Uniwersytet im. Adama Mickiewicza w Poznaniu

Wydział Biologii

Zastosowanie biodruku 3D oraz opracowanie biotuszy na bazie hydrożeli i nanomateriałów dla inżynierii tkankowej łąkotki

Rozprawa doktorska

Julia Anna Semba

Poznań, 2023

Adam Mickiewicz University, Poznan

Faculty of Biology

Application of 3D bioprinting and development of hydrogel/nanomaterial-based bioinks for meniscal tissue engineering

doctoral dissertation

by

Julia Anna Semba

Poznań, 2023

Supervisor

prof. UAM dr hab. inż. Jakub D. Rybka

the Laboratory of Applied Biotechnology,

Center for Advanced Technology, Adam Mickiewicz University

Auxiliary supervisor

dr Adam A. Mieloch

the Laboratory of Applied Biotechnology,

Center for Advanced Technology, Adam Mickiewicz University

Doctoral dissertation was performed at
the Laboratory of Applied Biotechnology
at Center for Advanced Technology,
Adam Mickiewicz University.

Acknowledgments

I would like to express my gratitude and appreciation to my supervisor Jakub Rybka for support, inspiration, unwavering faith in my work and ideas, and his insightful guidance.

I am grateful to Adam Mieloch for the effort and time he devoted to reviewing every sentence I wrote.

I truly value the help and motivation I have received from members of the Laboratory of Applied Biotechnology. Monika, Tomek, Filip, Ania, Piotr, Adam, Gosia – thank you!

My deepest thanks go to my family and friends – especially my parents, siblings, and Karol – for their support, encouragement, and love.

Contents

List of Scientific Papers Included in the Dissertation

1. **Semba J.A.**, Mieloch A.A., and Rybka J.D.

   Introduction to the state-of-the-art 3D bioprinting methods, design, and applications in orthopedics

   Bioprinting 18; 2020, https://doi.org/10.1016/j.bprint.2019.e00070

   IF: no data; CiteScore: 6,9 (2020)   MNiSW: 140 (2020)

2. Olejnik A., **Semba J.A.**, Kulpa A., Dańczak-Pazdrowska A., Rybka J.D., and Gornowicz-Porowska J.D.

   3D bioprinting in skin related research: Recent achievements and application perspectives

   ACS Synth. Biol. 11, 1, 26–38; 2022, https://doi.org/10.1021/acssynbio.1c00547

   IF: 5.249 (2021)   MNiSW: 140 (2022)

3. Mieloch A.A., **Semba J.A.**, and Rybka J.D.

   CNT-type dependent cellular adhesion on 3D-printed nanocomposite for tissue engineering

   Int J Bioprint 8(2), 548; 2022, http://doi.org/10.18063/ijb.v8i2.548

   IF: 7.422 (2021)   MNiSW: 40 (2022)

4. **Semba J.A.**, Mieloch A.A., Tomaszewska E., Cywoniuk P., and Rybka J.D.

   Formulation and evaluation of a bioink composed of alginate, gelatin, and nanocellulose for meniscal tissue engineering

   Int J Bioprint 9(1), 621; 2022, http://dx.doi.org/10.18063/ijb.v9i1.621

   IF: 7.422 (2021)   MNiSW: 40 (2022)

5. Szymański T., **Semba J.A.**, Mieloch A.A., Cywoniuk P., Kempa M., and Rybka J.D.

   Hyaluronic acid and multiwalled carbon nanotubes as bioink additives for cartilage tissue engineering

   Sci Rep 13, 646; 2023, https://doi.org/10.1038/s41598-023-27901-z

   IF: 4.997 (2021)   MNiSW: 140 (2023)

Unpublished papers

6. **Semba J.A.**, Mieloch A.A, Teixeira A.M., Martins P., and Rybka J.D.

   Mechanical testing of 3D printed constructs for meniscal tissue engineering

   Submitted on May 22th, 2023 to *European Polymer Journal* (manuscript number: EUROPOL-D-23-01256).

7. Mańkowska M., Stefańska M., Mleczko A.M., Kot W., Krych Ł., **Semba J.A.**, and Rybka J.D.

   Single-cell transcriptomic atlas of porcine meniscus: paving the way for advanced therapies

   Submitted on September 24th, 2023 to *Nature Communications* (manuscript number: NCOMMS-23-39377).

Streszczenie

Uszkodzone łąkotki mają niską zdolność do regeneracji, a żadna z dostępnych metod leczenia nie zapewnia powrotu stawu kolanowego do pełnej sprawności w długoterminowej perspektywie. Innowacyjne rozwiązanie stanowią biodrukowane 3D implanty mogące imitować złożoną architekturę łąkotki i przywrócić jej pełną funkcjonalność. Opracowanie biotuszy to kluczowy etap rozwoju techniki biodruku 3D, ponieważ jego kompozycja i struktura wpływa na właściwości tworzonej tkanki oraz oddziałuje na kondycję i różnicowanie komórek. Stąd, głównym celem niniejszej dysertacji było opracowanie biotuszu dla ekstruzyjnego biodruku 3D implantów łąkotki oraz wzbogacanie go wielościennymi nanorurkami węglowymi i kwasem hialuronowym w celu poprawienie właściwości mechanicznych i biologicznych.

Stężenie komponentów biotuszu – alginianu, żelatyny i karboksymetylowanej celulozy nanokrystalicznej – zostało wybrane na podstawie analizy reologicznej oraz dokładności wydruku. Wdrukowane chondrocyty wykazały żywotność powyżej 98% i wzrost ekspresji kolagenu typu II po 28 dniach od wydruku. Analiza pozostałych genów specyficznych dla tkanki chrzęstnej lub kostnej (*COL1A1*, *COL10A1*, *SOX9* i *RUNX2*) ukazała spadek ekspresji.

Ponadto, w rozprawie zawarto dowody wskazujące na korzyści płynące z suplementacji biotuszu wielościennymi nanorurkami węglowymi i kwasem hialuronowym. Analiza reologiczna i mechaniczna potwierdziły przydatność biotuszu dla inżynierii tkankowej łąkotki. Dodatek nanorurek węglowych prawie dwukrotnie zwiększył sztywność konstruktów, nawet przy tak niskim stężeniu jak 0,125 mg/ml. Połączenie tych dwóch dodatków miało pozytywny wpływ na żywotność macierzystych komórek mezenchymalnych wyizolowanych z ludzkiej tkanki tłuszczowej. Analiza real-time PCR genów *COL1A1*, *COL6A1*, *HIF1A*, *COMP*, *RUNX2* i *POU5F1* wykazała istotne zmiany w poziomie ekspresji.

Przeprowadzone analizy dostarczyły dowodów na przydatność materiału w inżynierii tkankowej łąkotki. W przyszłości, zasadne jest zbadanie zachowania konstruktu w długoterminowej hodowli *in vitro* oraz przeprowadzenie badań *in vivo*. Oprócz biodruku łąkotki, uważa się, że zaprezentowane wyniki mogą służyć jako podstawa dla rozwoju biotuszy dla biodruku 3D innych tkanek.

Słowa klucz: biodruk 3D, biotusz, łąkotka, inżynieria tkankowa

Abstract

Meniscus tears have a low capacity for self-repair and none of the available treatments reconstitute the full knee function in a long-term perspective. Considering the necessity for novel remedial solutions, the 3D bioprinted implant provides an opportunity to mimic the complex zonal architecture of the meniscus and restore its full functionality. The development of bioinks for 3D bioprinting is a pivotal step as its composition and structure affect the properties of the developing tissue and influence cell condition and differentiation. Therefore, the primary objective of this thesis was to develop a bioink for extrusion 3D bioprinting of meniscal constructs and to supplement the bioink with multiwalled carbon nanotubes and hyaluronic acid for enhanced mechanical and biological properties

The concentrations of bioink components – alginate, gelatin, and carboxymethylated cellulose nanocrystals – were chosen based on rheological analysis and printing accuracy. The encapsulated chondrocytes reached viability over 98% and increased expression of the collagen II gene after 28 days was observed. Examining the other genes specific to cartilage and bone tissue (*COL1A1*, *COL10A1*, *SOX9,* and *RUNX2*) revealed a decline in transcripts` levels.

What is more, the dissertation outlines the beneficial effect of multiwalled carbon nanotubes and hyaluronic acid addition to basal bioink. The rheological and mechanical characterization confirmed the usefulness of this bioink for cartilage tissue engineering. Carbon nanotube addition nearly doubled the stiffness of constructs, even at concentrations as low as 0.125 mg/ml. The combination of both additives had a beneficial influence on human adipose-derived mesenchymal stem cell viability. Real-time PCR analysis of *COL1A1*, *COL6A1*, *HIF1A*, *COMP*, *RUNX2*, and *POU5F1* genes revealed significant alterations in their expression profile.

Performed analyses proved its usefulness in meniscus tissue engineering. Prospectively, further development of the bioink should include long-term *in vitro* culture and *in vivo* studies. The published findings provide a foundation for the creation of bioinks for the 3D bioprinting of various tissues and organs.

Keywords: 3D bioprinting, bioink, meniscus, tissue engineering

List of Abbreviations

3D	Three-dimensional
BCNT	"Bamboo-like" Carbon Nanotube
CCNC	Carboxymethylated Cellulose Nanocrystal
COMP	Cartilage Oligomeric Matrix Protein
ECM	Extracellular Matrix
HIF	Hypoxia-Inducible Factor
hMSC-AT	Human Adipose Tissue-Derived Mesenchymal Stem Cell
MWCNT	Multiwalled Carbon Nanotube
NHAC	Normal Human Knee Articular Chondrocyte
PCL	Polycaprolactone
scRNA-seq	Single-Cell RNA Sequencing

Scientific achievements

Education

Since 01/2019	**Adam Mickiewicz University, Poznań** Doctoral Studies at Faculty of Biology I was transferred after II year from the Institute of Bioorganic Chemistry, Polish Academy of Sciences in Poznań.
2016–2018	**Adam Mickiewicz University, Poznań** Master's degree in Biotechnology in English Master thesis "The influence of nucleoside-diphosphate kinase (NDPK) inhibitors on respiration of the amoeba *Acanthamoeba castellanii* isolated mitochondria"
2013–2016	**Adam Mickiewicz University, Poznań** Bachelor degree in Biotechnology Bachelor thesis "Characterization of *Acanthamoeba castellanii* and *Trypanosoma brucei* fermentation processes"

Experience

Since 11/2018	**Center for Advanced Technology**, Adam Mickiewicz University, Poznań Position: PhD Student and co-investigator
07/2018–09/2018	**Department of Molecular Neurooncology**, Institute of Bioorganic Chemistry, Polish Academy of Sciences Position: Intern
07/2016–09/2016	**PozLab sp. z o. o.** Position: Intern
07/2015	**Chair and Department of Forensic Medicine**, Poznan University of Medical Sciences Position: Intern

Publications

Augustyniak A., Szymański T., Porzucek F., Mieloch A.A., **Semba J.A**., Hubert K.A., Grajek D., Krela R., Rogalska Z., Zalc-Budziszewska E., Wysocki S., Sobczak K., Kuczyński L., Rybka J.D.

A cohort study reveals different dynamics of SARS-CoV-2-specific antibody formation after Comirnaty and Vaxzevria vaccination

Vaccine, 2023, https://doi.org/10.1016/j.vaccine.2023.06.008

Szymański T., **Semba J.A.**, Mieloch A.A., Cywoniuk P., Kempa M., Rybka J.D.

Hyaluronic acid and multiwalled carbon nanotubes as bioink additives for cartilage tissue engineering

Sci Rep 13, 646, 2023, https://doi.org/10.1038/s41598-023-27901-z

Semba J.A., Mieloch A.A., Tomaszewska E., Cywoniuk P., Rybka J.D.

Formulation and evaluation of a bioink composed of alginate, gelatin, and nanocellulose for meniscal tissue engineering

Int J Bioprint, 2022, http://dx.doi.org/10.18063/ijb.v9i1.621

Mieloch A.A., **Semba J.A.**, Rybka J.D.

CNT-type dependent cellular adhesion on 3D-printed nanocomposite for tissue engineering

Int J Bioprint., 2022, http://doi.org/10.18063/ijb.v8i2.548

Olejnik A., **Semba J.A.**, Kulpa A., Dańczak-Pazdrowska A., Rybka J.D., Gornowicz-Porowska J.

3D bioprinting in skin related research: Recent achievements and application perspectives

ACS Synth. Biol., 11, 26–38, 2022, https://doi.org/10.1021/acssynbio.1c00547

Semba J.A., Mieloch A.A., Rybka J.D.

Introduction to the state-of-the-art 3D bioprinting methods, design, and applications in orthopedics

Bioprinting, 2020, 18, 2020 e00070, https://doi.org/10.1016/j.bprint.2019.e00070

Patent Applications

Porzucek F.W., Mańkowska-Woźniak M.M., Rybka J.D., Mieloch A.A., **Semba J.A.**

Polish Patent Application *"Biotusz na bazie macierzy zewnątrzkomórkowej (ECM) wyizolowanej z łąkotki świńskiej, sposób jego przygotowania oraz zastosowanie do biodruku 3D modelu łąkotki"*

P.443418 [WIPO ST 10/C PL443418]

Semba J.A., Tomaszewska E., Mieloch A.A., Rybka J.D.

Polish Patent Application *"Biotusz, sposób jego wytwarzania oraz zastosowanie do biodruku 3D łąkotki"*

P.440810 [WIPO ST 10/C PL440810]

Projects

"Selection of markers specific for cell population present in porcine meniscus for the future use in 3D bioprinted constructs assessment" MG/POWER17/2021/14 (2021–2022, 12 733 PLN) supported by the project "Passport to the future – Interdisciplinary doctoral studies at the Faculty of Biology Adam Mickiewicz University" – **principal investigator**

"Influence of collagen isolated from fish skin on cartilage-specific gene expression in adipose-derived mesenchymal stem cells encapsulated in 3D bioprinted constructs" 017/02/SNP/0019 (2022, 30 000 PLN) supported by the Excellence Innovative – Research University (ID-UB) Programme by Adam Mickiewicz University – **principal investigator**

"Development of bioinks for 3D bioprinting based on chemically modified porcines dECM, enriched with recombinant hybridproteins, nanomaterials and synthetic polymers" TECHMATSTRATEG-III/0027/2019 (2021–2023, 22 444 594 PLN) – **co-investigator**

"Development and verification of the effectiveness of the new covid-19 immunodiagnostic tool" founded by The National Centre for Research and Development SZPITALE-JEDNOIMIENNE/76/2020 (2021, 2 652 000 PLN) – **co-investigator**

"MeniScaff 3D - 3D bioprinted, carbon nanotube-enhanced scaffolds for stimulated chondrogenic differentiation of mesenchymal stem cells for meniscus regeneration" LIDER/34/0122/L-9/17/NCBR/2018 (2019–2022, 1 199 906 PLN) – **co-investigator**

Internships

One-month internship at the Institute of Science and Innovation in Mechanical and Industrial Engineering (INEGI), Faculty of Engineering, University of Porto, June 2022. The internship was financed by the project "Passport to the future – Interdisciplinary doctoral studies at the Faculty of Biology Adam Mickiewicz University" POWR.03.02.00-00-I006/17.

Aims of the Dissertation

Meniscus injuries lower the quality of life, and none of the currently available treatments completely reconstruct structure function long-term. Given the need for innovative repair solutions, the three dimensional (3D) bioprinted implants have the potential to recreate the complex zonal structure of the meniscus and restore its full functionality. The development of bioinks is pivotal as their composition impacts the phenotype of the developing tissue and strongly influences the cell fitness. Therefore, the primary objective was developing a bioink for 3D bioprinting of meniscal constructs. Along with the fundamental components of bioink, the dissertation outlines the benefits of multiwalled carbon nanotubes and hyaluronic acid as bioink additives. The rheological, mechanical, and biological characterization of the bioink determined the suitability of the bioink for cartilage tissue engineering.

Introduction

A thorough literature search was conducted to gain an in-depth understanding of 3D bioprinting. The acquired knowledge was published as two review articles. The review "**Introduction to the state-of-the-art 3D bioprinting methods, design, and applications in orthopedics**" in its first part describes the relevant features of cartilage and bone tissue [1]. Then, 3D bioprinting in tissue engineering is discussed – including a detailed description of applicable cell types, utilized materials, and available techniques. The final section presents the most relevant 3D bioprinting strategies in orthopedics. The second review article – "**3D Bioprinting in skin related research: Recent achievements and application perspectives**" – though focused on skin, not meniscus; involves details relevant to this dissertation: 3D bioprinting and bioink composition [2]. Highlights from these two publications are reconsidered below.

Menisci are cartilaginous structures located in the knee between the femur and tibia [3,4]. The extracellular matrix (ECM), vascularity, and cellular phenotype of the adult meniscus vary due to zonal architecture. The red-red zone has oval, fibroblast-like cells surrounded by ECM composed mainly of type I collagen [3]. The white-white zone, in contrast, contains round, chondrocyte-like cells encircled by ECM abundant in type II collagen and less amount of type I collagen. The vascularity is gradually diminishing from the red-red zone to the white-white zone (Fig. 1). The red-white zone displays intermediate features of red-red and white-white regions. Owing to these variations, the meniscus demonstrates heterogeneous biological and mechanical characteristics that facilitate the meniscus and knee joint's proper function.

Since menisci stabilize the knee and spread loads to reduce the stress applied to articular cartilage they are prone to injuries [5]. Healing of the meniscal lesions is directly connected to vascularization; therefore, the avascular zone has low regenerative properties. Meniscectomy and suturing – the most common therapeutic techniques – typically result in insubstantial and unsatisfactory results, particularly when complex or extensive injuries are treated. Moreover, meniscectomy increases contact stress on the articular cartilage, which leads to cartilage degeneration [6]. Due to the prevalence of meniscus injuries and the urgent need for innovative and effective treatment methods, the motivation for cartilage tissue engineering significantly increases.

Figure 1. *Extrusion 3D bioprinting of the meniscus implant. The vascularity gradually decreased from the outer zone to the inner zone of the meniscus. The black arrow indicates the applied pressure.*

Tissue engineering combines the principles of engineering and the life sciences to develop artificial tissues or organs for clinical use. One of the promising technologies for the commercial manufacturing of tissue constructs is 3D bioprinting, which implements computer-aided design to create 3D models through layer-by-layer assembly [7]. In extrusion, the constantly applied pneumatic pressure or mechanical pistons ejects bioinks comprised of viable cells, biomaterials (mainly hydrogels), and additional biological components (Fig. 1). This approach allows the production of implants and scaffolds with anatomical precision. The bioprinted cell-laden structures aimed to support new tissue development by providing an environment conducive to cell migration, proliferation, differentiation, or ECM secretion [8]. The enormous potential of this method is evidenced by the growing number of publications in the field of 3D bioprinting [9–12].

The dissertation was structured to align with three key aspects of bioink development: 1) Basal bioink development; 2) Bioink additives; 3) Mechanical testing. Core scientific achievements were grouped and briefly described according to the abovementioned criteria.

Development of Basal Bioink

The original research publication "**Formulation and evaluation of a bioink composed of alginate, gelatin, and nanocellulose for meniscal tissue engineering**" describes the bioink composed of 4.0% gelatin, 0.75% alginate, and 1.4% carboxymethylated cellulose nanocrystal (CCNC) dissolved in 4.6% D-mannitol (Fig. 2) [13]. Alginate is a common hydrogel used in tissue engineering that has gained popularity due to its biocompatibility, biodegradability, and affordability [14]. It crosslinks with divalent cations forming ionic bridges between polymer chains [15]. Unfortunately, alginates lack cell and protein binding properties due to their negative charge [16]. Therefore, it is commonly blended with positively charged biomaterials, like gelatin. In cartilage-related research, the stiffness of constructs is enhanced by reinforcing materials, such as nanocellulose.

Bioink properties

- ✓ Shear-thinning behavior
- ✓ Printable
- ✓ Stable in cell culture
- ✓ Biocompatible
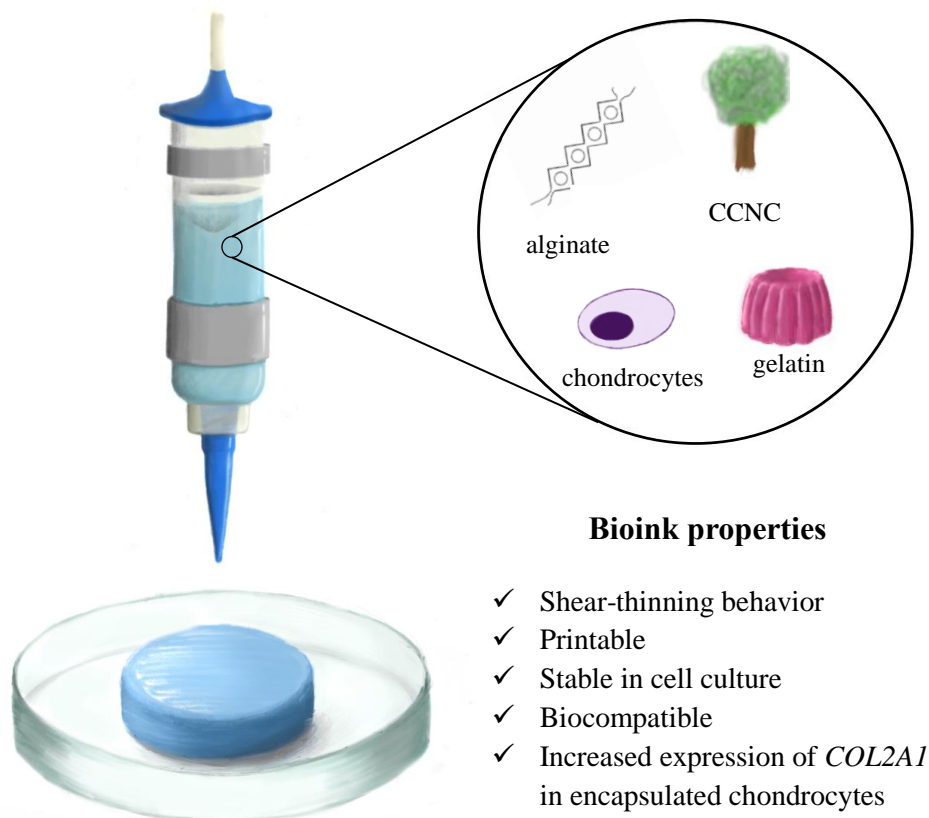- ✓ Increased expression of *COL2A1* in encapsulated chondrocytes

Figure 2. The 3D bioprinting with chondrocytes encapsulated in the bioink composed of 4.0% gelatin, 0.75% alginate, and 1.4% carboxymethylated cellulose nanocrystal. CCNC – carboxymethylated cellulose nanocrystal.

The bioink composition was chosen based on rheological analysis and printing accuracy measurements. The constructs encapsulated normal human knee articular chondrocytes (NHACs) exhibited > 98% viability in all measured time points (namely, 24 h and 7, 14, and 28 days). The RNA isolation with TriReagent and RNeasy Mini Kit (Qiagen) resulted in a low nucleic acid yield; therefore, only five chondrogenesis marker genes were selected - *COL1A1*, *COL2A1*, *COL10A1*, *SOX9*, and *RUNX2*. The expression of *COL2A1* increased during *in vitro* culture of bioprinted constructs, reaching statistical significance after four weeks. Expression of other studied genes dropped in time. The time point around 14 days of culture seems to be a peak in the expression of many genes, but the majority of the studies do not cover as extensive time points as 28 days [17–19]. Although, it is highly likely that at this stage cells may require further stimulation, for example, with growth factors.

The study proved, that formulated bioink is printable, stable under cell culture conditions, and biocompatible. It served as the basis for later development. The composition and preparation of this bioink are subjects of Polish Patent Application "*Biotusz na bazie macierzy zewnątrzkomórkowej (ECM) wyizolowanej z łąkotki świńskiej, sposób jego przygotowania oraz zastosowanie do biodruku 3D modelu łąkotki*".

Bioink Additives

Further, the usefulness and toxicity of carbon nanotubes as a bioink additive was evaluated. In the research entitled "**CNT-Type Dependent Cellular Adhesion on 3D-Printed Nanocomposite for Tissue Engineering**", 3D-printed grids made of polycaprolactone (PCL) were reinforced with multiwalled carbon nanotubes (MWCNTs) and "bamboo-like" carbon nanotubes (BCNTs) of the following concentrations: 0.005%, 0.01%, 0.02%, and 0.2% (Fig. 4) [20]. NHACs were seeded on grids to evaluate the toxicity of the material. After three and six days the highest viability was observed for 0.01% MWCNTs and 0.01% BCNTs supplemented grids.
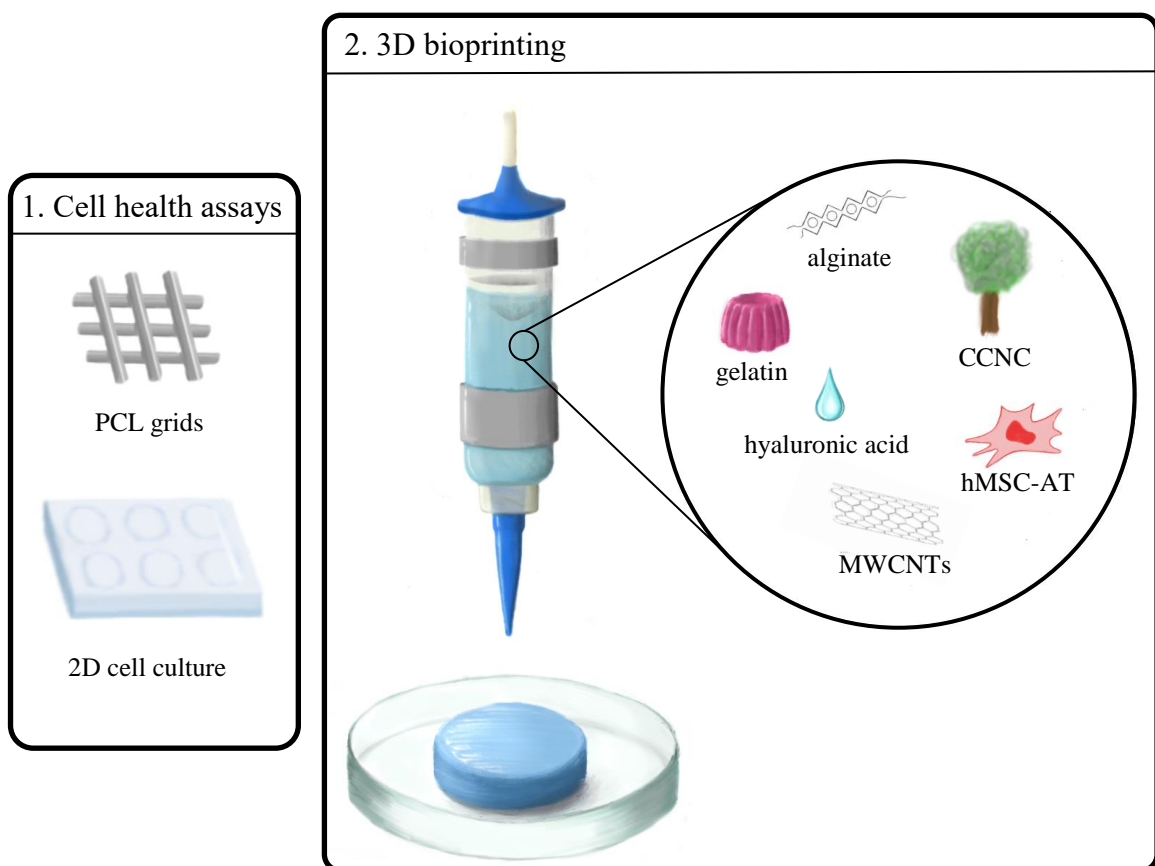
Figure 4. The workflow of testing carbon nanotubes and hyaluronic acid as bioink additives. The carbon nanotube-reinforced PCL grids were biologically assessed, followed by cell health assays made on hMSC-AT grown in medium supplemented with carbon nanotubes or hyaluronic acid. The obtained results were used to formulate the bioink for 3D bioprinting.
PCL – polycaprolactone, CCNC – carboxymethylated cellulose nanocrystal,
hMSC-AT – human adipose tissue-derived mesenchymal stem cells,
MWCNTs - multiwalled carbon nanotubes.

After two weeks, it was concluded, that pure PCL grids do not promote cell growth, since numerous apoptotic cells were noticed. The addition of 0.01% MWCNT enhanced cell proliferation; albeit, the cell shape remained spherical, indicating a suboptimal surface adhesion. More elongated cells were noted in PCL grids reinforced with 0.01% and 0.02% BCNTs, indicating that the BCNTs facilitated cellular attachment and proliferation.

In the next research published as "**Hyaluronic acid and multiwalled carbon nanotubes as bioink additives for cartilage tissue engineering**", the MWCNTs and hyaluronic acid were added to bioink and directly bioprinted with human adipose tissue-derived mesenchymal stem cells (hMSC-AT, PromoCell) [18]. The concentrations of these two additives were determined based on the cell viability, reactive oxygen species production, and apoptosis levels in 2D cell cultures of NHACs and hMSC-AT stimulated with investigated components (Fig. 4). The most beneficial effect was obtained with the addition of 0.25 mg/ml HA and 0.0625 mg/ml MWCNTs, hence, these concentrations were selected for 3D bioprinting.

Only the addition of MWCNTs and hyaluronic acid together positively impacted cell viability in 3D constructs. Gene expression analysis of *COL1A1*, *COL6A1*, *HIF1A*, *COMP*, *RUNX2*, and *POU5F1* genes revealed significant alterations in the expression level of all examined genes with a progressive loss of transcriptional activity in the majority of them. These findings suggest the necessity of conducting more complex gene expression analysis along with protein accumulation studies, over a longer period. The results from 3D bioprinted scaffolds encourage undertaking *in vivo* tests to investigate the mechanism of MWCNT interaction with cells.

Mechanical Testing

Attempts at meniscal tissue engineering using 3D bioprinted constructions should take mechanical concerns into account since the meniscus's functionality mostly depends on its mechanical properties. The majority of commercially available analytical equipment cannot handle such soft materials as hydrogels. Hence, to measure the mechanical properties of bioprinted constructs, I was at a one-month internship at the Institute of Science and Innovation in Mechanical and Industrial Engineering, Faculty of Engineering at the University of Porto, where the dedicated custom-made equipment for compression tests was available. The results are presented in the yet unpublished paper "**Mechanical testing of 3D printed constructs for meniscal tissue engineering**" (Fig. 3).

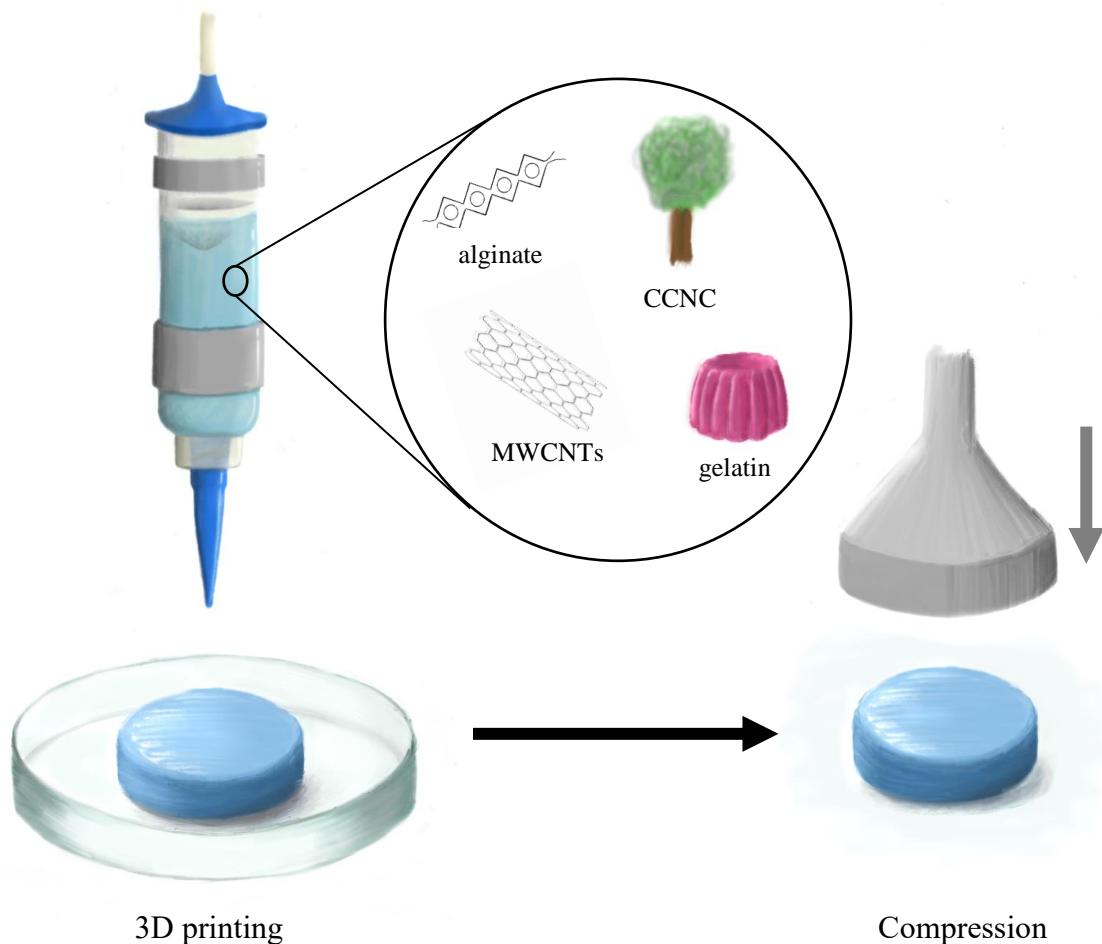alginate

CCNC

MWCNTs

gelatin

3D printing

Compression

Figure 3. The compression tests of 3D printed constructs (unpublished graphical abstract). CCNC – carboxymethylated cellulose nanocrystal. MWCNTs - multiwalled carbon nanotubes.

Compression tests were performed on bioprinted constructs with bioink described in "**Formulation and evaluation of a bioink composed of alginate, gelatin, and nanocellulose for meniscal tissue engineering**" [13]. At first, the protocol for compression testing of 3D bioprinted constructs was established. Then, it was applied to investigate the influence of time, hydrostatic pressure, and MWCNT addition on the mechanical properties of the 3D constructs. A significant increase in construct stiffness was observed for constructs with incorporated MWCNTs. The results confirmed the expediency of carbon nanotubes as reinforcement material. It is reasonable to test constructs with encapsulated cells. Such studies would have allowed for assessing the influence of MWCNTs on the mechanical properties of constructs and cell fitness over time. Additionally, the alteration in mechanical properties might facilitate monitoring the chondrogenesis process.

Additional Research

In the course of my PhD studies, I have acquired two minigrants thematically consistent with my research topic: "Influence of collagen isolated from fish skin on cartilage-specific gene expression in adipose-derived mesenchymal stem cells encapsulated in 3D bioprinted constructs" and "Selection of markers specific for cell population present in porcine meniscus for the future use in 3D bioprinted constructs assessment". The yet-unpublished results of these grants are presented below.

"Influence of collagen isolated from fish skin on cartilage-specific gene expression in adipose-derived mesenchymal stem cells encapsulated in 3D bioprinted constructs"

Collagens are a structural protein of the cartilaginous ECM. It has been proven that collagen type I gels offers appropriate biochemical and mechanical properties for cartilage tissue engineering [21]. Collagen addition (1.5%) to alginate bioink stimulates bone marrow-derived mesenchymal stem cell proliferation and enhances the expression of *SOX9* [22]. The expression of genes encoding cartilage ECM proteins (aggrecan and collagen type II) was also increased, with a decreased expression of the collagen type I gene. In another research, meniscal fibrochondrocytes viability was unaffected by collagen concentration (1% – 2%), when bioprinted with alginate/collagen bioink [23].

In the project, the influence of supplementation with various collagen concentrations (2%, 4%, 6%, and 8%) on the gene expression of hMSC-AT encapsulated in 3D bioprinted constructs was investigated. The collagens isolated from fish skin were obtained by courtesy of the Polish company COFACTOR. The research focused on analyzing fish skin collagens' influence on the cartilage- and osteogenic-specific marker genes that encode transcription factors and ECM proteins.

The bioink preparation and 3D bioprinting were conducted as described in "**Formulation and evaluation of a bioink composed of alginate, gelatin, and nanocellulose for meniscal tissue engineering**" [13]. After basal bioink preparation, various concentrations of fish skin collagen were added. The prepared bioinks were mixed with mesenchymal stem cells derived from adipose tissue (at a concentration 1×10^7 cells/ml of bioink). Adipose tissue was harvested by liposuction (by Mandala Beauty Clinic), and cells were isolated with collagenase I digestion. One, two, and four weeks after bioprinting, the constructs were collected for mRNA isolation with

Total RNA Midi (A&A Biotechnology) followed by reverse transcription (TranScriba 1step PCR Mix Probe, A&A Biotechnology). The expression of genes was measured with real-time PCR (QuantStudio 6K Flex, Applied Biosystem) where *RPS29* was chosen as the housekeeping gene.

The most profound variations were observed in *SOX9* and *SOX8* expression for constructs with 2%–6% collagen, at one- and two-week time points (Fig. 5A and B). The collagen addition lowered the expression of *RUNX2* at four weeks (Fig. 5C). In the case of genes encoding ECM proteins, the decrease of *COL1A1* expression was observed after four weeks in all collagen variants (Fig. 5D), while *COL6A1* expression dropped in all collagen variants except 8% (Fig. 5E). The concentration- and time-dependent changes in *COMP* expression were observed, with the most profound results in constructs with 4% collagen addition after four weeks (Fig. 5G). These results suggest that collagen addition in concentrations of 4% and 6% might have the highest chondrogenic potential.

The constructs with 8% collagen exhibited an intense expression of the collagen type X gene at one and two weeks, but an inverted pattern was observed at four weeks (Fig. 5F). The obtained results are insufficient to prove chondrocyte hypertrophy. Research on protein accumulation and more comprehensive gene expression analysis is required. Expression of *MMP13*, *HIF1A*, *COL2A2*, *COL11A1*, and *ACAN* genes expression was below the detection limit.

The weakness of the presented studies is only one biological replication; hence, there is no statistical analysis present. The lack of an adequate amount of analyzed constructs was caused by difficulty in the mesenchymal stem cell expansion. This problem could be solved by modification of cell culture procedure or change of a cell line (what was done in [18]). Nevertheless, the gene expression variations are noticeable and time-dependent. The most promising results are observed in samples with 4% and 6% collagen supplementation. It is feasible to investigate the gene expression and protein accumulation after a longer construct *in vitro* cultivation and with more biological replicates.
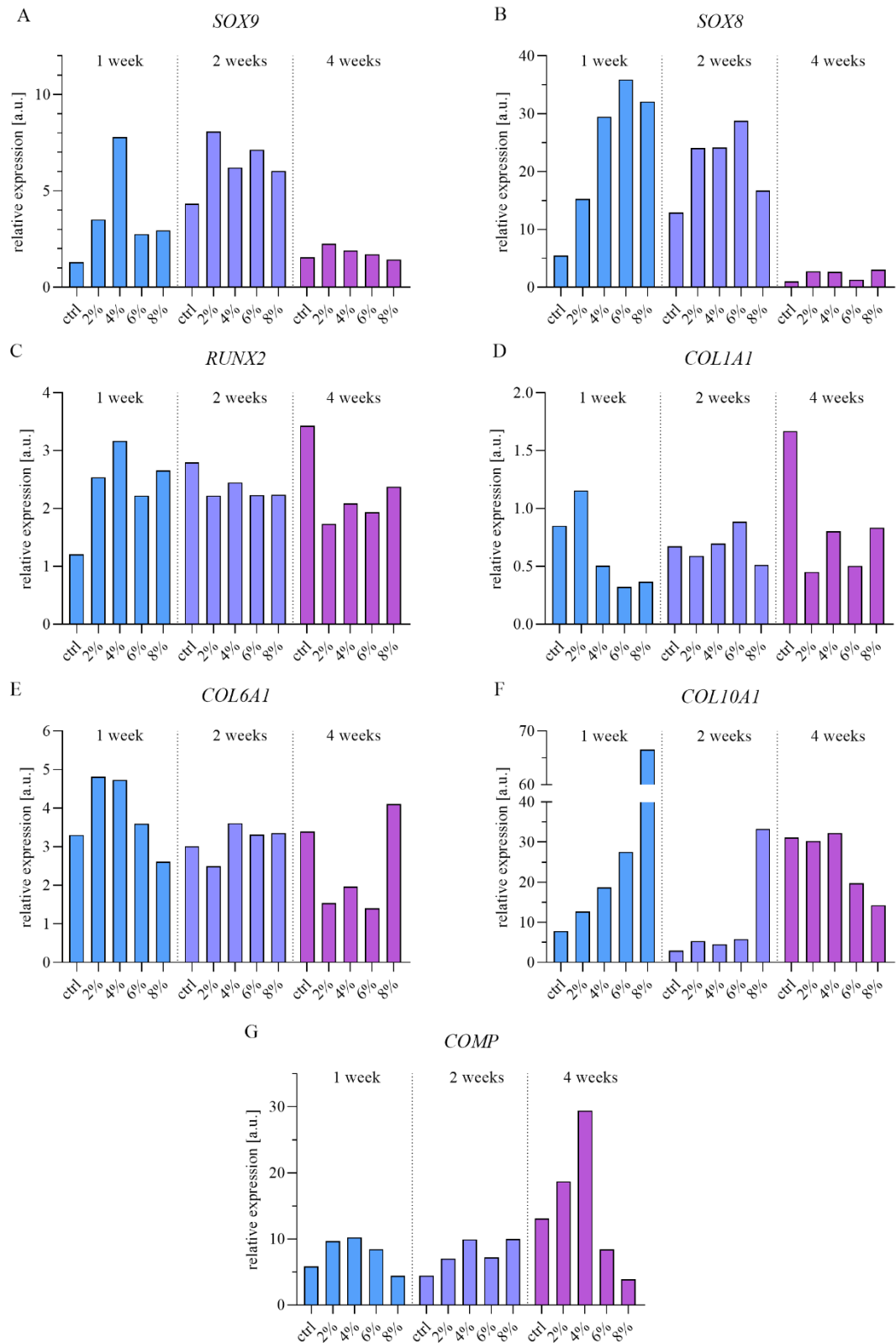
Figure 5. *Effect of collagen additives (2%, 4%, 6%, or 8%) on the expression of chondrogenic and osteogenic marker genes. Real-time analysis of SOX9 (A), SOX8 (B), RUNX2 (C), COL1A1 (D), COL6A1 (E), COL10A1 (F), and COMP (G) gene expression in hMSC-AT at one week, two weeks, and four weeks post-printing. The expression of each variant is normalized to the expression in hMSC-AT collected before bioprinting from 2D culture.*

"Selection of markers specific for cell population present in porcine meniscus for the future use in 3D bioprinted constructs assessment"

The research addressed the need for the identification of potential markers, which will be utilized for the assessment of cell differentiation inside 3D bioprinted meniscal constructs. At the time the project was been conducted, only one publication presenting the whole spectrum of cell subpopulations constituting the meniscus using a single-cell RNA sequencing (scRNA-seq) approach was published [24]. However, it was not focused on zonal characterization. So, the project aimed to optimize and perform scRNA-seq of meniscal zones: white-white and red-red.

Aggregated data showed high similarity between medial and lateral samples when representing the same zone, while red-red and white-white zones exhibited significant discrepancies regarding identified cell clusters. Preliminary data analysis enabled the identification of seven cell clusters corresponding to four major cell types (Fig. 6A). Most abundant cell cluster were chondrocytes (75% of cells); which were further divided into five subclusters due to differential genes expression (Fig. 6B and C). The distribution of chondrocyte subclusters differs among meniscus zones. It is anticipated that they fulfill different roles in the meniscus physiology. Next most abundant cell clusters are endothelial cells (with small population of proliferating endothelial cells) and smooth muscle cells (Fig. 6B). Cells expressing immune cells marker genes are also present in the sequencing data (Fig. 6A). Similar research published recently identified comparable clusters [25]. However, further data analysis is required for a more precise description of each cell cluster, unrevealing differentially expressed genes as well as identify up- and down-regulated pathways characteristic for each cluster.
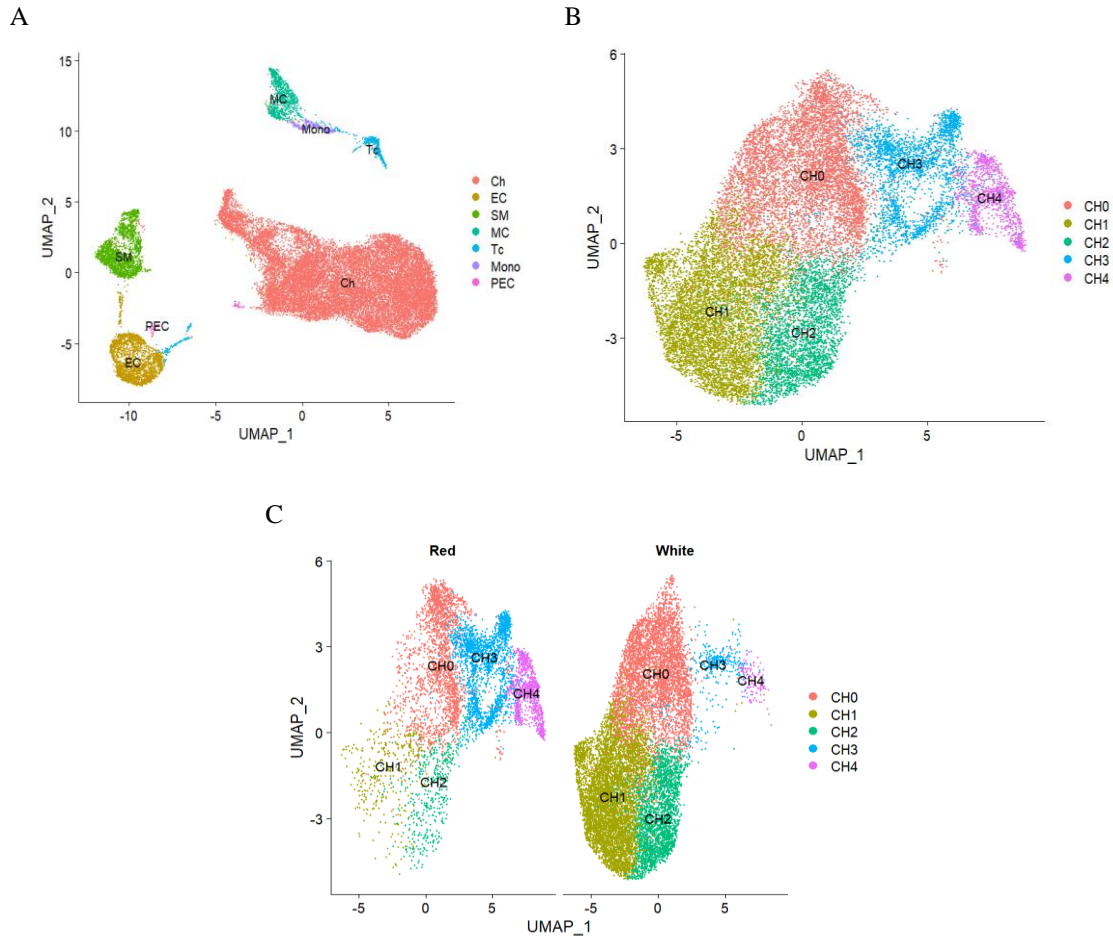
Figure 6. Analysis of sequencing data (unpublished).

A. Aggregated projection of identified cells. Ch – chondrocytes, EC – endothelial cells, SM – smooth muscle cells, MC – macrophages, Tc – T-cells, Mono – monocytes, PEC – proliferating endothelial cells. B. Identified chondrocyte subclusters. C. Chondrocyte subclusters distribution in red-red and white-white zones.

Other Investigations

Along with meniscal tissue engineering, I had the opportunity to bioprint skin constructs with CELLINK SKIN bioink, keratinocytes, and fibroblasts. The procedure was performed according to the Skin Tissue Model Kit protocol by CELLINK. Briefly, the model was designed in Tinkercad and sliced with Slic3r. The primary epidermal keratinocytes and fibroblasts HFF1 cell lines (both from ATCC) were handled according to the manufacturer's instructions. The cell suspension was mixed with bioink before being transferred to cartridges suitable for the BIO X printer (CELLINK). The nanofibrillar cellulose, sodium alginate, and fibrinogen in CELLINK SKIN bioink recapitulates the healing environment of the skin and preserves the construct structure in cell culture conditions. After bioprinting, the constructs underwent simultaneous ionic and thrombin crosslinking. Overall cell viability (checked as in [18]) was satisfactory after fourteen days post-printing ($> 81\%$) (unpublished results). The skin structures were sent for further research at Poznan University of Medical Sciences.

I have also collaborated with Dorota Gurda-Woźna (Institute of Bioorganic Chemistry, Polish Academy of Sciences) on her MINIATURA 5 project "*Optymalizacja warunków biodruku w celu stworzenia komórkowego modelu 3D raka wątroby, jako platformy skriningowej do selekcji związków o p000otencjale terapeutycznym*" (2021/05/X/NZ7/00450), on the optimization of bioprinting conditions in order to create a 3D model of liver cancer. I prepared bioink consisting of 4% gelatin from porcine skin and 1% sodium alginate dissolved in 4.6% D-mannitol. The bioprinting and crosslinking were as in [13], and the cell suspension was prepared by Dorota Gurda, PhD. The cell viability was $> 70\%$ in all tested time points (24h, 7d, 14d, 21d). The constructs were subjected to further studies by Dorota Gurda (results to be published).

Summary and Perspective

Currently, organ regeneration via bioprinting is relatively limited in clinical adoption. Despite many promising results from *in vitro* and *in vivo* studies, the gap between 3D bioprinting research and clinical use is still present. The results from this dissertation may be applied for upcoming research on bioink formulation, cell differentiation, and generation of the zonal-defined meniscus implant that has the potential of becoming the new therapeutic option in orthopedics.
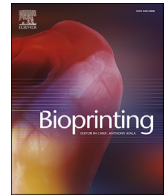
Reference

1. Semba, J. A., Mieloch, A. A. & Rybka, J. D. Introduction to the state-of-the-art 3D bioprinting methods, design, and applications in orthopedics. *Bioprinting* **18,** e00070 (2020).

2. Olejnik, A., Semba, J. A., Kulpa, A., Dańczak-Pazdrowska, A., Rybka, J. D. & Gornowicz-Porowska, J. 3D Bioprinting in Skin Related Research: Recent Achievements and Application Perspectives. *ACS Synth Biol* **11,** 26–38 (2022).

3. Murphy, C. A., Garg, A. K., Silva-Correia, J., Reis, R. L., Oliveira, J. M. & Collins, M. N. The Meniscus in Normal and Osteoarthritic Tissues: Facing the Structure Property Challenges and Current Treatment Trends. *Annu Rev Biomed Eng* **21,** 495–521 (2019).

4. Fox, A. J. S., Bedi, A. & Rodeo, S. A. The Basic Science of Human Knee Menisci: Structure, Composition, and Function. *Sports Health* **4,** 340–351 (2012).

5. Logerstedt, D. S., Ebert, J. R., MacLeod, T. D., Heiderscheit, B. C., Gabbett, T. J. & Eckenrode, B. J. Effects of and Response to Mechanical Loading on the Knee. *Sports Medicine* **52,** 201–235 (2022).

6. McDermott, I. D. & Amis, A. A. The consequences of meniscectomy. *J Bone Joint Surg Br* **88-B,** 1549–1556 (2006).

7. Skardal, A. in *3D Bioprinting in Regenerative Engineering: Principles and Applications* (eds. Khademhosseini, A. & Camci-Una, G.) 1–24 (CRC Press, 2018).

8. Kačarević, Ž. P., Rider, P. M., Alkildani, S., Retnasingh, S., Smeets, R., Jung, O., Ivanišević, Z. & Barbeck, M. An introduction to 3D bioprinting: Possibilities, challenges and future aspects. *Materials* **11,** (2018).

9. Vaishya, R., Patralekh, M. K., Vaish, A., Agarwal, A. K. & Vijay, V. Publication trends and knowledge mapping in 3D printing in orthopaedics. *J Clin Orthop Trauma* **9,** 194–201 (2018).

10. Tack, P., Victor, J., Gemmel, P. & Annemans, L. 3D-printing techniques in a medical setting: A systematic literature review. *Biomed Eng Online* **15,** 115 (2016).

11. Stanco, D., Urbán, P., Tirendi, S., Ciardelli, G. & Barrero, J. 3D bioprinting for orthopaedic applications: Current advances, challenges and regulatory considerations. *Bioprinting* **20,** e00103 (2020).

12. Ding, Z., Tang, N., Huang, J., Cao, X. & Wu, S. Global hotspots and emerging trends in 3D bioprinting research. *Front Bioeng Biotechnol* **11,** 1–20 (2023).

13. Semba, J. A., Mieloch, A. A., Tomaszewska, E., Cywoniuk, P. & Rybka, J. D. Formulation and evaluation of a bioink composed of alginate, gelatin, and nanocellulose for meniscal tissue engineering. *Int J Bioprint* **9,** 621 (2022).

14. Lee, K. Y. & Mooney, D. J. Alginate: Properties and biomedical applications. *Progress in Polymer Science (Oxford)* **37,** 106–126 (2012).

15. Grant, G., Morris, E., Rees, D., Smith, P. & Thom, D. Biological interactions between polysaccharides and divalent cations: The egg-box model. *FEBS Lett* **32,** 195–198 (1973).

16. Gargus, E., Lewis, P. & Shah, R. in *3D Bioprinting in Regenerative Engineering: Principles and Application* (eds. Khademhosseini, A. & Camci-Una, G.) 25–50 (Taylor & Francis, 2018).

17. Jian, Z., Zhuang, T., Qinyu, T., Liqing, P., Kun, L., Xujiang, L., Diaodiao, W., Zhen, Y., Shuangpeng, J., Xiang, S., Jingxiang, H., Shuyun, L., Libo, H., Peifu, T., Qi, Y. & Quanyi, G. 3D bioprinting of a biomimetic meniscal scaffold for application in tissue engineering. *Bioact Mater* **6,** 1711–1726 (2021).

18. Szymański, T., Semba, J. A., Mieloch, A. A., Cywoniuk, P., Kempa, M. & Rybka, J. D. Hyaluronic acid and multiwalled carbon nanotubes as bioink additives for cartilage tissue engineering. *Sci Rep* **13,** 646 (2023).

19. Haugh, M. G., Meyer, E. G., Thorpe, S. D., Vinardell, T., Duffy, G. P. & Kelly, D. J. Temporal and spatial changes in cartilage-matrix-specific gene expression in mesenchymal stem cells in response to dynamic compression. *Tissue Eng Part A* **17,** 3085–3093 (2011).

20. Mieloch, A. A., Semba, J. A. & Rybka, J. D. CNT-Type Dependent Cellular Adhesion on 3D-Printed Nanocomposite for Tissue Engineering. *Int J Bioprint* **8,** 70–79 (2022).

21. Puetzer, J. L. & Bonassar, L. J. High density type i collagen gels for tissue engineering of whole menisci. *Acta Biomater* **9,** 7787–7795 (2013).

22. Yang, X., Lu, Z., Wu, H., Li, W., Zheng, L. & Zhao, J. Collagen-alginate as bioink for three-dimensional (3D) cell printing based cartilage tissue engineering. *Mater Sci Eng C Mater Biol Appl.* **83,** 195–201 (2018).

23. Rhee, S., Puetzer, J. L., Mason, B. N., Reinhart-King, C. A. & Bonassar, L. J. 3D bioprinting of spatially heterogeneous collagen constructs for cartilage tissue engineering. *ACS Biomater Sci Eng* **2,** 1800–1805 (2016).

24. Sun, H., Wen, X., Li, H., Wu, P., Gu, M., Zhao, X., Zhang, Z., Hu, S., Mao, G., Ma, R., Liao, W. & Zhang, Z. Single-cell RNA-seq analysis identifies meniscus progenitors and reveals the progression of meniscus degeneration. *Ann Rheum Dis* **79,** 408–417 (2019).

25. Fu, W., Chen, S., Yang, R., Li, C., Gao, H., Li, J. & Zhang, X. Cellular features of localized microenvironments in human meniscal degeneration: a single-cell transcriptomic study. *Elife* **11,** (2022).

Publications and Author Statements

Review article

Introduction to the state-of-the-art 3D bioprinting methods, design, and applications in orthopedics

Julia Anna Semba [a], Adam Aron Mieloch [a,b], Jakub Dalibor Rybka [a,*]

[a] *Center for Advanced Technology, Adam Mickiewicz University in Poznan, Uniwersytetu Poznańskiego 10 Street, Poznan, 61-614, Poland*
[b] *Faculty of Chemistry, Adam Mickiewicz University in Poznan, Uniwersytetu Poznańskiego 8 Street, 61-614, Poznan, Poland*

A B S T R A C T

Cartilage injuries and bone loss become increasingly prevalent in modern societies. Articular cartilage and menisci have low or no capacity for self-repair and none of the available treatments provide satisfactory, long-term outcomes. Additionally, despite self-regenerating capabilities of bone tissue, the mechanism may fail or become insufficient, creating the need for surgical bone replacement, which is restrained by natural graft accessibility. 3D bioprinting is a rapidly developing technology emerging as a promising remedial therapy in orthopedics. The extensive and ongoing studies in this field are focused on such topics as cartilage and bone biology, standardization of cell culture protocols, bioink formulation, and 3D bioprinting technology. Recent results of these examinations, focused on applications in orthopedics, are presented in this review.

1. Introduction

Articular cartilage and menisci display a low or no capacity for self-repair and none of the available treatments reconstitute the organ's function [1–3]. In contrast, regenerative properties of the bone tissue are much greater but still burdened with the risk of failure or insufficiency [4]. Bioprinting is an emerging technology, providing promising and alternative ways of commercial manufacturing of tissue constructs for articular cartilage regeneration or bone replacement [3]. 3D bioprinting belongs to the family of additive manufacturing (AM) processes that utilize computer-aided design (CAD) for the generation of 3D models through layer-by-layer deposition [5]. The constructs are printed with bioink comprised of viable cells, biomaterials, and additional biological substances. These artificial, cell-laden scaffolds promote and support new tissue formation by providing a suitable environment for cell migration, proliferation, differentiation, and ensure a proper extracellular matrix (ECM) secretion [6,7]. Unsurprisingly, an increasing number of publications in the field of 3D bioprinting in orthopedics is observed, marking a tremendous potential of this technology [8,9].

2. Cartilage

Cartilage is an aneural, alymphatic, and avascular tissue, characterized by high fluid content and low oxygen consumption [10]. In vertebrates, three types of cartilages can be identified: hyaline cartilage, elastic cartilage, and fibrocartilage; which differ in terms of histology and ECM composition. Articular cartilage is composed of the hyaline cartilage, while menisci are made of the fibrous cartilage. This and the next chapter delve into the aspects of cartilage and bone biology that are relevant from the standpoint of tissue regeneration, tissue engineering (TE), and 3D bioprinting.

2.1. Chondrogenesis

During fetal development, chondrogenesis begins with the mesenchymal stem cell (MSC) condensation, followed by cell differentiation into chondrocytes, the sole cell type present in cartilage tissue [11]. Chondrocyte differentiation is regulated mainly by sex determining region Y (SRY)-box 9 (SOX9) [12,13]. There are multiple mechanisms involved in the control over the expression and activity of SOX9 that have been extensively described elsewhere [14]. SOX9, as a transcription factor, promotes *SOX5* and *SOX6* expression [15,16]. These three SOX proteins, called the SOX trio, initiate chondrogenic differentiation and are essential for the maintenance of the chondrocyte phenotype (Table 1) [16,17]. It has been demonstrated that the SOX trio provides signals that are sufficient for differentiation of MSCs into chondrocytes *in vitro* [16]. More molecular cues guiding chondrogenesis have been described in detail in other works, e.g. Wuelling & Vortkamp [18].

Table 1
Stage-specific marker genes of chondrogenesis.

	Transcription factors			Ligands	ECM proteins				
	SOX9 [15, 17]	SOX5/6 [17]	RUNX2 [19, 20]	VEGF [20]	ACAN [21, 22]	COL2α1 [17, 22]	COL11α1/2 [22]	COL10α1 [17]	MMP13 [23]
Prechondrocytic mesenchymal cells	+++	+++	+	–	+	+	+	–	–
Resting chondrocytes	+++	+++	–	–	++	++	++	–	–
Proliferating chondrocytes	+++	+++	–	–	+++	+++	+++	–	–
Prehypertrophic chondrocytes	+	+	++	+	+++	+++	+++	+	–
Hypertrophic chondrocytes	–	–	+++	+++	++	++	++	+++	+++

"+" low expression; "++" moderate expression; "+++" high expression; "-" no detectable expression.

2.2. Human articular cartilage composition, structure, and function

The SOX trio up-regulates *COL2α1, COL11α2,* and *ACAN* expression (Table 1) [16,17,24]. Products of these genes, namely collagen type II, type XI, and aggrecan, are structural proteins of the cartilaginous ECM, where collagen II is the most abundant one [25,26]. Aggrecan is an essential proteoglycan of the cartilage, that forms aggregates with hyaluronan [25]. Proteoglycans are made of a core protein covalently bond with glycosaminoglycan (GAG) chains, which are polysaccharide polymers [25]. Their main functions are to provide appropriate mechanical properties and facilitate ECM assembly [11,25]. Proteoglycans also affect signaling pathways by interacting with growth factors and its receptors [25]. In articular cartilage, the negatively-charged mesh of aggrecan and hyaluronan provides water absorption and retention properties within the tissue. As a result, articular cartilage is composed primarily of water (70–80% w/w), providing optimal mechanical properties to withstand recurrent compressive, tensile, shear, and frictional loading [11,25]. The biomechanical features of articular cartilage are zone-dependent and decrease with age or due to disease or injury [27]. Importantly, the similarity of mechanical properties between scaffolds and native, surrounding tissue is required to assert proper integration.

Mature articular cartilage displays zonal organization, differentiated by the ECM composition, collagen fiber orientation, and chondrocyte morphology [28]. According to these criteria, four zones can be distinguished: superficial (tangential), middle (transitional), deep (radial), and calcified zones (Fig. 1B). Cartilage calcification is induced by hypertrophic differentiation of chondrocytes that can be observed as an increase in cell volume and is subjected to regulation by multiple transduction pathways described in detail by Zhong et al. [11,29]. Importantly, healthy articular cartilage is able to resist hypertrophic differentiation and maintain its typical characteristics [29]. In terms of cartilage TE, it is pivotal to establish conditions that will prevent undesirable hypertrophy and the following ossification, in order to maintain the cartilage phenotype.

2.3. Lateral and medial menisci structure, composition and function

TE has been also focusing on developing novel treatment options for injuries of lateral and medial menisci, which are situated in the knee between the femoral condyle and the tibial plateau (Fig. 1A) [1]. Menisci stabilize the knee and spread loads to reduce the stress applied on articular cartilage. During fetal development, the meniscus is fully vascular; however, shortly after birth the vascularization gradually decreases. Ultimately, the mature meniscus can be divided into three
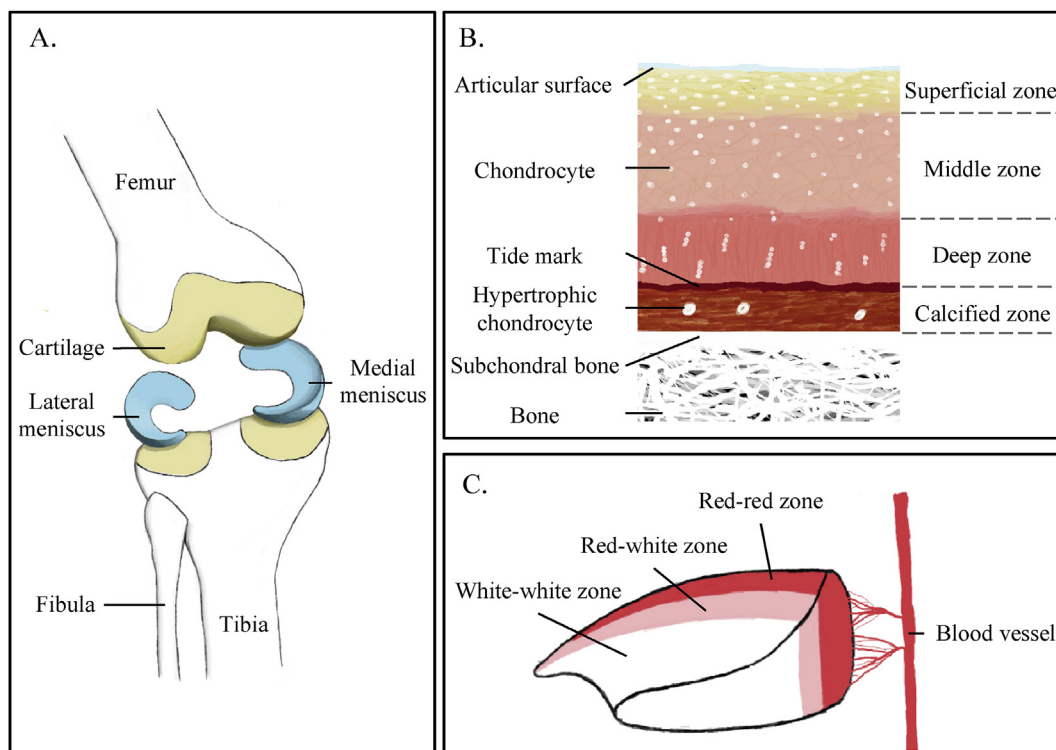

Fig. 1. Articular cartilage and menisci of the mature knee joint. **A.** Anatomy of the knee joint. **B.** The zonal organization of articular cartilage. **C.** The zonal organization of the meniscus.

regions: 1) the outer region (red-red zone), that is vascular and neural; 2) the intermediated region (red-white zone); and 3) the inner region (white-white zone), that is avascular and aneural (Fig. 1C). Meniscus zones vary in cell morphology and ECM composition. The red-red zone contains fibroblast-like cells embedded in ECM predominantly comprised of collagen type I. In contrast, the white-white zone has chondrocytes-like cells surrounded by ECM abundant in collagen II and GAGs, with less amount of collagen I in comparison to the outer region.

2.4. Motivation for cartilage tissue engineering

Due to the prevalence of articular cartilage and meniscus injuries, the importance of TE in their treatment significantly increases [11]. Cartilage injuries are usually localized at the medial femoral condyle and the patellar articular surface. They are caused mainly by mechanical stress such as impact or repetitive torsional loading [11,30]. Since the self-healing capabilities of the cartilage are fairly limited, injuries often lead to degenerative changes [11,31]. Meniscal lesions are also common injuries, especially prevalent in athletes and physically active people [1, 32]. Due to its dominant involvement in load transmission, the lateral meniscus is more prone to injuries in comparison to the medial meniscus [32]. The underlying mechanisms of meniscal tears usually involve twisting of the knee, hyperextension, torsional loading, and high compressive force [1,32]. Self-healing of the meniscal tears is directly dependent on the vascularization, therefore the avascular zone does not display regenerative properties [33]. In many cases, total or partial meniscectomy is the only available treatment option, which has poor long-term prognosis with a high risk of cartilage degeneration [34]. Therefore, the need for innovative treatment methods is urgent. 3D bioprinting is an excellent tool providing an opportunity to mimic the complex zonal structure of the meniscus and cartilage, restoring their full functionality.

3. Bone

3.1. Endochondral ossification

Bones of the appendicular skeleton (except for the clavicle) are formed by endochondral ossification, a process in which bones replace the initial cartilage [35]. This process starts in the primary (central parts of bones) or the secondary ossification centers (e.g. at the ends of long bones) and gradually expand [36]. Endochondral ossification is initiated by the slowdown of the chondrocyte proliferation, which subsequently leads to their hypertrophic transformation [35]. Chondrocyte transition is regulated by SOX9 and RUNX family transcription factor 2 (RUNX2), where RUNX2 with transcription factor Sp7, also called osterix (OSX), play a pivotal role in following endochondral ossification. Expression of *RUNX2* and *OSX* is regulated at different stages [35]. Increased expression of *SOX9* in prehypertrophic chondrocytes and its abolished expression in hypertrophic chondrocytes prove that SOX9 prevents hypertrophy in contrary to RUNX2, that is highly expressed in hypertrophic chondrocytes (Table 1) [15,29]. The change of *SOX9* and *RUNX2* expression influences the ECM synthesis, resulting in the decrease of *COL2α1* expression and initiation of collagen type X synthesis [37]. Collagen X is one of the hypotrophy markers (Table 1). Furthermore,

hypertrophic chondrocytes synthesize matrix metalloproteinase-13 (MMP13) that modulate ECM by the degradation of collagen II and aggrecan (Table 1) [38]. Hypertrophic chondrocytes ultimately undergo cell death or transform into osteoblasts or bone lining cells [10,38,39]. Osteoblasts are called the bone forming cells, while osteoclasts are responsible for cartilage matrix resorption [10]. Both cell types are requisite for bone matrix deposition. Osteoblast and osteoclast precursors are delivered to the center of the future bone in consequence of vascularization, stimulated by vascular endothelial growth factor (VEGF) (Table 2) [40]. Additionally, endothelial cells secrete growth factors controlling proliferation and differentiation of cells, including osteoblasts and osteoclasts. Therefore, the introduction of the vasculature to a construct is an essential requirement for the formation of a new bone tissue [41].

3.2. Human bone structure, composition, and function

The osteon is the basic structural unit of mineralized bone with a central canal (Haversian canal), occupied by a blood vessel [10]. The canal is encircled by lamellae, made of calcified matrix and collagen I. The canalicular system supplies metabolites and nutrients to cells, ensuring their survival during mineralization. Initial unmineralized matrix gradually transforms into mineralized bone tissue through impregnation with hydroxyapatite [47]. The mineralization is promoted by alkaline phosphatase (ALP) that catalyzes the hydrolysis of inorganic pyrophosphate into phosphate derivatives. Synthesis of ALP is a hallmark of the ECM mineralization (Table 2) [10]. Finally, maturation of the osteocytes occurs when cells are surrounded by the mineralized matrix. Osteocalcin (OCN) and osteopontin (OPN) are characteristic markers for bone mineralization and late osteoblast differentiation (Table 2) [48].

Mineralization leads to the production of hard bone tissue that, besides biomechanical functions, acts as the main metabolic storehouse for calcium and phosphorus [10]. The mechanical features of bone differ among bone tissue types and are affected by aging [48,49]. Moreover, mechanical stimuli enhance tissue formation and bone healing, although the mechanism is not fully comprehended [50]. The structural properties of native bone tissue and its response to the mechanical stimulation are crucial aspects that should be taken into account for successful implementation of TE.

3.3. Motivation for bone tissue engineering

Constant remodeling through the osteoblast and osteoclast activity is a prerequisite for proper bone healing [50]. Primary bone healing may occur only when bone fragments are tightly connected. Secondary bone healing is based on callus formation, followed by the new bone formation through intramembranous and endochondral ossifications. Nevertheless, healing mechanisms may fail leading to non-union, or become inadequate in the case of extensive bone loss caused by, e.g. tumor resection or osteomyelitis [4]. These defects engender discomfort, pain, functional disability, and may lead to pseudarthrosis. Bone lesions can be replaced by bone grafting; however, limitations of natural graft accessibility with increasing demand on bone substitutions are appreciable hurdles [51]. From that perspective, 3D bioprinting is an attractive strategy also for bone lesion treatment.

Table 2
Stage-specific marker genes of osteogenesis.

	Transcription factors		Ligands	ECM proteins			
	RUNX2 [42]	OSX [43,44]	VEGF [45]	COL1α1/2 [17,42]	ALP [23,46]	OPN [42,46]	OCN [42,46]
Preosteoblasts	+++	++	+	+	+++	+	+
Osteoblasts	+++	+++	+++	+++	++	+++	+++
Mature osteocytes	–	–	++	+	–	+	++[a]

"+" low expression; "++" moderate expression; "+++" high expression; "-" no detectable expression.
[a] Higher expression in early mature osteocytes.

4. Cells applied for cartilage and bone TE

4.1. Mesenchymal stem cells

One of commonly used cells in TE are multipotent MSCs, with self-renewal and differentiation potential [52,53]. Minimal criteria for identification of human MSCs are: 1) adherence to standard culture dishes; 2) negative or positive expression of surface antigens; and 3) multilineage differentiation capability into adipocytes, chondrocytes and osteoblasts [54].

4.1.1. MSC sources

Autologous MSCs are a preferable source of stem cells due to a lower failure rate and safety issues [55]. They can be harvested from bone marrow by invasive and painful bone marrow aspiration from the superior iliac crest, femur, or tibia [56]. Subsequently, bone marrow-derived MSCs (BMSCs) are usually isolated using density gradient centrifugation. The alternative for BMSCs are more accessible adipose-derived MSCs (ADSCs) [57]. ADSCs are frequently harvested through liposuction, which is a simple, relatively inexpensive, and low-risk procedure [58]. The infrapatellar fat pad is another source of ADSCs (IPFP-ADSCs), which are harvested intraoperatively [59–61]. For the first time, ADSCs were isolated by collagenase digestion [62]. With some modifications, it is still the most popular method while other, non-enzymatic methods, were also established [58,63–65].

4.1.2. MSC differentiation

Despite similarities in their genetic profile, BMSCs and ADSCs reveal different requirements for the induction of chondrogenesis and osteogenesis [66–68]. For example, it was demonstrated that BMSCs more easily differentiate into chondrogenic lineage than ADSCs, what favors them for cartilage TE [68]. Chondrogenic medium for MSC differentiation frequently contains transforming growth factor-β (TGF-β) and bone morphogenetic proteins (BMPs), while osteogenic medium includes, e.g. β-glycerolphosphate, dexamethasone, ascorbic acid, and BMPs [58,69]. Furthermore, to increase the cell chondrogenic potential, MSCs can be embedded into decellularized cartilage ECM [70,71].

The novel approach to stimulate chondrogenesis is a transfection of BMSCs to obtain permanently overexpression of nuclear receptor subfamily 2 group F member 2 (NR2F2) [72]. These cells were bioprinted and implanted subcutaneously into mice. The higher proteoglycan deposition was observed in constructs with transfected cells. Additionally, MSCs overexpressing NR2F2 cultured in hypoxic conditions showed improved chondrogenic differentiation and suppressed hypertrophy.

Oxygen tension is another crucial tool for manipulation of the cell fate since low oxygen level stimulates chondrogenesis and maintains articular cartilage phenotype, whereas normoxic conditions facilitate osteogenesis [10,53,73–75]. Tissues respond to changes in oxygen level trough hypoxia-inducible factors (HIFs) that are continuously expressed transcription factors [76]. HIFs are degraded by oxygen-driven hydroxylation, therefore diminishing oxygen level enhances HIFs activity. HIFs act on several signaling pathways. For instance, HIF-1α and HIF-2α positively regulate *SOX9* expression in articular cartilage [24,74,77]. Moreover, HIF-1α seems to inhibit RUNX2 [78], while HIF-2α and HIF-3α regulate expression of genes associated with terminal differentiation of chondrocytes [29,79]. Thereby, the balance between HIF-1α, HIF-2α, and HIF-3α determines the normal cartilage development [29]. Interestingly, hypoxia enhances chondrogenesis of ADSCs and suppresses the expression of osteogenic markers, even in osteogenic medium [80]. It was demonstrated that by controlling oxygen tension and mechanical properties of the construct, MSCs are able to form zonal gradient comparable to the native articular cartilage tissue [81].

MSC differentiation can be guided by bioink composition used for 3D bioprinting. It was shown that the formation of hyaline-like cartilage tissue from BMSCs is elicited by alginate hydrogel, while the formation of fibrocartilaginous tissue is enhanced by gelatin methacryloyl (GelMA)

and poly(ethylene glycol) dimethacrylate (PEGMA) [82]. Additionally, to induce BMSCs osteogenesis, bioink composed of alginate and nano-hydroxyapatite complexed with plasmid DNA was formulated and used for transfection with *BMP2* and *TGF-β3* genes [83]. Upon subcutaneous implantation in mice, enhanced osteogenesis, vascularization and mineralization of the scaffold were observed. Finally, cell-gradient patterning can be also utilized to facilitate bone and cartilage regeneration [84,85].

4.1.3. Challenges in MSC culture for the TE purpose

After the isolation, it is essential to maintain the chondrogenic and osteogenic potential of MSCs during the cell expansion. It was shown on BMSCs that *in vitro* aging can lead to genetic instability and directly affects differentiation potential [86]. Therefore, it is crucial to establish standardized protocols for culture and expansion of MSCs to create safe and effective therapies.

4.2. Chondrocytes

4.2.1. Chondrocyte sources

Autologous chondrocytes, another fine source of cells for TE purposes, are usually harvested from articular cartilage, ribs, or nasal septum and isolated by collagenase treatment [87]. Importantly, morphology and characteristics of chondrocytes isolated from articular cartilage are strictly correlated with the zone of origin [88]. In the case of *in vitro* expanded articular chondrocytes, TGF-β signaling is essential for cartilage formation, while fibroblast growth factor-2 (FGF-2) can stimulate cell proliferation [89,90]. Additionally, progenitor cells derived from human articular cartilage were also effectively used for cartilage repair [91,92].

4.2.2. Challenges in chondrocyte culture for the TE purpose

During the *in vitro* expansion, especially in low-density monolayer cultures, a commonly encountered issue is an uncontrolled dedifferentiation of chondrocytes [93]. Chondrocytes tend to change their phenotype to fibroblast-like cells and switch collagen synthesis from type II to type I [94]. The phenotypic changes can be observed in the early stages of the expansion, i.e. already after the first passage. To prevent dedifferentiation or restore chondrocytes phenotype, chondrogenic factors, especially BMP-2, can be employed [95]. Since chondrocyte dedifferentiation depends heavily on the ECM, 3D culture (e.g. in hyaluronic acid scaffold) may be an optimal solution [10,68].

Another considerable difficulty is posed by hypertrophic differentiation of chondrocytes [29,96]. Even though TGF-β prevents hypertrophy, its supplementation may not be sufficient for monolayer cultures [29]. This problem might be remediated by co-culture of mature chondrocytes with MSCs [96–98]. Co-culture of chondrocytes with ADSCs improved differentiation of stem cells and tissue forming abilities, while the addition of TGF-β1 up-regulated *COL2α1*, *ACAN*, and *COMP* expression [97]. Chondrogenic phenotype can be maintained in co-culture independently of oxygen tension [98]. In order to prevent irreversible cell mixing, stem cells can be also co-cultured with chondrocytes inactivated *via* irradiation [99]. This approach was effectively used for induced pluripotent stem cells (iPSCs) in bioprinted scaffold to support cartilage formation. Additionally, human BMSCs and chondrocytes encapsulated in 3D bioprinted silk-gelatin scaffolds have shown decreased hypertrophy as the effect of ECM remodeling, cell encapsulation and hypoxia [100]. Ultimately, articular cartilage-derived progenitor cells (ACPCs) were proposed as an alternative to overcome hypertrophic transformation [101]. ACPCs displayed lower expression of collagen X and higher expression of proteoglycan 4 (a marker of the superficial zone) in comparison to BMSCs. ACPCs and BMSCs have been successfully used for bioprinting zonal-like organized scaffolds [101]. In this study, one of the bioinks containing ACPCs was used for bioprinting of the superficial zone, while the second one, enriched with BMSCs, was used for the middle and deep zone printing.

5. Bioink composition for bone and cartilage TE

The development of bioinks for 3D bioprinting is a pivotal step as its composition and structure affect the phenotype of the developing tissue and strongly influence the cell condition and differentiation [102,103]. For instance, it was proved that the modulation of the construct stiffness can be used to direct cell differentiation [104,105]. Mechanical and physical properties (also during degradation), pore size, and architecture should match the properties of adjacent tissues [106]. Porosity is of particular importance since it contributes to the diffusion of oxygen, nutrients, and metabolic wastes. In the case of bone scaffolds, additional properties such as stimulation of the stem cell osteogenic differentiation (osteoinductivity), bone ingrowth (osteoconductivity), and vascular facilitation are required [41,49]. Biodegradation rate of bioink should be controlled and adjusted accordingly to the cells' ECM remodeling capacity, while the products of degradation cannot be toxic or immunogenic [106,107]. The entire and rapid removal of these products from the body is desired.

Hydrogels are an interesting group of biomaterials capable of absorbing and retaining large amounts of water without dissolution [108]. The ability to absorb water results from the presence of hydrophilic functional groups, while their resistance to dissolution is a consequence of a crosslinking between chains. Hydrogels can be biocompatible, biodegradable, and duly mimic natural tissue. The salient advantage of hydrogels is their permeability of oxygen, nutrients, and wastes.

This chapter focus on biomaterials that are the most promising in terms of cartilage and bone tissue engineering.

5.1. Alginate

Alginate is a natural polysaccharide produced by seaweeds or bacteria belonging to *Azotobacter* and *Pseudomonas* genera [109,110]. It is a linear and negatively charged polymer, comprised of two uronic acid monomers: β-D-mannuronic acid (M) residues and α-L-guluronic acid (G) residues, connected by 1,4-glycosidic bonds (Fig. 2) [109–112]. Uronic acid residues create blocks, namely G- or M-blocks (consecutive G or M acid residues), or MG-blocks (consist of alternating M and G residues). The proportion and the sequence of M and G monomers determine the properties of alginate and its hydrogels [109,110,113]. Alginates are biocompatible, biodegradable, non-toxic, and non-immunogenic [109]. Unfortunately, due to the negative charge, alginates lack cell and protein binding properties [112]. Thereby, it is frequently blended with positively charged biomaterials or modified to improve cell adhesion. It was demonstrated, that integrin-mediated chondrocyte attachment to alginate can be induced by RGD functionalization [114]. RGD motif is a cell binding amino acid sequence composed of arginine, glycine, and aspartate [115,116]. The attachment can be further enhanced by increasing stiffness of the RGD functionalized hydrogel, which additionally influence the chondrocyte morphology [114].

Alginate gelation can be induced by ionic crosslinking, where divalent cations form ionic bridges between G-blocks of different polymer chains [111]. These biding zones are described by the "egg-box" model (Fig. 2) [117]. The resulting hydrogel strength, stability, and mechanical properties differ according to the type of the interacting cations, the G blocks content, and variability within the polymer [110,113,118]. Alginates display a different binding affinity for different divalent cations, where the higher affinity is observed in alginates with higher G content and longer G blocks [119]. Hence, alginate gels rich in G residues are stronger but brittle, whereas these rich in M residues or GM blocks are weaker but more elastic. During 3D bioprinting, models are usually printed directly or immersed after processing in $CaCl_2$ solution [120, 121]. Calcium ions diffuse into alginate what result in rapid, poorly controlled gelation providing highly heterogeneous structure [109,122]. Crosslinker concentration and volume have been shown to affect not only mechanical features of hydrogels but also cell viability and proliferation [123]. The alginate bioink can be also partially pre-crosslinked with low concentration of $CaCl_2$ solution before printing [124]. The second
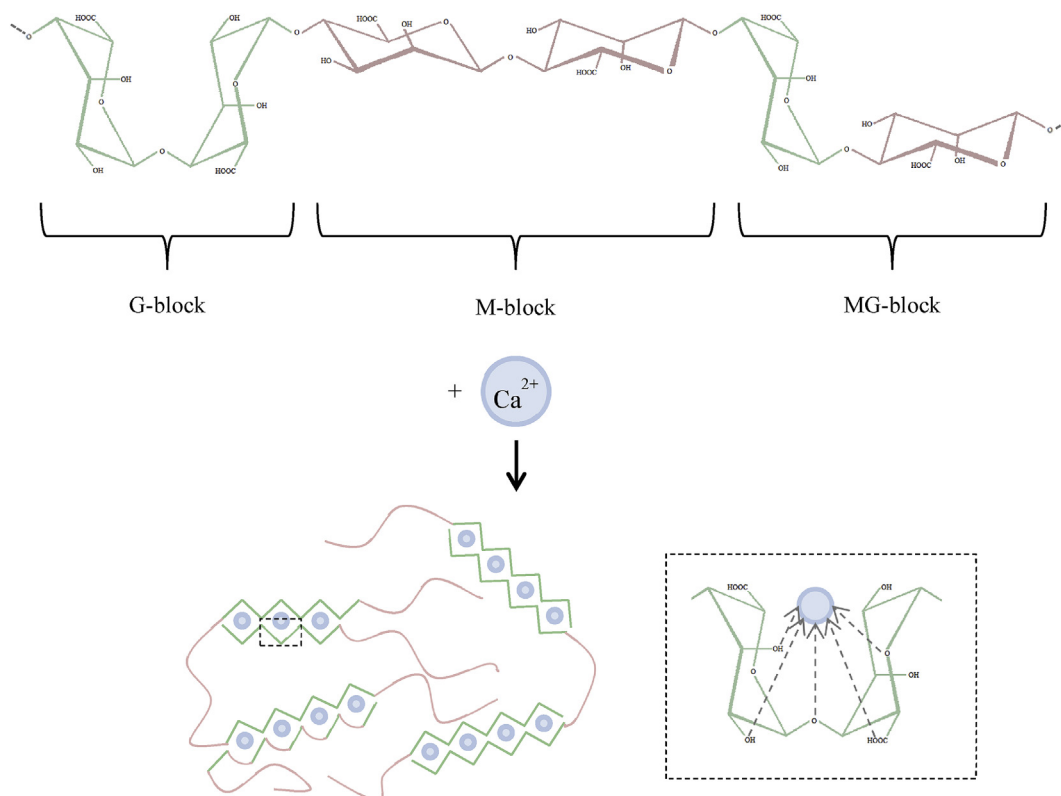

Fig. 2. The chemical structure of alginate and the "egg-box" model.

method used for alginate crosslinking is CaCO₃-GDL system [122]. Alginate solution is mixed with CaCO₃ suspension and subsequently, D-glucono-D-lactone (GDL) is added. GDL, as a slowly acting acid, lowers the pH, inducing the dissolution of CaCO₃ and dissociation of calcium ions. Slower gelation rate results in a uniform and mechanically stronger hydrogels. These two methods can be combined to obtain hydrogels injectable through a standard syringe [125].

Disintegration of alginate gels is a commonly observed event, triggered by the replacement of divalent cations by monovalent cations from the surrounding fluid [109,126]. The rate of disintegration depends on the molecular weight of the polymer [105,112]. Supplementing cell culture media with CaCl₂ decreases the degradation rate of alginate gels in long-term culture [127,128]. Moreover, an additional crosslinking with BaCl₂ enhances the stability of the gel [129]. Another approach to improve hydrogel stability utilizes the incorporation of orthosilicic acid, where stability is presumably achieved by interactions between the acid and Ca²⁺ [130]. Importantly, a human body is incapable of alginate degradation due to the lack of specific enzymes [131]. A study designed to monitor the faith of alginate in the body revealed that only the polymers with low molecular weight (below renal threshold, i.e. ≤48,000) can be excreted by the urinary system [132]. Molecular weights of commercially available alginates are higher than this threshold; therefore alginate is not entirely removed from the body. Remaining alginate was present mostly in blood and liver. To overcome this problem, alginate degradation can be enhanced by chemical modifications, e.g. oxidation of alginate chains [109,133].

Alginate is produced solely from brown seaweeds, commercially available as sodium or potassium salts, and is relatively cheap [119]. Depending on the genus, growth conditions, and age of the algae, the polysaccharide chain composition varies. Since alginate is obtained from natural sources, only highly purified alginates should be employed for TE [109]. Alginate is approved by the U.S. Food and Drug Administration (FDA) as a food ingredient [119].

5.2. Chitosan

Chitin is a natural polymer present in the exoskeleton of insects and crustaceans that ensures structural integrity and protection. It is also present in the cell wall of fungi and algae [134–136]. Chitin is composed of repeating N-acetyl-D-glucosamine residues linked by β-1,4-glycosidic bonds (Fig. 3) and can be found in three polymorphic forms: α, β, and γ; stemming from different organization and polarity of the chains. Due to its insolubility in water and most of the organic solvents, its usage in TE is limited. Chitosan is a deacetylated derivative of chitin (Fig. 3), soluble in aqueous acidic solutions and partially soluble in neutral pH. Chitosan

consists of N-acetyl-D-glucosamine and deacetylated D-glucosamine units. The ratio between those two constituents determines the degree of deacetylation. The degree of deacetylation and the molecular weight are determined by the source of initial polysaccharide and processing conditions. Physicochemical properties of chitosan are determined by these two factors [134]. For example, higher degree of deacetylation renders the material more flexible [137]. Chitosan, like other hydrogels, is biocompatible, biodegradable, and has low toxicity [134,136]. It is a positively charged copolymer with antimicrobial properties, that exhibits significant osteoconductivity but low osteoinductivity [135]. Ye et al. have demonstrated that IPFP-ADSCs seeded on the top of the 3D printed chitosan scaffold and cultured in chondrogenic media for 4 weeks, underwent chondrogenesis and formed a "cap" of tissue with chondrocytic morphology [60]. These results indicate that 3D printed chitosan hydrogels may also facilitate cell aggregation. However, chitosan shares a common drawback characteristic for the majority of hydrogels, which is a low mechanical resistance. Therefore, it is usually blended with other materials in order to improve mechanical properties.

Various physical and chemical methods can be applied for chitosan crosslinking. For example, 3D bioprintable chitosan hydrogels can be prepared by thermal polymerization [138]. Chitosan solution alkalized with glycerol phosphate disodium salt provides a printable bioink with gelling properties induced at 37 °C. *In vivo* studies revealed that the degradation rate of chitosan is proportional to the degree of deacetylation [139]. In a human body, chitosan is enzymatically degraded by lysozyme and N-acetyl-β-D-glucosaminidase [131,139].

Large scale production of chitin is based on crustaceans waste generated by the fishing industry, mainly shells of shrimp, crab, lobster, prawn, and krill [140]. Chitin deacetylation is performed *via* hydrolysis of acetamide groups at high temperature in alkaline conditions. Interestingly, chitosan-based bandage HemCon® has been approved by the FDA for clinical applications.

5.3. Collagen and its derivatives

Collagens are ubiquitous ECM proteins that are a right-handed helix comprised of three left-handed α-chains [115,141,142]. Depending on the type of collagen and source, homo- and heterotrimers can be formed. Collagens are composed of repeating amino acids sequence [Gly–X–Y]n, where X and Y are frequently occupied by proline and hydroxyproline, respectively, which stiffen the α-chains. Therefore, the superhelical structure is largely stabilized by hydrogen bonds between glycines, but also by the conformational restrictions and hydrogen bonds between hydroxyl groups of hydroxyproline. The ends of triple helixes contain non-helical regions, called telopeptides, that contribute to collagen
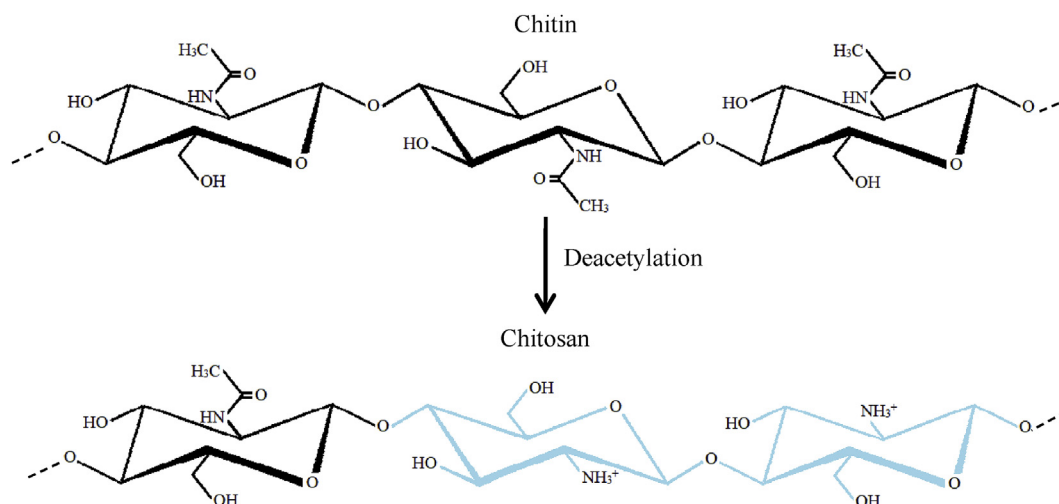

Fig. 3. The synthesis of chitosan by chitin deacetylation.

supramolecular assembly and hamper enzymatic degradation [141,143]. The lack of telopeptide regions alerts the collagen assembly pathway and prolongs the polymerization time [143]. This effect is associated with fiber nucleation, which is one of the network assembly steps. Collagen is a biocompatible and biodegradable polymer with low immunogenicity. It contains the cell binding RGD motif [144]. Collagen turnover is facilitated by the cells attached to its fibrils, which are responsible for both metalloproteinase-induced degradation and new ECM production [145]. Collagen thermal gelation has been successfully used in 3D bioprinting [146]. Although polymerization at 37 °C is usually used to facilitate cell viability, the utilization of lower temperatures (even down to 4 °C) has also been demonstrated [147].

The most commonly used collagen is collagen type I, isolated from rats, cattle, and pigs [141,147]. However, it was also demonstrated that pure collagen II scaffolds were able to induce and maintain MSC chondrogenesis [148]. It is noteworthy that collagens display source-dependent differences in, e.g. pore size within the formed scaffolds [147,149]. In the view of immunogenicity, religious aspects, and the risk of an animal disease transmission, human collagen is the most favorable one for TE applications [115]. Alternatively, human-like collagen can be synthesized by the means of recombinant genetic engineering.

Collagen denaturation caused by thermal treatment or hydrolysis results in a gelatin formation [150]. The gelatin composition and properties are similar to collagen, albeit the structure is non-homogenous and depends on the parameters of the denaturation process. Moreover, gelatin has better water solubility than collagen. Reversible thermal gelation at low temperatures or crosslinking by genipin, a chemical crosslinker, is used during 3D bioprinting [127,145,151]. Furthermore, gelatin methacryloyl (GelMA), a gelatin derivative with lysine and hydroxyl residues modified with methacrylamide and methacrylate groups, is photocrosslinkable under UV light with the assistance of a photoinitiator [152]. Under optimal bioprinting conditions, GelMA bioink is printable and cytocompatible with chondrocytes [153]. Bioink and bioprinting parameters, such as the degree of substitution, concentration, photoinitiator concentration, and UV exposure time, determine properties of GelMA based hydrogels and can be used to control the fate of encapsulated cells [152,154,155]. Gelatin is degraded by MMP-2, what was observed in bioprinted scaffolds laden with human MSCs [100].

5.4. Hyaluronic acid

Hyaluronic acid (HA), also called hyaluronan, is a ubiquitous glycosaminoglycan widely present in the ECM [156,157]. HA is produced by hyaluronan synthases localized on the inner face of plasma membrane and consists of repeating disaccharide units connected by β-1, 4-glycosidic bonds. Each unit is composed of N-acetyl-D-glucosamine and D-glucuronic acid linked by β-1,3-glycosidic bonds (Fig. 4). The balance of HA synthesis and degradation, together with the molecular weight of

HA, determines biological functions of the polymer [156]. For example, high molecular weight HA is anti-angiogenic and has beneficial effects on tissue repair, while low molecular weight HA displays pro-angiogenic and pro-inflammatory activity. HA is a biocompatible polymer interacting with cell surface receptors, capable of integration with the native bone tissue [156,158].

The addition of HA into a bioink promotes bone healing, MSC proliferation, and differentiation towards osteogenic lineage in 3D bioprinted scaffolds [159,160]. HA in its native form is brittle, degrades rapidly, and is not suitable for bioprinting. Hence, it is either blended with other biomaterials or modified [156–158,161]. For example, high molecular weight HA modified with methacrylate groups, similarly to GelMA, is compatible for 3D printing [162]. Methacrylated HA (MeHA) hydrogels are photopolymerizable and more resistant to degradation. BMSCs were shown to spontaneously differentiate towards osteogenic lineage in MeHA-based hydrogel, without any additional stimuli [162].

Currently, commercially available HA is extracted from animal tissues or produced by genetically modified bacteria [156,163]. Due to harsh extraction conditions, the risk of biological contamination, and costs, bacterial production of HA is recommended.

5.5. Synthetic materials

Synthetic materials are a frequent addition to bioinks, responsible for modulating their mechanical properties, crosslinking or printability [164]. Ones of the frequently used synthetic biomaterials are poloxamers (under trade name Pluronic), polycaprolactone (PCL) and polyethylene glycol (PEG). Poloxamers can be used as sacrificial bioink, due to their thermoreversible gelation [165]. Pluronic is liquid at <4 °C and forms gel at >16 °C. This material is not appropriate for long-term applications [126]. PCL is a hard, hydrophobic thermoplastic material that is used to increase mechanical properties and as a support [166]. This polymer easily blends with other materials. Interestingly, PCL improve chondrogenesis, what was demonstrated on IPFP-ADSC seeded scaffolds [167]. PEG success in TE application stems from the easiness of modification that can be utilized for fine-tuning of the materials properties, according to scaffold requirements [107,112]. For example, photocrosslinkable PEG dimethacrylate (PEGDA) can be obtained with methacrylate modification [107]. PEG was shown to improve the mechanical properties of bioprinted scaffolds for bone and cartilage TE [168].

5.6. Carbon nanotubes

An increasing interest is observed in the usage of nanomaterials in biomedicine, e.g. in bioimaging, drug delivery, or targeted therapy [169–171]. In the case of cartilage and bone TE, carbon nanotubes (CNTs) emerge as a promising nanomaterial [52,172,173]. In the preliminary studies, the incorporation of CNTs into scaffolds resulted in increased mechanical strength and stimulation of osteogenic and
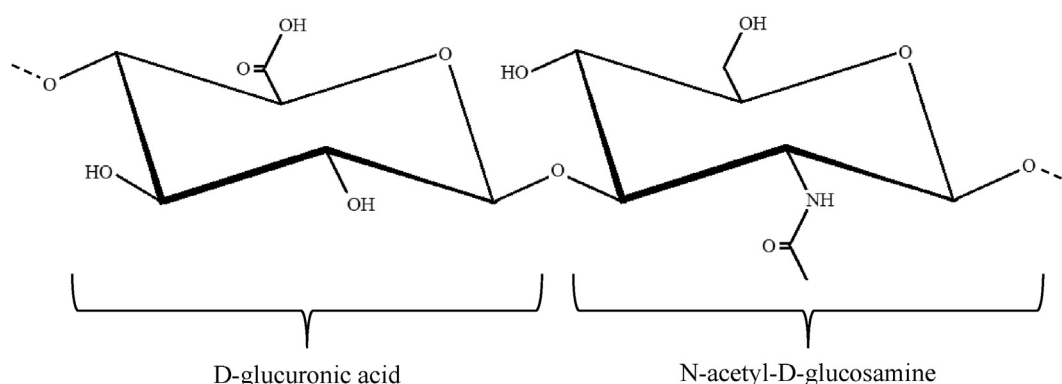

D-glucuronic acid   N-acetyl-D-glucosamine

Fig. 4. The structure of hyaluronic acid.

chondrogenic differentiation [52,173–175]. Nevertheless, careful approach should be undertaken regarding nanomaterials, as nanotoxicity is still largely unexplored territory [176–178].

6. 3D modeling and bioprinting techniques applied for cartilage and bone TE

3D bioprinting is a promising technique capable of fulfilling the unmet necessity for bone and cartilage scaffolds. It allows for easy production of tailored products with a significant architectural control [49].

It is essential to underline that the printing process itself affects cell biology what was demonstrated on the chondrogenic differentiation potential [185]. Shear forces exerted on cells during the transfer through the nozzle may elicit phenotypic expressions [11,53,186]. This effect is known as mechanotransduction.

6.1. 3D modeling

Computer-aided design (CAD) is a crucial component of 3D bioprinting workflow, determining structural properties of a model [179–181]. Anatomical conformity plays an indispensable role in proper integration of a scaffold, with surrounding tissues. Additionally, the introduction of designed lattices may be utilized to alter mechanical properties on a macroscopic level, while decreasing material consumption and increasing surface-to-volume ratio, providing more space for cell attachment and proliferation. CAD software spans from easy-to-use, beginner level (e.g. TinkerCAD, FreeCAD, BlocksCAD) through more advanced (e.g. Fusion360°), to professional level (e.g. AutoCAD, Solidworks, Catia, Rhino) [179]. Additional software can be employed for more specific purposes such as stress simulation, topology optimization, and generation of lattice structures (e.g. nTopology, Inventor Nastran). CAD models can be built from scratch, or generated *via* software dedicated to optimization and translation from .DICOM files [182]. Digital Imaging and Communications in Medicine (DICOM) is the standard for the communication and management of medical imaging information and related data [179]. This approach allows for creation of anatomically personalized implants and scaffolds. Examples of this software include D2P DICOM-to-PRINT, Materialise Mimics and open-source, 3DSlicer. 3D scanning is another promising technology that can be massively adopted for 3D printing of personalized ortheses, splints, and prostheses [183]. Obtained models can be saved and stored in various formats, however the most common file type recognized by various 3D printers is Standard Tesselation Language (.STL) [184]. Prior to printing , STL model needs to be converted by slicing software, which divides the object into a stack of flat layers. Each layer is then described as a linear movement of a printhead, laser path, or equivalent. During slicing, additional, printer-specific parameters can be introduced (e.g. infill density, layer height, printhead and print bed temp., printing speed). All this information is then saved in a format directly utilized by a printer, usually .GCODE.

6.2. Inkjet bioprinting

Inkjet bioprinting extrudes bioink out of a printing cartridge as a result of pressure generated in the printhead, fluid mechanics, and gravity [187]. According to the nature of the flow through the nozzle, droplets are formed in a continuous inkjet or drop-on-demand mode. The drop-on-demand printers achieve much higher resolution than continuous inkjet and are usually used for biological applications. The most popular methods to generate drop-on-demand printing mode utilize thermal or piezoelectric effects (Fig. 5) [187,188]. For thermal printing, a small part within the printhead is rapidly heated to nearly 300 °C what generates vapor bubbles within the bioink [188]. Created bubbles coalesce and expand, generating a pressure pulse. At the final stage, bubbles shrink and then collapse. Due to the short period of exposure to high temperature, this method has a negligible harmful impact on the
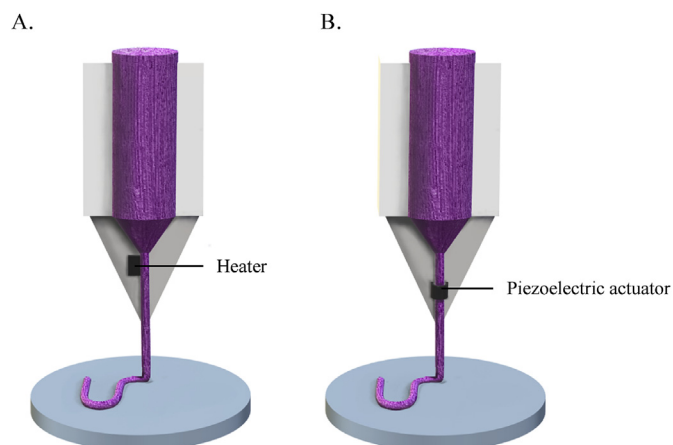

Fig. 5. Inkjet bioprinting. **A.** Thermal inkjet printer. **B.** Piezoelectric inkjet printer.

encapsulated cell viability [189]. The advantages of thermal inkjet printing are low costs and high printing speed [187]. However, the clogging of the nozzle is a frequently encountered issue. In piezoelectric printheads, piezoelectric actuator converts the applied voltage into a mechanical deformation of a crystal, which produces an acoustic wave generating pressure required for the drop ejection [187,188].

To form droplets, a bioink must be liquid inside the cartridge and quickly crosslink after extrusion [5]. Consequently, various platforms for inkjet bioprinting were established, including shear-thinning bioinks [112]. The thermal inkjet 3D bioprinter with simultaneous photopolymerization was used for precise positioning of encapsulated human chondrocytes during layer-by-layer deposition [190,191]. Whereas, the piezoelectric bioprinter was combined with $CaCl_2$ nebulizer to create alginate-based scaffolds [192]. $CaCl_2$ at low concentrations was sprayed over printed constructed and washed out immediately after gelation. Inkjet bioprinting can be also combined with electrospinning, which is a technique used for printing synthetic scaffolds [193]. This system utilizes electrostatic charge to pull fiber from the batch of a synthetic polymer (e.g. PCL) and therefore is not compatible with cell printing. However, the obtained material can be successfully used for TE purposes.

6.3. Extrusion bioprinting

Extrusion bioprinting, also called a direct writing system, is a technology able to print continuously [194]. Pneumatic pressure or mechanical pistons are applied for extrusion-based deposition (Fig. 6A). The constant applied force enables bioprinting of highly viscous bioinks. This method is compatible with high cell densities, albeit the mechanical
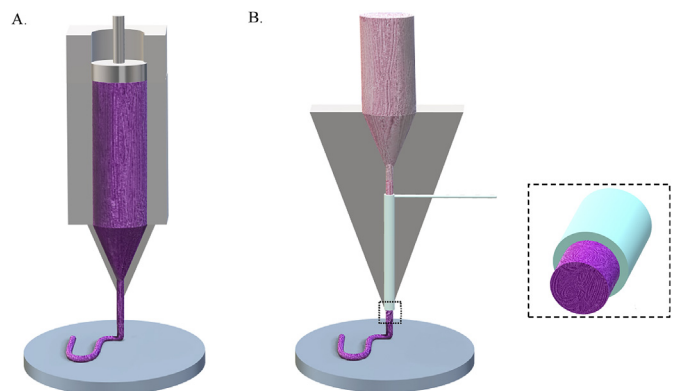

Fig. 6. A. Extrusion bioprinting. **B.** Extrusion bioprinting with a coaxial printhead.

stresses may reduce cell viability [7,184].

The co-axial printheads are used in extrusion printers for simultaneous delivery of the bioink through the core flow and the crosslinker trough the sheath flow (Fig. 6B) [195]. This construction is frequently applied for printing alginate-based bioinks forming the core and $CaCl_2$ solution used as the sheath [196,197]. Nevertheless, this system is also applicable for printing different types of bioinks [124,198]. An interesting strategy is a handheld, 3D core/shell bioprinting device, called Biopen, dedicated for *in situ* 3D bioprinting for cartilage tissue repair [199–201]. More complex bioprinting of multi-layered constructs for cartilage and osteochondral tissue regeneration can be performed with the multihead deposition system (MHDS) [202] and multi-head tissue/organ building system (MtoBS) [203,204]. MHDS is equipped with four heads that utilize pneumatic pressure for dispensing [202], while MtoBS has several printheads that can use pneumatic pressure, plunger system, and individual heating systems to dispense different types of biomaterials [203,204]. The bioprinting of high melting point thermoplastic constructs is possible with the volume-by-volume (VbV) process [205]. The thermoplastic polymer is extruded first and then, bioink fills the printed scaffold. In this way, high temperature does not affect cell viability. VbV process was applied for printing poly lactic acid (PLA) scaffold where the spaces were filled with chondrocytes encapsulated in alginate.

6.4. Laser-assisted bioprinting

Laser-assisted bioprinting (LAB) is a nozzle-free, noncontact technique, where the laser is pulsed on a ribbon composed of three layers: laser-transparent layer, laser-absorbing layer, and bioink layer [206]. The laser beam energy is absorbed by the ribbon what generates a local bubble on the opposite side (Fig. 7). Rapid formation of the bubble ejects a desired amount of bioink on a receiving stage. LAB is applicable for high cell densities and high viscosity inks. The main three, laser-based techniques are: 1) laser-induced forward transfer (LIFT); 2) absorbing film-assisted laser-induced forward transfer (AFA-LIFT); and 3) matrix-assisted pulsed laser evaporation direct writing (MAPLE-DW). LIFT was successfully applied for *in situ* bioprinting of BMSCs on a bone defect in mice [207].

6.5. Stereolithography and digital light projection

Stereolithography (SLA) and digital light projection (DLP) are nozzle-free techniques that create 3D objects through layer-by-layer photo-polymerization. In SLA, liquid resin is solidified by UV laser beam [7, 208], while in DLP, visible light is projected in the shape of the layer (Fig. 8) [7,208]. Final structures made of SLA or DLP are drained and washed. Scaffolds are often subjected to post-curing, in order to improve their mechanical properties. These methods utilize photosensitive polymers or bioinks, usually requiring photoinitiators [7]. Alternatively, if photoinitiators are undesirable, polymers with polymerization based on a
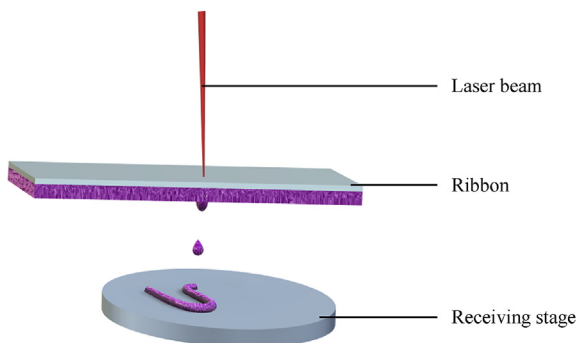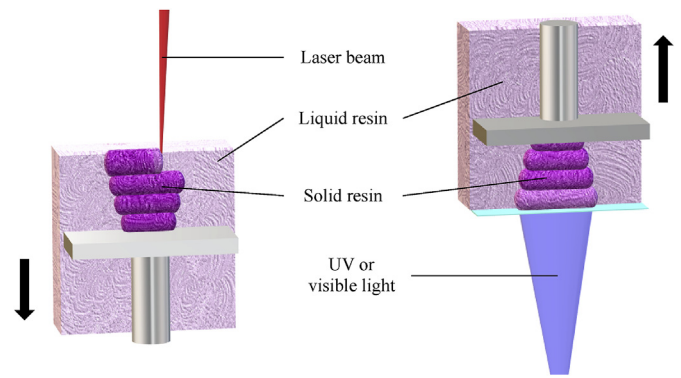
Fig. 8. Stereolithography approaches. Left: a bottom-up approach with laser beam. Right: a top-down approach with light projection.

thiol-ene reaction can be applied. SLA and DLP can be performed in two ways, i.e. bottom-up and top-down approach (Fig. 8). In bottom-up fabrication, a layer of resin is cured by the light from above and the structure is built on a support platform. While in the top-down approach, the source of the light is localized beneath the transparent plate.

SLA was proposed for bioprinting of methacrylated poly-D,L-lactica-cid/polyethyleneglycol/poly-D,L-lactic acid (PDLLA-PEG)–HA bioink with human ADSCs for cartilage TE [209]. The cells maintained high viability and retained the potential to differentiate into chondrocytes. GelMA and MeHA bioinks were also used in SLA bioprinting to create constructs with variable cell densities [210]. Both bioinks maintained the phenotype of chondrocytes and sustained cartilage-specific ECM formation.

7. Application of 3D bioprinting for bone and cartilage TE

7.1. The templating strategy

For alginate-based bioinks, the templating strategy can be applied where alginate serves only as a temporary support (Table 3) [197]. During bioprinting, alginate is immediately crosslinked with $CaCl_2$ solution, which can be co-extruded through outer sheath flow. Once a secondary crosslinking of other bio-macromolecular components is finished, alginate is gradually dissociated through incubation of the construct in a solution containing monovalent ions. This process can be accelerated by the addition of a chelating agent targeting divalent cations, such as ethylenediaminetetraacetic acid (EDTA). This method was established for extrusion bioprinting of gelatin scaffolds in which genipin was used to induce secondary crosslinking. The resultant gel is composed mostly of gelatin and the viability of encapsulated human MSCs is high (>90%). Dual-stage gelation can be applied also for the GelMA-alginate bioinks, where alginate crosslinking is followed by UV light crosslinking. Subsequently, the gradual removal of the alginate enlarges microfiber pores of the hydrogel, which may support cell growth. This bioink laden with human umbilical vein endothelial cells (HUVECs) was proposed for the formation of vascularized constructs by microfluidic bioprinting [195]. Endothelial cells form lumen-like structures that act as a vascular bed, which can be subsequently seeded with secondary cell type, like cardiomyocytes, to form vascularized tissue. Dual-stage gelation was applied as well for collagen I-alginate bioink [197]. The printing is followed by incubation at 37 °C to induce collagen crosslinking. Subsequently, supportive alginate is washed out leaving the scaffold composed of collagen I. This bioink effectively maintained the phenotype of chondrocytes what was observed by abundant expression of cartilage marker genes and GAGs synthesis [120]. Moreover, the bioink suppressed dedifferentiation of chondrocytes and exhibited favorable mechanical properties, suitable for cartilage TE. Alginate-templated bioprinting was also used for the formation of scaffolds composed of GelMA and chondroitin sulfate amino ethyl methacrylate (CS-AEMA) for

Fig. 7. Laser-assisted bioprinting.

Table 3
The examples of the templating strategy.

Ref.	Supporting material	Crosslinking of supporting material	Bio-macromolecule	Crosslinking of biomacromolecule	Removal of supporting material
[197]	Alginate	Physical crosslinking by co-delivered $CaCl_2$ solution	GelMA	Photo-crosslinking by UV light	Incubation in a culture medium
			Gelatin	Chemical crossliniking by genipin	Incubation in a culture medium
			Collagen I	Physical crosslinking at 37 °C	Incubation in a culture medium
[128]	Pluronic F127	Sol–gel transition onto heated stage set to 37 °C	Alginate	Physical crosslinking by incubation in $CaCl_2$ solution	Washing at RT

cartilage TE [211]. In the scaffold, BMSC expression of collagen I and collagen X genes was limited, while the expression of collagen II gene was enhanced in chondrogenic medium. Interestingly, the incorporation of MeHA resulted in hypertrophic differentiation of BMSCs as the effect of excessive crosslinking.

The pluronic-alginate bioink was developed for cartilage and bone tissue bioprinting, where the Pluronic F-127 serves as a template [128]. The bioink extrusion on a heated plate set to 37 °C induces the sol-gel transition of the Pluronic. Subsequently, the alginate gelation is induced by immersion in $CaCl_2$ solution. In this procedure, Pluronic was finally dissolved and washed-out at room temperature leaving homogenously distributed channels. The scaffold possessed desired mechanical properties and BMSCs showed high cell viability (83%) after encapsulation. The differentiation of BMSCs into osteoblasts and chondrocytes was elicited with differentiation media.

7.2. Addition of cellulose for cartilage scaffolds

Nanofibrillated cellulose is an interesting biomaterial for bioprinting of cartilage constructs. Nanofibrillated cellulose-alginate bioink in combination with electromagnetic inkjet technology was used to bioprint human chondrocytes [212]. The mechanical support was provided by nanocellulose, while the gelation was based on alginate crosslinking. It was demonstrated that nanocellulose-alginate scaffolds are more suitable for iPSCs to support cartilage formation than nanocellulose-HA scaffolds [99]. Moreover, nanofibrillated cellulose-alginate scaffolds laden with human chondrocytes, human BMSCs, or co-cultures of both cell types were tested *in vivo* in a murine model [213,214]. The most abundant synthesis of GAGs, representing cartilage formation, was observed in constructs with chondrocytes or co-cultures of chondrocytes and BMSCs. BMSCs enhanced chondrocyte proliferation and biomaterials revealed proper integration with native tissues *in vivo*.

7.3. Addition of tricalcium phosphate (TCP) for calcified tissues scaffolds

Tricalcium phosphate (TCP) is a promising material for bone and calcified cartilage TE. TCP exists in two different forms: α-tricalcium phosphate (α-TCP) and β-tricalcium phosphate (β-TCP) [215]. Scaffolds made of α-TCP–collage I laden with preosteoblasts MC3T3-E1 were shown to effectively support osteogenic differentiation [216]. The construct was printed alternately with α-TCP–collagen I ink and collage I laden with cells. Cementation of α-TCP to calcium-deficient hydroxyapatite (CDHA) was induced by hydrolysis in culture medium. Another interesting process was established to bioprint core/shell-structured scaffolds made of CDHA and alginate [124]. The α-TCP as the core provided stiffness, while alginate blended with preosteoblast MC3T3-E1 cells as the shell contributed to elasticity. Once the bioprinting was finished, the construct was crosslinked in $CaCl_2$ solution, followed by cementation in PBS and then in culture medium. Encapsulated cells survived bioprinting and maintained their viability for 35 days of culture. For calcified cartilage tissue, bioink comprised of alginate-GelMA mixed with ceramic β-TCP microparticles was developed [196]. This bioink was extruded co-axially with $CaCl_2$ sheath flow in order to induce alginate

polymerization. Subsequently, UV light induced GelMA gelation was performed. The analysis of gene expression revealed the enhanced synthesis of cartilage ECM and overexpression of ALP, indicating the potential of BMSC to form calcified cartilage tissue.

7.4. Addition of HA for bone scaffolds

Gelatin-alginate bioinks are commonly used for TE, where gelatin contributes to cell attachment and alginate ensures stability [127,217, 218]. For this bioink, the two-step gelation may be applied [127,217]. The hydrogel is firstly heated and bioprinted on a cold plate to induce reversible thermal gelation of gelatin and then crosslinked in $CaCl_2$. The bioink is compatible with MG-63 osteoblast-like cells and cell attachment was confirmed by the actin cytoskeleton staining [219]. For bone TE, the additional inclusion of HA to gelatin-alginate hydrogel enhance hydrogel mechanical strength, viscoelastic properties, and matrix mineralization [127]. Interestingly, MC3T3-E1 preosteoblasts encapsulated in chitosan-HA hydrogels showed higher cell viability, proliferation, and osteogenic differentiation in comparison to alginate constructs [138]. These results reveal osteoconductive nature of chitosan-HA hydrogels and favor the use of this bioink for bone TE applications.

For the bioprinting of bone substitutions, a new approach, based on a two-channel bioink system, was proposed [220]. One channel carried bioink A, a prehydrogel solution of PEG-Clay, and the other channel was filled with bioink B, composed of HA used as a primary rat osteoblast carrier. The first layer of the construct was made of bioink A, whereas the consecutive layers were printed alternately with bioink A and bioink B. PEG-Clay scaffolds promoted osteogenic differentiation by a gradual release of Mg^{2+} and Si^{4+} ions, while HA protected cells during UV crosslinking and facilitated the release of encapsulated cells after bioprinting. This construct had excellent osteogenic properties *in vitro* and stimulated new bone formation *in vivo*. The alginate-polyvinyl alcohol (PVA)-HA bioink was another bioink formulated for the regeneration of bone defects [221,222]. The addition of PVA-HA suspension increased the viscosity and improved viability of murine calvaria 3T3-E1 cells after bioprinting [222]. However, collagen incorporation was required to promote cell attachment and to provide an appropriate mechanical rigidity, crucial for cell migration [221]. Although HA is frequently applied for building bone constructs, this biomaterial is also used for cartilage bioprinting. For example, MeHA addition to PEG-based bioink improved thermo-sensitive profile and degradation time of bioprinted constructs for cartilage regeneration [223].

7.5. Vascularized scaffolds for bone TE

As it was mentioned above, the reconstruction of large bone deficits requires the incorporation of a vascular network [40]. To address this challenge, GelMA hydrogels laden with blood-derived HUVECs and human BMSCs were made [224,225]. The construct can be dually 3D bioprinted by alternate deposition of PLA and GelMA layers [225]. BMP2 and VEGF have been successfully incorporated into this construct to induce angiogenesis and osteogenesis. In another study, BMP2 was also effectively bound to GelMA and controllably released from BMSCs-laden

bioprinted constructs [226]. The incorporation of BMP2 was shown to induce MSC differentiation into osteocytes with higher efficacy in comparison to osteogenic medium. Alternatively, vascularized scaffolds can be obtained by printing a central, vessel-like structure with soft GelMA that quickly degrades leaving an open lumen [224]. GelMA was conjugated with VEGF at different ratios and used to print a gradient of HUVECs embedded in hydrogel. An enhanced capillary formation was observed and improved upon by the co-culture of HUVECs and MSCs. The incorporation of osteoinductive silicate nanoplatelets (dissociating into Na^+, Mg^{2+}, $Si(OH)_4$, and Li^+ in aqueous solution) together with VEGF enhanced osteogenic differentiation of MSCs. Fibrin-based bioink encapsulating either MSCs or HUVECs was likewise applied for bioprinting of constructs with improved neovascularization [227]. In this example, mechanical strength of the construct was reinforced with PCL scaffold. Two bioinks were used to bioprint osteon-like patterns that hold the potential to develop vascularized scaffold and stimulate osteogenic differentiation of MSCs *in vivo*.

The problem of vascular network formation can be overcome by bioprinting a template for *in vivo* neovascularization [228]. For the whole bone engineering, RGD-functionalized alginate hydrogel laden with BMSCs and reinforced with PCL scaffold was used. This bone precursor was chondrogenically primed and implanted subcutaneously into mice. After twelve weeks, the construct was extensively vascularized and mineralized with detectable bone marrow like tissue. These results lead to the conclusion that the bioprinted scaffold is able to stimulate endochondral ossification *in vivo*.

7.6. 3D biopaper

The bioink can be deposited into a receiving sheet, called biopaper, that supports a tissue formation. Collagen type I frequently serve as a biopaper [126,207]. For cartilage repair, osteochondral plugs were used as the 3D biopaper for bioprinting with photopolymerizable PEGMA and human chondrocytes [190]. The cells maintained chondrogenic phenotype within the scaffold, which integrated with native cartilage and bone tissues. The native cartilage has a positive effect on chondrogenesis and improves ECM deposition. Besides, an enhanced proteoglycan production at the interface between the scaffold and the host cartilage demonstrated the importance of the remaining native cartilage in promoting neocartilage formation.

7.7. Multilayered 3D scaffolds

The more complex multilayer scaffolds were created for the reconstruction of osteochondral defects. For instance, the 3D fiber deposition technique was applied for building the tissue-like structure with BMSCs or chondrocytes encapsulated in alginate [229]. BMSCs were additionally blended with HA and β-TCP. *In vivo* study showed that the scaffolds sustained not only cell phenotype but also stable cellular organization. However, the hydrogel displayed insufficient mechanical strength and cells were unable to adhere or degrade the alginate, indicating that the bioink composition should be reconsidered. Alternatively, a multilayer construct with two different ECM-derived materials was built with the use of four printheads and applied for reconstruction of osteochondral defects in the rabbit knee joint. First, a PCL framework was formed and then, the voids were filled with the bioink [203,204]. The bottom layer of the construct (atelocollagen with BMP2) constituted a subchondral bone and the top layer (cucurbit [6]uril(CB [6])-conjugated HA with TGF-β) constituted superficial cartilage [204]. Both layers were laden with human turbinate-derived MSCs. 1,6-diaminohexane(DAH)-conjugated HA was dispensed on the top layer to self-assemble CB [6]/DAH-HA hydrogel. *In vivo* constructs revealed an excellent ability for the osteochondral regeneration in comparison to PCL constructs seeded with MSCs and PCL constructs filled with alginate hydrogel encapsulating MSCs, enriched with growth factors. The zonal organization characteristic of native cartilage was observed. Moreover, the PCL fibers were

shown to interact with newly formed bone within the bottom layer of the scaffolds. In similar studies, the construct composed of alternating layers of PCL and chondrocytes encapsulated in collagen I-fibrin gel maintained cell phenotype and synthesis of cartilage ECM [193].

In order to mimic the native organization of the meniscus, the regionally defined construct was bioprinted with alginate-based hydrogel functionalized with decellularized ECM, isolated from the inner or the outer region of the meniscus [230]. The bioink was combined with IPFP-ADSC. In the absence of exogenous growth factors, inner meniscus ECM supported the development of chondrogenic phenotype, while outer meniscus ECM supported the fibrogenic phenotype. The addition of TGF-β3 to inner meniscal ECM enhanced chondrogenic phenotype, whereas the connective tissue growth factor (CTGF) supplementation in outer meniscal ECM supported fibrogenic phenotype. To obtain mechanical properties similar to the native meniscal tissue, the structure was reinforced with PCL. The viability of stem cells was not affected by the bioprinting process.

8. Perspectives for future development

Currently, the organ regeneration *via* bioprinting is fairly limited in clinical adoption [49,231]. Despite many promising results from *in vitro* and *in vivo* studies, the gap between 3D bioprinting research and clinical use is still present [49]. Further development is highly dependent on the progress in the biomaterials science, without which, large-scale adoption of the 3D bioprinting will not be possible [232]. Finding a balance between optimal environment for cell growth and mechanical properties congruent with native tissue remains a challenge [6]. In addition, the establishment of cell expansion protocols for 3D bioprinting is a considerable hurdle. Another widely discussed topic involves introduction of the functional vasculature [195,225,232–234]. Despite several advancements in this filed, fully vascularized tissue constructs have not yet been obtained. Nonetheless, there are several breakthrough examples of successful organ-bioprinting, highlighting the tremendous potential of this technology (Table 4).

9. Summary

In this review, recent studies of 3D bioprinting applications for bone and cartilage repair are discussed. The extensive research conducted in this field indicates high expectations for 3D bioprinting success. Currently, the community of 3D bioprinting researchers is faced with the development of the fabrication processes that include standardization of optimal cell culture protocols, bioink formulation, and adjusting 3D bioprinting parameters. Potential risks involved with the clinical application of 3D bioprinted constructs need to be thoroughly investigated and legal ramifications specifying a permitted biomedical use are urgently required [238,239]. Nevertheless, 3D bioprinting may become the

Table 4
Examples of organ-bioprinting.

Ref.	Bioprinted model	Bioprinting technique	Bioink	
			Material	Cells
[235]	The vascularized alveolar model	SLA	PEGDA and GelMA	Human lung epithelial cells (seeded) and human lung fibroblasts (bioprinted)
[236]	The left ventricle of the heart	Freeform reversible embedding of suspended hydrogels (FRESH)	Collagen	human embryonic stem cell–derived cardiomyocytes and cardiac fibroblasts
[237]	The trachea	Extrusion bioprinting	PCL and alginate	nasal epithelial and auricular cartilage cells

new therapeutic option that resolves current treatment insufficiencies regarding bone and cartilage repair and provides satisfactory, long-term outcomes.

Author contributions

Conceptualization, Adam Mieloch and Jakub Rybka; Funding acquisition, Jakub Rybka; Investigation, Julia Semba; Project administration, Jakub Rybka; Supervision, Jakub Rybka; Writing – original draft, Julia Semba; Writing – review & editing, Adam Mieloch and Jakub Rybka.

Funding

Declaration of competing interest

The authors declare that they have no known competing financial interests or personal relationships that could have appeared to influence the work reported in this paper.

Acknowledgments

References

[1] E.A. Makris, P. Hadidi, K.A. Athanasiou, The knee meniscus: structure-function, pathophysiology, current repair techniques, and prospects for regeneration, Biomaterials 32 (2011) 7411–7431, https://doi.org/10.1016/j.biomaterials.2011.06.037.

[2] C.R. Fellows, C. Matta, R. Zakany, I.M. Khan, A. Mobasheri, Adipose, bone marrow and synovial joint-derived mesenchymal stem cells for cartilage repair, Front. Genet. 7 (2016) 213, https://doi.org/10.3389/fgene.2016.00213.

[3] C. Di Bella, A. Fosang, D.M. Donati, G.G. Wallace, P.F.M. Choong, 3D bioprinting of cartilage for orthopedic surgeons: reading between the lines, Front. Surg. 2 (2015) 39, https://doi.org/10.3389/fsurg.2015.00039.

[4] C.R. Fellows, K. Gauthaman, P.N. Pushparaj, M. Abbas, C. Matta, R. Lewis, C. Buhrmann, M. Shakibaei, A. Mobasheri, Stem cells in bone and articular cartilage tissue regeneration, in: P. Van Pham (Ed.), Bone Cartil. Regen., Springer, Cham, 2016, pp. 177–204, https://doi.org/10.1007/978-3-319-40144-7.

[5] A. Skardal, Principles and applications of bioprinting, in: A. Khademhosseini, G. Camci-Una (Eds.), 3D Bioprinting Regen. Eng. Princ. Appl., CRC Press, 2018, pp. 1–24.

[6] G. Bouet, D. Marchat, M. Cruel, L. Malaval, L. Vico, In vitro three-dimensional bone tissue models: from cells to controlled and dynamic environment, Tissue Eng. B Rev. 21 (2015) 133–156, https://doi.org/10.1089/ten.TEB.2013.0682.

[7] Ž.P. Kačarević, P.M. Rider, S. Alkildani, S. Retnasingh, R. Smeets, O. Jung, Z. Ivanišević, M. Barbeck, An introduction to 3D bioprinting: possibilities, challenges and future aspects, Materials 11 (2018), https://doi.org/10.3390/ma11112199.

[8] P. Tack, J. Victor, P. Gemmel, L. Annemans, 3D-printing techniques in a medical setting: a systematic literature review, Biomed. Eng. Online 15 (2016) 115, https://doi.org/10.1186/s12938-016-0236-4.

[9] R. Vaishya, M.K. Patralekh, A. Vaish, A.K. Agarwal, V. Vijay, Publication trends and knowledge mapping in 3D printing in orthopaedics, J. Clin. Orthop. Trauma 9 (2018) 194–201, https://doi.org/10.1016/j.jcot.2018.07.006.

[10] B.K. Hall, Bones and Cartilage, second ed., Elsevier, 2015.

[11] K.A. Athanasiou, E.M. Darling, J.C. Hu, Articular Cartilage Tissue Engineering, Morgan & Claypool, 2010, https://doi.org/10.2200/S00213ED1V01Y200910TIS003.

[12] W. Bi, J.M. Deng, Z. Zhang, R.R. Behringer, B. De Crombrugghe, Sox9 is required for cartilage formation, Nat. Genet. 22 (1999) 85–89.

[13] E. Kozhemyakina, A.B. Lassar, E. Zelzer, A pathway to bone: signaling molecules and transcription factors involved in chondrocyte development and maturation, Development 142 (2015) 817–831, https://doi.org/10.1242/dev.105536.

[14] V. Lefebvre, M. Dvir-Ginzberg, SOX9 and the many facets of its regulation in the chondrocyte lineage, Connect, Tissue Res. 58 (2017) 2–14, https://doi.org/10.1080/03008207.2016.1183667.

[15] H. Akiyama, M.-C. Chaboissier, J.F. Martin, A. Schedl, B. de Crombrugghe, The transcription factor Sox9 has essential roles in successive steps of the chondrocyte differentiation pathway and is required for expression of Sox5 and Sox6, Genes Dev. 16 (2002) 2813–2828, https://doi.org/10.1101/gad.1017802.overt.

[16] T. Ikeda, S. Kamekura, A. Mabuchi, I. Kou, S. Seki, T. Takato, K. Nakamura, H. Kawaguchi, S. Ikegawa, U. Il Chung, The combination of SOX5, SOX6, and SOX9 (the SOX trio) provides signals sufficient for induction of permanent cartilage, Arthritis Rheum. 50 (2004) 3561–3573, https://doi.org/10.1002/art.20611.

[17] V. Lefebvre, R.R. Behringer, B. de Crombrugghe, L-Sox5, Sox6 and Sox9 control essential steps of the chondrocyte differentiation pathway, Osteoarthr. Cartil. 9 (2001) S69–S75, https://doi.org/10.1053/joca.2001.0447.

[18] M. Wuelling, A. Vortkamp, Molecular control of cartilage differentiation, in: S. Grässel, A. Aszódi (Eds.), Cartil, vol. 1, Physiol. Dev., Springer International Publishing, 2016, pp. 191–213, https://doi.org/10.1007/978-3-319-29568-8.

[19] I.S. Kim, F. Otto, B. Zabel, S. Mundlos, Regulation of chondrocyte differentiation by Cbfa1, Mech. Dev. 80 (1999) 159–170, https://doi.org/10.1016/S0925-4773(98)00210-X.

[20] E. Zelzer, D.J. Glotzer, C. Hartmann, D. Thomas, N. Fukai, S. Soker, B.R. Olsen, Tissue specific regulation of VEGF expression during bone development requires Cbfa1/Runx2, Mech. Dev. 106 (2001) 97–106, https://doi.org/10.1016/S0925-4773(01)00428-2.

[21] S. Shibata, K. Fukada, H. Imai, T. Abe, Y. Yamashita, In situ hybridization and immunohistochemistry of versican, aggrecan and link protein, and histochemistry of hyaluronan in the developing mouse limb bud cartilage, J. Anat. 203 (2003) 425–432, https://doi.org/10.1046/j.1469-7580.2003.00226.x.

[22] S.I. Vornehm, J. Dudhia, K. Von der Mark, T. Aigner, Expression of collagen types IX and XI and other major cartilage matrix components by human fetal chondrocytes in vivo, Matrix Biol. 15 (1996) 91–98.

[23] J.P. Tuckermann, K. Pittois, N.C. Partridge, J. Merregaert, P. Angel, Collagenase-3 (MMP-13) and integral membrane protein 2a (Itm2a) are marker genes of chondrogenic/osteoblastic cells in bone formation: sequential temporal, and spatial expression of Itm2a, alkaline phosphatase, MMP-13, and osteocalcin in the mouse, J. Bone Miner. Res. 15 (2000) 1257–1265.

[24] J.E. Lafont, S. Talma, C.L. Murphy, Hypoxia-inducible factor 2α is essential for hypoxic induction of the human articular chondrocyte phenotype, Arthritis Rheum. 56 (2007) 3297–3306, https://doi.org/10.1002/art.22878.

[25] A. Aspberg, Cartilage proteoglycans, in: S. Grässel, A. Aszódi (Eds.), Cartil, vol. 1, Physiol. Dev., Springer International Publishing, 2016, pp. 1–22, https://doi.org/10.1007/978-3-319-29568-8.

[26] S. Grässel, Collagens in hyaline cartilage, in: S. Grässel, A. Aszódi (Eds.), Cartil, vol. 1, Physiol. Dev., Springer International Publishing, 2016, pp. 23–53, https://doi.org/10.1007/978-3-319-29568-8.

[27] A.A. Mieloch, M. Richter, T. Trzeciak, M. Giersig, J.D. Rybka, Osteoarthritis severely decreases the elasticity and hardness of knee joint Cartilage : a nanoindentation study, J. Clin. Med. 8 (2019), https://doi.org/10.3390/jcm8111865.

[28] X. Wang, W.C. Chan, D. Chan, Joint development, in: S. Grässel, A. Aszódi (Eds.), Cartil, vol. 1, Physiol. Dev., Springer, Cham, 2016, pp. 169–189, https://doi.org/10.1007/978-3-319-29568-8.

[29] L. Zhong, X. Huang, M. Karperien, J.N. Post, The regulatory role of signaling crosstalk in hypertrophy of MSCs and human articular chondrocytes, Int. J. Mol. Sci. 16 (2015) 19225–19247, https://doi.org/10.3390/ijms160819225.

[30] D.S. Logerstedt, D.A. Scalzitti, K.L. Bennell, R.S. Hinman, H. Silvers-Granelli, J. Ebert, K. Hambly, J.L. Carey, L. Snyder-Mackler, M.J. Axe, C.M. McDonough, Knee pain and mobility impairments: meniscal and articular cartilage lesions Revision 2018, J. Orthop. Sport. Phys. Ther. 48 (2018) A1–A50, https://doi.org/10.2519/jospt.2018.0301.

[31] M. Richter, T. Trzeciak, J.D. Rybka, W. Suchorska, E. Augustyniak, M. Lach, M. Kaczmarek, J. Kaczmarczyk, Correlations between serum adipocytokine concentrations, disease stage, radiological status and total body fat content in the patients with primary knee osteoarthritis, Int. Orthop. 41 (2017) 983–989, https://doi.org/10.1007/s00264-016-3370-5.

[32] H. Pereira, R. Varatojo, N. Sevivas, L. Serratosa, P.L. Ripoll, J.M. Oliveira, R.L. Reis, J. Espregueira-Mendes, Physiopathology of the meniscal lesions, in: C. Hulet, H. Pereira, G. Peretti, M. Denti (Eds.), Surg. Meniscus, ESSKA, 2016, pp. 47–61, https://doi.org/10.1007/978-3-662-49188-1.

[33] H. Yu, A.B. Adesida, N.M. Jomha, Meniscus repair using mesenchymal stem cells - a comprehensive review, Stem Cell Res. Ther. 6 (2015) 86, https://doi.org/10.1186/s13287-015-0077-2.

[34] I.D. McDermott, A.A. Amis, The consequences of meniscectomy, J. Bone Joint Surg. Br. 88-B (2006) 1549–1556, https://doi.org/10.1302/0301-620x.88b12.18140.

[35] M. Witkowska-Zimny, Transcriptional control of osteogenesis, in: Y. Lin (Ed.), Osteogenesis, InTech, 2012, pp. 1–20.

[36] L.T. Staheli, Fundamentals of Pediatric Orthopedics, Lippincott Williams & Wilkins, 2008.

[37] E.J. Mackie, Y.A. Ahmed, L. Tatarczuch, K.S. Chen, M. Mirams, Endochondral ossification: how cartilage is converted into bone in the developing skeleton, Int. J. Biochem. Cell Biol. 40 (2008) 46–62, https://doi.org/10.1016/j.biocel.2007.06.009.

[38] K. von der Mark, X. Zhou, Cell fate of growth plate chondrocytes in endochondral ossification: cell death or reprogramming into osteogenic lineage?, in: S. Grässel, A. Aszódi (Eds.), Cartil, vol. 1 Physiol. Dev., Springer, Cham, 2016, pp. 115–142, https://doi.org/10.1007/978-3-319-29568-8.

[39] L. Yang, K.Y. Tsang, H.C. Tang, D. Chan, K.S.E. Cheah, Hypertrophic chondrocytes can become osteoblasts and osteocytes in endochondral bone formation, Proc. Natl. Acad. Sci. U.S.A. 111 (2014) 12097–12102, https://doi.org/10.1073/pnas.1302703111.

[40] J. Zhou, J. Dong, Vascularization in the bone repair, in: Y. Lin (Ed.), Osteogenesis, InTech, 2012, pp. 287–296, https://doi.org/10.5772/36325.

[41] L. Roseti, V. Parisi, M. Petretta, C. Cavallo, G. Desando, I. Bartolotti, B. Grigolo, Scaffolds for bone tissue engineering: state of the art and new perspectives, Mater. Sci. Eng. C 78 (2017) 1246–1262, https://doi.org/10.1016/j.msec.2017.05.017.

[42] Z. Maruyama, C.A. Yoshida, T. Furuichi, N. Amizuka, M. Ito, R. Fukuyama, T. Miyazaki, H. Kitaura, K. Nakamura, T. Fujita, N. Kanatani, T. Moriishi, K. Yamana, W. Liu, H. Kawaguchi, K. Nakamura, T. Komori, Runx2 determines bone maturity and turnover rate in postnatal bone development and is involved in bone loss in estrogen deficiency, Dev. Dynam. 236 (2007) 1876–1890, https://doi.org/10.1002/dvdy.21187.

[43] L.A. Kaback, D.Y. Soung, A. Naik, N. Smith, E.M. Schwarz, R.J. O'Keefe, H. Drissi, Osterix/Sp7 regulates mesenchymal stem cell mediated endochondral ossification, J. Cell. Physiol. 214 (2007) 173–182, https://doi.org/10.1002/jcp.21176.

[44] K. Nakashima, X. Zhou, G. Kunkel, Z. Zhang, J.M. Deng, R.R. Behringer, B. de Crombrugghe, The novel zinc finger-containing transcription factor osterix is required for osteoblast differentiation and bone formation, Cell 108 (2002) 17–29, https://doi.org/10.1016/S0092-8674(01)00622-5.

[45] M.M.L. Deckers, M. Karperien, C. Van Der Bent, T. Yamashita, S.E. Papapoulos, C.W.G.M. Löwik, Expression of vascular endothelial growth factors and their receptors during osteoblast differentiation, Endocrinology 141 (2000) 1667–1674, https://doi.org/10.1210/endo.141.5.7458.

[46] M. Weinreb, D. Shinar, G.A. Rodan, Different pattern of alkaline phosphatase, osteopontin, and osteocalcin expression in developing rat bone visualized by in situ hybridization, J. Bone Miner. Res. 5 (1990) 831–842, https://doi.org/10.1002/jbmr.5650050806.

[47] H. Orimo, The mechanism of mineralization and the role of alkaline phosphatase in health and disease, J. Nippon Med. Sch. 77 (2010) 4–12, https://doi.org/10.1272/jnms.77.4.

[48] E. Bonucci, Bone mineralization, Front. Biosci. 17 (2012) 100–128, https://doi.org/10.5772/54591.

[49] J. Henkel, M.A. Woodruff, D.R. Epari, R. Steck, V. Glatt, I.C. Dickinson, P.F.M. Choong, M.A. Schuetz, D.W. Hutmacher, Bone regeneration based on tissue engineering conceptions — a 21st century perspective, Bone Res. 1 (2013) 216–248, https://doi.org/10.4248/br201303002.

[50] M.S. Ghiasi, J. Chen, A. Vaziri, E.K. Rodriguez, A. Nazarian, Bone fracture healing in mechanobiological modeling: a review of principles and methods, BoneKEy Rep. 6 (2017) 87–100, https://doi.org/10.1016/j.bonr.2017.03.002.

[51] W. Wang, K.W.K. Yeung, Bone grafts and biomaterials substitutes for bone defect repair: a review, Bioact. Mater. 2 (2017) 224–247, https://doi.org/10.1016/j.bioactmat.2017.05.007.

[52] T. Trzeciak, J.D. Rybka, M. Richter, J. Kaczmarczyk, M. Ramalingam, M. Giersig, Cells and nanomaterial-based tissue engineering techniques in the treatment of bone and cartilage injuries, J. Nanosci. Nanotechnol. 16 (2016) 8948–8952, https://doi.org/10.1166/jnn.2016.12732.

[53] D.A. Parate, S. Zhang, J.H.P. Hui, W.S. Toh, Stem cells for articular cartilage repair and regeneration, in: P. Van Pham (Ed.), Bone Cartil. Regen., Springer, Cham, 2016, pp. 119–147, https://doi.org/10.1007/978-3-319-40144-7.

[54] M. Dominici, K. Le Blanc, I. Mueller, I. Slaper-Cortenbach, F. Marini, D. Krause, R. Deans, A. Keating, D. Prockop, E. Horwitz, Minimal criteria for defining multipotent mesenchymal stromal cells. The International Society for Cellular Therapy position statement, Cytotherapy 8 (2006) 315–317, https://doi.org/10.1080/14653240600855905.

[55] M. Hinsenkamp, L. Muylle, T. Eastlund, D. Fehily, L. Noël, D.M. Strong, Adverse reactions and events related to musculoskeletal allografts: reviewed by the world health organisation Project NOTIFY, Int. Orthop. 36 (2012) 633–641, https://doi.org/10.1007/s00264-011-1391-7.

[56] S. Hosseini, M. Baghaban Eslaminejad, Mesenchymal stem cells: an optimistic cell source in tissue engineering for bone regeneration, in: P. Van Pham (Ed.), Bone Cartil. Regen., Springer, Cham, 2016, pp. 205–243, https://doi.org/10.1007/978-3-319-40144-7.

[57] P.A. Zuk, M. Zhu, P. Ashjian, D.A. De Ugarte, J.I. Huang, H. Mizuno, Z.C. Alfonso, J.K. Fraser, P. Benhaim, M.H. Hedrick, Human adipose tissue is a source of multipotent stem cells, Mol. Biol. Cell 13 (2002) 4279–4295, https://doi.org/10.1091/mbc.E02-02-0105.

[58] P. Palumbo, F. Lombardi, G. Siragusa, M.G. Cifone, B. Cinque, M. Giuliani, Methods of isolation, characterization and expansion of human adipose-derived stem cells (ASCs): an overview, Int. J. Mol. Sci. 19 (2018), https://doi.org/10.3390/ijms19071897.

[59] C.T. Buckley, T. Vinardell, S.D. Thorpe, M.G. Haugh, E. Jones, D. McGonagle, D.J. Kelly, Functional properties of cartilaginous tissues engineered from infrapatellar fat pad-derived mesenchymal stem cells, J. Biomech. 43 (2010) 920–926, https://doi.org/10.1016/j.jbiomech.2009.11.005.

[60] K. Ye, R. Felimban, K. Traianedes, S.E. Moulton, G.G. Wallace, J. Chung, A. Quigley, P.F.M. Choong, D.E. Myers, Chondrogenesis of infrapatellar fat pad derived adipose stem cells in 3D printed chitosan scaffold, PLoS One 9 (2014), e99410, https://doi.org/10.1371/journal.pone.0099410.

[61] R.I. Felimban, Engineering Articular Cartilage from Human Infrapatellar Fat Pad Stem Cells for Transplantation Therapy, 2015.

[62] P.A. Zuk, M. Zhu, H. Mizuno, J. Huang, J.W. Futrell, A.J. Katz, P. Benhaim, J.P. Lorenz, M. Hedrick, Multilineage cells from human adipose tissue: implications for cell-based therapies, Tissue Eng. 7 (2001) 211–228.

[63] H. Busser, C. De Bruyn, F. Urbain, M. Najar, K. Pieters, G. Raicevic, N. Meuleman, D. Bron, L. Lagneaux, Isolation of adipose-derived stromal cells without enzymatic treatment: expansion, phenotypical, and functional characterization, Stem Cells Dev. 23 (2014) 2390–2400, https://doi.org/10.1089/scd.2014.0071.

[64] G. Zeng, K. Lai, J. Li, Y. Zou, H. Huang, J. Liang, X. Tang, J. Wei, P. Zhang, A rapid and efficient method for primary culture of human adipose-derived stem cells, Organogenesis 9 (2013) 287–295, https://doi.org/10.4161/org.27153.

[65] A.D. Gojanovich, M.C. Gimenez, D. Masone, T.M. Rodriguez, R.A. Dewey, L.R. Delgui, D.M. Bustos, M. Uhart, Human adipose-derived mesenchymal stem/stromal cells handling protocols. Lipid droplets and proteins double-staining, Front. Cell Dev. Biol. 6 (2018) 33, https://doi.org/10.3389/fcell.2018.00033.

[66] Y. Sakaguchi, I. Sekiya, K. Yagishita, T. Muneta, Comparison of human stem cells derived from various mesenchymal tissues: superiority of synovium as a cell source, Arthritis Rheum. 52 (2005) 2521–2529, https://doi.org/10.1002/art.21212.

[67] S. Boeuf, W. Richter, Chondrogenesis of mesenchymal stem cells: role of tissue source and inducing factors, Stem Cell Res. Ther. 1 (2010) 31, https://doi.org/10.1186/scrt31.

[68] R.B. Jakobsen, A. Shahdadfar, F.P. Reinholt, J.E. Brinchmann, Chondrogenesis in a hyaluronic acid scaffold: comparison between chondrocytes and MSC from bone marrow and adipose tissue, Knee Surgery, Sport, Traumatol. Arthrosc. 18 (2010) 1407–1416, https://doi.org/10.1007/s00167-009-1017-4.

[69] D.-A. Yu, J. Han, B.-S. Kim, Stimulation of chondrogenic differentiation of mesenchymal stem cells, Int. J. Stem Cells 5 (2012) 16–22, https://doi.org/10.15283/ijsc.2012.5.1.16.

[70] F. Pati, J. Jang, D.H. Ha, S. Won Kim, J.W. Rhie, J.H. Shim, D.H. Kim, D.W. Cho, Printing three-dimensional tissue analogues with decellularized extracellular matrix bioink, Nat. Commun. 5 (2014) 3935, https://doi.org/10.1038/ncomms4935.

[71] S. Rathan, L. Dejob, R. Schipani, B. Haffner, M.E. Möbius, D.J. Kelly, Fiber reinforced cartilage ECM functionalized bioinks for functional cartilage tissue engineering, Adv. Healthc. Mater. 8 (2019), https://doi.org/10.1002/adhm.201801501.

[72] G. Gao, X.F. Zhang, K. Hubbell, X. Cui, NR2F2 regulates chondrogenesis of human mesenchymal stem cells in bioprinted cartilage, Biotechnol. Bioeng. 114 (2017) 208–216, https://doi.org/10.1002/bit.26042.

[73] C.B. Foldager, A.B. Nielsen, S. Munir, M. Ulrich-Vinther, K. Søballe, C. Bünger, M. Lind, Combined 3D and hypoxic culture improves cartilage-specific gene expression in human chondrocytes, Acta Orthop. 82 (2011) 234–240, https://doi.org/10.3109/17453674.2011.566135.

[74] B.L. Thoms, K.A. Dudek, J.E. Lafont, C.L. Murphy, Hypoxia promotes the production and inhibits the destruction of human articular cartilage, Arthritis Rheum. 65 (2013) 1302–1312, https://doi.org/10.1002/art.37867.

[75] S. Riis, V. Zachar, S. Boucher, M.C. Vemuri, C.P. Pennisi, T. Fink, Critical steps in the isolation and expansion of adipose-derived stem cells for translational therapy, Expert Rev. Mol. Med. 17 (2015) e11, https://doi.org/10.1017/erm.2015.10.

[76] C.J. Schofield, P.J. Ratcliffe, Oxygen sensing by HIF hydroxylases, Nat. Rev. Mol. Cell Biol. 5 (2004) 343–354, https://doi.org/10.1038/nrm1366.

[77] C. Zhang, F. Yang, R. Cornelia, W. Tang, S. Swisher, H. Kim, Hypoxia-inducible factor-1 is a positive regulator of Sox9 activity in femoral head osteonecrosis, Bone 48 (2011) 507–513, https://doi.org/10.1016/j.bone.2010.10.006.

[78] J. Huang, F. Deng, L. Wang, X.R. Xiang, W.W. Zhou, N. Hu, L. Xu, Hypoxia induces osteogenesis-related activities and expression of core binding factor α1 in mesenchymal stem cells, Tohoku J. Exp. Med. 224 (2011) 7–12, https://doi.org/10.1620/tjem.224.7.

[79] B.D. Markway, H. Cho, J. Zilberman-Rudenko, P. Holden, A. McAlinden, B. Johnstone, Hypoxia-inducible factor 3-alpha expression is associated with the stable chondrocyte phenotype, J. Orthop. Res. 33 (2015) 1561–1570, https://doi.org/10.1002/jor.22930.

[80] C. Merceron, C. Vinatier, S. Portron, M. Masson, J. Amiaud, L. Guigand, Y. Chérel, P. Weiss, J. Guicheux, Differential effects of hypoxia on osteochondrogenic potential of human adipose-derived stem cells, Am. J. Physiol. 298 (2010) C355–C364, https://doi.org/10.1152/ajpcell.00398.2009.

[81] S.D. Thorpe, T. Nagel, S.F. Carroll, D.J. Kelly, Modulating gradients in regulatory signals within mesenchymal stem cell seeded hydrogels: a novel strategy to engineer zonal articular cartilage, PLoS One 8 (2013), e60764, https://doi.org/10.1371/journal.pone.0060764.

[82] A.C. Daly, S.E. Critchley, E.M. Rencsok, D.J. Kelly, A comparison of different bioinks for 3D bioprinting of fibrocartilage and hyaline cartilage, Biofabrication 8 (2016), 045002, https://doi.org/10.1088/1758-5090/8/4/045002.

[83] G.M. Cunniffe, T. Gonzalez-Fernandez, A. Daly, B.N. Sathy, O. Jeon, E. Alsberg, D.J. Kelly, Three-dimensional bioprinting of polycaprolactone reinforced gene activated bioinks for bone tissue engineering, Tissue Eng. A 23 (2017) 891–900, https://doi.org/10.1089/ten.tea.2016.0498.

[84] A. Carlier, G.A. Skvortsov, F. Hafezi, E. Ferraris, J. Patterson, B. Koc, H. Van Oosterwyck, Computational model-informed design and bioprinting of cell-patterned constructs for bone tissue engineering, Biofabrication 8 (2016), 025009, https://doi.org/10.1088/1758-5090/8/2/025009.

[85] X. Ren, F. Wang, C. Chen, X. Gong, L. Yin, L. Yang, Engineering zonal cartilage through bioprinting collagen type II hydrogel constructs with biomimetic chondrocyte density gradient, BMC Muscoskelet. Disord. 17 (2016), https://doi.org/10.1186/s12891-016-1130-8.

[86] Y.H.K. Yang, C.R. Ogando, C. Wang See, T.Y. Chang, G.A. Barabino, Changes in phenotype and differentiation potential of human mesenchymal stem cells aging in vitro, Stem Cell Res. Ther. 9 (2018) 131, https://doi.org/10.1186/s13287-018-0876-3.

[87] A.O. Oseni, P.E. Butler, A.M. Seifalian, Optimization of chondrocyte isolation and characterization for large-scale cartilage tissue engineering, J. Surg. Res. 181 (2013) 41–48, https://doi.org/10.1016/j.jss.2012.05.087.

[88] F. You, B.F. Eames, X. Chen, Application of extrusion-based hydrogel bioprinting for cartilage tissue engineering, Int. J. Mol. Sci. 18 (2017), https://doi.org/10.3390/ijms18071597.

[89] X. Cui, K. Breitenkamp, M. Lotz, D. D'Lima, Synergistic action of fibroblast growth factor-2 and transforming growth factor-beta1 enhances bioprinted human neocartilage formation, Biotechnol. Bioeng. 109 (2012) 2357–2368, https://doi.org/10.1158/0008-5472.CAN-10-4002.

[90] A. Tekari, R. Luginbuehl, W. Hofstetter, R.J. Egli, Transforming growth factor beta signaling is essential for the autonomous formation of cartilage-like tissue by expanded chondrocytes, PLoS One 10 (2015), e0120857, https://doi.org/10.1371/journal.pone.0120857.

[91] R. Williams, I.M. Khan, K. Richardson, L. Nelson, H.E. McCarthy, T. Analbelsi, S.K. Singhrao, G.P. Dowthwaite, R.E. Jones, D.M. Baird, H. Lewis, S. Roberts, H.M. Shaw, J. Dudhia, J. Fairclough, T. Briggs, C.W. Archer, Identification and clonal characterisation of a progenitor cell sub-population in normal human articular cartilage, PLoS One 5 (2010), e13246, https://doi.org/10.1371/journal.pone.0013246.

[92] Y. Jiang, Y. Cai, Z. Wei, Z. Yin, C. Hu, T. Tong, P. Lu, S. Zhang, D. Neculai, R.S. Tuan, W.H. Ouyang, Human cartilage-derived progenitor cells from committed chondrocytes for efficient cartilage repair and regeneration, Stem Cells Transl. Med. 5 (2016) 733–744, https://doi.org/10.5966/sctm.2015-0192.

[93] K. von der Mark, V. Gauss, H. von der Mark, P. Müller, Relationship between cell shape and type of collagen synthesised as chondrocytes lose their cartilage phenotype in culture, Nature 267 (1977) 531–532.

[94] E.M. Darling, K.A. Athanasiou, Rapid phenotypic changes in passaged articular chondrocyte subpopulations, J. Orthop. Res. 23 (2005) 425–432, https://doi.org/10.1016/j.orthres.2004.08.008.

[95] F. Legendre, D. Ollitrault, M. Hervieu, C. Baugé, L. Maneix, D. Goux, H. Chajra, F. Mallein-Gerin, K. Boumediene, P. Galera, M. Demoor, Enhanced Hyaline Cartilage Matrix Synthesis in Collagen Sponge Scaffolds by Using siRNA to Stabilize Chondrocytes Phenotype Cultured with BMP-2 under Hypoxia, ((n.d.)).

[96] S. Chen, P. Fu, R. Cong, H.S. Wu, M. Pei, Strategies to minimize hypertrophy in cartilage engineering and regeneration, Genes Dis. 2 (2015) 76–95, https://doi.org/10.1016/j.gendis.2014.12.003.

[97] N.S. Hwang, S.G. Im, P.B. Wu, D.A. Bichara, X. Zhao, M.A. Randolph, R. Langer, D.G. Anderson, Chondrogenic priming adipose-mesenchymal stem cells for cartilage tissue regeneration, Pharm. Res. 28 (2011) 1395–1405, https://doi.org/10.1007/s11095-011-0445-2.

[98] V.V. Meretoja, R.L. Dahlin, S. Wright, F.K. Kasper, A.G. Mikos, The effect of hypoxia on the chondrogenic differentiation of co-cultured articular chondrocytes and mesenchymal stem cells in scaffolds, Biomaterials 34 (2013) 4266–4273, https://doi.org/10.1016/j.biomaterials.2013.02.064.

[99] D. Nguyen, D.A. Hgg, A. Forsman, J. Ekholm, P. Nimkingratana, C. Brantsing, T. Kalogeropoulos, S. Zaunz, S. Concaro, M. Brittberg, A. Lindahl, P. Gatenholm, A. Enejder, S. Simonsson, Cartilage tissue engineering by the 3D bioprinting of iPS cells in a nanocellulose/alginate bioink, Sci. Rep. 7 (2017), https://doi.org/10.1038/s41598-017-00690-y.

[100] S. Chameettachal, S. Midha, S. Ghosh, Regulation of chondrogenesis and hypertrophy in silk fibroin-gelatin-based 3D bioprinted constructs, ACS Biomater. Sci. Eng. 2 (2016) 1450–1463, https://doi.org/10.1021/acsbiomaterials.6b00152.

[101] R. Levato, W.R. Webb, I.A. Otto, A. Mensinga, Y. Zhang, M. van Rijen, R. van Weeren, I.M. Khan, J. Malda, The bio in the ink: cartilage regeneration with bioprintable hydrogels and articular cartilage-derived progenitor cells, Acta Biomater. 61 (2017) 41–53, https://doi.org/10.1016/j.actbio.2017.08.005.

[102] H.A. Awad, M.Q. Wickham, H.A. Leddy, J.M. Gimble, F. Guilak, Chondrogenic differentiation of adipose-derived adult stem cells in agarose, alginate, and gelatin scaffolds, Biomaterials 25 (2004) 3211–3222, https://doi.org/10.1016/j.biomaterials.2003.10.045.

[103] A.C. Daly, F.E. Freeman, T. Gonzalez-Fernandez, S.E. Critchley, J. Nulty, D.J. Kelly, 3D bioprinting for cartilage and osteochondral tissue engineering, Adv. Healthc. Mater. 6 (2017) 1–20, https://doi.org/10.1002/adhm.201700298.

[104] D.F. Duarte Campos, A. Blaeser, A. Korsten, S. Neuss, J. Jäkel, M. Vogt, H. Fischer, The stiffness and structure of three-dimensional printed hydrogels direct the differentiation of mesenchymal stromal cells toward adipogenic and osteogenic lineages, Tissue Eng. A 21 (2015) 740–756, https://doi.org/10.1089/ten.tea.2014.0231.

[105] F.E. Freeman, D.J. Kelly, Tuning alginate bioink stiffness and composition for controlled growth factor delivery and to spatially direct MSC fate within bioprinted tissues, Sci. Rep. 7 (2017), https://doi.org/10.1038/s41598-017-17286-1.

[106] A. Parak, P. Pradeep, L.C. du Toit, P. Kumar, Y.E. Choonara, V. Pillay, Functionalizing bioinks for 3D bioprinting applications, Drug Discov. Today 24 (2018) 198–205, https://doi.org/10.1016/j.drudis.2018.09.012.

[107] L.J. Min, T.Y.S. Edgar, Z. Zicheng, Y.W. Yee, Biomaterials for bioprinting, in: L.G. Zhang, J.P. Fisher, K.W. Leong (Eds.), 3D Bioprinting Nanotechnol. Tissue Eng. Regen. Med., Elsevier, 2015, pp. 129–148.

[108] E.M. Ahmed, Hydrogel: preparation, characterization, and applications: a review, J. Adv. Res. 6 (2015) 105–121, https://doi.org/10.1016/j.jare.2013.07.006.

[109] K.Y. Lee, D.J. Mooney, Alginate: properties and biomedical applications, Prog. Polym. Sci. 37 (2012) 106–126, https://doi.org/10.1016/j.progpolymsci.2011.06.003.

[110] M.F. Moradali, S. Ghods, B.H.A. Rehm, Alginate biosynthesis and biotechnological production, in: B.H.A. Rehm, M.F. Moradali (Eds.), Alginates Their Biomed. Appl., Springer Nature, 2018, pp. 1–26, https://doi.org/10.1007/978-981-10-6910-9.

[111] S.H. Ching, N. Bansal, B. Bhandari, Alginate gel particles–A review of production techniques and physical properties, Crit. Rev. Food Sci. Nutr. 57 (2017) 1133–1152, https://doi.org/10.1080/10408398.2014.965773.

[112] E. Gargus, P. Lewis, R. Shah, Bioinks for 3D printing, in: A. Khademhosseini, G. Camci-Una (Eds.), 3D Bioprinting Regen. Eng. Princ. Appl., Taylor & Francis, 2018, pp. 25–50.

[113] K.I. Draget, G. Skjåk-Bræk, B.T. Stokke, Similarities and differences between alginic acid gels and ionically crosslinked alginate gels, Food Hydrocolloids 20 (2006) 170–175, https://doi.org/10.1016/j.foodhyd.2004.03.009.

[114] N.G. Genes, J.A. Rowley, D.J. Mooney, L.J. Bonassar, Effect of substrate mechanics on chondrocyte adhesion to modified alginate surfaces, Arch. Biochem. Biophys. 422 (2004) 161–167, https://doi.org/10.1016/j.abb.2003.11.023.

[115] F.-M. Chen, X. Liu, Advancing Biomaterials of Human Origin for Tissue Engineering, vol. 53, 2016, pp. 86–168, https://doi.org/10.1016/j.progpolymsci.2015.02.004.

[116] S.E. D'Souza, M.H. Ginsberg, E.F. Plow, Arginyl-glycyl-aspartic acid (RGD): a cell adhesion motif, Trends Biochem. Sci. 16 (1991) 246–250.

[117] G. Grant, E. Morris, D. Rees, P. Smith, D. Thom, Biological interactions between polysaccharides and divalent cations: the egg-box model, FEBS Lett. 32 (1973) 195–198.

[118] M. Mancini, M. Moresi, R. Rancini, Mechanical properties of alginate gels: empirical characterisation, J. Food Eng. 39 (1999) 369–378, https://doi.org/10.1016/S0260-8774(99)00022-9.

[119] C. Peteiro, Alginate production from marine macroalgae, with emphasis on kelp farming, in: B.H.A. Rehm, M.F. Moradali (Eds.), Alginates Their Biomed. Appl., Springer Singapore, 2018, pp. 27–66.

[120] X. Yang, Z. Lu, H. Wu, W. Li, L. Zheng, J. Zhao, Collagen-alginate as bioink for three-dimensional (3D) cell printing based cartilage tissue engineering, Mater. Sci. Eng. C Mater. Biol. Appl. 83 (2018) 195–201, https://doi.org/10.1016/j.msec.2017.09.002.

[121] S. Naghieh, M.R. Karamooz-Ravari, M.D. Sarker, E. Karki, X. Chen, Influence of crosslinking on the mechanical behavior of 3D printed alginate scaffolds: experimental and numerical approaches, J. Mech. Behav. Biomed. Mater. 80 (2018) 111–118, https://doi.org/10.1016/j.jmbbm.2018.01.034.

[122] C.K. Kuo, P.X. Ma, Ionically crosslinked alginate hydrogels as scaffolds for tissue engineering: Part 1. Structure, gelation rate and mechanical properties, Biomaterials 22 (2001) 511–521, https://doi.org/10.1016/S0142-9612(00)00201-5.

[123] N. Cao, X.B. Chen, D.J. Schreyer, Influence of calcium ions on cell survival and proliferation in the context of an alginate hydrogel, ISRN Chem. Eng. 2012 (2012), https://doi.org/10.5402/2012/516461.

[124] R. Naren, Y. Hui-Suk, A simultaneous 3D printing process for the fabrication of bioceramic and cell-laden hydrogel core/shell scaffolds with potential application in bone tissue regeneration, J. Mater. Chem. B. 4 (2016) 4707–4716, https://doi.org/10.1039/c6tb00849f.

[125] A. Schmitt, P. Rödel, C. Anamur, C. Seeliger, A.B. Imhoff, E. Herbst, S. Vogt, M. Van Griensven, G. Winter, J. Engert, Calcium alginate gels as stem cell matrix - making paracrine stem cell activity available for enhanced healing after surgery, PLoS One 10 (2015), e0118937, https://doi.org/10.1371/journal.pone.0118937.

[126] P.S. Gungor-Ozkerim, I. Inci, Y.S. Zhang, A. Khademhosseini, M.R. Dokmeci, Bioinks for 3D bioprinting: an overview, Biomater. Sci. 6 (2018) 915–946, https://doi.org/10.1039/c7bm00765e.

[127] S. Wüst, M.E. Godla, R. Müller, S. Hofmann, Tunable hydrogel composite with two-step processing in combination with innovative hardware upgrade for cell-based three-dimensional bioprinting, Acta Biomater. 10 (2014) 630–640, https://doi.org/10.1016/j.actbio.2013.10.016.

[128] J.P.K. Armstrong, M. Burke, B.M. Carter, S.A. Davis, A.W. Perriman, 3D bioprinting using a templated porous bioink, Adv. Healthc. Mater. 5 (2016) 1724–1730, https://doi.org/10.1002/adhm.201600022.

[129] A.G. Tabriz, M.A. Hermida, N.R. Leslie, W. Shu, Three-dimensional bioprinting of complex cell laden alginate hydrogel structures, Biofabrication 7 (2015), 45012, https://doi.org/10.1088/1758-5090/7/4/045012.

[130] G. Birdi, R.H. Bridson, A.M. Smith, S.P. Mohd Bohari, L.M. Grover, Modification of alginate degradation properties using orthosilicic acid, J. Mech. Behav. Biomed. Mater. 6 (2012) 181–187, https://doi.org/10.1016/j.jmbbm.2011.10.001.

[131] V. Guarino, T. Caputo, R. Altobelli, L. Ambrosio, Degradation properties and metabolic activity of alginate and chitosan polyelectrolytes for drug delivery and tissue engineering applications, AIMS Mater. Sci. 2 (2015) 497–502, https://doi.org/10.3934/matersci.2015.4.497.

[132] A. Al-Shamkhani, R. Duncan, Radioiodination of alginate via covalently-bound tyrosinamide allows monitoring of its fate in vivo, J. Bioact. Compat Polym. 10 (1995) 4–13, https://doi.org/10.1177/088391159501000102.

[133] J. Jia, D.J. Richards, S. Pollard, Y. Tan, J. Rodriguez, R.P. Visconti, T.C. Trusk, M.J. Yost, H. Yao, R.R. Markwald, Y. Mei, Engineering alginate as bioink for bioprinting, Acta Biomater. 10 (2014) 4323–4331, https://doi.org/10.1016/j.actbio.2014.06.034.

[134] S. Islam, M.A.R. Bhuiyan, M.N. Islam, Chitin and chitosan: structure, properties and applications in biomedical engineering, J. Polym. Environ. 25 (2017) 854–866, https://doi.org/10.1007/s10924-016-0865-5.

[135] R. Logith Kumar, A. Keshav Narayan, S. Dhivya, A. Chawla, S. Saravanan, N. Selvamurugan, A review of chitosan and its derivatives in bone tissue engineering, Carbohydr. Polym. 151 (2016) 172–188, https://doi.org/10.1016/j.carbpol.2016.05.049.

[136] A. Padmanabhan, L.S. Nair, Chitosan hydrogels for regenerative engineering, in: P.K. Dutta (Ed.), Chitin Chitosan Regen. Med., Springer India, 2016, pp. 3–40.

[137] Y. Yuan, B.M. Chesnutt, W.O. Haggard, J.D. Bumgardner, Deacetylation of chitosan: material characterization and in vitro evaluation via albumin adsorption and pre-osteoblastic cell cultures, Materials 4 (2011) 1399–1416, https://doi.org/10.3390/ma4081399.

[138] T.T. Demirtaş, G. Irmak, M. Gümüşderelioğlu, Bioprintable form of chitosan hydrogel for bone tissue engineering, Biofabrication 9 (2017), 035003, https://doi.org/10.1088/1758-5090/aa7b1d.

[139] S.M. Lim, D.K. Song, S.H. Oh, D.S. Lee-Yoon, E.H. Bae, J.H. Lee, In vitro and in vivo degradation behavior of acetylated chitosan porous beads, J. Biomater. Sci. Polym. 19 (2008) 453–466, https://doi.org/10.1163/156856208783719482.

[140] C. Peniche, W. Argüelles-Monal, F.M. Goycoolea, Chitin and chitosan: major sources, properties and application, in: M.N. Belgacem, A. Gandin (Eds.), Monomers, Polym. Compos. From Renew. Resour., Elsevier, 2008, pp. 517–542.

[141] D. Liu, M. Nikoo, G. Boran, P. Zhou, J.M. Regenstein, Collagen and gelatin, Annu. Rev. Food Sci. Technol. 6 (2015) 527–557, https://doi.org/10.1146/annurev-food-031414-111800.

[142] A. Sorushanova, L.M. Delgado, Z. Wu, N. Shologu, A. Kshirsagar, R. Raghunath, A.M. Mullen, Y. Bayon, A. Pandit, M. Raghunath, D.I. Zeugolis, The collagen suprafamily: from biosynthesis to advanced biomaterial development, Adv. Mater. 31 (2019) 1–39, https://doi.org/10.1002/adma.201801651.

[143] R.S. Walton, D.D. Brand, J.T. Czernuszka, Influence of telopeptides, fibrils and crosslinking on physicochemical properties of type I collagen films, J. Mater. Sci. Mater. Med. 21 (2010) 451–461, https://doi.org/10.1007/s10856-009-3910-2.

[144] A.M. Ferreira, P. Gentile, V. Chiono, G. Ciardelli, Collagen for bone tissue regeneration, Acta Biomater. 8 (2012) 3191–3200, https://doi.org/10.1016/j.actbio.2012.06.014.

[145] B.D. Walters, J.P. Stegemann, Strategies for directing the structure and function of 3D collagen biomaterials across length scales, Acta Biomater. 10 (2014) 1488–1501, https://doi.org/10.1016/j.actbio.2013.08.038.

[146] S. Rhee, J.L. Puetzer, B.N. Mason, C.A. Reinhart-King, L.J. Bonassar, 3D bioprinting of spatially heterogeneous collagen constructs for cartilage tissue engineering, ACS Biomater. Sci. Eng. 2 (2016) 1800–1805, https://doi.org/10.1021/acsbiomaterials.6b00288.

[147] E.E. Antoine, P.P. Vlachos, M.N. Rylander, Review of collagen I hydrogels for bioengineered tissue microenvironments: characterization of mechanics, structure, and transport, Tissue Eng. B Rev. 20 (2014) 683–696, https://doi.org/10.1089/ten.teb.2014.0086.

[148] D. Bosnakovski, M. Mizuno, G. Kim, S. Takagi, M. Okumura, T. Fujinaga, Chondrogenic differentiation of bovine bone marrow mesenchymal stem cells (MSCs) in different hydrogels: influence of collagen type II extracellular matrix on MSC chondrogenesis, Biotechnol. Bioeng. 93 (2006) 1152–1163, https://doi.org/10.1002/bit.20828.

[149] R. Parenteau-Bareil, R. Gauvin, S. Cliche, C. Gariépy, L. Germain, F. Berthod, Comparative study of bovine, porcine and avian collagens for the production of a tissue engineered dermis, Acta Biomater. 7 (2011) 3757–3765, https://doi.org/10.1016/j.actbio.2011.06.020.

[150] M. Nikkhah, M. Akbari, A. Memic, A. Dolatshahi-pirouz, A. Khademhosseini, Gelatin-based biomaterials for tissue engineering and stem cell bioengineering, in: N.M. Neves, R.L. Reis (Eds.), Biomater. From Nat. Adv. Devices Ther., I, John Wiley & Sons, Inc., 2016, pp. 37–62.

[151] S.K. Williams, J.B. Hoying, Bioinks for bioprinting, in: K. Turksen (Ed.), Bioprinting Regen. Med., Humana Press, 2015, pp. 1–137, https://doi.org/10.1007/978-3-319-21386-6.

[152] K. Yue, G.T. Santiago, A. Tamayol, N. Annabi, A. Khademhosseini, W. Hospital, S. Arabia, Synthesis, properties, and biomedical applications of gelatin methacryloyl (GelMA) hydrogels, Biomaterials 73 (2015) 254–271, https://doi.org/10.1016/j.biomaterials.2015.08.045.

[153] Y. Gu, L. Zhang, X. Du, Z. Fan, L. Wang, W. Sun, Y. Cheng, Y. Zhu, C. Chen, Reversible physical crosslinking strategy with optimal temperature for 3D bioprinting of human chondrocyte-laden gelatin methacryloyl bioink, J. Biomater. Appl. 33 (2018) 609–618, https://doi.org/10.1177/0885328218805864.

[154] W. Schuurman, P.A. Levett, M.W. Pot, P.R. van Weeren, W.J.A. Dhert, D.W. Hutmacher, F.P.W. Melchels, T.J. Klein, J. Malda, Gelatin-methacrylamide hydrogels as potential biomaterials for fabrication of tissue-engineered cartilage constructs, Macromol. Biosci. 13 (2013) 551–561, https://doi.org/10.1002/mabi.201200471.

[155] I. Pepelanova, K. Kruppa, T. Scheper, A. Lavrentieva, Gelatin-methacryloyl (GelMA) hydrogels with defined degree of functionalization as a versatile toolkit for 3D cell culture and extrusion bioprinting, Bioengineering 5 (2018), https://doi.org/10.3390/bioengineering5030055.

[156] A. Fallacara, E. Baldini, S. Manfredini, S. Vertuani, Hyaluronic acid in the third millennium, Polymers (2018) 10, https://doi.org/10.3390/polym10070701.

[157] M.A. Serban, A. Skardal, Hyaluronan chemistries for three-dimensional matrix applications, Matrix Biol. 78–79 (2018) 337–345, https://doi.org/10.1016/j.matbio.2018.02.010.

[158] H.D. Kim, S. Amirthalingam, S.L. Kim, S.S. Lee, J. Rangasamy, N.S. Hwang, Biomimetic materials and fabrication approaches for bone tissue engineering, Adv. Healthc. Mater. 6 (2017), https://doi.org/10.1002/adhm.201700612.

[159] G. Gao, A.F. Schilling, T. Yonezawa, J. Wang, G. Dai, X. Cui, Bioactive nanoparticles stimulate bone tissue formation in bioprinted three-dimensional scaffold and human mesenchymal stem cells, Biotechnol. J. 9 (2014) 1304–1311, https://doi.org/10.1002/biot.201400305.

[160] L. Benning, L. Gutzweiler, K. Tröndle, J. Riba, R. Zengerle, P. Koltay, S. Zimmermann, G.B. Stark, G. Finkenzell, Cytocompatibility testing of hydrogels

[161] C. Chircov, A.M. Grumezescu, L.E. Bejenaru, Hyaluronic acid-based scaffolds for tissue engineering, Rom. J. Morphol. Embryol. 59 (2018) 71–76, https://doi.org/10.1016/j.carbpol.2012.10.028.

[162] M.T. Poldervaart, B. Goversen, M. De Ruijter, A. Abbadessa, F.P.W. Melchels, F.C. Öner, W.J.A. Dhert, T. Vermonden, J. Alblas, 3D bioprinting of methacrylated hyaluronic acid (MeHA) hydrogel with intrinsic osteogenicity, PLoS One 12 (2017), e0177628, https://doi.org/10.1371/journal.pone.0177628.

[163] J.H. Sze, J.C. Brownlie, C.A. Love, Biotechnological production of hyaluronic acid: a mini review, Biotechnology 3 (2016) 6, https://doi.org/10.1007/s13205-016-0379-9.

[164] J. Gopinathan, I. Noh, Recent trends in bioinks for 3D printing, Biomater. Res. 22 (2018), https://doi.org/10.1186/s40824-018-0122-1.

[165] M. Hospodiuk, M. Dey, D. Sosnoski, I.T. Ozbolat, The bioink: a comprehensive review on bioprintable materials, Biotechnol. Adv. 35 (2017) 217–239, https://doi.org/10.1016/j.biotechadv.2016.12.006.

[166] V.J. Mkhabela, S.S. Ray, Poly(ε-caprolactone) nanocomposite scaffolds for tissue engineering: a brief overview, J. Nanosci. Nanotechnol. 14 (2014) 535–545, https://doi.org/10.1166/jnn.2014.9055.

[167] P. Vahedi, S. Jarolmasjed, H. Shafaei, L. Roshangar, J. Soleimani Rad, E. Ahmadian, In vivo articular cartilage regeneration through infrapatellar adipose tissue derived stem cell in nanofiber polycaprolactone scaffold, Tissue Cell 57 (2019) 49–56, https://doi.org/10.1016/j.tice.2019.02.002.

[168] G. Gao, A.F. Schilling, K. Hubbell, T. Yonezawa, D. Truong, Y. Hong, G. Dai, X. Cui, Improved properties of bone and cartilage tissue from 3D inkjet-bioprinted human mesenchymal stem cells by simultaneous deposition and photocrosslinking in PEG-GelMA, Biotechnol. Lett. 37 (2015) 2349–2355, https://doi.org/10.1007/s10529-015-1921-2.

[169] A.A. Mieloch, M. Kręcisz, J.D. Rybka, A. Strugała, M. Krupiński, A. Urbanowicz, M. Kozak, B. Skalski, M. Figlerowicz, M. Giersig, The influence of ligand charge and length on the assembly of Brome mosaic virus derived virus-like particles with magnetic core, AIP Adv. 8 (2018), https://doi.org/10.1063/1.5011138.

[170] K. Kucharczyk, J.D. Rybka, M. Hilgendorff, M. Krupinski, M. Slachcinski, A. Mackiewicz, M. Giersig, H. Dams-Kozlowska, Composite spheres made of bioengineered spider silk and iron oxide nanoparticles for theranostics applications, PLoS One 14 (2019), e0219790, https://doi.org/10.1371/journal.pone.0219790.

[171] K.R. Wierzbinski, T. Szymanski, N. Rozwadowska, J.D. Rybka, A. Zimna, T. Zalewski, K. Nowicka-Bauer, A. Malcher, M. Nowaczyk, M. Krupinski, M. Fiedorowicz, P. Bogorodzki, P. Grieb, M. Giersig, M.K. Kurpisz, Potential use of superparamagnetic iron oxide nanoparticles for in vitro and in vivo bioimaging of human myoblasts, Sci. Rep. 8 (2018) 1–17, https://doi.org/10.1038/s41598-018-22018-0.

[172] I. Firkowska, M. Giersig, Carbon nanotube - based three - dimensional matrices for tissue engineering, in: C.S.S.R. Kumar (Ed.), Nanomater. Life Sci. Vol.9 Carbon Nanomater., WILEY-VCH, 2011, pp. 161–185.

[173] N.O. Chahine, N.M. Collette, C.B. Thomas, D.C. Genetos, G.G. Loots, Nanocomposite scaffold for chondrocyte growth and cartilage tissue engineering: effects of carbon nanotube surface functionalization, Tissue Eng. A 20 (2014) 2305–2315, https://doi.org/10.1089/ten.tea.2013.0328.

[174] T. Trzeciak, J.D. Rybka, E.M. Akinoglu, M. Richter, J. Kaczmarczyk, M. Giersig, In vitro evaluation of carbon nanotube-based scaffolds for cartilage tissue engineering, J. Nanosci. Nanotechnol. 16 (2016) 9022–9025, https://doi.org/10.1166/jnn.2016.12733.

[175] E.M. Gonçalves, F.J. Oliveira, R.F. Silva, M.A. Neto, M.H. Fernandes, M. Amaral, M. Vallet-Regí, M. Vila, Three-dimensional printed PCL-hydroxyapatite scaffolds filled with CNTs for bone cell growth stimulation, J. Biomed. Mater. Res. B Appl. Biomater. 104 (2016) 1210–1219, https://doi.org/10.1002/jbm.b.33432.

[176] M. Kręcisz, J.D. Rybka, A.J. Strugała, B. Skalski, M. Figlerowicz, M. Kozak, M. Giersig, Interactions between magnetic nanoparticles and model lipid bilayers - fourier transformed infrared spectroscopy (FTIR) studies of the molecular basis of nanotoxicity, J. Appl. Phys. 120 (2016), https://doi.org/10.1063/1.4962951.

[177] R. Eivazzadeh-Keihan, A. Maleki, M. de la Guardia, M.S. Bani, K.K. Chenab, P. Pashazadeh-Panahi, B. Baradaran, A. Mokhtarzadeh, M.R. Hamblin, Carbon based nanomaterials for tissue engineering of bone: building new bone on small black scaffolds: a review, J. Adv. Res. 18 (2019) 185–201, https://doi.org/10.1016/j.jare.2019.03.011.

[178] A.P. Francis, T. Devasena, Toxicity of carbon nanotubes: a review, Toxicol. Ind. Health 34 (2018) 200–210, https://doi.org/10.1177/0748233717747472.

[179] N. Sahai, M. Gogoi, Techniques and software used in 3D printing for nanomedicine applications, in: 3D Print. Technol. Nanomedicine, Elsevier, 2019, pp. 23–41, https://doi.org/10.1016/b978-0-12-815890-6.00002-5.

[180] M. Varkey, A. Atala, Current challenges and future perspectives of bioprinting, in: A. Khademhosseini, G. Camci-Unal (Eds.), 3D Bioprinting Regen. Eng., CRC Press, 2018, pp. 359–373.

[181] J. Li, M. Chen, X. Fan, H. Zhou, Recent advances in bioprinting techniques: approaches, applications and future prospects, J. Transl. Med. 14 (2016) 1–15, https://doi.org/10.1186/s12967-016-1028-0.

[182] G. Filardo, M. Petretta, C. Cavallo, L. Roseti, S. Durante, U. Albisinni, B. Grigolo, Patient-specific meniscus prototype based on 3D bioprinting of human cell-laden scaffold, Bone Joint Res. 8 (2019) 101–106, https://doi.org/10.1302/2046-3758.82.BJR-2018-0134.R1.

[183] L. Li, F. Yu, J. Shi, S. Shen, H. Teng, J. Yang, X. Wang, Q. Jiang, In situ repair of bone and cartilage defects using 3D scanning and 3D printing, Sci. Rep. 7 (2017) 1–12, https://doi.org/10.1038/s41598-017-10060-3.

[184] C. Mandrycky, Z. Wang, K. Kim, D. Kim, 3D bioprinting for engineering complex tissues, Biotechnol. Adv. 34 (2016) 422–434, https://doi.org/10.1016/j.biotechadv.2015.12.011.

[185] V.H.M. Mouser, R. Levato, A. Mensinga, W.J.A. Dhert, D. Gawlitta, J. Malda, Bio-ink development for three-dimensional bioprinting of hetero-cellular cartilage constructs, Connect. Tissue Res. (2018), https://doi.org/10.1080/03008207.2018.1553960.

[186] C.V.B. de Gusmo, J.R. Lenzi Mariolani, W. Dias, Mechanotransduction and osteogenesis, in: Y. Lin (Ed.), Osteogenesis, InTech, 2012, pp. 153–182, https://doi.org/10.5772/34504.

[187] S. Chameettachal, F. Pati, Inkjet-based 3D bioprinting, in: A. Khademhosseini, G. Camci-Unal (Eds.), 3D Bioprinting Regen. Eng. Princ. Appl., Taylor & Francis Group, 2018, pp. 99–118.

[188] N. Morita, A.A. Khalate, A.M. van Buul, H. Wijshoff, Inkjet printheads, in: S.D. Hoath (Ed.), Fundam. Inkjet Print., Wiley-VCH Verlag GmbH & Co., 2016, pp. 57–92.

[189] K. Hölzl, S. Lin, L. Tytgat, S. Van Vlierberghe, Linxia Gu, A. Ovsianikov, Bioink properties before, during and after 3D bioprinting, Biofabrication 8 (2016).

[190] X. Cui, K. Breitenkamp, M.G. Finn, M. Lotz, D.D. D'Lima, Direct human cartilage repair using three-dimensional bioprinting technology, Tissue Eng. A 18 (2012) 1304–1312, https://doi.org/10.1089/ten.tea.2011.0543.

[191] X. Cui, G. Gao, T. Yonezawa, G. Dai, Human cartilage tissue fabrication using three-dimensional inkjet printing technology, J. Vis. Exp. (2014), https://doi.org/10.3791/51294.

[192] L. Raddatz, A. Lavrentieva, I. Pepelanova, J. Bahnemann, D. Geier, T. Becker, T. Scheper, S. Beutel, Development and application of an additively manufactured calcium chloride nebulizer for alginate 3D-bioprinting purposes, J. Funct. Biomater. 9 (2018), https://doi.org/10.3390/jfb9040063.

[193] T. Xu, K.W. Binder, M.Z. Albanna, D. Dice, W. Zhao, J.J. Yoo, A. Atala, Hybrid printing of mechanically and biologically improved constructs for cartilage tissue engineering applications, Biofabrication 5 (2013), 015001, https://doi.org/10.1088/1758-5082/5/1/015001.

[194] Y. Huang, X.F. Zhang, G. Gao, T. Yonezawa, X. Cui, 3D bioprinting and the current applications in tissue engineering, Biotechnol. J. 12 (2017), https://doi.org/10.1002/biot.201600734.

[195] Y.S. Zhang, Q. Pi, A.M. van Genderen, Microfluidic bioprinting for engineering vascularized tissues and organoids, J. Vis. Exp. (2017), e55957, https://doi.org/10.3791/55957.

[196] A. Kosik-Kozioł, M. Costantini, A. Mróz, J. Idaszek, M. Heljak, J. Jaroszewicz, E. Kijeńska, K. Szöke, N. Frerker, A. Barbetta, J.E. Brinchmann, W. Święszkowski, 3D bioprinted hydrogel model incorporating β-tricalcium phosphate for calcified cartilage tissue engineering, Biofabrication 11 (2019), 035016, https://doi.org/10.1088/1758-5090/ab15cb.

[197] K. Zhu, N. Chen, X. Liu, X. Mu, W. Zhang, C. Wang, Y.S. Zhang, A general strategy for extrusion bioprinting of bio-macromolecular bioinks through alginate-templated dual-stage crosslinking, Macromol. Biosci. 18 (2018), https://doi.org/10.1002/mabi.201800127.

[198] W. Zhu, H. Cui, B. Boualam, F. Masood, E. Flynn, R.D. Rao, Z.Y. Zhang, L.G. Zhang, 3D bioprinting mesenchymal stem cell-laden construct with core-shell nanospheres for cartilage tissue engineering, Nanotechnology 29 (2018) 185101, https://doi.org/10.1088/1361-6528/aaafa1.

[199] C. Di Bella, S. Duchi, C.D. O'Connell, R. Blanchard, C. Augustine, Z. Yue, F. Thompson, C. Richards, S. Beirne, C. Onofrillo, S.H. Bauquier, S.D. Ryan, P. Pivonka, G.G. Wallace, P.F. Choong, In situ handheld three-dimensional bioprinting for cartilage regeneration, J. Tissue Eng. Regenerat. Med. 12 (2018) 611–621, https://doi.org/10.1002/term.2476.

[200] S. Duchi, C. Onofrillo, C.D. O'Connell, R. Blanchard, C. Augustine, A.F. Quigley, R.M.I. Kapsa, P. Pivonka, G. Wallace, C. Di Bella, P.F.M. Choong, Handheld co-axial bioprinting: application to in situ surgical cartilage repair, Sci, For. Rep. 7 (2017), https://doi.org/10.1038/s41598-017-05699-x.

[201] C. Onofrillo, S. Duchi, C.D. O'Connell, R. Blanchard, A.J. O'Connor, M. Scott, G.G. Wallace, P.F.M. Choong, C. Di Bella, Biofabrication of human articular cartilage: a path towards the development of a clinical treatment, Biofabrication 10 (2018), 045006, https://doi.org/10.1088/1758-5090/aad8d9.

[202] J. Kundu, J.H. Shim, J. Jang, S.W. Kim, D.W. Cho, An additive manufacturing-based PCL–alginate–chondrocyte bioprinted scaffold for cartilage tissue engineering, J. Tissue Eng. Regenerat. Med. 9 (2013) 1286–1297, https://doi.org/10.1002/term.1682.

[203] J.H. Shim, J.S. Lee, J.Y. Kim, D.W. Cho, Bioprinting of a mechanically enhanced three-dimensional dual cell-laden construct for osteochondral tissue engineering using a multi-head tissue/organ building system, J. Micromech. Microeng. 22 (2012), https://doi.org/10.1088/0960-1317/22/8/085014.

[204] J.H. Shim, K.M. Jang, S.K. Hahn, J.Y. Park, H. Jung, K. Oh, K.M. Park, J. Yeom, S.H. Park, S.W. Kim, J.H. Wang, K. Kim, D.W. Cho, Three-dimensional bioprinting of multilayered constructs containing human mesenchymal stromal cells for osteochondral tissue regeneration in the rabbit knee joint, Biofabrication 8 (2016), 014102, https://doi.org/10.1088/1758-5090/8/1/014102.

[205] J.M. Baena, G. Jiménez, E. López-Ruiz, C. Antich, C. Griñán-Lisón, M. Perán, P. Gálvez-Martín, J.A. Marchal, Volume-by-volume bioprinting of chondrocytes-alginate bioinks in high temperature thermoplastic scaffolds for cartilage regeneration, Exp. Biol. Med. 244 (2019) 13–21, https://doi.org/10.1177/1535370218821128.

[206] B.T. Vinson, S.C. Sklare, Y. Huang, D.B. Chrisey, Laser-based 3D bioprinting, in: A. Khademhosseini, G. Camci-Unal (Eds.), 3D Bioprinting Regen. Eng. Princ. Appl., Taylor & Francis Group, 2018, pp. 77–98.

[207] V. Keriquel, H. Oliveira, M. Rémy, S. Ziane, S. Delmond, B. Rousseau, S. Rey, S. Catros, J. Amédée, F. Guillemot, J.C. Fricain, In situ printing of mesenchymal stromal cells, by laser-assisted bioprinting, for in vivo bone regeneration applications, Sci. Rep. 7 (2017), https://doi.org/10.1038/s41598-017-01914-x.

[208] F.P.W. Melchels, J. Feijen, D.W. Grijpma, A review on stereolithography and its applications in biomedical engineering, Biomaterials 31 (2010) 6121–6130, https://doi.org/10.1016/j.biomaterials.2010.04.050.

[209] A.X. Sun, H. Lin, A.M. Beck, E.J. Kilroy, R.S. Tuan, Projection stereolithographic fabrication of human adipose stem cell-incorporated biodegradable scaffolds for cartilage tissue engineering, Front. Bioeng. Biotechnol. 3 (2015) 115, https://doi.org/10.3389/fbioe.2015.00115.

[210] T. Lam, T. Dehne, J.P. Krüger, S. Hondke, M. Endres, A. Thomas, R. Lauster, M. Sittinger, L. Kloke, Photopolymerizable gelatin and hyaluronic acid for stereolithographic 3D bioprinting of tissue-engineered cartilage, J. Biomed. Mater. Res. B Appl. Biomater. (2019), https://doi.org/10.1002/jbm.b.34354.

[211] M. Costantini, J. Idaszek, K. Szöke, J. Jaroszewicz, M. Dentini, A. Barbetta, J.E. Brinchmann, W. Święszkowski, 3D bioprinting of BM-MSCs-loaded ECM biomimetic hydrogels for in vitro neocartilage formation, Biofabrication 8 (2016), 035002, https://doi.org/10.1088/1758-5090/8/3/035002.

[212] K. Markstedt, A. Mantas, I. Tournier, H. Martínez Ávila, D. Hägg, P. Gatenholm, 3D bioprinting human chondrocytes with nanocellulose-alginate bioink for cartilage tissue engineering applications, Biomacromolecules 16 (2015) 1489–1496, https://doi.org/10.1021/acs.biomac.5b00188.

[213] P. Apelgren, M. Amoroso, A. Lindahl, C. Brantsing, N. Rotter, P. Gatenholm, L. Kölby, Chondrocytes and stem cells in 3D-bioprinted structures create human cartilage in vivo, PLoS One 12 (2017), e0189428, https://doi.org/10.1371/journal.pone.0189428.

[214] T. Möller, M. Amoroso, D. Hägg, C. Brantsing, N. Rotter, P. Apelgren, A. Lindahl, L. Kölby, P. Gatenholm, In vivo chondrogenesis in 3D bioprinted human cell-laden hydrogel constructs, Plast. Reconstr. Surg. Glob. Open 5 (2017) e1227, https://doi.org/10.1097/GOX.0000000000001227.

[215] M. Kamitakahara, C. Ohtsuki, T. Miyazaki, Review paper: behavior of ceramic biomaterials derived from tricalcium phosphate in physiological condition, J. Biomater. Appl. 23 (2008) 197–212, https://doi.org/10.1177/0885328208096798.

[216] W.J. Kim, H.S. Yun, G.H. Kim, An innovative cell-laden α-TCP/collagen scaffold fabricated using a two-step printing process for potential application in regenerating hard tissues, Sci. Rep. 7 (2017), https://doi.org/10.1038/s41598-017-03455-9.

[217] Z. Li, S. Huang, Y. Liu, B. Yao, T. Hu, H. Shi, J. Xie, X. Fu, Tuning alginate-gelatin bioink properties by varying solvent and their impact on stem cell behavior, Sci. Rep. 8 (2018), https://doi.org/10.1038/s41598-018-26407-3.

[218] M. Di Guiseppe, N. Law, B. Webb, R.A. Macrae, L.J. Liew, T.B. Sercombe, R.J. Dilley, B.J. Doyle, Mechanical behaviour of alginate-gelatin hydrogels for 3D bioprinting, J. Mech. Behav. Biomed. Mater. 79 (2018) 150–157, https://doi.org/10.1016/j.jmbbm.2017.12.018.

[219] T. Zehnder, B. Sarker, A.R. Boccaccini, R. Detsch, Evaluation of an alginate-gelatine crosslinked hydrogel for bioplotting, Biofabrication 7 (2015), 025001, https://doi.org/10.1088/1758-5090/7/2/025001.

[220] X. Zhai, C. Ruan, Y. Ma, D. Cheng, M. Wu, W. Liu, X. Zhao, H. Pan, W.W. Lu, 3D-bioprinted osteoblast-laden nanocomposite hydrogel constructs with induced microenvironments promote cell viability, differentiation, and osteogenesis both in vitro and in vivo, Adv. Sci. 5 (2018), 1700550, https://doi.org/10.1002/advs.201700550.

[221] S.T. Bendtsen, M. Wei, In vitro evaluation of 3D bioprinted tri-polymer network scaffolds for bone tissue regeneration, J. Biomed. Mater. Res. A 105 (2017) 3262–3272, https://doi.org/10.1002/jbm.a.36184.

[222] S.T. Bendtsen, S.P. Quinnell, M. Wei, Development of a novel alginate-polyvinyl alcohol-hydroxyapatite hydrogel for 3D bioprinting bone tissue engineered scaffolds, J. Biomed. Mater. Res. A 105 (2017) 1457–1468, https://doi.org/10.1002/jbm.a.36036.

[223] A. Abbadessa, V.H.M. Mouser, M.M. Blokzijl, D. Gawlitta, W.J.A. Dhert, W.E. Hennink, J. Malda, T. Vermonden, A synthetic thermosensitive hydrogel for cartilage bioprinting and its biofunctionalization with polysaccharides, Biomacromolecules 17 (2016) 2137–2147, https://doi.org/10.1021/acs.biomac.6b00366.

[224] B. Byambaa, N. Annabi, K. Yue, G. Trujillo-de Santiago, M.M. Alvarez, W. Jia, M. Kazemzadeh-Narbat, S.R. Shin, A. Tamayol, A. Khademhosseini, Bioprinted osteogenic and vasculogenic patterns for engineering 3D bone tissue, Adv. Healthc. Mater. 6 (2017), https://doi.org/10.1002/adhm.201700015.

[225] H. Cui, W. Zhu, M. Nowicki, X. Zhou, A. Khademhosseini, L.G. Zhang, Hierarchical fabrication of engineered vascularized bone biphasic constructs via dual 3D bioprinting: integrating regional bioactive factors into architectural design, Adv. Healthc. Mater. 5 (2016) 2174–2181, https://doi.org/10.1002/adhm.201600505.

[226] M. Du, B. Chen, Q. Meng, S. Liu, X. Zheng, C. Zhang, H. Wang, H. Li, N. Wang, J. Dai, 3D printing of BMSC-laden methacrylamide gelatin scaffolds with CBD-BMP2-collagen microfibers, Biofabrication 7 (2015), 044104, https://doi.org/10.1088/1758-5090/7/4/044104.

[227] C. Piard, H. Baker, T. Kamalitdinov, J. Fisher, Bioprinted osteon-like scaffolds enhance in vivo neovascularization, Biofabrication 11 (2019), 025013, https://doi.org/10.1088/1758-5090/ab078a.

[228] A.C. Daly, G.M. Cunniffe, B.N. Sathy, O. Jeon, E. Alsberg, D.J. Kelly, 3D bioprinting of developmentally inspired templates for whole bone organ engineering, Adv. Healthc. Mater. 5 (2016) 2353–2362, https://doi.org/10.1002/adhm.201600182.

[229] N.E. Fedorovich, W. Schuurman, H.M. Wijnberg, H.-J. Prins, P.R. van Weeren, J. Malda, J. Alblas, W.J.A. Dhert, Biofabrication of osteochondral tissue equivalents by printing topologically defined, cell-laden hydrogel scaffolds, Tissue Eng. C Methods 18 (2012) 33–44, https://doi.org/10.1089/ten.tec.2011.0060.

[230] S. Romanazzo, S. Vedicherla, C. Moran, D.J. Kelly, Meniscus ECM-functionalised hydrogels containing infrapatellar fat pad-derived stem cells for bioprinting of regionally defined meniscal tissue, J. Tissue Eng. Regenerat. Med. 12 (2018) e1826–e1835, https://doi.org/10.1002/term.2602.

[231] S.L. Francis, C. Di Bella, G.G. Wallace, P.F.M. Choong, Cartilage tissue engineering using stem cells and bioprinting technology—barriers to clinical translation, Front. Surg. 5 (2018) 1–12, https://doi.org/10.3389/fsurg.2018.00070.

[232] A. Kumar, J. Ahlawat, M. Narayan, 3D bioprinting for organs, skin, and engineered tissues, in: N. Ahmad, P. Gopinath, R. Dutta (Eds.), 3D Print. Technol. Nanomedicine, Elsevier, 2019, pp. 115–128, https://doi.org/10.1016/b978-0-12-815890-6.00006-2.

[233] Y. Huang, X.F. Zhang, G. Gao, T. Yonezawa, X. Cui, 3D bioprinting and the current applications in tissue engineering, Biotechnol. J. 12 (2017), https://doi.org/10.1002/biot.201600734.

[234] A.C. Daly, P. Pitacco, J. Nulty, G.M. Cunniffe, D.J. Kelly, 3D printed microchannel networks to direct vascularisation during endochondral bone repair, Biomaterials 162 (2018) 34–46, https://doi.org/10.1016/j.biomaterials.2018.01.057.

[235] B. Grigoryan, S.J. Paulsen, D.C. Corbett, D.W. Sazer, C.L. Fortin, A.J. Zaita, P.T. Greenfield, N.J. Calafat, J.P. Gounley, A.H. Ta, F. Johansson, A. Randles, J.E. Rosenkrantz, J.D. Louis-Rosenberg, P.A. Galie, K.R. Stevens, J.S. Miller, Multivascular networks and functional intravascular topologies within biocompatible hydrogels, Science 364 (80) (2019) 458–464, https://doi.org/10.1126/science.aav9750.

[236] A. Lee, A.R. Hudson, D.J. Shiwarski, J.W. Tashman, T.J. Hinton, S. Yerneni, J.M. Bliley, P.G. Campbell, A.W. Feinberg, 3D bioprinting of collagen to rebuild components of the human heart, Science 365 (80) (2019) 482–487, https://doi.org/10.1126/science.aav9051.

[237] J.H. Park, J.K. Yoon, J.B. Lee, Y.M. Shin, K.W. Lee, S.W. Bae, J.H. Lee, J.J. Yu, C.R. Jung, Y.N. Youn, H.Y. Kim, D.H. Kim, Experimental tracheal replacement using 3-dimensional bioprinted artificial trachea with autologous epithelial cells and chondrocytes, Sci. Rep. 9 (2019) 1–11, https://doi.org/10.1038/s41598-019-38565-z.

[238] F. Gilbert, J.N.M. Viaña, C.D. O'Connell, S. Dodds, Enthusiastic portrayal of 3D bioprinting in the media: ethical side effects, Bioethics 32 (2018) 94–102, https://doi.org/10.1111/bioe.12414.

[239] F. Gilbert, C.D. O'Connell, T. Mladenovska, S. Dodds, Print me an organ? Ethical and regulatory issues emerging from 3D bioprinting in medicine, Sci. Eng. Ethics 24 (2018) 73–91, https://doi.org/10.1007/s11948-017-9874-6.

Julia Semba

Laboratory of Applied Biotechnology
Center for Advanced Technology
Adam Mickiewicz University in Poznan
e-mail: jsemba@amu.edu.pl
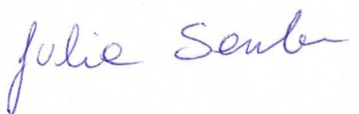
Author contribution statement

I declare that I am the first author of the article "Introduction to the state-of-the-art 3D bioprinting methods, design, and applications in orthopedics" by Julia Anna Semba, Adam Aron Mieloch, and Jakub Dalibor Rybka, published in *Bioprinting* in 2020. The author's contribution is as follows:

Julia Semba reviewed the literature and wrote the original draft with all the figures.

Adam Mieloch designed the study and revised the manuscript.

Jakub Rybka designed the study, supervised the technical part of the research, and revised the manuscript. Jakub Rybka acquired funding and corresponded with the journal and reviewers.

Date: 18.08.2023
Signature: *Julie Semba*

prof. UAM dr hab. Inż. Jakub D. Rybka

Dr Adam Mieloch

Laboratory of Applied Biotechnology
Center for Advanced Technology
Adam Mickiewicz University in Poznan
e-mail: amieloch@amu.edu.pl

Author contribution statement

I declare that I am the co-author of the article "Introduction to the state-of-the-art 3D bioprinting methods, design, and applications in orthopedics" by Julia Anna Semba, Adam Aron Mieloch, and Jakub Dalibor Rybka, published in *Bioprinting* in 2020 and I am aware that this publication is a part of Julia Semba PhD dissertation. The author's contribution is as follows:

Julia Semba reviewed the literature and wrote the original draft with all the figures.

Adam Mieloch designed the study and revised the manuscript.

Jakub Rybka designed the study, supervised the technical part of the research, and revised the manuscript. Jakub Rybka acquired funding and corresponded with the journal and reviewers.

Date: 21. 08. 2023

Signature:

Dr hab. inż. Jakub Rybka, prof. UAM

Laboratory of Applied Biotechnology
Center for Advanced Technology
Adam Mickiewicz University in Poznan
e-mail: jrybka@amu.edu.pl

Author contribution statement

I declare that I am the corresponding author of the article "Introduction to the state-of-the-art 3D bioprinting methods, design, and applications in orthopedics" by Julia Anna Semba, Adam Aron Mieloch, and Jakub Dalibor Rybka, published in *Bioprinting* in 2020 and I am aware that this publication is a part of Julia Semba PhD dissertation. The author's contribution is as follows:

Julia Semba reviewed the literature and wrote the original draft with all the figures.

Adam Mieloch designed the study and revised the manuscript.

Jakub Rybka designed the study, supervised the technical part of the research, and revised the manuscript. Jakub Rybka acquired funding and corresponded with the journal and reviewers.

Date: 1 8. 08. 2023

Signature:

prof. UAM dr hab. inż. Jakub D. Rybka

3D Bioprinting in Skin Related Research: Recent Achievements and Application Perspectives

Anna Olejnik, Julia Anna Semba, Adam Kulpa, Aleksandra Dańczak-Pazdrowska, Jakub Dalibor Rybka,* and Justyna Gornowicz-Porowska*

ACCESS | Metrics & More | Article Recommendations

ABSTRACT: In recent years, significant progress has been observed in the field of skin bioprinting, which has a huge potential to revolutionize the way of treatment in injury and surgery. Furthermore, it may be considered as an appropriate platform to perform the assessment and screening of cosmetic and pharmaceutical formulations. Therefore, the objective of this paper was to review the latest advances in 3D bioprinting dedicated to skin applications. In order to explain the boundaries of this technology, the architecture and functions of the native skin were briefly described. The principles of bioprinting methods were outlined along with a detailed description of key elements that are required to fabricate the skin equivalents. Next, the overview of recent progress in 3D bioprinting studies was presented. The article also highlighted the potential applications of bioengineered skin substituents in various fields including regenerative medicine, modeling of diseases, and cosmetics/drugs testing. The advantages, limitations, and future directions of this technology were also discussed.

KEYWORDS: *bioequivalents, three-dimensional skin bioprinting, bioinks, skin substituents, bioprinting methods, 3D bioprinters*
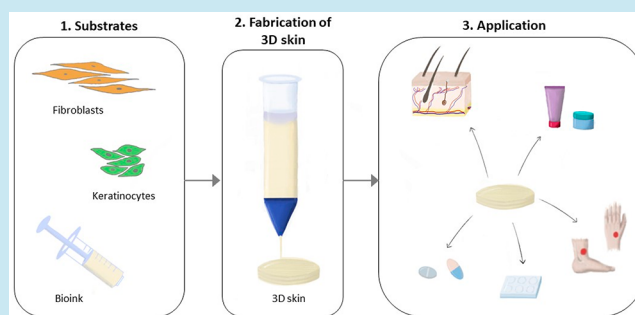
1. INTRODUCTION

Over the past decade, 3D bioprinting has gained worldwide significant attention from scientists involved in biological, medical, and pharmaceutical studies. In the beginning, it is essential to understand the difference between 3D printing and 3D bioprinting. In the first technique, layers of materials (plastics, metal, polymer resins, rubber) are created to obtain a three-dimensional structure. It is used to manufacture 3D-shaped objects. This technology has found applications in various fields including medicine, dentistry, engineering, architecture, agriculture, aerospace, and product design.[1−3] In the medical area, it serves to produce anatomical models, implants, prosthetics, therapeutic devices, surgical instruments, specialized tools, and 3D plastic models that assist surgeons in operations.[4,5] In radiology, patient-specific physical three-dimensional models can be designed from medical images that enable us to solve and analyze surgical problems.[6] The possibility to use data from computed tomography or magnetic resonance imaging is the appreciable advantage in preoperative planning of complex operations, in particular in transplantology, oral and maxillofacial surgery, or congenital heart disease.[7−9] The clinical trials in preoperative planning were also registered in orthopedics and maxillofacial surgery.[10] Likewise, there is activity to print synthetic, personalized implants and patient specific instruments. Moreover, 3D printing is useful to

recognize visible abnormalities and confront them with imaging techniques.[4] In turn, bioprinting is an innovative technology that is applied to obtain three-dimensional complex structures using cells, biomaterials, and biological molecules.[11,12] In simple terms, bioprinting functions in a similar way to standard 3D printing; however, the conventional ink is replaced by bioink that comprises cells and biomaterials required to form tissue constructs with a high degree of repeatability, flexibility, and accuracy.[11,13] Due to the computer-driven bioprinters, the cells and biomaterials can be deposited precisely in order to achieve the predefined structures. Generally, three stages can be distinguished in bioprinting. Initially, precise information about tissues/organs should be collected to select appropriate materials and to define models. Second, the information is transferred into an electrical signal to provide the control under the printer to fabricate the tissues. In the last step, the stable structure is developed.[14−17] 3D bioprinting belongs to the Additive Manufacturing technology that may have a broad
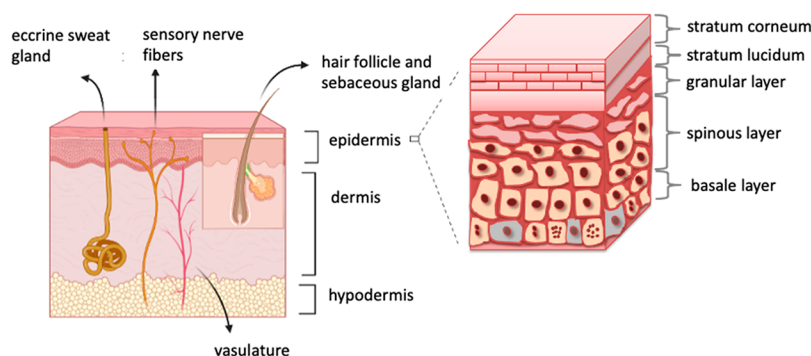
Figure 1. Schematic structure of the skin: the stratum corneum (the outmost layer), the viable epidermis, and the dermis.

spectrum of applications including tissue engineering,[18] transplantation,[16] drug screening, cancer research,[19] cardiovascular and regenerative medicine,[20] as well as dentistry.[21] This method can be applied to regenerate the tooth-like composite tissues and enables us to control their shapes. Furthermore, bioprinting was also used to regenerate cartilage and bones.[22,23]

This technology also gives the opportunity to fabricate skin by using selected types of cells. Up until now, a skin equivalent that contains all skin elements has not been printed. However, the technology is still in the developing stage. The bioprinted skin constructs were first fabricated by Lee and collaborators in 2009, who added human dermal fibroblasts to a collagen hydrogel.[24] At the same time Koch et al.[25] focused attention on bioprinting skin equivalents by adding to collagen bioink keratinocytes and fibroblasts. In 2010, Binder et al. applied for the first time the 3D inkjet-printer skin substitutes using human fibroblasts and keratinocytes to repair wounds.[26] Since that time, significant progress in this field has been observed. The aim of this paper is to review the latest advances in 3D bioprinting dedicated to skin applications.

2. SKIN ARCHITECTURE AND FUNCTION

The skin is the largest organ of the human body, which is characterized by multidimensional architecture. It consists of unique, structurally different layers with specific properties: epidermis, dermis, and hypodermis (Figure 1). The skin is responsible for many vital functions which are compartment-dependent; however, skin layers often act synergistically.[27−33] Thus, one of the key problems of skin fabrication using bioprinting techniques is not only to deposit the skin layers but also to precisely reproduce a biomimetic tissue.[34] The epidermis is the outermost layer of the skin. It is a stratified structure composed of several well-defined layers: basal (which is a germinal layer), spinous, granular, and stratum corneum. The latter is the result of the maturation and differentiation of keratinocytes, which account for 95% of all epidermal cells. The enucleated, densely packed keratinocytes of the stratum corneum, called corneocytes, are surrounded by a lipid matrix and form a "brick and mortar" structure, which is the main component of a proper epidermal barrier protecting against external insults (biological, physical, chemical) and restricting water loss. However, it should be stressed that keratinocytes are also a part of immunological defense. Other epidermal cells which play an important role in skin physiology include melanocytes (pigment-producing cells responsible for the protection of mitotically active cells from UV damage) and Langerhans cells (antigen-presenting cells that have a key role in the adaptive immune response).

There is a dermo-epidermal junction between the epidermis and the dermis made of proteins and proteoglycans. It is involved in the signaling between cells and in cell migration during the healing process. The dermis is a fibrous connective tissue made up of fibers (mainly collagen and elastic in smaller amounts), various cells (of which fibroblasts are the most numerous, but also some others like mast cells, histiocytes, or dendrocytes can be found), and a ground substance (with high water binding capacity). It is worth emphasizing that contrary to the epidermis, the dermis is largely acellular. Besides its role in adaptive and innate immunological defense, the dermis is responsible for the mechanical strength, resilience, and elasticity of the skin. Additionally, unlike the epidermis, the dermis houses blood and lymphatic vessels, several kinds of nerve endings, and appendages (apocrine and eccrine sweat glands as well as the complex structures called pilosebaceous units). Nerve endings are responsible for one of the most important functions of the skin, which is receiving stimuli from the environment. The eccrine glands together with blood vessels play a role in thermoregulation. Sebum from sebaceous glands creates a lipid film at the epidermal surface, thus enhancing the function of the epidermal barrier. The innermost layer of the skin is the subcutaneous tissue, which consists mainly of adipocytes and connective tissue septa. Their role includes insulation, mechanical cushioning, and energy storage, but they are also immunologically active.[35,36]

In the end, inhabiting microbiota together with the correct skin structure play an integral role for optimal barrier function, pathogen defense, and tissue repair with the production of essential anti-inflammatory and antimicrobial molecules to maintain skin homeostasis.[37] Eventually, future perspectives of skin biofabrication should include research on ecosystems of obtained equivalents. The skin disruptions and declining microbial diversity may be linked to allergic as well inflammatory skin diseases. As described above, the complete architecture and function of the skin depend on all layers and their microstructure, which determine the skin's proper function. In light of this, obtaining a tissue-engineered skin equivalent reflecting biomechanical properties seems to be a real challenge.

3. BIOPRINTING

Bioprinting is a promising technique for the commercial manufacturing of tissue constructs for regenerative medicine. This method utilizes a computer-controlled three-dimensional (3D) printer for the precise depositing of bioinks composed of viable cells, biomaterials, and additional biological substances in a layer-by-layer manner.[38] The bioprinted cell-laden scaffolds aimed to promote and support new tissue formation by

Table 1. Comparison of Methods Applied in Skin Bioprinting[47−50]

method	printing process	accuracy	pros	cons	ref.
Extrusion bioprinting	line by line	medium-low	low cost, simplicity, printability of high cell density and highly viscous bioinks	clogging nozzles, mechanical stresses generated while bioink deposition	34,51−53
Inkjet-based biopritning	drop by drop	medium	low cost, high cell viability, high resolution, high throughput, noncontact printing	limited bioink, low strength, nozzle clogging, risk of exposing cells to mechanical and thermal stress, possibility of cell agglomeration and sedimentation	28,41,54,55
Laser-assisted bioprinting	drop by drop	high	high cell viability, noncontact, nozzle-free, high precision and resolution	low scalability, low flow rate caused by fast gelation, time-consuming	28,56,57

providing a suitable environment for cell migration, proliferation, differentiation, and ensuring proper ECM secretion. Furthermore, this technique enables the creation of constructs that mimic the architecture of patient-specific spatial geometry with the control position of cells similar to native tissue structure.[39] There are even attempts to create a methodology for in situ skin bioprinting.[40,41]

3.1. 3D Bioprinting Methods. There are three main techniques of 3D bioprinting, which were compared in Table 1. The most popular one is extrusion bioprinting that applied pneumatic pressure or mechanical pistons for continuous deposition of bioinks.[42,43] In skin tissue engineering, it is also the most widely used method. It is characterized by high printing speed, affordability, and scalability of printed models. Extrusion bioprinting allows using wider types of biomaterials since high viscous materials can be utilized. However, the clogging of the nozzle is a frequently observed problem.

Another technology applied in skin construct production is inkjet-based bioprinting.[44,45] The technique uses a drop-on-demand printing mode usually by utilization of thermal or piezoelectric effects. In thermal bioprinting, a small heater in the printhead uses high temperatures to generate vapor bubbles within the bioink.[46] These bubbles create the pressure pulse that extrudes bioink. In the second approach, the piezoelectric actuator converts the applied voltage into the deformation of a crystal.

These changes produce the pressure required for the drop ejection. The bioink for inkjet bioprinting should have low viscosities that affect the mechanical properties of final scaffolds.[11] Nevertheless, this method is fast and relatively cheap. Lastly, laser-assisted bioprinting (LAB) is also applied for skin biofabrication.[56,58,59] This is a noncontact, nozzle-free method where a laser beam is absorbed by the ribbon that generates a local bubble in bioink on the opposite side. LAB is applied for bioprinting with high cell density bioinks at a resolution of nearly a single cell. The final constructs can be printed in three different forms such as cell-suspensions, cell-encapsulated hydrogels, or cell-free models.[60]

3.2. Bioink. The bioink formulation is a pivotal step as its composition and structure affect the phenotype of the developing tissue.[11,39] The mechanical and physical properties of bioink need to ensure printability and correspond to engineering tissue. The biodegradation rate of bioink should be adjusted to the cell capacity to remodel the extracellular matrix (ECM), while the products of degradation cannot be toxic or immunogenic. Despite the growing number of biomaterials used in bioprinting, only a subset of them is suitable for skin bioprinting. These biomaterials are briefly described below.

3.2.1. Collagen. Collagen is the most abundant protein in the mammalian ECM and, hence, it is widely used in tissue engineering.[39] It has excellent biocompatibility with low immunogenicity and toxicity. There are 28 types of collagen present in vertebrates.[61] Collagen type I makes up most of the protein mass in the connective tissues of mammals; hence, it is frequently utilized for bioink production. Unfortunately, the main limitations of collagen use are its low mechanical stability, poor solubility, cost, and fibrotic tissue formation. Neutralized collagen solution heated to a temperature of 20−37 °C self-assembles into a physically cross-linked hydrogel that provides structural and biological support for cells.[62,63] However, collagen gelation at physiological temperatures is slow so it is frequently mixed with other biomaterials. Collagen type I-based bioink has been used for extrusion skin bioprinting.[24,45] In these studies, the collagen layers and the cell layers (fibroblast and keratinocytes) were printed separately. The printed model retained form, shape, and was morphologically and biologically similar to human skin tissue. In addition, constructs were cultured at the air−liquid interface to promote epidermal maturation.[45]

3.2.2. Gelatin. Gelatin, an irreversibly denatured form of collagen, is frequently used for bioink formulation instead of collagen. Gelatin retains many similar features of collagen including cell adhesion sites and cytocompatibility; however, it has a significantly lower price and better water solubility than collagen.[64] Gelatin is unable to form long fibrils.[65] Instead, local regions of triple helices on different gelatin strands interact to form physical cross-links that are responsible for gelation at lower temperatures (below 30 °C).[65] Hence, the viscosity of gelatin-based bioinks can be easily changed by altering the temperature and concentration of gelatin. The application of gelatin-based bioinks for skin tissue engineering showed promising results in the promotion of epithelialization and granulation in the wound healing process.[66] However, the gelation of gelatin is a thermoreversible process, so its bonds are easily broken in a physiologic environment. Hence, gelatin is frequently blended with alginate for bioink production.

3.2.3. Alginate. Alginate, the most popular biomaterial used for 3D bioprinting, is a linear and negatively charged polymer composed of two uronic acid monomers.[67] This material has low toxicity and is cheap and nonimmunogenic. Alginate lacks cell and protein binding properties, so the addition of extra positively charged biomaterials is required to achieve cell adhesion.[68,69] Alginate-based bioinks are cross-linked by divalent cations, which is described by the "egg-box" model.[70] The most popular cross-linking solution is $CaCl_2$.[39,71] This cross-linking method is fast and heterogeneous, but is hard to bioprint. Hence, as mentioned previously, alginate is mixed with other materials, like gelatin. In terms of skin fabrication, the alginate/gelatin bioink with proper rheological parameters was also proposed.[69] This bioink composition is subjected to two-step polymerization, namely thermal and ionic.

3.2.4. Chitosan. Chitosan is a deacetylated derivative of natural chitin present in the exoskeleton of invertebrates and fungi.[72] Chitosan is a biodegradable, biocompatible, and hemostatic polymer, which can be modified as an antimicrobial and anti-inflammatory agent for wound healing patches.[72,73] Various physical and chemical methods can be applied for chitosan cross-linking. Chitosan has been widely used for skin tissue engineering where it has shown a positive influence on the proliferation and adhesion of keratinocytes and fibroblasts in constructed models.[74] Nevertheless, it suffers from weak mechanical properties and slow gelation time. Therefore, it is preferred that it should be combined with the other polymers or cross-linked.[75] The chitosan-based bioink cytocompatibility and toxicity toward human fibroblasts and keratinocytes were tested in terms of in vitro and in vivo skin tissue regeneration in rats.[76] The results proved chitosan biocompatibility. Moreover, chitosan showed a beneficial influence on the regeneration of wounds in a rat model.

3.2.5. Fibrin. Fibrinogen is a protein found in blood and has shown unique characteristics as a hemostatic agent and structural support for wound healing.[77] It has also shown excellent biocompatibility and has a natural cell-binding site. Fibrinogen can be enzymatically converted by thrombin to fibrin. In recent years, fibrin has been used as an additive for bioinks for skin bioprinting. The diluted plasma-derived fibrin showed higher expression of type I and III collagen in keratinocytes and fibroblasts and improved cell adhesion in a printed model of skin.[64] In the case of skin bioprinting, as an example, the fibrinogen/collagen bioink with fibroblasts and keratinocytes was engrafted in wounds on mice and pigs.[41] This construct showed a dermal composition and accelerated re-epithelialization. Interestingly, vascular formation in regenerated tissue was observed.

4. TYPES OF CELLS APPLIED IN SKIN BIOPRINTING

Commercially available cell lines for fibroblasts, keratinocytes, melanocytes, and hair follicles are commonly applied in skin bioprinting.[34] Furthermore, it is also possible to isolate the specific cell phenotypes from skin biopsies. Cell cultures are usually used to generate the millions of cells required for bioprinting.

So far fibroblasts have been widely applied to develop 3D-bioprinted skin constructs.[78−81] These cells are essential for dermal formation and wound healing. In the presence of proper stimuli such as transforming growth factor beta β-1, platelet-derived growth factor, and insulin-like growth factor (IGF-1), they synthesize ECM. The majority of publications report 3D skin equivalents comprise usually two types of cells such as keratinocytes (human epidermal keratinocytes),[45] or keratinocytes and fibroblasts. Human dermal fibroblasts were the most frequently involved in the bioprinting process.[41,45,82−85] However, T3T mouse fibroblasts[86−88] and L929 mouse fibroblasts[89] were also used in some studies.

In order to mimic the natural skin, it is important to incorporate melanocytes that produce melanin, a pigment that provides photoprotection. Min et al.[90] introduced these cells into the full-thickness skin model. Initially, a dermal layer composed of collagen and fibroblasts was printed. Afterward, the melanocytes and keratinocytes were successively bioprinted on the top of the dermis. The histological analysis confirmed the presence of melanocytes in the epidermal layer recognized as freckle-like pigmentation. Recently, more attempts have been performed to introduce melanocytes into skin models by 3D bioprinting.[91−93]

Up to now, the progress in bioprinting of blood and lymphatic vessels has been limited. These systems can be found in the dermis and are crucial for the appropriate transfer of oxygen and nutrients. In spite of their significance, there are only several articles that presented the combination of fibroblasts with endothelial cells and pericytes.[94−97] Baltazar et al.[94] produced multilayered vascularized skin using two types of bioinks to form the dermis and epidermis. The first one contained human foreskin dermal fibroblasts, endothelial cells, and placental pericytes. The second one constituted human foreskin keratinocytes. Other research groups applied human fibroblasts, keratinocytes, pericytes, and induced pluripotent stem cell-derived endothelial cells to fabricate skin equivalents.[96] Li et al.[69] employed in their studies Wharton's jelly mesenchymal stem cells and amniotic epithelial cells, while Nocera et al.[88] involved epithelial Vero cells in their research. Kim et al.[95] fabricated a perfusable vascularized 3D skin model made up of the epidermis, dermis, and hypodermis. In should be mentioned that the cells that can cause skin disease can also be introduced to the biomaterials. This kind of tissue containing pathogenic cells can be applied to perform research on pathophysiology skin disorders.[45] It should be stressed that in order to obtain the appropriate environment for cell/tissue growth the knowledge regarding cell membrane composition should be taken into account while designing 3D bioprinted skin models. It has been presented by Ferreri and Chatgilialoglu that dermatological problems strictly correlate with the functions of cell membranes.[98,99] Well-balanced composition of fatty acids in cell membranes is crucial for their proper fluidity, permeability, hydration, and skin aging.[98] The importance of this aspect, when cultured cells are applied, was also demonstrated by Symons et al.[100]

5. THE REQUIRED PROPERTIES OF BIOPRINTED SKIN

The bioprinted skin should fulfill the special functional and compositional features. It should be biocompatible and should have required mechanical properties and appropriate surface chemistry. The ideal skin model should be able to transfer nutrients and reduce wound exudates.[11] In order to reproduce the native skin, the bioprinted equivalent of the appropriate cells (keratinocytes, melanocytes, Merkel and Langerhans cells, fibroblasts, adipocytes) should be accurately deposited at certain locations in the particular layer. It is essential to control the density and ratio between the populations of cells that are applied to fabricate the skin construct. It is also crucial to determine the mechanical strength, porosity, and degradation rate of bioprinted construct. The desirable skin equivalent should be porous to provide the appropriate cells' aeration. The pores should be interconnected to allow cells to attach. In addition, they should be of small size in order to protect from microbials.[101] The desirable skin equivalent should have a pore size between 200 and 400 μm.[102] Furthermore, they should be biodegradable and should maintain their 3D structure for minimum 3 weeks to enable the ingrowth of fibroblasts and blood vessels and to proliferate epithelial cells.[103]

6. OVERVIEW OF 3D SKIN BIOPRINTING STUDIES

In the past years, significant progress has been observed in the field of skin bioprinting.[51,52,96] The studies on fabrication of skin equivalents started from printing only dermis,[80,91] then the next

Table 2. Selected 3D Skin Bioprinting Studies

| biomaterials/bioink	cell types	bioprinting method	main findings	ref
Collagen	NIH3T3 fibroblasts, human keratinocytes	Laser-based	Fabrication of viable skin constructs, formation of multilayered epidermis within 11 days.	56
Collagen type-I on Matriderm	Human immortalized keratinocyte, NIH 3T3 fibroblasts	Laser-based	Histological analysis: high density of fibroblasts and keratinocytes, expression of laminin protein (a component of basement membrane in the skin).	59
Collagen type I	Fibroblasts, keratinocytes	Extrusion based	Densely packed cells in epidermis layers and low density of cells in the dermis.	45
Collagen hydrogel precursor	Fibroblast, melanocytes, keratinocytes	Extrusion based	Fabrication of full-thickness skin model containing pigmentation.	90
Collagen and fibrinogen	Amniotic fluid-based stem cell or mesenchymal stem cells	Inkjet	The presence of blood vessels in the subcutaneous adipose tissue revealed in histological analysis.	108
Hydrogel fibrinogen and collagen type I	Fibroblast, keratinocyte	Inkjet (in situ)	Design of a system for in situ skin bioprinting. Acceleration of wound regeneration by bioprinted fibroblasts and keratinocytes compared to the controls.	109
Collagen hydrogel, gelatin, PCL (polycaprolatone)	Fibroblast, keratinocyte	Extrusion and inkjet based	Fabrication of skin model with functional transwell system containing stabilized fibroblast-stretched dermis and stratified epidermis layers	107
Gelatin, Fibrinogen, alginate	Fibroblasts, keratinocytes	Extrusion based	Generation of a full-thickness skin by scaffold-free bioprinting strategy.	43
Plasma-derived fibrin	Human fibroblast, human keratinocyte	Extrusion based	The structural and functional features and consistency of bioprinted skin are comparable to human skin.	50
Skin differentiation medium, Collagen I, fetal bovine serum,	Human keratinocytes, human fibroblast, human endothelial cells, human pericytes	Extrusion based	Fabrication of multilayered vascularized bioengineered skin graft biologically and morphologically similar to native skin.	94
Collagen, Thrombin, Fibrinogen	Neonatal human dermal fibroblasts and epidermal keratinocytes, dermal microvascular endothelial cells	Inkjet-based	Bioprinted scaffold revealed 17% better wound contraction	110
Gelatin, Glycerol, Fibrinogen, Hyaluronic acid, Poly(urethane)	Human fibroblasts, Human keratinocytes	Extrusion based	Development of 3D printed BioMask for facial skin regeneration. Histological analyses revealed the regeneration of skin tissue on complex wounds.	111
Fibrinogen, Glycerol, Gelatin, Hyaluronic acid, Aprotinin	Human keratinocytes, Human melanocytes, Primary human fibroblasts, follicle dermal papillary cells, preadipocytes	Extrusion based	The bioprinted skin enhanced the closure of the wound by promoting the formation of the epidermal barrier.	92
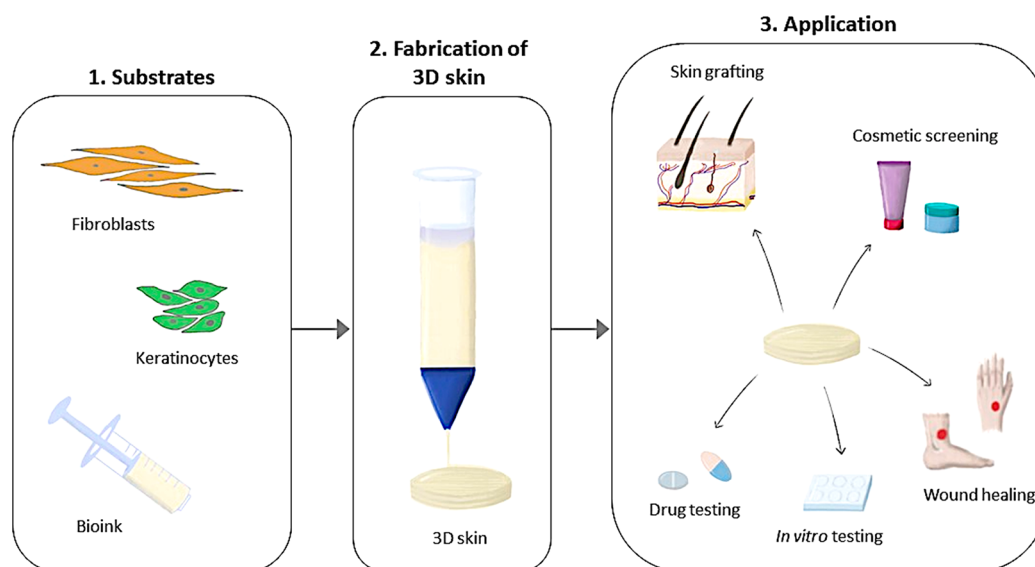
Figure 2. Overview of 3D skin bioprinting concept.

two layers (epidermis and dermis) were generated,[52,85,94] and subsequently trilayers (epidermis, dermis, and hypodermis)[92,95] were obtained. Table 2 summarizes the most important studies on the fabrication of skin equivalents using bioprinting technology. Some details concerning the selected approaches are presented in this paragraph.

Pourchet et al.[43] fabricated a two-layered skin substituent using a bioink mixture of gelatin and fibrinogen. The thickness of this construct was 5 mm. After 26 days of culture, the 3D printed skin revealed the histological features of native skin. In turn, Cubo et al.[50] developed a full-thickness human skin using fibroblasts and keratinocytes embedded in human plasma with fibrinogen. Both in vitro and in vivo results revealed that the bioprinted skin equivalent resembled the native human skin and both dermis and epidermis layers were clearly identified. Lee et al.[45] fabricated a two-layer skin equivalent by using keratinocytes and fibroblasts as constituent cells of the epidermis and dermis. The collagen was applied to form the skin dermal matrix. The histology and immunofluorescence studies showed that 3D printed skin constructs were morphologically and biologically similar to human native skin. However, some studies proved that biomaterials based on collagen have poor printability and long cross-linking time. Therefore, Ng et al.[104] obtained polyelectrolyte-gelatin-chitosan hydrogels and reported that they had good biocompatibility with fibroblast skin cells and appropriate printability at room temperature. In turn, Rimann et al.[105] reported an all-in-one solution for the fabrication of soft tissue skin models using bioprinting process with human primary fibroblasts and keratinocytes. In another study, Yanez et al.[106] employed the 3D bioprinting technology to integrate capillary-like endothelial networks into a dermo-epidermal skin graft including neonatal human epidermal keratinocytes and neonatal human dermal fibroblasts. Moreover, histological characterization of obtained constructs demonstrated the formation of dermal and epidermal skin layers comparable to the native skin, which is accompanied by the presence of new microvessels in the mouse tissue. Min et al.[90] elaborated the procedure of developing thick skin with pigmentations containing melanocytes. In turn, Kim et al.[107] proposed a novel single-step 3D cell-printing using a functional transwell system. A hybrid approach was developed which involved extrusion and inkjet modules

simultaneously. The construct based on collagen with polycaprolactone mesh (that inhibited the collagen contraction during maturation of tissue) was applied in this procedure. The skin model obtained exhibited promising biological properties. It contained steady fibroblast-stretched dermis and thick epidermis layers. Moreover, it was proved that due to this method, the costs and time consumption were lower compared to the stereotyped culture. Next, Hakimi et al.[40] developed a hand-held skin printer allowing in situ formation of skin tissue sheets of different homogeneous and architected compositions. They also demonstrated that this system is compatible with dermal and epidermal cells incorporated with ionic cross-linkable alginate, enzymatically cross-linkable proteins, and their mixtures with collagen type I and hyaluronic acid. Admane et al.[52] obtained a full-thickness human cell-based skin equivalent that exhibited structural, mechanical, and biomechanical properties similar to human skin. They fabricated the unique undulated pattern of the dermal-epidermal junction. Due to the great advances in 3D bioprinting presented above, the researchers started to search for the possibility of applications of skin equivalents that will be presented in the next paragraph.

7. APPLICATION OF 3D BIOPRINTING IN SKIN-RELATED RESEARCH

Human bioengineered skin substitutes may be used for different clinical and research applications.[30,112−115] With spreading interest in cosmetic/aesthetic procedures and rising rates of obesity, diabetes, and aging populations, the repair of damaged or lost tissue is a worldwide concern, and the demand for skin biofabrication is still growing. It is postulated that skin bioprints represent an alternative approach for the following:

- Regenerative medicine clinical applications (chronic wounds, burn injuries, ulcerations, reconstructive surgery after large oncological resections).
- Modeling physiological/pathological conditions (wound healing, UV response, aging, permeability of skin barrier, drug reaction, photoirradiation, skin cancer, genodermatoses, inflammatory conditions).
- Cosmetic/pharmaceutical industry (safety and efficacy of active agents, drug absorbance, drugs metabolization, personalized therapies).

Also, the models of bioprinted skins may serve as a platform for the development of new formulations. Some legal conditions and regulations and ethical reasons related to the tests of safety and efficacy of new formulas in animal models by the cosmetic and pharmaceutical industry force the search for new solutions in the field of cosmetology, pharmacy, and medicine. Moreover, ex vivo skin represents a valuable model for skin penetration studies, but due to logistical and viability limitations, the development of alternatives is required. On the other hand, the traditional 2D cell culture has essential limitations, thus innovative technologies such as 3D bioprinting are needed. Figure 2 illustrates the 3D skin fabrication process and the main applications of this technology.

7.1. Treatment of Burn Injuries and Wound Healing. A lot of people suffer from nonhealing skin wounds. Traditionally, transplants from patients' bodies or from donors are used to treat skin injuries. 3D bioprinting could be applied as an alternative for the above-mentioned method. The main advantage of this innovative technology is that the skin equivalents can be easily created in lesser time and cost.[4] 3D bioprinting gives an opportunity to revolutionize the way of treatment in injury and surgery. Especially it can be useful to heal the burned skin. 3D bioprinters were created that provide an opportunity to print skin for injured patients.[4] Two strategies such as ex vivo and in situ bioprinting are applied to fabricate skin for wound healing treatment. In ex vivo methods (inkjet-, extrusion-, laser-based bioprinting), a skin construct containing dermis and epidermis is printed, and next if necessary it is matured in vitro. Afterward, it is grafted to the wound of the patient. The simplest and the quickest ex vivo method is extrusion-based bioprinting. In this technique all components (such as human fibroblasts, human plasma, calcium chloride) necessary to form the dermis are deposited at the same time. Afterward, on the top of this layer, human keratinocytes are placed to create an epidermis. Michael et al.[56] used laser-assisted bioprinting to develop skin equivalents and transplanted the mice's wounds. After 11 days, the transplant adhered to the tissues located around the wound; in addition, the cells in the graft proliferated and differentiated. Cubo et al.[50] demonstrated the suitability of a 3D bioprinter and primary human fibroblasts and keratinocytes to produce a human-plasma-derived bilayered skin to treat burn injuries and traumatic and surgical wounds. Xiong et al.[116] reported that the rate of wound healing increased by using 3D printed gelatin-silk fibroin composite scaffolds. The addition of fibroblast growth factor might improve the treatment effectiveness. In turn, Lian et al.[117] added to hydrogel (that contained gelatin, sodium alginate, gelatin methacrylate) normal human dermal fibroblasts and normal human keratinocytes to fabricate a skin substituent that was applied to reduce scars in nude mice. The bioprinted skin revealed much better results in healing the wound than the bioprinted hydrogel or untreated wound control. The histology and immunofluorescence analyses performed 28 days after grafting showed that the thickness of both dermis and epidermis was comparable to that of mice. Additionally, the microvascular formation in the dermis layer was also detected.

In turn, in an in situ bioprinting approach, the skin cells suspended in hydrogels are directly printed on the injured part of the patient's body. Subsequently, the cross-linking of the bioinks is performed to reproduce the 3D skin structure.[33] Binder et al.[26,109] created a computer software and bioprinting tool that consisted of a cartridge delivery system composed of a series of inkjet nozzles and laser scanner. On the basis of the data acquired from the laser, the 3D model of the wound was reconstructed. In the next step, the printing heads filled dropwise the wound with bioink composed of fibroblasts, collagen I, and fibrinogen. At the same time, thrombin was added which is required to cross-link fibrinogen into a fibrin hydrogel. In the last stage, keratinocytes were printed. The experiments performed on the nude mice proved that the wound was repaired by printed skin within 3 weeks, which was faster than the controls (5 weeks). This method is original and promising, but it is still at the developing stage and more trials are required.

Skardal et al.[118] created a special type of bioink (photo-crosslinkable heparin-conjugated hyaluronic acid) that was capable of releasing cell-secreted growth factors. This complex system was dedicated for in situ skin printing and tested in wound healing treatment. The bioink and amniotic fluid-derived stem cells were printed directly on the wound of the murine model. Afterward, with the usage of thiol−ene photopolymerization process under exposure of ultraviolet light, the bioink was cross-linked. Wounds treated with the presented above procedure revealed a higher closure rate compared to non-treated control. In turn, Albanna et al.[41] reported a new type of mobile skin bioprinting procedure that quickly healed the complex injuries. The biomaterials included fibrinogen and thrombin. The immunohistochemistry analysis of human cells showed that human fibroblasts, keratinocytes, and endogenous cells were present in the skin layers. The authors also proved that the treatment of wounds with autologous fibroblasts and keratinocytes, which were applied immediately to the target place, improved the wound healing process. The performed studies proved that the cells (such as keratinocytes, fibroblasts, melanocytes) isolated from patients can be applied during the bioprinting process. After in vitro culturing, the cells can be mixed with appropriate biopolymer and printed to obtain a skin construct that after maturation can be implanted into the injured area of the patient.

The main limitation of 3D bioprinting technology regarding wound healing treatments is that the time required to obtain sufficient autologous cells to fabricate a large skin surface is not diminished sufficiently yet. It is essential to mention that the patients who suffer from extensive burns require treatment in as short of a time as possible. Therefore, the immediate application of bioprinted skin equivalents is essential to accelerate the wound recovery and decrease the hypertrophic scar tissue.[119]

7.2. Modeling of Skin Diseases. 3D tumor models may help to analyze the mode of action in cancer proliferation and metastasis and reaction to the selected drug. The bioprinted tissues can be combined with tumor cells to obtain the new model of diseases. Thus, melanoma was introduced to the human in vitro skin equivalent.[120] Liu et al.[96] fabricated skin tissues to generate disease models of Atopic Dermatitis (AD). Several characteristic features of AD were distinguished in these models such as hyperplasia and spongiosis; elevated level of proinflammatory cytokines; early and terminal expression of differentiation proteins. This study revealed that bioprinting can be applied to fabricate human skin substituents with different types of cellular complexity for modeling a certain disease. This method gives an opportunity to understand the mechanisms of various pathologies.

7.3. The Cosmetic and Pharmaceutical Industry. In light of the entry into force of the EU Cosmetic Regulation (EU/1223/2009) with the complete ban of animal testing for cosmetic purposes, there is a strong demand to obtain skin

equivalents that could serve as an alternative to animal trials. It should be added that the use of animal models is not only restricted due to ethical reasons but also due to their incomplete similarity to human skin. Therefore, the research results in some cases are not clear enough.[121] The human physiological system is different than the animal one. Consequently, ca. 50% of drugs that passed positively the animal trials proved to be toxic for humans and inversely.[122] The worldwide trend in both pharmaceutical and cosmetics industries is to search for skin models that could be applied to test new substances and novel topical formulations.[123,124]

Therefore, 3D bioprinting has attracted the blooming attention of skincare companies. It is expected that this new technology may revolutionize the testing of cosmetic and topical products. As it was presented above, skin is multilayered and contains various cell types. 3D bioprinting gives the opportunity to deposit cells in this arrangement. 3D bioprinted skin may bring a lot of advantages for both cosmetic and pharmaceutical industries. Before clinical studies of each new substance/drug, their safety should be examined in in vitro tests. The pharmaceutical/chemical companies may test the medicines and chemicals by applying skin models fabricated using 3D bioprinters,[29] whereas cosmetic formulations must be assessed for potential toxic and allergic effects prior launching to the market.[30] Therefore, 3D bioprinted skin may be considered as an appropriate platform to perform assessment and screening of cosmetic and pharmaceutical formulations. Due to this technology the drug and product testing could be faster, cheaper, and more effective. In addition, it can be more ethical. The method can be fully standardized and automated, thus the production costs will be reduced. For cosmetic testing different types of skin such as normal, dry, oily, and sensitive should be fabricated.[125] In addition, the 3D skin bioprinting has the potential to be applied to study drug/active compound penetration and absorption through the skin. This technology attracted the attention of global cosmetic leaders such as L'Oreal and Proctor & Gamble, who invested in the research and development of 3D bioprinted skin models.[126]

7.4. Clinical Application of 3D Skin Bioprinting. The translation of skin bioprinting from academic research to clinical practice is promising. Different forms of potential clinical applications involving regenerative medicine like cell therapy (cell-based immunotherapy, stem cell therapeutics) and tissue engineering were found[4,41,127−129] 3D bioprinting may be used for the regeneration of skin tissue and appendages. In light of this, one of the most important clinical needs is skin grafts. The print of skin biological scaffold may serve as an alternative to painful traditional skin grafts to minimize donor requirements and provide better treatment of skin grafting.[4,41] Moreover, this technology can be used to treat chronic and nonhealing wounds such as diabetic, venous, or pressure ulcers and burn wounds.[41] Günther et al.[40] developed hand-held 3D bioprinting instruments that ameliorated healing in porcine models of full-thickness burns. The system promotes the skin regeneration and reduces scars; therefore, it has potential to be introduced in clinical settings in the near future. In addition, the skin bioprinting may also revolutionize aesthetic medical procedures. 3D skin bioprinting has the potential for reconstituting the cancer microenvironment.[4,129] It can be used to create tumor models from patients' cancerous cells, which can be further helpful for the personalization of anticancer drugs. Furthermore, this procedure may serve as a powerful tool for studying various biochemical pathways' roles in carcinoma initiation and

progression.[129] Another clinical application of 3D skin bioprinting is precision medicine.[4] In light of this, it can be used for providing individualized medication as per the genetic profile and health condition of the patient. In addition, personalized skin bioprinting is pointed out as one of the promising techniques of tissue engineering for astronauts in future, long-distance space missions.[130] However, despite these great perspectives, we should be aware that skin bioprinting is still in its clinical infancy. The automated procedures need to be adopted in order to efficiently translate bioprinted skin to the clinical settings. Multiple experimental, ethical, budgetary, and regulatory difficulties hinder its rapid clinical application.[131]

8. ADVANTAGES AND LIMITATIONS OF 3D BIOPRINTING

Due to the bioprinting technique, it is possible to produce 3D skin models in an automated way, which is faster than manual methods. During the skin fabrication process, there is an opportunity to introduce different molecules and cells that promote pigmentation, vascularization, and innervation, which enable us to create biomimetic equivalents.[132] 3D bioprinting allows the precise deposition of different cells and biomaterials with high reproducibility and flexibility.[22] The skin constructs developed using this method have good plasticity, extensibility, and can be printed in high yield.[119] Therefore, the main advantage of skin bioprinting is the development of clinically relevant skin constructs that closely mimic the native skin architecture and heterogeneity via precise positioning of multiple cell types. Large-scale fabrication is another benefit of 3D-bioprinting that could be favorable for the cosmetics and pharmaceuticals screening process. Furthermore, specific skin equivalents dedicated to the selected patients can be developed by printing autologous cells.[133] This may contribute to developing personalized therapies for skin diseases.

Despite many advantages of 3D bioprinting, it is important to mention the obstacles that may be encountered during skin fabrication. The whole system is of high complexity. Therefore, specialized staff are required to carry out the production process. In addition, the 3D bioprinter is of a professional level and its maintenance is high cost. Therefore, the rapid promotion of the application of bioprinting technology could be limited. The challenges for skin bioprinting are primarily associated with selecting appropriate printable bioinks to support the function of cells and stimulate the fabrication of new ECM after printing. A critical issue is also to develop the large skin equivalent with highly developed vasculature. Some researchers have worked on fabricating the multiscale vascular networks including dendritic channels[134] and straight pipeline;[135] however, they were still far from the blood vessels of native skin. Another bottleneck of bioprinting concerns the difficulty to fabricate the skin constructs that contain hair follicles, sweat glands, and sebaceous glands. An important challenge is also to fabricate the skin with the appropriate color and texture that mimic the native skin. Furthermore, cell viability may be affected by different factors such as bioprinting method applied, the printing speed, and types of seeding cells.[37,104,105] Furthermore, the heat that is generated while printing may damage the cells. Another limitation is related to patient safety. The skin 3D bioprinting process is not yet mature. Therefore, some security concerns may occur in the future concerning safety problems when the bioprinted skin will be directly applied to patients in clinical studies. There are also legal challenges that need to be taken into

consideration before the product can be released to the market.[136−138]

9. CONCLUSIONS

3D bioprinting can bring different advantages in various fields. It can eliminate the need for donors of organs. Moreover, this technology may improve the drug discovery process. Additionally, it may eliminate animal testing. The main challenge seems to be the creation of functional skin with sufficient vascularity, innervation, and functions such as touch sensation and perception.[29] In addition, the color, texture, and individual traits of native skin are other difficulties. An upcoming direction is to generate more complex skin models. Future perspectives also involved producing dry, oily skin with different textures, pigmented with various shades/tones. It should be noted that there are some ethical, social, and legal challenges requiring attention before the technology and product may be successfully used in a large scale and enter the clinical world.

AUTHOR INFORMATION

Corresponding Authors

Jakub Dalibor Rybka − *Center for Advanced Technology, Adam Mickiewicz University, 61-614 Poznań, Poland;* ⦿ orcid.org/0000-0002-9633-9900; Email: jrybka@amu.edu.pl

Justyna Gornowicz-Porowska − *Department and Division of Practical Cosmetology and Skin Diseases Prophylaxis, Poznan University of Medicinal Sciences, 60-623 Poznań, Poland;* Email: justyna.gornowicz-porowska@ump.edu.pl

Authors

Anna Olejnik − *Faculty of Chemistry, Adam Mickiewicz University in Poznań, 61-614 Poznań, Poland*

Julia Anna Semba − *Center for Advanced Technology, Adam Mickiewicz University, 61-614 Poznań, Poland; Faculty of Biology, Adam Mickiewicz University in Poznań, 61-614 Poznań, Poland*

Adam Kulpa − *Center for Advanced Technology, Adam Mickiewicz University, 61-614 Poznań, Poland; Faculty of Biology, Adam Mickiewicz University in Poznań, 61-614 Poznań, Poland*

Aleksandra Dańczak-Pazdrowska − *Department of Dermatology, Poznan University of Medical Sciences, 60-356 Poznań, Poland*

Complete contact information is available at:
https://pubs.acs.org/10.1021/acssynbio.1c00547

Author Contributions

Conceptualization, Anna Olejnik, Justyna Gornowicz-Porowska, and Jakub Rybka; Funding acquisition, Jakub Rybka; Investigation, Anna Olejnik, Julia Semba; Project administration, Anna Olejnik, Justyna Gornowicz-Porowska, and Jakub Rybka; Supervision, Justyna Gornowicz-Porowska and Jakub Rybka; Writing (original draft), Anna Olejnik, Julia Semba, Adam Kulpa, Aleksandra Danczak-Pazdrowska; Writing (review and editing), Justyna Gornowicz-Porowska and Jakub Rybka.

Notes

The authors declare no competing financial interest.

REFERENCES

(1) Shaw, M. *3D Printing Technology: Its Applications and Scope in Fashion Industry*. https://www.researchgate.net/publication/318128860_3D_Printing_TechnologyIts_application_and_scope_in_Fashion_Industry.

(2) Ventola, C. L. Medical Applications for 3D Printing: Current and Projected Uses. *Pharm. Ther.* **2014**, *39* (10), 704.

(3) Haleem, A.; Javaid, M.; Khan, S.; Khan, M. I. Retrospective Investigation of Flexibility and Their Factors in Additive Manufacturing Systems. *Int. J. Ind. Syst. Eng.* **2020**, *36* (3), 400−429.

(4) Javaid, M.; Haleem, A. 3D Bioprinting Applications for Printing of Skin: A Brief Study. *Sensors Int.* **2021**, *2*, 100123.

(5) Mason, J.; Visintini, S.; Quay, T. An Overview of Clinical Applications of 3-D Printing and Bioprinting. *CADTH Issues Emerg. Health Technol.* **2019**.

(6) Marconi, S.; Pugliese, L.; Botti, M.; Peri, A.; Cavazzi, E.; Latteri, S.; Auricchio, F.; Pietrabissa, A. Value of 3D Printing for the Comprehension of Surgical Anatomy. *Surg. Endosc.* **2017**, *31* (10), 4102−4110.

(7) Sheikh, A.; Chepelev, L.; Christensen, A. M.; Mitsouras, D.; Schwarz, B. A.; Rybicki, F. J. Beginning and Developing a Radiology-Based in-Hospital 3D Printing Lab. In *3D Printing in Medicine*; Springer, 2017; pp 35−41.

(8) Xu, J. J.; Luo, Y. J.; Wang, J. H.; Xu, W. Z.; Shi, Z.; Fu, J. Z.; Shu, Q. Patient-Specific Three-Dimensional Printed Heart Models Benefit Preoperative Planning for Complex Congenital Heart Disease. *World J. Pediatr.* **2019**, *15* (3), 246−254.

(9) Mehra, P.; Miner, J.; D'Innocenzo, R.; Nadershah, M. Use of 3-D Stereolithographic Models in Oral and Maxillofacial Surgery. *J. Maxillofac. Oral Surg.* **2011**, *10* (1), 6−13.

(10) Witowski, J.; Sitkowski, M.; Zuzak, T.; Coles-Black, J.; Chuen, J.; Major, P.; Pdziwiatr, M. From Ideas to Long-Term Studies: 3D Printing Clinical Trials Review. *Int. J. Comput. Assist. Radiol. Surg.* **2018**, *13* (9), 1473−1478.

(11) Murphy, S. V.; Atala, A. 3D Bioprinting of Tissues and Organs. *Nat. Biotechnol.* **2014**, *32* (8), 773−785.

(12) Moroni, L.; Boland, T.; Burdick, J. A.; De Maria, C.; Derby, B.; Forgacs, G.; Groll, J.; Li, Q.; Malda, J.; Mironov, V. A.; et al. Biofabrication: A Guide to Technology and Terminology. *Trends Biotechnol.* **2018**, *36* (4), 384−402.

(13) Hospodiuk, M.; Dey, M.; Sosnoski, D.; Ozbolat, I. T. The Bioink: A Comprehensive Review on Bioprintable Materials. *Biotechnol. Adv.* **2017**, *35* (2), 217−239.

(14) Yeong, W. Y.; Chua, C. K. *Bioprinting: Principles and Applications*; World Scientific Publishing Co. Inc., 2014; Vol. 1.

(15) Gu, Q.; Hao, J.; Lu, Y.; Wang, L.; Wallace, G. G.; Zhou, Q. Three-Dimensional Bio-Printing. *Sci. China Life Sci.* **2015**, *58* (5), 411−419.

(16) Ozbolat, I. T. Bioprinting Scale-up Tissue and Organ Constructs for Transplantation. *Trends Biotechnol.* **2015**, *33* (7), 395−400.

(17) Shafiee, A.; Atala, A. Printing Technologies for Medical Applications. *Trends Mol. Med.* **2016**, *22* (3), 254−265.

(18) Jakab, K.; Norotte, C.; Marga, F.; Murphy, K.; Vunjak-Novakovic, G.; Forgacs, G. Tissue Engineering by Self-Assembly and Bio-Printing of Living Cells. *Biofabrication* **2010**, *2* (2), 22001.

(19) Perkins, J. D. Are We Reporting the Same Thing? *Liver Transplant. Off. Publ. Am. Assoc. Study Liver Dis. Int. Liver Transplant. Soc.* **2007**, *13* (3), 465−466.

(20) Saini, G.; Segaran, N.; Mayer, J. L.; Saini, A.; Albadawi, H.; Oklu, R. Applications of 3D Bioprinting in Tissue Engineering and Regenerative Medicine. *J. Clin. Med.* **2021**, *10* (21), 4966.

(21) Teerdha, P. D.; Admali, M.; Smriti, K.; Pentapati, K. C.; Vineetha, R.; Gadicherla, S. 3D Bio-Printing−A Review on Current

Application and Future Prospects in Dentistry. *J. Int. Dent. Med. Res.* **2019**, *12* (3), 1202−1210.

(22) Cui, X.; Boland, T.; D'Lima, D. D.; Lotz, M. K. Thermal Inkjet Printing in Tissue Engineering and Regenerative Medicine. *Recent Pat. Drug Delivery Formul.* **2012**, *6* (2), 149−155.

(23) Keriquel, V.; Oliveira, H.; Rémy, M.; Ziane, S.; Delmond, S.; Rousseau, B.; Rey, S.; Catros, S.; Amédée, J.; Guillemot, F.; Fricain, J. C. In Situ Printing of Mesenchymal Stromal Cells, by Laser-Assisted Bioprinting, for in Vivo Bone Regeneration Applications. *Sci. Rep.* **2017**, DOI: 10.1038/s41598-017-01914-x.

(24) Lee, W.; Debasitis, J. C.; Lee, V. K.; Lee, J. H.; Fischer, K.; Edminster, K.; Park, J. K.; Yoo, S. S. Multi-Layered Culture of Human Skin Fibroblasts and Keratinocytes through Three-Dimensional Freeform Fabrication. *Biomaterials* **2009**, *30* (8), 1587−1595.

(25) Koch, L.; Kuhn, S.; Sorg, H.; Gruene, M.; Schlie, S.; Gaebel, R.; Polchow, B.; Reimers, K.; Stoelting, S.; Ma, N.; et al. Laser Printing of Skin Cells and Human Stem Cells. *Tissue Eng. Part C: Methods* **2010**, *16* (5), 847−854.

(26) Binder, K. W.; Zhao, W.; Aboushwareb, T.; Dice, D.; Atala, A.; Yoo, J. J. In Situ Bioprinting of the Skin for Burns. *J. Am. Coll. Surg.* **2010**, *211* (3), S76.

(27) Randall, M. J.; Jüngel, A.; Rimann, M.; Wuertz-Kozak, K. Advances in the Biofabrication of 3D Skin in Vitro: Healthy and Pathological Models. *Front. Bioeng. Biotechnol.* **2018**, *6*, 154.

(28) Pereira, R. F.; Sousa, A.; Barrias, C. C.; Bayat, A.; Granja, P. L.; Bártolo, P. J. Advances in Bioprinted Cell-Laden Hydrogels for Skin Tissue Engineering. *Biomanuf. Rev.* **2017**, *2* (1), 1−26.

(29) Millás, A.; Lago, J.; Vasquez-Pinto, L.; Massaguer, P.; Maria-Engler, S. S. Approaches to the Development of 3d Bioprinted Skin Models: The Case of Natura Cosmetics. *Int. J. Adv. Med. Biotechnol.* **2019**, *2* (1), 3−13.

(30) Sarkiri, M.; Fox, S. C.; Fratila-Apachitei, L. E.; Zadpoor, A. A. Bioengineered Skin Intended for Skin Disease Modeling. *Int. J. Mol. Sci.* **2019**, *20* (6), 1407.

(31) Pereira, R. F.; Barrias, C. C.; Granja, P. L.; Bartolo, P. J. Advanced Biofabrication Strategies for Skin Regeneration and Repair. *Nanomedicine* **2013**, *8* (4), 603−621.

(32) Varkey, M.; Visscher, D. O.; van Zuijlen, P. P. M.; Atala, A.; Yoo, J. J. Skin Bioprinting: The Future of Burn Wound Reconstruction? *Burn. Trauma* **2019**, *7*, 1−12.

(33) Velasco, D.; Quílez, C.; Garcia, M.; del Cañizo, J. F.; Jorcano, J. L. 3D Human Skin Bioprinting: A View from the Bio Side. *J. 3D Print. Med.* **2018**, *2*, 141−162.

(34) Perez-Valle, A.; Del Amo, C.; Andia, I. Overview of Current Advances in Extrusion Bioprinting for Skin Applications. *Int. J. Mol. Sci.* **2020**, *21* (18), 6679.

(35) Muroyama, A.; Lechler, T. Polarity and Stratification of the Epidermis. In *Seminars in Cell & Developmental Biology*; Elsevier, 2012; Vol. 23, pp 890−896.

(36) Richmond, J. M.; Harris, J. E. Immunology and Skin in Health and Disease. *Cold Spring Harb. Perspect. Med.* **2014**, *4* (12), a015339.

(37) Parrado, C.; Mercado-Saenz, S.; Perez-Davo, A.; Gilaberte, Y.; Gonzalez, S.; Juarranz, A. Environmental Stressors on Skin Aging. Mechanistic Insights. *Front. Pharmacol.* **2019**, *10*, 759.

(38) Kačarević, Ž. P.; Rider, P. M.; Alkildani, S.; Retnasingh, S.; Smeets, R.; Jung, O.; Ivanišević, Z.; Barbeck, M. An Introduction to 3D Bioprinting: Possibilities, Challenges and Future Aspects. *Materials (Basel)* **2018**, *11* (11), 2199.

(39) Semba, J. A.; Mieloch, A. A.; Rybka, J. D. Introduction to the State-of-the-Art 3D Bioprinting Methods, Design, and Applications in Orthopedics. *Bioprinting* **2020**, *18*, e00070.

(40) Hakimi, N.; Cheng, R.; Leng, L.; Sotoudehfar, M.; Ba, P. Q.; Bakhtyar, N.; Amini-Nik, S.; Jeschke, M. G.; Günther, A. Handheld Skin Printer:: In Situ Formation of Planar Biomaterials and Tissues. *Lab Chip* **2018**, *18* (10), 1440−1451.

(41) Albanna, M.; Binder, K. W.; Murphy, S. V.; Kim, J.; Qasem, S. A.; Zhao, W.; Tan, J.; El-Amin, I. B.; Dice, D. D.; Marco, J.; Green, J.; Xu, T.; Skardal, A.; Holmes, J. H.; Jackson, J. D.; Atala, A.; Yoo, J. J. In Situ Bioprinting of Autologous Skin Cells Accelerates Wound Healing of Extensive Excisional Full-Thickness Wounds. *Sci. Rep.* **2019**, *9* (1), 1−15.

(42) Derakhshanfar, S.; Mbeleck, R.; Xu, K.; Zhang, X.; Zhong, W.; Xing, M. 3D Bioprinting for Biomedical Devices and Tissue Engineering: A Review of Recent Trends and Advances. *Bioact. Mater.* **2018**, *3* (2), 144−156.

(43) Pourchet, L. J.; Thepot, A.; Albouy, M.; Courtial, E. J.; Boher, A.; Blum, L. J.; Marquette, C. A. Human Skin 3D Bioprinting Using Scaffold-free Approach. *Adv. Healthc. Mater.* **2017**, *6* (4), 1601101.

(44) Chameettachal, S.; Pati, F. Inkjet-Based 3D Bioprinting. In *3D Bioprinting in Regenerative Engineering: Principles and Applications*; Khademhosseini, A., Camci-Unal, G., Eds.; Taylor & Francis Group, 2018; pp 99−118.

(45) Lee, V.; Singh, G.; Trasatti, J. P.; Bjornsson, C.; Xu, X.; Tran, T. N.; Yoo, S. S.; Dai, G.; Karande, P. Design and Fabrication of Human Skin by Three-Dimensional Bioprinting. *Tissue Eng. - Part C Methods* **2014**, *20* (6), 473−484.

(46) Hutchings, I. M.; Martin, G.; Hoath, S. D. Introductory Remarks. *J. Nutr. Sci. Vitaminol. (Tokyo)* **2011**, *38*, 372−374.

(47) Heinrich, M. A.; Liu, W.; Jimenez, A.; Yang, J.; Akpek, A.; Liu, X.; Pi, Q.; Mu, X.; Hu, N.; Schiffelers, R. M.; et al. 3D Bioprinting: From Benches to Translational Applications. *Small* **2019**, *15* (23), 1805510.

(48) Fayyazbakhsh, F.; Leu, M. C. A Brief Review on 3D Bioprinted Skin Substitutes. *Procedia Manuf.* **2020**, *48*, 790−796.

(49) Retting, K. N.; Nguyen, D. G. Additive Manufacturing in the Development of 3D Skin Tissues. *Ski. Tissue Model.* **2018**, 377−397.

(50) Cubo, N.; Garcia, M.; Del Cañizo, J. F.; Velasco, D.; Jorcano, J. L. 3D Bioprinting of Functional Human Skin: Production and in Vivo Analysis. *Biofabrication* **2017**, *9* (1), 15006.

(51) Derr, K.; Zou, J.; Luo, K.; Song, M. J.; Sittampalam, G. S.; Zhou, C.; Michael, S.; Ferrer, M.; Derr, P. Fully Three-Dimensional Bioprinted Skin Equivalent Constructs with Validated Morphology and Barrier Function. *Tissue Eng. Part C Methods* **2019**, *25* (6), 334−343.

(52) Admane, P.; Gupta, A. C.; Jois, P.; Roy, S.; Lakshmanan, C. C.; Kalsi, G.; Bandyopadhyay, B.; Ghosh, S. Direct 3D Bioprinted Full-Thickness Skin Constructs Recapitulate Regulatory Signaling Pathways and Physiology of Human Skin. *Bioprinting* **2019**, *15*, e00051.

(53) Askari, M.; Naniz, M. A.; Kouhi, M.; Saberi, A.; Zolfagharian, A.; Bodaghi, M. Recent Progress in Extrusion 3D Bioprinting of Hydrogel Biomaterials for Tissue Regeneration: A Comprehensive Review with Focus on Advanced Fabrication Techniques. *Biomater. Sci.* **2021**, *9* (3), 535−573.

(54) Miguel, S. P.; Cabral, C. S. D.; Moreira, A. F.; Correia, I. J. Production and Characterization of a Novel Asymmetric 3D Printed Construct Aimed for Skin Tissue Regeneration. *Colloids Surfaces B Biointerfaces* **2019**, *181*, 994−1003.

(55) Li, J.; Chen, M.; Fan, X.; Zhou, H. Recent Advances in Bioprinting Techniques: Approaches, Applications and Future Prospects. *J. Transl. Med.* **2016**, *14* (1), 1−15.

(56) Michael, S.; Sorg, H.; Peck, C. T.; Koch, L.; Deiwick, A.; Chichkov, B.; Vogt, P. M.; Reimers, K. Tissue Engineered Skin Substitutes Created by Laser-Assisted Bioprinting Form Skin-Like Structures in the Dorsal Skin Fold Chamber in Mice. *PLoS One* **2013**, *8* (3), e57741.

(57) Ventura, R. D. An Overview of Laser-Assisted Bioprinting (LAB) in Tissue Engineering Applications. *Med. Lasers; Eng. Basic Res. Clin. Appl.* **2021**, *10* (2), 76−81.

(58) Vinson, B. T.; Sklare, S. C.; Huang, Y.; Chrisey, D. B. Laser-Based 3D Bioprinting. In *3D Bioprinting in Regenerative Engineering: Principles and Applications*; Khademhosseini, A., Camci-Unal, G., Eds.; Taylor & Francis Group, 2018; pp 77−98.

(59) Koch, L.; Deiwick, A.; Schlie, S.; Michael, S.; Gruene, M.; Coger, V.; Zychlinski, D.; Schambach, A.; Reimers, K.; Vogt, P. M.; Chichkov, B. Skin Tissue Generation by Laser Cell Printing. *Biotechnol. Bioeng.* **2012**, *109* (7), 1855−1863.

(60) Kathawala, M. H.; Ng, W. L.; Liu, D.; Naing, M. W.; Yeong, W. Y.; Spiller, K. L.; Van Dyke, M.; Ng, K. W. Healing of Chronic Wounds:

An Update of Recent Developments and Future Possibilities. *Tissue Eng. Part B Rev.* **2019**, *25* (5), 429−444.

(61) Ricard-Blum, S. The Collagen Family. *Cold Spring Harb. Perspect. Biol.* **2011**, *3*, 1−19.

(62) Sorushanova, A.; Delgado, L. M.; Wu, Z.; Shologu, N.; Kshirsagar, A.; Raghunath, R.; Mullen, A. M.; Bayon, Y.; Pandit, A.; Raghunath, M.; Zeugolis, D. I. The Collagen Suprafamily: From Biosynthesis to Advanced Biomaterial Development. *Adv. Mater.* **2019**, *31* (1), 1−39.

(63) Antoine, E. E.; Vlachos, P. P.; Rylander, M. N. Review of Collagen I Hydrogels for Bioengineered Tissue Microenvironments: Characterization of Mechanics, Structure, and Transport. *Tissue Eng. Part B Rev.* **2014**, *20* (6), 683−696.

(64) Yan, W. C.; Davoodi, P.; Vijayavenkataraman, S.; Tian, Y.; Ng, W. C.; Fuh, J. Y. H.; Robinson, K. S.; Wang, C. H. 3D Bioprinting of Skin Tissue: From Pre-Processing to Final Product Evaluation. *Adv. Drug Delivery Rev.* **2018**, *132*, 270−295.

(65) Benwood, C.; Chrenek, J.; Kirsch, R. L.; Masri, N. Z.; Richards, H.; Teetzen, K.; Willerth, S. M. Natural Biomaterials and Their Use as Bioinks for Printing Tissues. *Bioengineering* **2021**, *8* (2), 27.

(66) Tanaka, A.; Nagate, T.; Matsuda, H. Acceleration of Wound Healing by Gelatin Film Dressings with Epidermal Growth Factor. *J. Vet. Med. Sci.* **2005**, *67*, 909.

(67) Lee, K. Y.; Mooney, D. J. Alginate: Properties and Biomedical Applications. *Prog. Polym. Sci.* **2012**, *37* (1), 106−126.

(68) Genes, N. G.; Rowley, J. A.; Mooney, D. J.; Bonassar, L. J. Effect of Substrate Mechanics on Chondrocyte Adhesion to Modified Alginate Surfaces. *Arch. Biochem. Biophys.* **2004**, *422* (2), 161−167.

(69) Liu, P.; Shen, H.; Zhi, Y.; Si, J.; Shi, J.; Guo, L.; Shen, S. G. 3D Bioprinting and in Vitro Study of Bilayered Membranous Construct with Human Cells-Laden Alginate/Gelatin Composite Hydrogels. *Colloids Surf., B* **2019**, *181*, 1026−1034.

(70) Grant, G.; Morris, E.; Rees, D.; Smith, P.; Thom, D. Biological Interactions between Polysaccharides and Divalent Cations: The Egg-Box Model. *FEBS Lett.* **1973**, *32*, 195−198.

(71) Naghieh, S.; Karamooz-Ravari, M. R.; Sarker, M. D.; Karki, E.; Chen, X. Influence of Crosslinking on the Mechanical Behavior of 3D Printed Alginate Scaffolds: Experimental and Numerical Approaches. *J. Mech. Behav. Biomed. Mater.* **2018**, *80*, 111−118.

(72) Islam, S.; Bhuiyan, M. A. R.; Islam, M. N. Chitin and Chitosan: Structure, Properties and Applications in Biomedical Engineering. *J. Polym. Environ.* **2017**, *25* (3), 854−866.

(73) Cheung, R. C.; Ng, T. B.; Wong, J. H.; C, W. Chitosan: An Update on Potential Biomedical and Pharmaceutical Applications. *Mar. Drugs* **2015**, *13*, 5156−5186.

(74) Revi, D.; Paul, W.; Anilkumar, T.V.; Sharma, C. P. Chitosan Scaffold Co-Cultured with Keratinocyte and Fibroblast Heals Full Thickness Skin Wounds in Rabbit. *J. Biomed Mater. Res. A* **2014**, *102* (9), 3273−3281.

(75) Hafezi, F.; Shorter, S.; Tabriz, A. G.; Hurt, A.; Elmes, V.; Boateng, J.; Douroumis, D. Bioprinting and Preliminary Testing of Highly Reproducible Novel Bioink for Potential Skin Regeneration. *Pharmaceutics* **2020**, *12* (6), 550.

(76) Intini, C.; Elviri, L.; Cabral, J.; Mros, S.; Bergonzi, C.; Bianchera, A.; Flammini, L.; Govoni, P.; Barocelli, E.; Bettini, R.; McConnell, M. 3D-Printed Chitosan-Based Scaffolds: An in Vitro Study of Human Skin Cell Growth and an in-Vivo Wound Healing Evaluation in Experimental Diabetes in Rats. *Carbohydr. Polym.* **2018**, *199*, 593.

(77) Williams, S. K.; Hoying, J. B. Bioinks for Bioprinting. In *Bioprinting in Regenerative Medicine*; Turksen, K., Ed.; Humana Press, 2015; pp 1−137. DOI: 10.1007/978-3-319-21386-6.

(78) Shi, P.; Laude, A.; Yeong, W. Y. Investigation of Cell Viability and Morphology in 3D Bio-printed Alginate Constructs with Tunable Stiffness. *J. Biomed. Mater. Res. Part A* **2017**, *105* (4), 1009−1018.

(79) He, Y.; Yang, F.; Zhao, H.; Gao, Q.; Xia, B.; Fu, J. Research on the Printability of Hydrogels in 3D Bioprinting. *Sci. Rep.* **2016**, *6* (1), 1−13.

(80) Zidarič, T.; Milojević, M.; Gradišnik, L.; Stana Kleinschek, K.; Maver, U.; Maver, T. Polysaccharide-Based Bioink Formulation for 3D

Bioprinting of an in Vitro Model of the Human Dermis. *Nanomaterials* **2020**, *10* (4), 733.

(81) Pereira, R. F.; Sousa, A.; Barrias, C. C.; Bártolo, P. J.; Granja, P. L. A Single-Component Hydrogel Bioink for Bioprinting of Bioengineered 3D Constructs for Dermal Tissue Engineering. *Mater. Horizons* **2018**, *5* (6), 1100−1111.

(82) Shi, L.; Hu, Y.; Ullah, M. W.; Ou, H.; Zhang, W.; Xiong, L.; Zhang, X. Cryogenic Free-Form Extrusion Bioprinting of Decellularized Small Intestinal Submucosa for Potential Applications in Skin Tissue Engineering. *Biofabrication* **2019**, *11* (3), 35023.

(83) Xu, C.; Molino, B. Z.; Wang, X.; Cheng, F.; Xu, W.; Molino, P.; Bacher, M.; Su, D.; Rosenau, T.; Willför, S. 3D Printing of Nanocellulose Hydrogel Scaffolds with Tunable Mechanical Strength towards Wound Healing Application. *J. Mater. Chem. B* **2018**, *6* (43), 7066−7075.

(84) Shi, L.; Xiong, L.; Hu, Y.; Li, W.; Chen, Z.; Liu, K.; Zhang, X. Three-dimensional Printing Alginate/Gelatin Scaffolds as Dermal Substitutes for Skin Tissue Engineering. *Polym. Eng. Sci.* **2018**, *58* (10), 1782−1790.

(85) Kim, B. S.; Kwon, Y. W.; Kong, J.-S.; Park, G. T.; Gao, G.; Han, W.; Kim, M.-B.; Lee, H.; Kim, J. H.; Cho, D.-W. 3D Cell Printing of in Vitro Stabilized Skin Model and in Vivo Pre-Vascularized Skin Patch Using Tissue-Specific Extracellular Matrix Bioink: A Step towards Advanced Skin Tissue Engineering. *Biomaterials* **2018**, *168*, 38−53.

(86) Heidenreich, A. C.; Pérez-Recalde, M.; Wusener, A. G.; Hermida, É. B. Collagen and Chitosan Blends for 3D Bioprinting: A Rheological and Printability Approach. *Polym. Test.* **2020**, *82*, 106297.

(87) Xu, W.; Molino, B. Z.; Cheng, F.; Molino, P. J.; Yue, Z.; Su, D.; Wang, X.; Willför, S.; Xu, C.; Wallace, G. G. On Low-Concentration Inks Formulated by Nanocellulose Assisted with Gelatin Methacrylate (GelMA) for 3D Printing toward Wound Healing Application. *ACS Appl. Mater. Interfaces* **2019**, *11* (9), 8838−8848.

(88) Nocera, A. D.; Comín, R.; Salvatierra, N. A.; Cid, M. P. Development of 3D Printed Fibrillar Collagen Scaffold for Tissue Engineering. *Biomed. Microdevices* **2018**, *20* (2), 1−13.

(89) Chen, C.-S.; Zeng, F.; Xiao, X.; Wang, Z.; Li, X.-L.; Tan, R.-W.; Liu, W.-Q.; Zhang, Y.-S.; She, Z.-D.; Li, S.-J. Three-Dimensionally Printed Silk-Sericin-Based Hydrogel Scaffold: A Promising Visualized Dressing Material for Real-Time Monitoring of Wounds. *ACS Appl. Mater. Interfaces* **2018**, *10* (40), 33879−33890.

(90) Min, D.; Lee, W.; Bae, I.; Lee, T. R.; Croce, P.; Yoo, S. Bioprinting of Biomimetic Skin Containing Melanocytes. *Exp. Dermatol.* **2018**, *27* (5), 453−459.

(91) Shi, Y.; Xing, T. L.; Zhang, H. B.; Yin, R. X.; Yang, S. M.; Wei, J.; Zhang, W. J. Tyrosinase-Doped Bioink for 3D Bioprinting of Living Skin Constructs. *Biomed. Mater.* **2018**, *13* (3), 35008.

(92) Jorgensen, A. M.; Varkey, M.; Gorkun, A.; Clouse, C.; Xu, L.; Chou, Z.; Murphy, S. V.; Molnar, J.; Lee, S. J.; Yoo, J. J.; et al. Bioprinted Skin Recapitulates Normal Collagen Remodeling in Full-Thickness Wounds. *Tissue Eng. Part A* **2020**, *26* (9−10), 512−526.

(93) Ng, W. L.; Qi, J. T. Z.; Yeong, W. Y.; Naing, M. W. Proof-of-Concept: 3D Bioprinting of Pigmented Human Skin Constructs. *Biofabrication* **2018**, *10* (2), 25005.

(94) Baltazar, T.; Merola, J.; Catarino, C.; Xie, C. B.; Kirkiles-Smith, N. C.; Lee, V.; Hotta, S.; Dai, G.; Xu, X.; Ferreira, F. C.; et al. Three Dimensional Bioprinting of a Vascularized and Perfusable Skin Graft Using Human Keratinocytes, Fibroblasts, Pericytes, and Endothelial Cells. *Tissue Eng. Part A* **2020**, *26* (5−6), 227−238.

(95) Kim, B. S.; Gao, G.; Kim, J. Y.; Cho, D. 3D Cell Printing of Perfusable Vascularized Human Skin Equivalent Composed of Epidermis, Dermis, and Hypodermis for Better Structural Recapitulation of Native Skin. *Adv. Healthc. Mater.* **2019**, *8* (7), 1801019.

(96) Liu, X.; Michael, S.; Bharti, K.; Ferrer, M.; Song, M. J. A Biofabricated Vascularized Skin Model of Atopic Dermatitis for Preclinical Studies. *Biofabrication* **2020**, *12* (3), 35002.

(97) Attalla, R.; Puersten, E.; Jain, N.; Selvaganapathy, P. R. 3D Bioprinting of Heterogeneous Bi-and Tri-Layered Hollow Channels within Gel Scaffolds Using Scalable Multi-Axial Microfluidic Extrusion Nozzle. *Biofabrication* **2019**, *11* (1), 15012.

(98) Ferreri, C.; Chatgilialoglu, C. *Membrane Lipidomics for Personalized Health*; John Wiley & Sons Ltd.: Chichester, UK, 2015.

(99) Chatgilialoglu, C.; Ferreri, C. Nutrilipidomics: A Tool for Personalized Health. *J. Glycomics Lipidomics* 2012, 2, e109.

(100) Symons, J. L.; Cho, K.-J.; Chang, J. T.; Du, G.; Waxham, M. N.; Hancock, J. F.; Levental, I.; Levental, K. R. Lipidomic Atlas of Mammalian Cell Membranes Reveals Hierarchical Variation Induced by Culture Conditions, Subcellular Membranes, and Cell Lineages. *Soft Matter* 2021, 17 (2), 288−297.

(101) Augustine, R.; Kalarikkal, N.; Thomas, S. Microbial Barrier Property and Blood Compatibility Studies of Electrospun Poly-ξ-Caprolactone/Zinc Oxide Nanocomposite Scaffolds. *J. Sib. Fed. Univ., Biol.* 2017, 10, 226.

(102) Park, Y. R.; Ju, H. W.; Lee, J. M.; Kim, D.-K.; Lee, O. J.; Moon, B. M.; Park, H. J.; Jeong, J. Y.; Yeon, Y. K.; Park, C. H. Three-Dimensional Electrospun Silk-Fibroin Nanofiber for Skin Tissue Engineering. *Int. J. Biol. Macromol.* 2016, 93, 1567−1574.

(103) Sekine, H.; Shimizu, T.; Sakaguchi, K.; Dobashi, I.; Wada, M.; Yamato, M.; Kobayashi, E.; Umezu, M.; Okano, T. In Vitro Fabrication of Functional Three-Dimensional Tissues with Perfusable Blood Vessels. *Nat. Commun.* 2013, 4 (1), 1−10.

(104) Ng, W. L.; Yeong, W. Y.; Naing, M. W. Polyelectrolyte Gelatin-Chitosan Hydrogel Optimized for 3D Bioprinting in Skin Tissue Engineering. *Int. J. Bioprinting* 2016, DOI: 10.18063/IJB.2016.01.009.

(105) Rimann, M.; Bono, E.; Annaheim, H.; Bleisch, M.; Graf-Hausner, U. Standardized 3D Bioprinting of Soft Tissue Models with Human Primary Cells. *J. Lab. Autom.* 2016, 21 (4), 496−509.

(106) Yanez, M.; Rincon, J.; Dones, A.; De Maria, C.; Gonzales, R.; Boland, T. In Vivo Assessment of Printed Microvasculature in a Bilayer Skin Graft to Treat Full-Thickness Wounds. *Tissue Eng. Part A* 2015, 21 (1−2), 224−233.

(107) Kim, B. S.; Lee, J.-S.; Gao, G.; Cho, D.-W. Direct 3D Cell-Printing of Human Skin with Functional Transwell System. *Biofabrication* 2017, 9 (2), 25034.

(108) Skardal, A.; Mack, D.; Kapetanovic, E.; Atala, A.; Jackson, J. D.; Yoo, J.; Soker, S. Bioprinted Amniotic Fluid-derived Stem Cells Accelerate Healing of Large Skin Wounds. *Stem Cells Transl. Med.* 2012, 1 (11), 792−802.

(109) Binder, K. W. *In Situ Bioprinting of the Skin*; Wake Forest University, 2011.

(110) Marchioli, G; van Gurp, L; van Krieken, P P; Stamatialis, D; Engelse, M; van Blitterswijk, C A; Karperien, M B J; de Koning, E; Alblas, J; Moroni, L; van Apeldoorn, A A Fabrication of Three-Dimensional Bioplotted Hydrogel Scaffolds for Islets of Langerhans Transplantation. *Biofabrication* 2015, 7 (2), 25009.

(111) Seol, Y.-J.; Lee, H.; Copus, J. S.; Kang, H.-W.; Cho, D.-W.; Atala, A.; Lee, S. J.; Yoo, J. J. 3D Bioprinted Biomask for Facial Skin Reconstruction. *Bioprinting* 2018, 10, e00028.

(112) Prescott, S. L.; Larcombe, D.-L.; Logan, A. C.; West, C.; Burks, W.; Caraballo, L.; Levin, M.; Van Etten, E.; Horwitz, P.; Kozyrskyj, A. The Skin Microbiome: Impact of Modern Environments on Skin Ecology, Barrier Integrity, and Systemic Immune Programming. *World Allergy Org. J.* 2017, 10 (1), 1−16.

(113) Tavakoli, S.; Klar, A. S. Bioengineered Skin Substitutes: Advances and Future Trends. *Appl. Sci.* 2021, 11 (4), 1493.

(114) Smandri, A.; Nordin, A.; Hwei, N. M.; Chin, K. Y.; Abd Aziz, I.; Fauzi, M. B. Natural 3D-Printed Bioinks for Skin Regeneration and Wound Healing: A Systematic Review. *Polymers (Basel)* 2020, 12 (8), 1782.

(115) Velasquillo, C.; Galue, E. A.; Rodriquez, L.; Ibarra, C.; Ibarra-Ibarra, L. G. Skin 3D Bioprinting. Applications in Cosmetology. *J. Cosmet., Dermatol. Sci. Appl.* 2013, 03, 85.

(116) Xiong, S.; Zhang, X.; Lu, P.; Wu, Y.; Wang, Q.; Sun, H.; Heng, B. C.; Bunpetch, V.; Zhang, S.; Ouyang, H. A Gelatin-Sulfonated Silk Composite Scaffold Based on 3D Printing Technology Enhances Skin Regeneration by Stimulating Epidermal Growth and Dermal Neo-vascularization. *Sci. Rep.* 2017, 7 (1), 1−12.

(117) Lian, Q.; Jiao, T.; Zhao, T.; Wang, H.; Yang, S.; Li, D. 3D Bioprinted Skin Substitutes for Accelerated Wound Healing and Reduced Scar. *J. Bionic Eng.* 2021, 18 (4), 900−914.

(118) Skardal, A.; Murphy, S. V.; Crowell, K.; Mack, D.; Atala, A.; Soker, S. A Tunable Hydrogel System for Long-term Release of Cell-secreted Cytokines and Bioprinted in Situ Wound Cell Delivery. *J. Biomed. Mater. Res. Part B Appl. Biomater.* 2017, 105 (7), 1986−2000.

(119) He, P.; Zhao, J.; Zhang, J.; Li, B.; Gou, Z.; Gou, M.; Li, X. Bioprinting of Skin Constructs for Wound Healing. *Burn. Trauma* 2018, DOI: 10.1186/s41038-017-0104-x.

(120) Mathes, S. H.; Ruffner, H.; Graf-Hausner, U. The Use of Skin Models in Drug Development. *Adv. Drug Delivery Rev.* 2014, 69, 81−102.

(121) Garcia, M.; Escamez, M. J.; Carretero, M.; Mirones, I.; Martinez-Santamaria, L.; Navarro, M.; Jorcano, J. L.; Meana, A.; Del Rio, M.; Larcher, F. Modeling Normal and Pathological Processes through Skin Tissue Engineering. *Mol. Carcinog. Publ. Coop. with Univ. Texas MD Anderson Cancer Cent.* 2007, 46 (8), 741−745.

(122) Hansen, K.; Khanna, C. Spontaneous and Genetically Engineered Animal Models: Use in Preclinical Cancer Drug Development. *Eur. J. Cancer* 2004, 40 (6), 858−880.

(123) Jung, K.-M.; Lee, S.-H.; Jang, W.-H.; Jung, H.-S.; Heo, Y.; Park, Y.-H.; Bae, S.; Lim, K.-M.; Seok, S. H. KeraSkin-VM: A Novel Reconstructed Human Epidermis Model for Skin Irritation Tests. *Toxicol. Vitr.* 2014, 28 (5), 742−750.

(124) Catarino, C. M.; do Nascimento Pedrosa, T.; Pennacchi, P. C.; de Assis, S. R.; Gimenes, F.; Consolaro, M. E. L.; de Moraes Barros, S. B.; Maria-Engler, S. S. Skin Corrosion Test: A Comparison between Reconstructed Human Epidermis and Full Thickness Skin Models. *Eur. J. Pharm. Biopharm.* 2018, 125, 51−57.

(125) Vijayavenkataraman, S. 3D Bioprinted Skin: The First 'to-Be' Successful Printed Organ? *J. 3D Print. Med.* 2017, 1, 143.

(126) Tarassoli, S. P.; Jessop, Z. M.; Al-Sabah, A.; Gao, N.; Whitaker, S.; Doak, S.; Whitaker, I. S. Skin Tissue Engineering Using 3D Bioprinting: An Evolving Research Field. *J. Plast. Reconstr. Aesthetic Surg.* 2018, 71 (5), 615−623.

(127) Yang, R.; Yang, S.; Zhao, J.; Hu, X.; Chen, X.; Wang, J.; Xie, J.; Xiong, K. Progress in Studies of Epidermal Stem Cells and Their Application in Skin Tissue Engineering. *Stem Cell Res. Ther.* 2020, 11 (1), 1−13.

(128) Phua, Q. H.; Han, H. A.; Soh, B.-S. Translational Stem Cell Therapy: Vascularized Skin Grafts in Skin Repair and Regeneration. *J. Transl. Med.* 2021, 19 (1), 1−11.

(129) Datta, P.; Dey, M.; Ataie, Z.; Unutmaz, D.; Ozbolat, I. T. 3D Bioprinting for Reconstituting the Cancer Microenvironment. *NPJ. Precis. Oncol.* 2020, 4 (1), 1−13.

(130) Ghidini, T. Regenerative Medicine and 3D Bioprinting for Human Space Exploration and Planet Colonisation. *J. Thorac. Dis.* 2018, 10 (Suppl20), S2363−S2375.

(131) Gilbert, F.; O'Connell, C. D.; Mladenovska, T.; Dodds, S. Print Me an Organ? Ethical and Regulatory Issues Emerging from 3D Bioprinting in Medicine. *Sci. Eng. Ethics* 2018, 24 (1), 73−91.

(132) Rosenberg, E. S.; Dufort, E. M.; Udo, T.; Wilberschied, L. A.; Kumar, J.; Tesoriero, J.; Weinberg, P.; Kirkwood, J.; Muse, A.; DeHovitz, J.; et al. Association of Treatment with Hydroxychloroquine or Azithromycin with In-Hospital Mortality in Patients with COVID-19 in New York State. *JAMA, J. Am. Med. Assoc.* 2020, 323 (24), 2493−2502.

(133) Ng, W. L.; Wang, S.; Yeong, W. Y.; Naing, M. W. Skin Bioprinting: Impending Reality or Fantasy? *Trends Biotechnol.* 2016, 34 (9), 689−699.

(134) Wong, L.; Pegan, J. D.; Gabela-Zuniga, B.; Khine, M.; McCloskey, K. E. Leaf-Inspired Microcontact Printing Vascular Patterns. *Biofabrication* 2017, 9 (2), 21001.

(135) Lee, V. K.; Kim, D. Y.; Ngo, H.; Lee, Y.; Seo, L.; Yoo, S.-S.; Vincent, P. A.; Dai, G. Creating Perfused Functional Vascular Channels Using 3D Bio-Printing Technology. *Biomaterials* 2014, 35 (28), 8092−8102.

(136) Mandrycky, C.; Wang, Z.; Kim, K.; Kim, D. 3D Bioprinting for Engineering Complex Tissues. *Biotechnol. Adv.* **2016**, *34* (4), 422−434.

(137) Zhu, W.; Ma, X.; Gou, M.; Mei, D.; Zhang, K.; Chen, S. 3D Printing of Functional Biomaterials for Tissue Engineering. *Curr. Opin. Biotechnol.* **2016**, *40*, 103−112.

(138) Vijayavenkataraman, S.; Lu, W. F.; Fuh, J. Y. H. 3D Bioprinting−an Ethical, Legal and Social Aspects (ELSA) Framework. *Bioprinting* **2016**, *1*, 11−21.

Julia Semba

Laboratory of Applied Biotechnology
Center for Advanced Technology
Adam Mickiewicz University in Poznan
e-mail: jsemba@amu.edu.pl

Author contribution statement

I declare that I am the co-author of the article "3D bioprinting in skin related research: recent achievements and application perspectives" by Anna Olejnik, Julia Anna Semba, Adam Kulpa, Aleksandra Dańczak-Pazdrowska, Jakub Dalibor Rybka, and Justyna Gornowicz-Porowska, published in *ACS Synthetic Biology* in 2022. The author contribution is as follows:

Anna Olejnik designed the study, reviewed the literature, and wrote the original draft of introduction, Chapter 4 "Types of cells applied in skin bioprinting", Chapter 5 "The required properties of bioprinted skin", Chapter 6 "Overview of 3D skin bioprinting studies", Chapter 7 "Application of 3D bioprinting in skin-related research", Chapter 8 "Advantages and limitations of 3D bioprinting" and conclusions, drawn part of Figure 1.

Julia Semba reviewed the literature and wrote the original draft of Chapter 3 "Bioprinting" (with Adam Kulpa), and drawn Figure 2.

Adam Kulpa reviewed the literature and wrote the original draft of Chapter 3 "Bioprinting" (with Julia Semba)

Aleksandra Dańczak-Pazdrowska wrote the original draft of Chapter 2 "Skin architecture and function".

Jakub Rybka designed the study, supervised the technical part of the research, and revised the manuscript. Jakub Rybka also corresponded with the journal and reviewers.

Justyna Gornowicz-Porowska designed the study, supervised the research, and revised the manuscript, drawn part of Figure 1 and wrote the original draft of Chapter 2 "Skin architecture and function", Chapter 5 "The required properties of bioprinted skin", Chapter 6 "Overview of 3D skin bioprinting studies" and Chapter 7 "Application of 3D bioprinting in skin-related research" and conclusions.

Date: 18. 08. 2023
Signature: *Julia Semba*

prof. UAM dr hab. Inż. Jakub D. Rybka

Dr Anna Olejnik

Faculty of Chemistry
Adam Mickiewicz University in Poznan
e-mail: annamar@amu.edu.pl

Author contribution statement

I declare that I am the first author of the article "3D bioprinting in skin related research: recent achievements and application perspectives" by Anna Olejnik, Julia Anna Semba, Adam Kulpa, Aleksandra Dańczak-Pazdrowska, Jakub Dalibor Rybka, and Justyna Gornowicz-Porowska, published in *ACS Synthetic Biology* in 2022 and I am aware that this publication is a part of Julia Semba PhD dissertation. The author's contribution is as follows:

Anna Olejnik designed the study, reviewed the literature, and wrote the original draft of introduction, Chapter 4 "Types of cells applied in skin bioprinting", Chapter 5 "The required properties of bioprinted skin", Chapter 6 "Overview of 3D skin bioprinting studies", Chapter 7 "Application of 3D bioprinting in skin-related research", Chapter 8 "Advantages and limitations of 3D bioprinting" and conclusions, drawn part of Figure 1.

Julia Semba reviewed the literature and wrote the original draft of Chapter 3 "Bioprinting" (with Adam Kulpa), and drawn Figure 2.

Adam Kulpa reviewed the literature and wrote the original draft of Chapter 3 "Bioprinting" (with Julia Semba)

Aleksandra Dańczak-Pazdrowska wrote the original draft of Chapter 2 "Skin architecture and function".

Jakub Rybka designed the study, supervised the technical part of the research, and revised the manuscript. Jakub Rybka also corresponded with the journal and reviewers.

Justyna Gornowicz-Porowska designed the study, supervised the research, and revised the manuscript, drawn part of Figure 1 and wrote the original draft of Chapter 2 "Skin architecture and function", Chapter 5 "The required properties of bioprinted skin", Chapter 6 "Overview of 3D skin bioprinting studies" and Chapter 7 "Application of 3D bioprinting in skin-related research" and conclusions.

Date: 21.08.2023

Signature:

Adam Kulpa

Oklahoma Medical Research Foundation
e-mail: adam.kulpa97@gmail.com

Author contribution statement

I declare that I am the co-author of the article "3D bioprinting in skin related research: recent achievements and application perspectives" by Anna Olejnik, Julia Anna Semba, Adam Kulpa, Aleksandra Dańczak-Pazdrowska, Jakub Dalibor Rybka, and Justyna Gornowicz-Porowska, published in *ACS Synthetic Biology* in 2022 and I am aware that this publication is a part of Julia Semba PhD dissertation. The author's contribution is as follows:

Anna Olejnik designed the study, reviewed the literature, and wrote the original draft of introduction, Chapter 4 "Types of cells applied in skin bioprinting", Chapter 5 "The required properties of bioprinted skin", Chapter 6 "Overview of 3D skin bioprinting studies", Chapter 7 "Application of 3D bioprinting in skin-related research", Chapter 8 "Advantages and limitations of 3D bioprinting" and conclusions, drawn part of Figure 1.

Julia Semba reviewed the literature and wrote the original draft of Chapter 3 "Bioprinting" (with Adam Kulpa), and drawn Figure 2.

Adam Kulpa reviewed the literature and wrote the original draft of Chapter 3 "Bioprinting" (with Julia Semba)
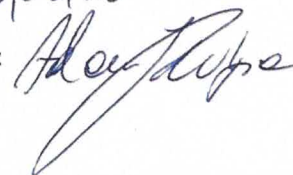
Aleksandra Dańczak-Pazdrowska wrote the original draft of Chapter 2 "Skin architecture and function".

Jakub Rybka designed the study, supervised the technical part of the research, and revised the manuscript. Jakub Rybka also corresponded with the journal and reviewers.

Justyna Gornowicz-Porowska designed the study, supervised the research, and revised the manuscript, drawn part of Figure 1 and wrote the original draft of Chapter 2 "Skin architecture and function", Chapter 5 "The required properties of bioprinted skin", Chapter 6 "Overview of 3D skin bioprinting studies" and Chapter 7 "Application of 3D bioprinting in skin-related research" and conclusions.

Date: 23/08/23

Signature:

Dr hab. inż. Jakub Rybka, prof. UAM

Laboratory of Applied Biotechnology
Center for Advanced Technology
Adam Mickiewicz University in Poznan
e-mail: jrybka@amu.edu.pl

Author contribution statement

I declare that I am the corresponding author of the article "3D bioprinting in skin related research: recent achievements and application perspectives" by Anna Olejnik, Julia Anna Semba, Adam Kulpa, Aleksandra Dańczak-Pazdrowska, Jakub Dalibor Rybka, and Justyna Gornowicz-Porowska, published in *ACS Synthetic Biology* in 2022 and I am aware that this publication is a part of Julia Semba PhD dissertation. The author's contribution is as follows:

Anna Olejnik designed the study, reviewed the literature, and wrote the original draft of introduction, Chapter 4 "Types of cells applied in skin bioprinting", Chapter 5 "The required properties of bioprinted skin", Chapter 6 "Overview of 3D skin bioprinting studies", Chapter 7 "Application of 3D bioprinting in skin-related research", Chapter 8 "Advantages and limitations of 3D bioprinting" and conclusions, drawn part of Figure 1.

Julia Semba reviewed the literature and wrote the original draft of Chapter 3 "Bioprinting" (with Adam Kulpa), and drawn Figure 2.

Adam Kulpa reviewed the literature and wrote the original draft of Chapter 3 "Bioprinting" (with Julia Semba)

Aleksandra Dańczak-Pazdrowska wrote the original draft of Chapter 2 "Skin architecture and function".

Jakub Rybka designed the study, supervised the technical part of the research, and revised the manuscript. Jakub Rybka also corresponded with the journal and reviewers.

Justyna Gornowicz-Porowska designed the study, supervised the research, and revised the manuscript, drawn part of Figure 1 and wrote the original draft of Chapter 2 "Skin architecture and function", Chapter 5 "The required properties of bioprinted skin", Chapter 6 "Overview of 3D skin bioprinting studies" and Chapter 7 "Application of 3D bioprinting in skin-related research" and conclusions.

Date: 1 8. 08. 2023

Signature:

of. UAM dr hab. inż. Jakub D. Rybka

Dr hab. Justyna Gornowicz-Porowska

Department and Division of Practical Cosmetology and Skin Diseases Prophylaxis
University of Medicinal Sciences, Poznan
e-mail: justyna.gornowicz-porowska@ump.edu.pl

Author contribution statement

I declare that I am the corresponding author of the article "3D bioprinting in skin related research: recent achievements and application perspectives" by Anna Olejnik, Julia Anna Semba, Adam Kulpa, Aleksandra Dańczak-Pazdrowska, Jakub Dalibor Rybka, and Justyna Gornowicz-Porowska, published in *ACS Synthetic Biology* in 2022 and I am aware that this publication is a part of Julia Semba PhD dissertation. The author's contribution is as follows:

Anna Olejnik designed the study, reviewed the literature, and wrote the original draft of introduction, Chapter 4 "Types of cells applied in skin bioprinting", Chapter 5 "The required properties of bioprinted skin", Chapter 6 "Overview of 3D skin bioprinting studies", Chapter 7 "Application of 3D bioprinting in skin-related research", Chapter 8 "Advantages and limitations of 3D bioprinting" and conclusions, drawn part of Figure 1.

Julia Semba reviewed the literature and wrote the original draft of Chapter 3 "Bioprinting" (with Adam Kulpa), and drawn Figure 2.

Adam Kulpa reviewed the literature and wrote the original draft of Chapter 3 "Bioprinting" (with Julia Semba)

Aleksandra Dańczak-Pazdrowska wrote the original draft of Chapter 2 "Skin architecture and function".

Jakub Rybka designed the study, supervised the technical part of the research, and revised the manuscript. Jakub Rybka also corresponded with the journal and reviewers.

Justyna Gornowicz-Porowska designed the study, supervised the research, and revised the manuscript, drawn part of Figure 1 and wrote the original draft of Chapter 2 "Skin architecture and function", Chapter 5 "The required properties of bioprinted skin", Chapter 6 "Overview of 3D skin bioprinting studies" and Chapter 7 "Application of 3D bioprinting in skin-related research" and conclusions.

Date: 28. 06 23

Signature:

dr hab. n. med. Justyna Gornowicz-Porowska, prof. UMP

CNT-Type Dependent Cellular Adhesion on 3D-Printed Nanocomposite for Tissue Engineering

Adam A. Mieloch[1]*, Julia A. Semba[1,2], Jakub D. Rybka[1]*

[1]Center for Advanced Technology, Adam Mickiewicz University, Poznan, Poland
[2]Faculty of Biology, Adam Mickiewicz University, Poznan, Poland

Abstract: At present, one of the main limitations of three-dimensional (3D) bioprinting in tissue engineering stems from a scarcity of biomaterials tailored for specific applications. Widely used hydrogels offer an optimal printability and a suitable environment for cell growth; however, they lack the mechanical strength required for non-soft tissues, for example, cartilage, tendons, and meniscus. This work investigated the physicochemical, mechanical, and biological characteristics of a 3D-printed polycaprolactone (PCL) reinforced with multiwalled carbon nanotubes (MWCNT) and "bamboo-like" carbon nanotubes (BCNT) with the following w/w % concentrations: 0.005%, 0.01%, 0.02%, and 0.2%. The materials were analyzed with subsequent techniques: Scanning electron microscopy, nanoindentation, parallel plate rheometry, and differential scanning calorimetry. Biological evaluations were performed with normal human articular chondrocytes by confocal microscopy and proliferation assay. The study revealed that the carbon nanotubes (CNT) addition improved the rheological properties of the material by increasing the setting temperature. Moderate enhancement was observed in terms of mechanical properties. The most significant difference was noted in cell adhesion and proliferation. Pure PCL did not facilitate cell growth and mainly apoptotic cells were observed on its surface. The addition of 0.01% MWCNT resulted in enhanced adhesion and proliferation; however, the morphology of the cells remained spherical, signifying a suboptimal surface for proliferation. Interestingly, PCL reinforced with 0.02% BCNT displayed excellent facilitation of cellular adhesion and proliferation, which is uncharacteristic of pure PCL. In summary, this study investigated the potential of CNT-reinforced PCL for 3D bioprinting and tissue engineering, highlighting key physicochemical, mechanical, and biological aspects of this biomaterial.

Keywords: 3D bioprinting; Polycaprolactone; Carbon nanotubes; Tissue engineering nanocomposite

1. Introduction

Polycaprolactone (PCL) is a semicrystalline biodegradable polyester with a melting temperature of ~60°C. It is FDA-approved for use in surgical implants and drug delivery devices and is widely studied for applications in tissue engineering and regenerative medicine[1]. Due to its low melting temperature and proven biocompatibility, it is the most commonly used thermoplastic polymer for three-dimensional (3D) bioprinting[2-5]. However, its mechanical and bioadhesive properties are suboptimal for non-soft tissue engineering and can be improved on by implementing additives. Carbon nanotubes (CNT)

are an excellent additive candidate, supplementing both inadequacies of the PCL. Structurally, CNT can be viewed as sheets of graphene rolled into cylinders. There are several morphologically distinct forms of CNT, resulting in varying physicochemical properties. Nonetheless, CNT are one of the strongest materials in nature with Young's modulus on the order of $270 - 950$ GPa and tensile strength of $11 - 63$ GPa[6]. In terms of biocompatibility, they have been extensively studied for tailored biomaterial engineering of tissues such as cardiac tissue, neural tissue, bone, and cartilage[7-10]. In addition, a significant body of work regarding CNT-reinforced nanocomposites and their characteristics can be found in

the literature[11-13]. For the purpose of this study, two types of CNT were selected: "bamboo-like" CNT (BNCT) and multiwalled CNT (MWCNT). "Bamboo-like" CNT (BCNT) resemble the cup-in-cup structure characteristic of the bamboo stem, with a high presence of surface defects. This type of CNT is comparatively inexpensive as its imperfect morphology does not require stringent synthesis conditions. MWCNT are composed of multiple single-walled CNT with diminishing diameters, arranged concentrically. Due to the diminished quantity of structural defects in comparison to BCNT, MWNCT can be used for tissue engineering applications requiring electrical conductivity[14]. In recent years, a lot of research has been devoted to electrospun PCL/CNT nanocomposites for tissue engineering purposes, indicating a growing interest in biopolymers with CNT additives[15-19]. In regard to PCL/CNT composites, a staggering amount of variables, such as CNT aspect ratios, purity, defects, functionalizations, entanglement within a polymer matrix, and interfacial interactions reduce any predictive attempts of resulting properties to an educated guess. In addition, the potential cytotoxicity of a nanocomposite material depends on the biodegradation rate and subsequent gradual release of the nanofiller into the tissue environment. Therefore, despite a plethora of relevant research, a specific application-driven design of CNT-reinforced polymers still requires extensive laboratory work. This work aimed to evaluate mechanical and biological properties of PCL reinforced with BCNT and MWCNT from a 3D bioprinting and tissue engineering point of view.

2. Materials and methods

2.1. Materials

CNT were purchased from NanoLab Inc. (USA, MA). MWCNT have a purity >85%, diameter 10 – 30 nm, and length 5 – 20 µm. BCNT have a purity >85%, diameter 10 – 30 nm, and length 5 – 20 µm. PCL used in this work was in powder (~50 000 MW, Polysciences Europe GmbH). LIVE/DEAD Viability/Cytotoxicity Kit for mammalian cells (Invitrogen) was also used in this study.

2.2. Cell culture

Human knee articular chondrocytes (NHAC-kn, Cat No: CC-2550, LONZA) were cultured in DMEM/F12 with L-glutamine (Corning) supplemented with 10% fetal bovine serum (FBS), 50 µg/mL 2-phospho-L-ascorbic acid, 50 U/ml penicillin, and 50 µg/ml streptomycin at standard culture conditions. The medium was changed every 3 days. Cells were subcultured at 80 – 90% confluence with the TrypLE Express Enzyme (Gibco). Chondrocytes up to the ninth passage and with cell viability above 95% were used for cell experiments.

2.3. Material preparation

The PCL and CNT powders were mixed in 15 ml Falcon tubes by shaking until a visually homogeneous powder was obtained. Subsequently, the powder was placed on a glass Petri dish and heated on a magnetic stirrer until melting occurred. The melt was cooled down and folded several times to improve the homogeneity of the material. Finally, the melt was cut into pellet-like pieces, which were suitable for the thermoplastic printhead.

2.4. 3D printing

3D printing was performed with the Cellink BioX printer. In the process, the thermoplastic printhead was utilized. The 3D model of the grid was prepared by manual writing of a.gcode file. The printing was performed with the following parameters: printhead nozzle diameter, 0.4 mm; printhead temperature, 180°C; printing speed, 4 mm/s; and extrusion pressure, 510 kPa.

2.5. Nanoindentation

The nanoindentation study was performed on a G200 (Agilent) nanoindenter equipped with a DCM head. Each sample was subjected to 12 indentations of 2000 nm in-depth, with a Berkovich-type probe, at room temperature. Analyses were performed at 500 – 1800 nm depth. Due to the uneven topography of the surface, extreme results were excluded from further analysis.

2.6. Parallel plate rheometry

The rheology study was performed with the Discovery Hybrid HR20 Rheometer (TA instruments). A 20 mm aluminum parallel plate was used for the measurements. A temperature sweep analysis was performed in two ranges: 120 – 40°C and 50 – 80°C. For both ranges, the temp. step was set to 2°C, 1% strain, and angular frequency at 10 rad/s. The soak time was set to 30 s. A flow sweep analysis was performed at three temperatures: 180°C, 120°C, and 60°C. The range of shear rate was set from 1×10^{-3} 1/s to 500.0 1/s, at logarithmic step. Data were analyzed using TA Instruments TRIOS Software version 5.1.1.46572.

2.7. Differential scanning calorimetry (DSC)

DSC analysis was performed on a DSC 8500 apparatus (Perkin Elmer) in the temperature range of $-90 – 180°C$, with nitrogen flow (20 ml/min). The temperature change rate was set at 10°C/min. The thermal history of the raw material was erased before measurement. 3D-printed grids were not subjected to thermal history erasure.

2.8. LIVE/DEAD viability/cytotoxicity kit for mammalian cells

3D-printed grids were cut and sterilized by ultraviolet (UV) light (30 min on each side). This experiment was carried out on 24-well Ultra-Low Attachment plates (Corning) in three biological replications. The chondrocytes were seeded on the grids at a density of 2×10^4 cells per well. The culture medium was changed every three days. The assay was carried out after 2 weeks of culture under standard conditions. The final concentrations of calcein-AM and EthD-1 were 2 and 4 µM, respectively. The labeled cells were visualized under confocal microscopy (Olympus XI83).

2.9. Cell Titer-Glo 2.0 cell viability assay

To investigate the potential toxicity of the materials, 3D-printed PCL grids were cut and sterilized with UV light (30 min on each side). This experiment was carried out on 24-well plates in three biological replications. Chondrocytes were seeded at a density of 2×10^4 cells per well. Positive control was cells seeded without the grid. After 3 and 6 days, the CellTiter-Glo 2.0 cell viability assay was carried out according to the manufacturer's manual with slight modifications. Briefly, 500 µl of fresh medium was added to each well, equilibrated to room temperature, followed by the addition of the CellTiter reagent. The plates were mixed for 2 min and incubated for 10 min at room temperature. Then, 200 µl of the solution was transferred to 96-well opaque-walled plates in at least two technical repeats. The luminescence was recorded using the Infinite 200 PRO plate reader (TECAN).

2.10. Statistical analysis

Statistical analysis was performed using GraphPad Prism ver. 8.0.1.

3. Results

3.1. Scanning electron microscopy (SEM) imaging

SEM imaging of the printed constructs revealed that the addition of CNT, regardless of their type and concentration, resulted in a much smoother surface in comparison to the pure PCL (**Figure S1**). The initial assumption was that the decrease in surface roughness will result in diminished cell attachment.

3.2. Parallel plate rheometry

Rheological properties are crucial from the standpoint of 3D printing and polymer manufacturing. It also provides valuable insight into the supramolecular interactions present within a material. The materials were subjected to the temperature sweep in the 120 – 40°C range, followed by a 50 – 80°C range sweep. Subsequently, flow sweep analysis was performed at three temperatures: 180°C, 120°C, and 60°C. Exemplary results of a pure PCL are presented in **Figure 1**.

The rest can be found in Supplementary File (**Figures S2-S4**). From the temperature sweep analysis, a point of modulus cross-over was obtained. The modulus cross-over signifies a temperature at which a change of the dominant modulus occurs. If the storage modulus (G') dominates, a material presents more elastic (solid-like) behavior. Conversely, if the loss modulus (G'') dominates, the material presents a more viscous (liquid-like) behavior. From the flow sweep analysis, zero-rate viscosity was calculated. The results are presented in **Table 1**.

The addition of CNT resulted in elevated temperature of modulus cross-over during cooling, regardless of CNT type. The highest increase was observed for 0.2% addition of BCNT and 0.2% MWCNT: 6.3°C and 5.2°C increase, respectively, in comparison to pure PCL. The temperature of modulus cross-over during heating was not pronouncedly affected by CNT addition. These observations indicate that CNT influence the solidification of PCL, but not melting. This led us to the suspicion that CNT may affect the crystallization of PCL either by acting as nucleation centers or by facilitating heat transfer through the polymer. Such phenomena have been described previously[20-22]. Regarding zero-rate viscosity, 0.01% addition of BCNT and MWCNT increased the polymer's viscosity. Interestingly, at the highest concentrations, a decrease in zero-rate viscosity was observed instead. Congruous data were obtained for all three temperatures. This result could be attributed to a gradual shift in dominant interactions between the CNT and PCL chains. At 0.01%, PCL/CNT interactions may predominate over PCL/PCL and CNT/CNT. With increasing CNT concentrations, the balance shifts toward CNT/CNT interactions, resulting in a decrease in zero-rate viscosity. The best fit flow analysis of viscosity vs. strain curve confirmed the pseudoplastic behavior of all tested materials. In most cases, the Carreau-Yasuda model was attributed to the experimental data[23,24]. Regardless of CNT addition, all samples showed similarity in viscosity vs. strain curve (**Figure S4**). At 60°C, the Newtonian plateau persisted until the shear rate of c.a. 6 1/s, where the transition region occurred. Due to limitations of the apparatus, further measurements beyond this point were unattainable. At 120°C, a prolonged Newtonian plateau was observed, followed by a well-pronounced transition region starting at c.a. 25 1/s, and a precipitous drop in viscosity, signifying the power-law region. At 180°C, the Newtonian plateau extended to the shear viscosity of c.a. 100 1/s. The transition region and the power-law were, in general, more flattened in comparison to 120°C.
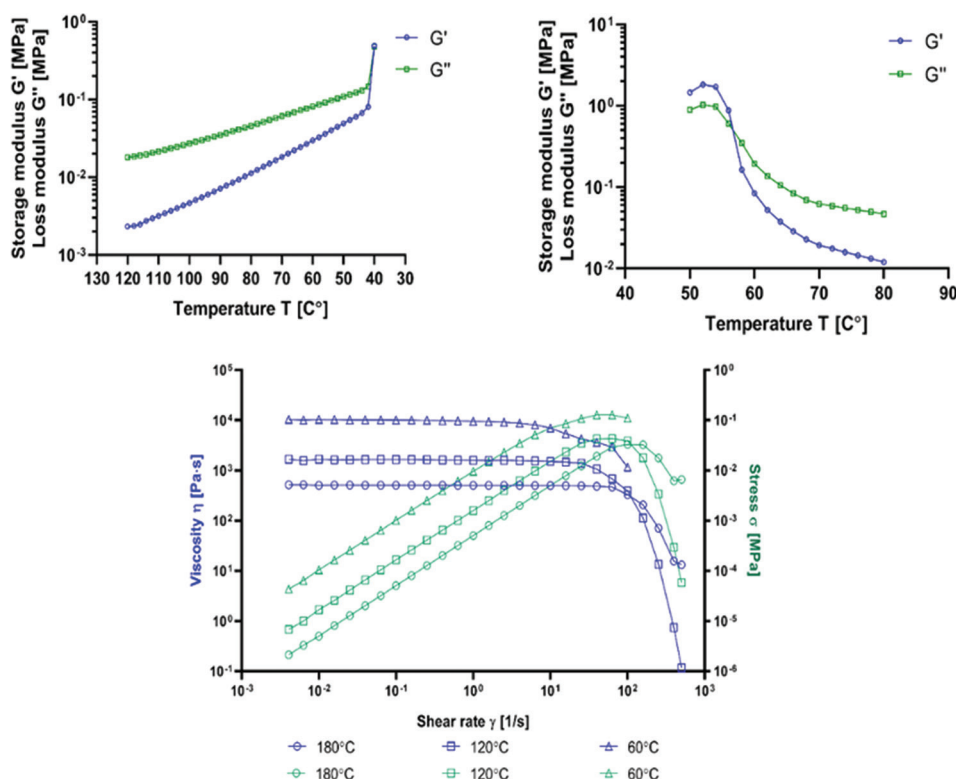
Figure 1. Example results of the temperature sweep and the flow sweep analysis (pure PCL).

Table 1. The modulus cross-over and zero-rate viscosity of the PCL at various CNTs concentrations.

CNT content (w/w)		Modulus cross-over (°C)		Zero-rate viscosity (Pa·s)		
		120-40°C	50-80°C	180°C	120°C	60°C
PCL	0%	40.0	56.7	502.2	1579.6	10162.1
BCNT	0.005%	44.0	56.8	542.3	1662.8	10762.9
	0.01%	44.0	57.1	605.8	1892.9	10694.7
	0.02%	44.4	56.9	573.7	1775.7	9027.3
	0.2%	46.3	57.4	485.6	1536.2	7090.8
MWCNT	0.005%	42.8	57.0	555.4	1655.7	9729.2
	0.01%	42.6	56.9	579.7	1825.2	10252.4
	0.02%	44.0	57.1	569.8	1718.9	9377.6
	0.2%	45.2	57.2	452.6	1394.2	8445.1

In blue – minimum values; in red – maximum values. Zero-rate viscosity was calculated using best fit flow (viscosity vs. flow).

Obtained data indicates that the CNT addition does not affect the dynamics of shear-thinning behavior, displaying comparable viscosity versus strain curves across all samples at given temperatures. From this perspective, 120°C seems to be the most optimal for 3D printing of PCL, as it allows to fully utilize its shear-thinning behavior.

3.3. DSC

First, a DSC analysis was performed to assess the crystallinity of the raw material and the 3D 3D-printed grids. From the standpoint of a material investigation, it was vital to differentiate which factors affect crystallinity,

namely, CNT addition or the 3D printing process. Therefore, the analysis of 3D printed grids was run without erasing the thermal history of the material, retaining its crystalline structure. The degree of crystallinity was calculated based on the heat of melting as:

$$\chi(\%) = \frac{\Delta H_m}{\Delta H_{m^0}} \cdot 100\%$$

where:

ΔH_m – the heat of melting (J/g)

$\Delta H_m{}^0$ – the heat of melting (J/g) for 100% crystalline polymer

The melting heat for 100% crystalline PCL is 139.5 J/g, which was adopted from the literature[25]. The results are summarized in **Table 2**.

The analysis revealed that the CNT addition does not affect substantially the overall crystallinity of the PCL. Interestingly, the process of 3D printing itself was much more influential, providing an 8.7% mean increase of crystallinity. Second, DSC analysis was utilized to investigate the crystallization dynamics of PCL + CNT blends. The rheological behavior of the samples suggests that the addition of CNT accelerates the solidification of the melts, which is associated with the crystallization of the material. The results confirmed the observations from the rheological analysis. The addition of CNT increases the temperature of crystallization onset (Tc) and the Tc (**Figure 2**). BCNT addition resulted in a mean increase of 4.0°C in the Tc onset and 6.9°C in the Tc. MWCNT addition provided a 2.9°C mean increase in the Tc onset and a 5.1°C mean increase in the Tc (**Table 3**). Despite not increasing overall crystallinity, CNT addition did enhance the crystallization rate of the PCL, calculated as Tc onset - Tc.

Table 2. The degree of crystallinity of the PCL at various CNTs concentrations.

	CNT content (w/w)	Degree of crystallinity (%)	
		Raw material	Grids
PCL	0%	50.75	59.00
BCNT	0.005%	51.38	59.94
	0.01%	50.68	60.20
	0.02%	50.14	60.26
	0.2%	50.91	61.92
MWCNT	0.005%	51.52	57.64
	0.01%	51.31	58.89
	0.02%	51.11	59.81
	0.2%	49.77	58.24

In blue – minimum values; in red – maximum values.

Table 3. The Tc and Tc onset the PCL at various CNTs concentrations.

	CNTs content (w/w)	Tc onset (°C)	Tc (°C)	Tc onset - Tc (°C)
PCL	0%	32.89	25.3	7.6
BCNT	0.005%	36.22	32.29	3.9
	0.01%	35.97	31.27	4.7
	0.02%	37.25	32.69	4.6
	0.2%	38.13	32.38	5.8
MWCNT	0.005%	33.66	27.93	5.7
	0.01%	35.43	29.65	5.8
	0.02%	36.54	31.91	4.6
	0.2%	37.62	32.01	5.6

In blue – minimum values; in red – maximum values.

3.4. Nanoindentation

Mean elastic modulus and mean hardness were measured via the nanoindentation method (**Figure 3**). Measurement was performed only on raw materials, as the curvature of 3D printed grids hinders reliable measurement. Therefore, we were unable to assess the effects of increased crystallinity on the mechanical properties of PCL reinforced with CNTs. The sole addition of CNTs did improve the mechanical properties of the material, however, in a nonlinear fashion. The highest increase in mean elastic modulus and hardness was observed for PCL with a concentration of 0.02% MWCNT.

3.5. LIVE/DEAD viability/cytotoxicity assay

Normal human knee articular chondrocytes (NHAC-kn) were seeded on the 3D printed grids and cultured for 2 weeks in standard conditions on non-adherent culture plates. After 2 weeks, cells were dyed with the LIVE/DEAD assay (**Figure 4**). The addition of CNTs did significantly affect the biocompatibility of the PCL. Chondrocytes seeded on pure PCL were mostly dead, while even the smallest concentration of 0.005% BCNT enhanced the viability. The enhancement was observed up to 0.02% concentration. At the highest tested concentration, BCNT decreased the viability of the chondrocytes in comparison to lower concentrations. The biocompatibility enhancement effect was less pronounced for PCL/MWCNT. A visible improvement was observed for the concentration of 0.01% MWCNT; however, it was still markedly worse compared to BCNT. Interestingly, BCNT addition facilitated a proper, elongated morphology of the chondrocytes, while this effect was absent in MWCNT-containing samples. In addition, the elongation occurred in parallel to the printhead movement, suggesting extrusion-driven topography alterations, dictating the direction of filopodia elongation. Cells on the PCL/MWCNT grids remained spherical and were rather loosely attached.

3.6. Cell Titer-Glo 2.0 cell viability assay

PCL is a biodegradable polymer; therefore, there is a risk of CNT-mediated cytotoxicity elicited by free-floating CNT, which are released from the polymer. To provide a quantitative analysis of cell viability, the CellTiter-Glo 2.0 Cell Viability assay was performed after three and 6 days of culture. In this experiment, cells were seeded on standard culture plates with inserted grids. After 3 days of culture, a slight increase of viability was observed for 0.01% MWCNT samples (**Figure 5**). On the other hand, 0.2% BCNT samples displayed markedly lower viability. As expected, the highest concentrations of CNT significantly decreased cell viability after 6 days of culture. Compared to control samples, 0.005 – 0.01%
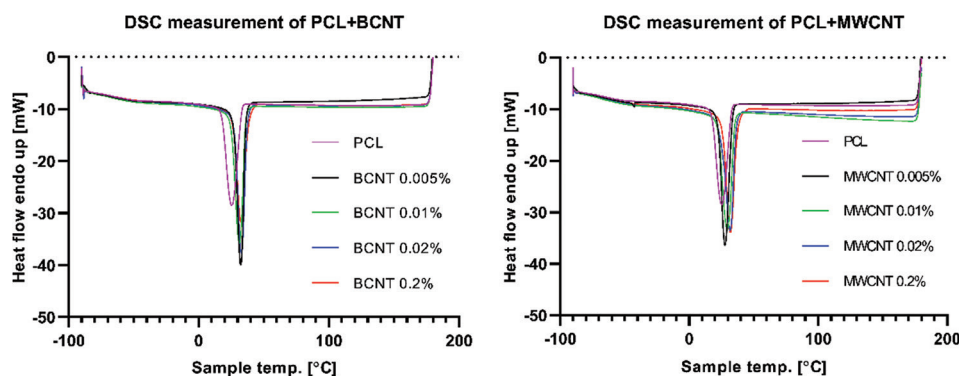
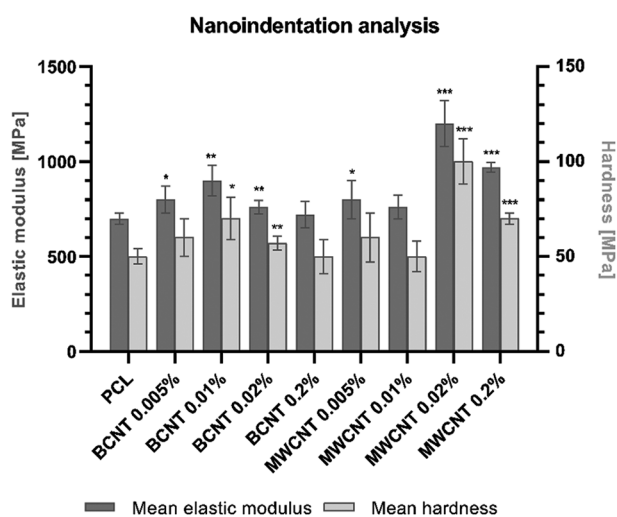**Figure 2.** DSC measurement. Cooling step of raw materials (after thermal history erasure).

Figure 3. Mean elastic modulus and mean hardness of raw materials measured through nanoindentation. Statistical analysis was performed using one-way ANOVA and *post hoc* Dunnett's T3 multiple comparisons test. The mean of each column was compared to the mean of PCL column. CI = 95%, *P* value: 0.12 (ns), 0.033(*), 0.002 (**), <0.001 (***).

concentration range of both CNT types provided no statistically significant differences in viability. Pure PCL grids did have a minor effect on cell viability. The statistical significance of differences between samples against pure PCL was presented in the Supplementary File (**Table S1**).

4. Discussion

The data presented highlights several physicochemical, mechanical, and biological characteristics of PCL reinforced with CNT for 3D printing and tissue engineering. It is important to underline that the polymer mixing methodology most likely resulted in nonhomogeneous CNT dispersions within the polymer matrix, contributing to various characteristics of the resulting biomaterial. For an extensive overview of CNT/polymer nanocomposites and their interfacial characteristics, see the following article[26]. In our study, the addition of CNT resulted in a smoothened surface of the 3D-printed grids in comparison to pure PCL. As the data suggest, this effect cannot be explained by changes in viscosity or crystallinity of the samples. It could, however, be a result of an increased rate of crystallization, calculated as Tc onset - Tc. Presumably, CNT facilitate heat transfer through the polymer providing uniform temperature distribution, preventing local tensions arising from a nonequal rate of crystallization due to regional temperature differences. Contrary to this hypothesis, low concentrations of a thermoconductive filler are believed to facilitate phonons scattering at the filler/polymer interfaces, resulting in the "interface thermal resistance" phenomenon[27,28]. At this point, the mechanism of surface smoothening remains unsettled. However, taking into consideration the increase of the modulus cross-over temperature, Tc and Tc onset, with concomitant lack of increased overall crystallinity for CNT-reinforced PCL, supports the notion of enhanced thermal transfer.

Rheology analysis provided insight into the properties of the CNT/polymer interface. The initial increase of zero-rate viscosity at low to medium concentrations of CNT suggests that the strength of polymer/polymer interface interactions is lower than the polymer/CNT. However, at high CNT concentrations, zero-rate viscosity decreased below pure PCL, signifying the CNT/CNT interface being weaker in comparison to the polymer/polymer interface. Furthermore, the lack of increased viscosity at lower shear rates indicates that the CNT-filled PCL does not behave like a yield stress fluid (represented by the Herschel-Bulkley model)[29]. Therefore, it can be concluded that the CNT do not form cross-linked networks with the polymer chains. Moreover, it suggests that CNT do not act as nucleation centers for PCL crystallization, as was demonstrated for other polymers[30-32]. This finding is corroborated by the DSC data, revealing that the degree of crystallinity was not significantly affected by the CNT addition. Interestingly,
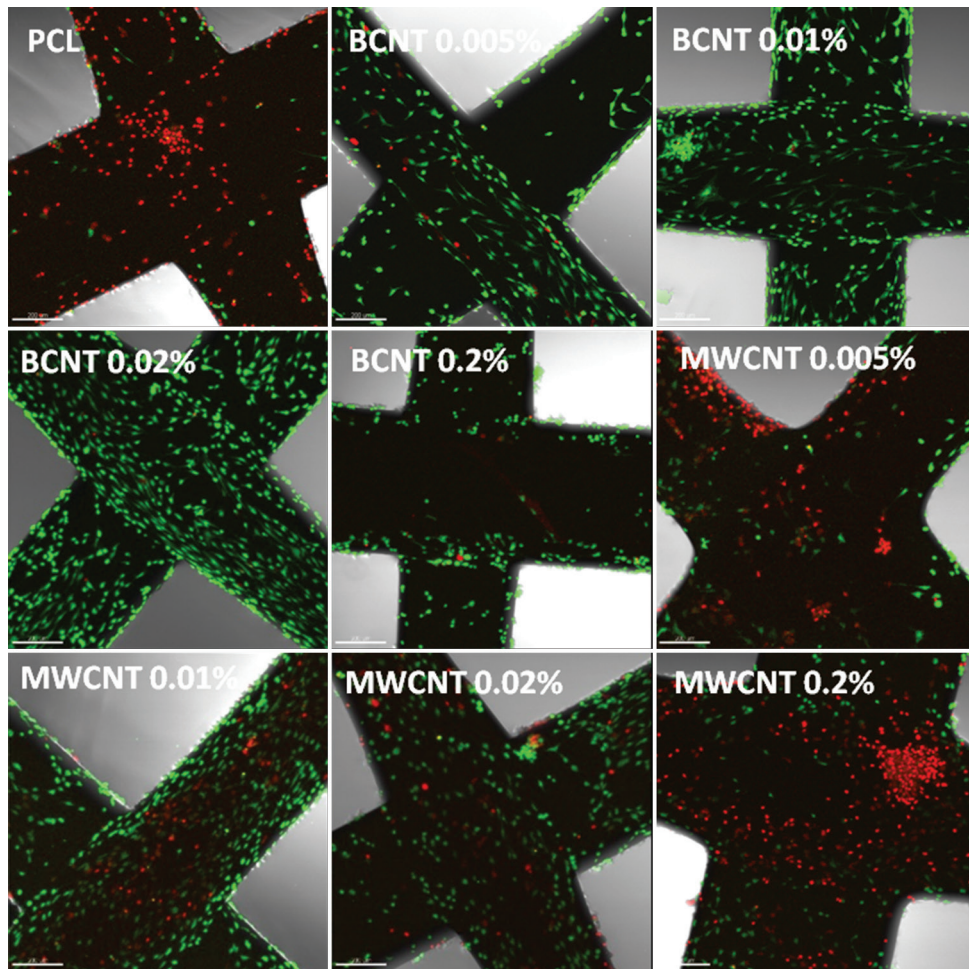
Figure 4. Confocal microscopy of LIVE/DEAD assay. Normal human knee articular chondrocytes (NHAC-kn) cultured for 2 weeks in standard conditions. Scale bars represent 200 μm.
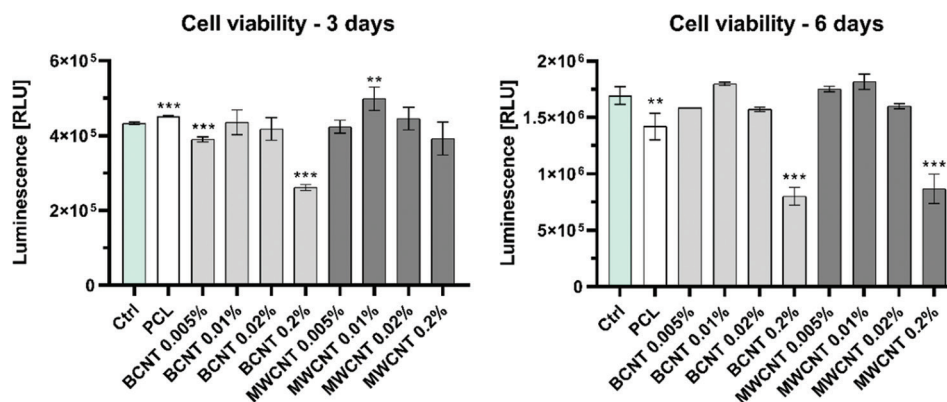

Figure 5. CellTiter-Glo 2.0 cell viability assay. Statistical analysis was performed using one-way ANOVA and *post hoc* Dunnett's T3 multiple comparisons test. The mean of each column was compared to the mean of the control (Ctrl) column. CI = 95%, *P* value: 0.12 (ns), 0.033(*), 0.002 (**), <0.001 (***).

the 3D printing process itself resulted in a significantly increased crystallinity compared to the raw material.

Regarding the mechanical properties assessed by nanoindentation, the addition of CNT did increase the hardness and elastic modulus of the PCL. The effect was the most pronounced for high concentrations of MWCNT. As mentioned previously, the main limitation of the study was the inability to measure 3D-printed grids

due to the cylindrical shape of the sample, which was unsuitable for nanoindentation. This obstacle prevented the comparison between more crystalline 3D-printed grids and raw material. Another factor that has to be taken into consideration is the nonhomogeneous dispersion of the nanotubes, which may form clusters within the material, potentially affecting the measurement.

Biological assessment of the materials revealed an extraordinary improvement in human knee chondrocyte proliferation and viability after the addition of BCNT. At 0.02 w/w% BCNT concentration, cells displayed an optimal morphology and enhanced proliferation. Interestingly, MWCNT addition also enhanced proliferation in comparison to pure PCL; however, cell morphology remained spherical, signifying nonoptimal adhesion to the surface. We suspect two potential mechanisms responsible for the observed effect: (i) Alterations of the surface zeta potential; and (ii) CNT protrusion from the polymer matrix, providing additional anchoring for the cells. In addition, the 3D printing process forces the alignment of CNT along the principal axis of the polymer extrusion, which coincides with the direction of the chondrocytes' filopodia projection, supporting the latter hypothesis. Unfortunately, no direct cause of the enhanced adhesion/proliferation has been found.

As mentioned previously, PCL is a biodegradable polymer, which entails a risk of gradual release of a filler into the environment[33-35]. Our cell viability assay performed after six days of culture showed a significant decrease in cell viability for the highest concentrations of CNT. The rate of biodegradation is a crucial factor, especially for potentially cytotoxic fillers. In theory, however, this could be mitigated by rapid extracellular matrix production, counteracting PCL degradation, and subsequently preventing CNT from being released into the environment.

5. Conclusions

Our study evaluated BCNT and MWCNT as fillers for PCL nanocomposites, dedicated for 3D bioprinting and tissue engineering. The following summary statements could be derived from this study: (i) CNT decreases the roughness of the 3D-printed constructs; (ii) CNT increases the temperature of modulus crossover, Tc, and Tc onset; (iii) the degree of crystallinity depends on the process of 3D printing rather than the CNT addition; (iv) BCNT addition favors cell growth and proliferation of human chondrocytes, facilitating their natural morphology; and (v) at high concentrations, CNT elicit cytotoxic effect and render the material rather unsuitable for tissue engineering purposes. In summary, this work provides novel aspects of PCL-based nanocomposites reinforced with CNT for 3D printing and tissue engineering.

Conflict of interest

The authors declare no competing interests.

Author contributions

J.D.R. guided and supervised the project. A. A. M. designed and supervised the experiments. A. A. M., J.A.S., and J.D.R. conducted experiments and contributed intellectually to the scientific design of the project. A.A.M. and J.D.R. mentored the technical part of the project; manuscript preparation A.A.M and J.A.S.; manuscript edition J.D.R.

References

1. Li L, LaBarbera DV, 2017, 3D High-Content Screening of Organoids for Drug Discovery. In: Comprehensive Medicinal Chemistry III. Vol. 2-8. Amsterdam, Netherlands: Elsevier, p388–415.

2. Ramasamy S, Davoodi P, Vijayavenkataraman S, *et al.*, 2021, Optimized Construction of a Full Thickness Human Skin Equivalent using 3D Bioprinting and a PCL/Collagen Dermal Scaffold. *Bioprinting*, 21:e00123.
   https://doi.org/10.1016/j.bprint.2020.e00123

3. Hassanajili S, Karami-Pour A, Oryan A, *et al.*, 2019, Preparation and Characterization of PLA/PCL/HA Composite Scaffolds Using Indirect 3D Printing for Bone Tissue Engineering. *Mater Sci Eng C*, 104:109960.
   https://doi.org/10.1016/j.msec.2019.109960

4. Zhang W, Ullah I, Shi L, *et al.*, 2019, Fabrication and Characterization of Porous Polycaprolactone Scaffold Via Extrusion-Based Cryogenic 3D Printing for Tissue Engineering. *Mater Des*, 180:107946.
   https://doi.org/10.1016/j.matdes.2019.107946

5. Duymaz BT, Erdiler FB, Alan T, *et al.*, 2019, 3D Bio-Printing of Levan/Polycaprolactone/Gelatin Blends for Bone Tissue Engineering: Characterization of the Cellular Behavior. *Eur Polym J*, 119:426–37.
   https://doi.org/10.1016/j.eurpolymj.2019.08.015

6. Yu MF, Lourie O, Dyer MJ, *et al*., 2000, Strength and Breaking Mechanism of Multiwalled Carbon Nanotubes Under Tensile Load. *Science,* 287:637–40.
    https://doi.org/10.1126/science.287.5453.637

7. Szymański T, Mieloch AA, Richter M, *et al*., 2020, Utilization of Carbon Nanotubes in Manufacturing of 3D Cartilage and Bone Scaffolds. *Materials (Basel)*, 13:4039.

8. Patel DK, Dutta SD, Ganguly K, *et al*., 2021, Enhanced Osteogenic Potential of Unzipped Carbon Nanotubes for Tissue Engineering. *J Biomed Mater Res A*, 109:1869–80.
    https://doi.org/10.1002/jbm.a.37179

9. Edwards SL, Werkmeister JA, Ramshaw JA, 2009, Carbon Nanotubes in Scaffolds for Tissue Engineering. *Expert Rev Med. Dev*, 6:499–505.

10. Haniu H, Saito N, Matsuda Y, *et al*., 2012, Basic Potential of Carbon Nanotubes in Tissue Engineering Applications. *J Nanomater*, 2012:343747.

11. Soni SK, Thomas B, Kar VR, 2020, A Comprehensive Review on CNTs and CNT-Reinforced Composites: Syntheses, Characteristics and Applications. *Mater Today Commun*, 25:101546.

12. Stocco TD, Antonioli E, Romagnolli ML, *et al*., 2020, Aligned Biomimetic Scaffolds Based on Carbon Nanotubes-Reinforced Polymeric Nanofibers for Knee Meniscus Tissue *Eng Mater Lett*, 264:127351.
    https://doi.org/10.1016/j.matlet.2020.127351

13. Lebedev SM, 2020, PCL-CNT Nanocomposites Prepared by Melt Compounding and Evaluation of Their Basic Properties. *Polym Compos*, 41:1830–40.
    https://doi.org/10.1002/pc.25501

14. Abdal-Hay A, Taha M, Mousa HM, *et al*., 2019, Engineering of Electrically-Conductive Poly(E-Caprolactone)/Multi-Walled Carbon Nanotubes Composite Nanofibers for Tissue Engineering Applications. *Ceram Int*, 45:15736–40.
    https://doi.org/10.1016/j.ceramint.2019.04.206

15. Zadehnajar P, Akbari B, Karbasi S, *et al*., 2019, Preparation and Characterization of Poly ε-Caprolactone-Gelatin/Multi-Walled Carbon Nanotubes Electrospun Scaffolds for Cartilage Tissue Engineering Applications. *Int J Polym Mater Polym Biomater*, 69:326–37.
    https://doi.org/10.1080/00914037.2018.1563088

16. Jahanmard F, Eslaminejad MB, Amani-Tehran M, *et al*., 2020, Incorporation of F-MWCNTs into Electrospun Nanofibers Regulates Osteogenesis Through Stiffness and Nanotopography. *Mater Sci Eng C,* 106:110163.
    https://doi.org/10.1016/j.msec.2019.110163

17. Zadehnajar P, Karbasi S, Akbari B, *et al*., 2020, Incorporation of Multi-Walled Carbon Nanotubes Into Electrospun PCL/Gelatin Scaffold: The Influence on the Physical, Chemical and Thermal Properties and Cell Response for Tissue Engineering. *Mater Technol*, 35:39–49.
    https://doi.org/10.1080/10667857.2019.1651539

18. Wu T, Chen X, Sha J, *et al*., 2019, Fabrication of Shish-Kebab-Structured Carbon Nanotube/Poly(E-Caprolactone) Composite Nanofibers for Potential Tissue Engineering Applications. *Rare Met*, 38:64–72.
    https://doi.org/10.1007/s12598-017-0965-y

19. Zou Y, Zhang C, Wang P, *et al*., 2020, Electrospun Chitosan/Polycaprolactone Nanofibers Containing Chlorogenic Acid-Loaded Halloysite Nanotube for Active Food Packaging. *Carbohydr Polym*, 247:116711.
    https://doi.org/10.1016/j.carbpol.2020.116711

20. Yu W, Liu C, Fan S, 2021, Advances of CNT-Based Systems in Thermal Management. *Nano Res*, 14:2471–90.

21. Konstantopoulos G, Maroulas P, Dragatogiannis DA, *et al*., 2021, The Effect of Interfacial Resistance and Crystallinity on Heat Transfer Mechanism in Carbon Nanotube Reinforced Polyethylene. *Mater Des*, 199:109420.
    https://doi.org/10.1016/J.MATDES.2020.109420

22. Avramenko TG, Khutoryanskaya NV, Naumenko SM, *et al*., 2019, Effect of Carbon Nanofillers on Processes of Structural Relaxation in the Polymer Matrixes. In: Proceedings of the Springer Proceedings in Physics. Vol. 221. Cham: Springer, p293–305.

23. Carreau PJ, 1972, Rheological Equations from Molecular Network Theories. *Trans Soc Rheol,* 16:99–127.
    https://doi.org/10.1122/1.549276

24. Yasuda K, 1979, Investigation of the Analogies between Viscometric and Linear Viscoelastic Properties of Polystyrene Fluids, Massachusetts Institute of Technology.

25. Pitt CG, Chasalow FI, Hibionada YM, *et al*., 1981, Aliphatic Polyesters. I. The Degradation of Poly(ε-Caprolactone) *In Vivo*. *J Appl Polym Sci*, 26:3779–87.
    https://doi.org/10.1002/app.1981.070261124

26. Chen J, Liu B, Gao X, *et al*., 2018, A Review of the Interfacial Characteristics of Polymer Nanocomposites Containing Carbon Nanotubes. *RSC Adv*, 8:28048–85.

27. Evans W, Prasher R, Fish J, *et al*., 2008, Effect of Aggregation and Interfacial Thermal Resistance on Thermal Conductivity of Nanocomposites and Colloidal Nanofluids. *Int J Heat Mass Transf*, 51:1431–8.
    https://doi.org/10.1016/j.ijheatmasstransfer.2007.10.017

28. Klonos PA, Peoglos V, Bikiaris DN, *et al*., 2020, Rigid Amorphous Fraction and Thermal Diffusivity in

Nanocomposites Based on Poly(L-Lactic Acid) Filled with Carbon Nanotubes and Graphene Oxide. *J Phys Chem C*, 124:5469–79.

https://doi.org/10.1021/acs.jpcc.9b11843

29. Zhu H, Kim YD, de Kee D, 2005, Non-Newtonian Fluids with a Yield Stress. *J Nonnewton Fluid Mech*, 129:177–81.

https://doi.org/10.1016/j.jnnfm.2005.06.001

30. Wurm A, Herrmann A, Cornelius M, *et al.*, 2015, TEMPERATURE dependency of Nucleation Efficiency of Carbon Nanotubes in Pet and PBT. *Macromol Mater Eng*, 300:637–49.

https://doi.org/10.1002/mame.201400405

31. Schawe JE, Pötschke P, Alig I, 2017, Nucleation Efficiency of Fillers in Polymer Crystallization Studied by Fast Scanning Calorimetry: Carbon Nanotubes in Polypropylene. *Polymer (Guildf)*, 116:160–72.

https://doi.org/10.1016/j.polymer.2017.03.072

32. Zhang S, Minus ML, Zhu L, *et al.*, 2008, Polymer Transcrystallinity induced by Carbon Nanotubes. *Polymer (Guildf)*, 49:1356–64.

https://doi.org/10.1016/j.polymer.2008.01.018

33. Sun H, Mei L, Song C, *et al.*, 2006, The *In Vivo* Degradation, Absorption and Excretion of PCL-Based Implant. *Biomaterials,* 27:1735–40.

https://doi.org/10.1016/j.biomaterials.2005.09.019

34. Goodwin DG, Boyer I, Devahif T, *et al.*, 2018, Biodegradation of Carbon Nanotube/Polymer Nanocomposites Using a Monoculture. *Environ Sci Technol*, 52:40–51.

https://doi.org/10.1021/acs.est.7b02062

35. Frank BP, Goodwin DG, Bohutskyi P, *et al.*, 2020, Influence of Polymer Type and Carbon Nanotube Properties on Carbon Nanotube/Polymer Nanocomposite Biodegradation. *Sci Total Environ*, 742:140642.

https://doi.org/10.1016/j.scitotenv.2020.140512

Publisher's note

Whioce Publishing remains neutral with regard to jurisdictional claims in published maps and institutional affiliations.
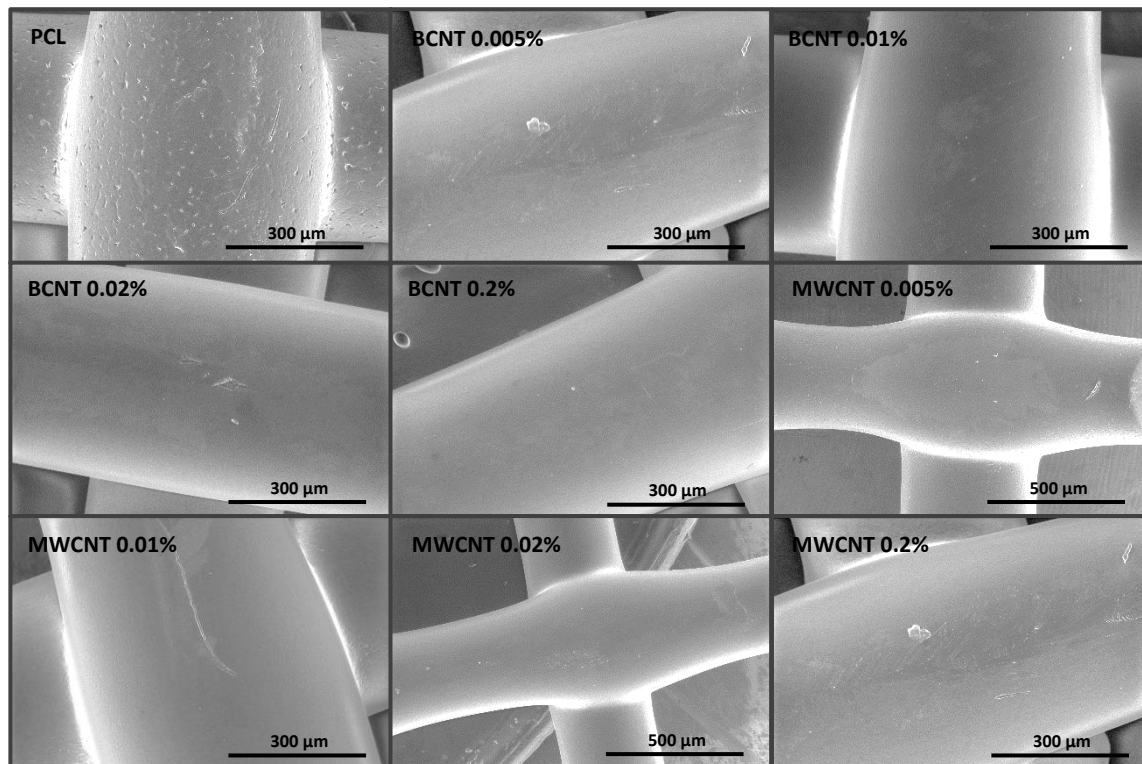
Supplementary File

PCL | BCNT 0.005% | BCNT 0.01%
300 µm | 300 µm | 300 µm
BCNT 0.02% | BCNT 0.2% | MWCNT 0.005%
300 µm | 300 µm | 500 µm
MWCNT 0.01% | MWCNT 0.02% | MWCNT 0.2%
300 µm | 500 µm | 300 µm
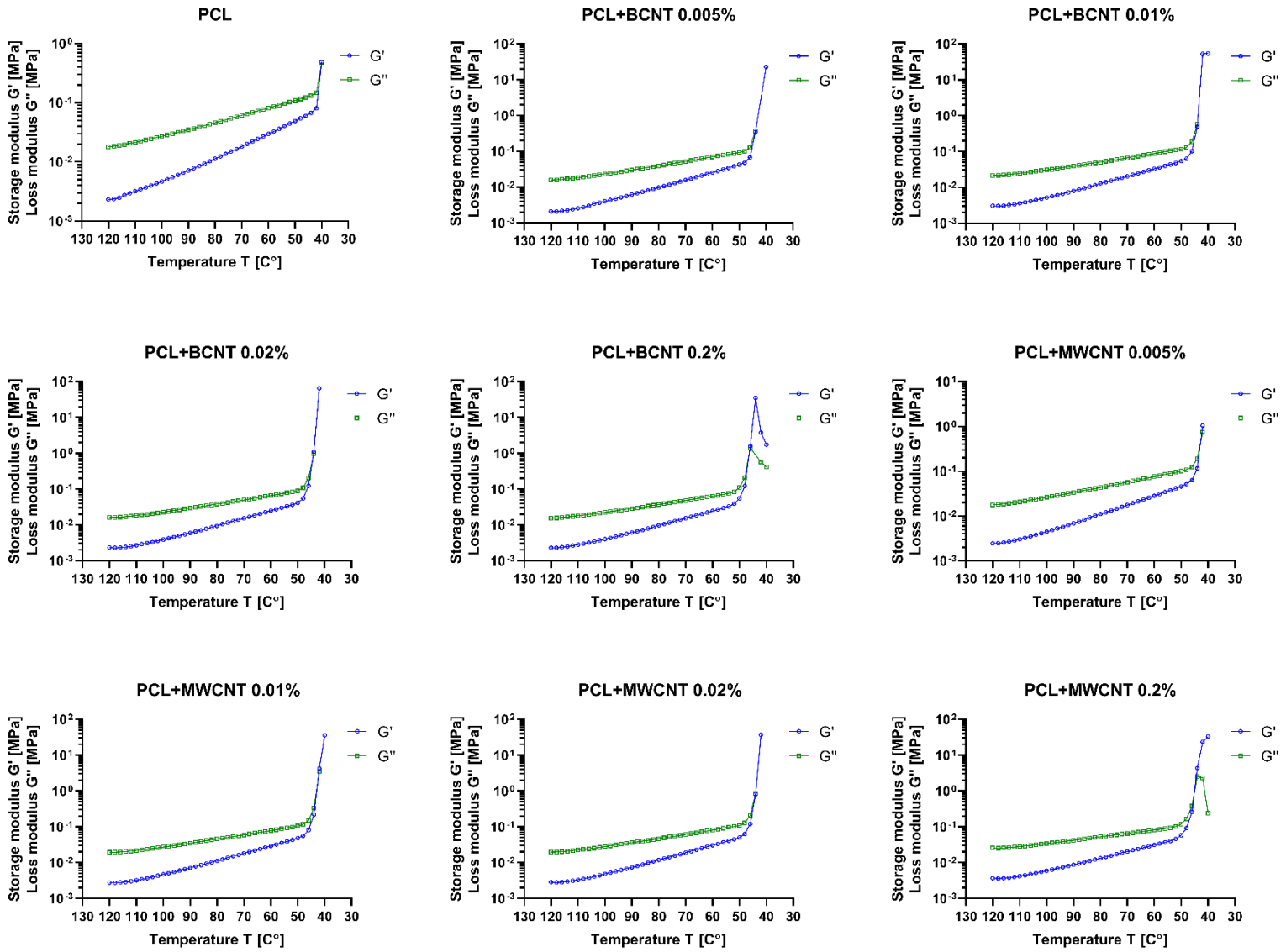
Figure S1. SEM images of 3D-printed grids

Figure S2. Temperature sweep analysis for 120–40°C range
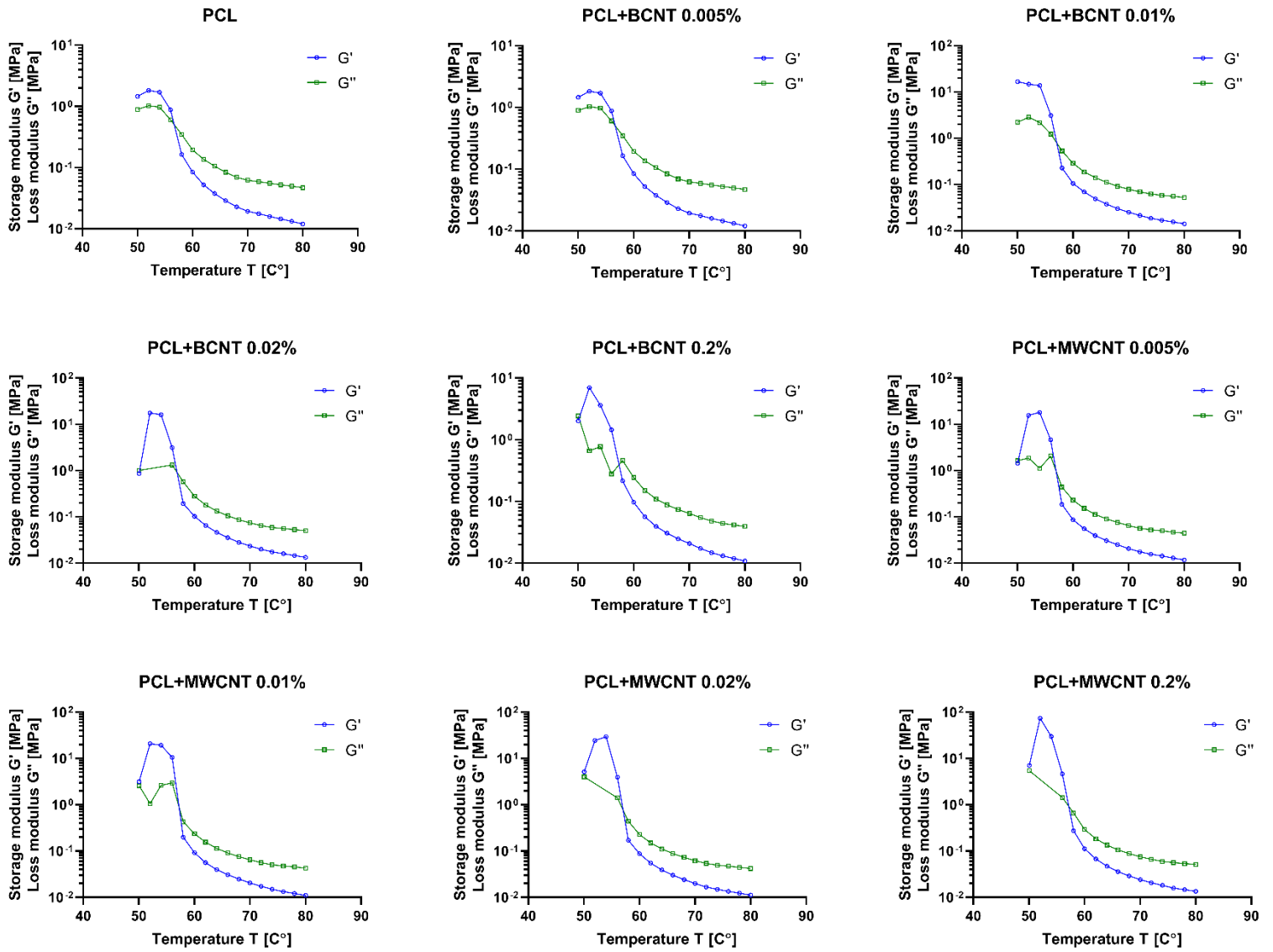
Figure S3. Temperature sweep analysis for 50–80°C range
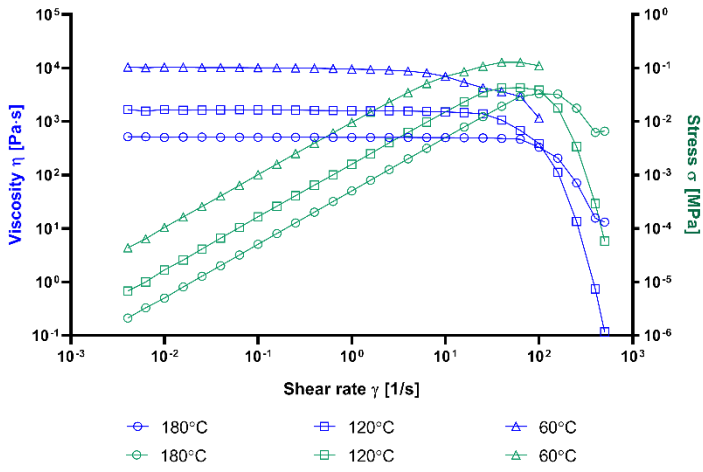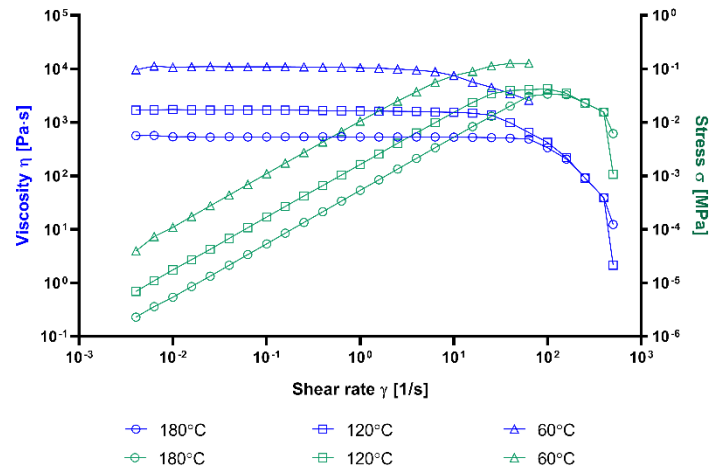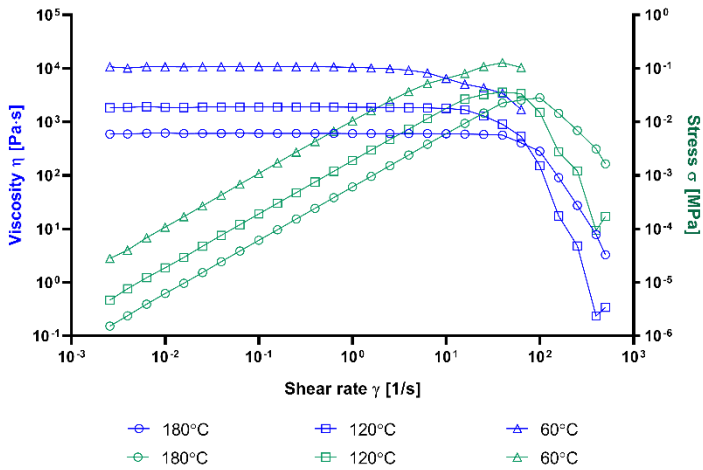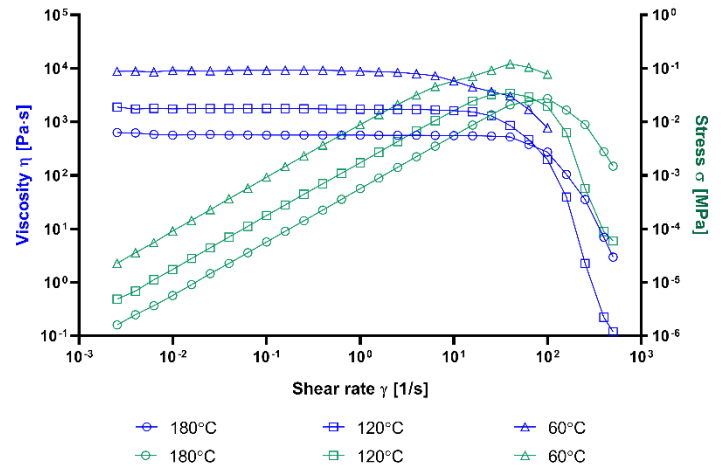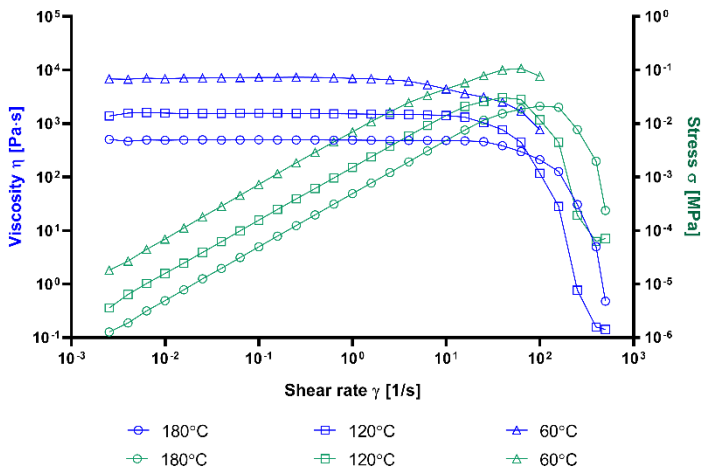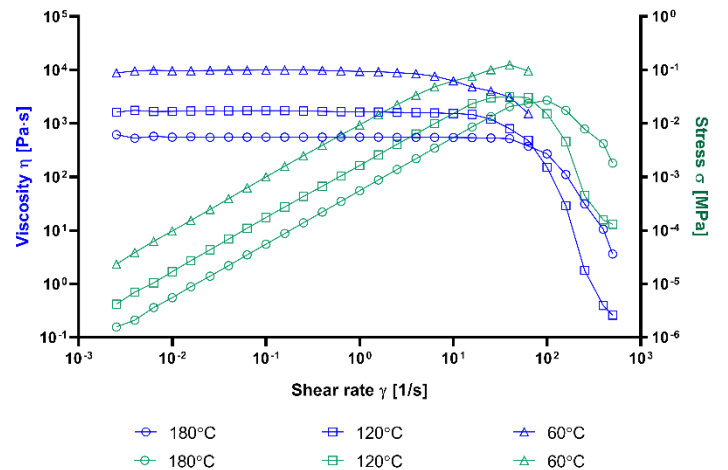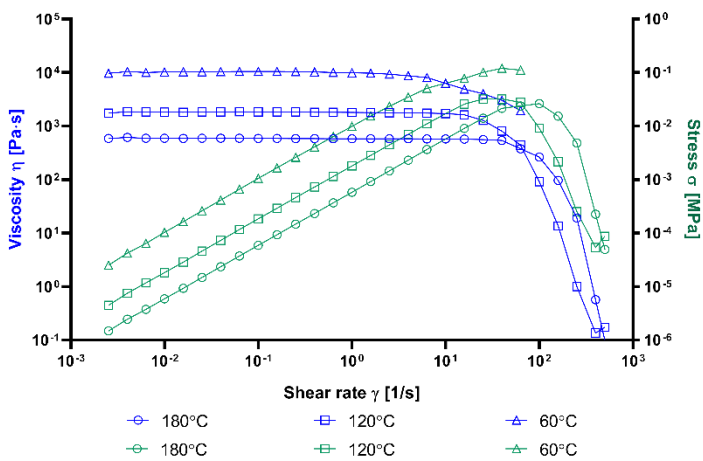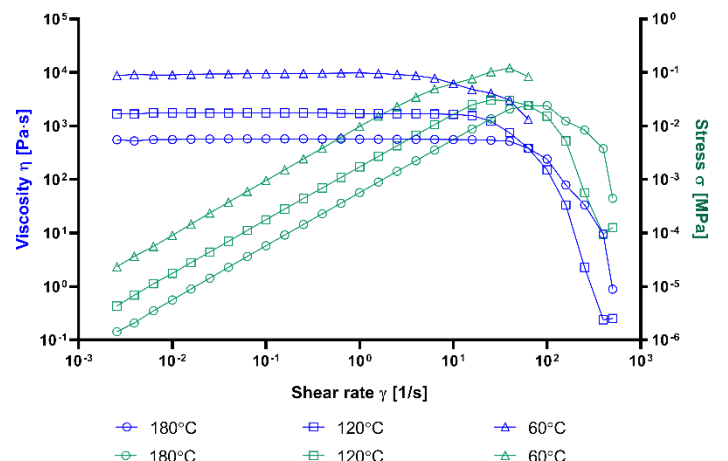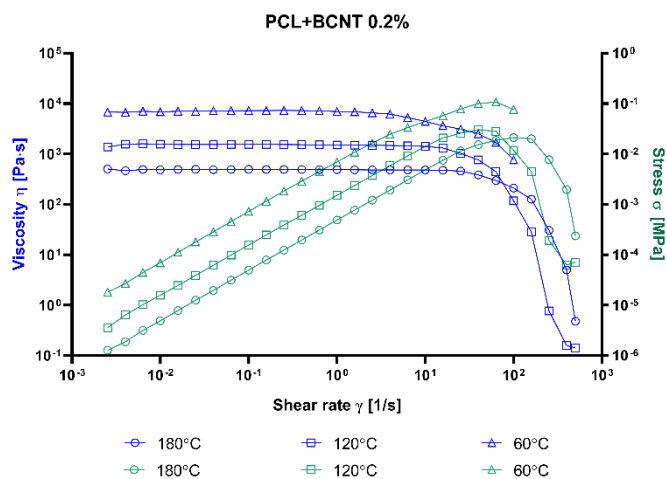
Figure S4. Flow sweep analysis at 180°C, 120°C and 60°C

Table S1. Results of the CellTiter-Glo 2.0 cell viability assay.

Pair	Statistical significance	
	3 days	6 days
PCL vs. Ctrl	***	**
PCL vs. BCNT 0.005%	***	ns
PCL vs. BCNT 0.01%	ns	**
PCL vs. BCNT 0.02%	ns	ns
PCL vs. BCNT 0.2%	***	***
PCL vs. MWCNT 0.005%	**	**
PCL vs. MWCNT 0.01%	*	***
PCL vs. MWCNT 0.02%	ns	ns
PCL vs. MWCNT 0.2%	*	***

Statistical analysis was performed using one-way Anova and post -hoc Dunnett`s T3 multiple comparisons test. The mean of each column was compared to the mean of PCL column.

CI=95%, P value: 0.12 (ns), 0.033(*), 0.002 (**), <0.001 (***).

Julia Semba

Laboratory of Applied Biotechnology
Center for Advanced Technology
Adam Mickiewicz University in Poznan
e-mail: jsemba@amu.edu.pl

Author contribution statement

I declare that I am the co-author of the article "CNT-Type Dependent Cellular Adhesion on 3D-Printed Nanocomposite for Tissue Engineering" by Adam Aron Mieloch, Julia Anna Semba, and Jakub Dalibor Rybka, published in *International Journal of Bioprinting* in 2022. The author's contribution is as follows:

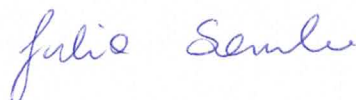**Adam Mieloch** designed the study, supervised the experiments and the technical part of the project. Adam Mieloch carried out material preparation, 3D printing, nanoindentation tests, rheological analysis, and differential scanning calorimetry analysis. Adam Mieloch wrote the original draft of introduction, methodology (except sections 2.2., 2.8., and 2.9.), results (except sections 3.5. and 3.6.), and discussion. Adam Mieloch prepared all figures except Figure 4 and Figure 5.

Julia Semba prepared, made, and analyzed the cell viability with the LIVE/DEAD viability/cytotoxicity kit and the Cell Titer-Glo 2.0 cell viability assay. Julia Semba papered the original draft of methodology (sections 2.2., 2.8., and 2.9.) and results (sections 3.5. and 3.6.) with Figure 4 and Figure 5.

Jakub Rybka designed the study, supervised the technical part of the project, analyzed the results, and revised the manuscript. Jakub Rybka also acquired funding and corresponded with the journal and reviewers.

Date: 18.08.2023

Signature: *Julia Semba*

prof. UAM dr hab. Inż. Jakub D. Rybka

Dr Adam Mieloch

Laboratory of Applied Biotechnology
Center for Advanced Technology
Adam Mickiewicz University in Poznan
e-mail: amieloch@amu.edu.pl

Author contribution statement

I declare that I am the first author of the article "CNT-Type Dependent Cellular Adhesion on 3D-Printed Nanocomposite for Tissue Engineering" by Adam Aron Mieloch, Julia Anna Semba, and Jakub Dalibor Rybka, published in *International Journal of Bioprinting* in 2022 and I am aware that this publication is a part of Julia Semba PhD dissertation. The author's contribution is as follows:

Adam Mieloch designed the study, supervised the experiments and the technical part of the project. Adam Mieloch carried out material preparation, 3D printing, nanoindentation tests, rheological analysis, and differential scanning calorimetry analysis. Adam Mieloch wrote the original draft of introduction, methodology (except sections 2.2., 2.8., and 2.9.), results (except sections 3.5. and 3.6.), and discussion. Adam Mieloch prepared all figures except Figure 4 and Figure 5.

Julia Semba prepared, made, and analyzed the cell viability with the LIVE/DEAD viability/cytotoxicity kit and the Cell Titer-Glo 2.0 cell viability assay. Julia Semba papered the original draft of methodology (sections 2.2., 2.8., and 2.9.) and results (sections 3.5. and 3.6.) with Figure 4 and Figure 5.

Jakub Rybka designed the study, supervised the technical part of the project, analyzed the results, and revised the manuscript. Jakub Rybka also acquired funding and corresponded with the journal and reviewers.

Date: 21.08.2023

Signature:

Dr hab. inż. Jakub Rybka, prof. UAM

Laboratory of Applied Biotechnology
Center for Advanced Technology
Adam Mickiewicz University in Poznan
e-mail: jrybka@amu.edu.pl

Author contribution statement

I declare that I am the corresponding author of the article "CNT-Type Dependent Cellular Adhesion on 3D-Printed Nanocomposite for Tissue Engineering" by Adam Aron Mieloch, Julia Anna Semba, and Jakub Dalibor Rybka, published in *International Journal of Bioprinting* in 2022. The author's contribution is as follows:

Adam Mieloch designed the study, supervised the experiments and the technical part of the project. Adam Mieloch carried out material preparation, 3D printing, nanoindentation tests, rheological analysis, and differential scanning calorimetry analysis. Adam Mieloch wrote the original draft of introduction, methodology (except sections 2.2., 2.8., and 2.9.), results (except sections 3.5. and 3.6.), and discussion. Adam Mieloch prepared all figures except Figure 4 and Figure 5.

Julia Semba prepared, made, and analyzed the cell viability with the LIVE/DEAD viability/cytotoxicity kit and the Cell Titer-Glo 2.0 cell viability assay. Julia Semba papered the original draft of methodology (sections 2.2., 2.8., and 2.9.) and results (sections 3.5. and 3.6.) with Figure 4 and Figure 5.

Jakub Rybka designed the study, supervised the technical part of the project, analyzed the results, and revised the manuscript. Jakub Rybka also acquired funding and corresponded with the journal and reviewers.

Date: 1 8. 08. 2023

Signature: prof. UAM dr hab. Inż. Jakub D. Rybka

RESEARCH ARTICLE

Formulation and evaluation of a bioink composed of alginate, gelatin, and nanocellulose for meniscal tissue engineering

Julia Anna Semba[1,2], Adam Aron Mieloch[1], Ewa Tomaszewska[3], Piotr Cywoniuk[1], Jakub Dalibor Rybka[1]*

[1]Center for Advanced Technology, Adam Mickiewicz University, Poznan, Poland

[2]Faculty of Biology, Adam Mickiewicz University, Poznan, Poland

[3]Faculty of Mechanical Engineering, Poznan University of Technology, Poznan, Poland

*Corresponding author:
Jakub Dalibor Rybka
(jrybka@amu.edu.pl)

Abstract

The necessity to preserve meniscal function prompts the research and development of novel treatment options, like three-dimensional (3D) bioprinting. However, bioinks for meniscal 3D bioprinting have not been extensively explored. Therefore, in this study, a bioink composed of alginate, gelatin, and carboxymethylated cellulose nanocrystal (CCNC) was formulated and evaluated. Firstly, bioinks with varying concentrations of the aforementioned components were subjected to rheological analysis (amplitude sweep test, temperature sweep test, and rotation). The optimal bioink formulation of 4.0% gelatin, 0.75% alginate, and 1.4% CCNC dissolved in 4.6% D-mannitol was further used for printing accuracy analysis, followed by 3D bioprinting with normal human knee articular chondrocytes (NHAC-kn). The encapsulated cells' viability was > 98%, and collagen II expression was stimulated by the bioink. The formulated bioink is printable, stable under cell culture conditions, biocompatible, and able to maintain the native phenotype of chondrocytes. Aside from meniscal tissue bioprinting, it is believed that this bioink could serve as a basis for the development of bioinks for various tissues.

Keywords: Meniscus; 3D bioprinting; Bioink; Alginate; Gelatin; Carboxymethylated cellulose nanocrystal

1. Introduction

Meniscal lesions are one of the most common injuries to the human knee, stemming from its biomechanical role as a shock absorber[1]. The clinical results of meniscus repair have direct correlations with the vascularization of the area in which the lesion occurs. The vascularized zone has higher regenerative potential in comparison to the avascular zone. The routine treatment methods include stitching and partial meniscectomy, which pose a risk of detachment and limitation to joint mobility[2,3]. There is also a risk of late-age osteoarthritis with meniscectomy, as it decreases the contact area and increases the contact stress on the articular cartilage. In the case of complex and extensive meniscal tears, the treatment options include allograft transplantation; however, tissue

accessibility is a major limitation. Therefore, cartilage regeneration or substitute through a tissue-engineered scaffold is extensively explored.

Three-dimensional (3D) bioprinting emerges as a versatile method to manufacture structurally defined constructs[4]. In short, 3D bioprinting utilizes a carrier matrix termed bioink to provide a microenvironment for cells suspended within it[5]. The main advantage of 3D bioprinting is the architectural control over products[6]. A perfectly tailored scaffold can be developed using data from various imaging techniques, like magnetic resonance imaging (MRI)[7]. The growing interest in this field of research is anticipated[8]. Presently, 3D bioprinting is used to manufacture tissues, organs, or cancer models for research, including orthopedic applications[9].

Literature presents various bioink compositions developed for orthopedic 3D bioprinting[5]. An interesting idea is to formulate bioink based solely on the decellularized extracellular matrix (ECM) from porcine menisci[10,11]. This low immunogenic component exhibits good biocompatibility and stimulates chondrogenesis. However, constructs suffer from poor mechanical stability, which is an issue that has to be addressed. Polycaprolactone (PCL) is frequently used as a reinforcement in orthopedic applications[12,13]. For example, PCL supports alginate-based bioinks mixed with porcine inner or outer meniscal ECM[10,14]. Nevertheless, ECM extraction requires the use of surfactants that may elicit cytotoxic effects even at low concentrations[15]. Alternative methods of supercritical carbon dioxide (CO_2) extraction require advanced and costly equipment. As a result, alginate, collagen derivatives, chitosan, nanocellulose, and hyaluronic acid are some of the more widely investigated biomaterials[5].

The most commonly used bioink component is an accessible and affordable alginate that crosslinks with divalent cations, usually calcium ions (Ca^{2+}). Nonetheless, the rapid alginate gelation limits the control over this process during bioprinting[16]. Therefore, it is usually mixed with other materials, like gelatin, to obtain bioinks with dual-stage gelation[7]. The gelation of gelatin is temperature-dependent; it is fluid above 30°C but solid at lower temperatures. In addition, gelatin, unlike alginate, has a positive charge that ensures cell and protein binding[17]. Alginate-gelatin bioink is commonly used as a basis for bone and cartilage tissue engineering[18–20].

In cartilage-related research, the addition of nanocellulose enhances the mechanical properties and shear forces affecting cells and printability[7,21,22]. The cell mobility inside constructs and phenotypic changes are related to the mechanical properties of bioink[23]. Cells detect mechanical stress through mechanoreceptors,

which convert mechanical stimuli into biochemical signals that regulate various cellular pathways[24]. The mechanical stimulation is further enhanced by shear forces exerted on cells during 3D bioprinting[7,25]. This phenomenon is known as mechanotransduction and is one of the chondrogenesis stimulators.

Extrusion-based bioprinting, which is the most popular type of bioprinting, utilizes compressed air or a mechanical piston to extrude bioink from a cartridge[5,26]. It is a relatively affordable technique and is compatible with various materials, including alginate- and gelatine-based bioinks[27,28]. The applicability of extrusion-based bioprinting can be expanded by integrating additional modules, such as the microfluidic printhead or the UV module for photo-curable materials[29,30]. Inkjet bioprinting is another 3D bioprinting technology that ejects droplets; hence, it allows the manufacturing of constructs in a drop-on-demand fashion[31,32]. Laser-assisted bioprinting systems, such as laser-induced forward transfer (LIFT) and vat polymerization-based bioprinting, can also be used as 3D bioprinting techniques for cartilage tissue engineering. LIFT is a nozzle-free and noncontact technique that is applicable for high-viscosity bioinks with high cell densities[5]. The laser is pulsed on a ribbon that absorbs energy and generates a bubble of bioink on the opposite side[5,33]. Vat polymerization is based on the polymerization of photo-curable inks in vats and is mainly used for 3D printing with inks without cells. Nevertheless, digital light processing is a vat polymerization technology that has been successfully used for bioprinting with bioinks mixed with cells[34,35]. A bioink composed of alginate, gelatin, and carboxymethylated cellulose nanocrystal (CCNC) was formulated and evaluated for meniscal tissue engineering. The addition of CCNC is a novelty selected for its carboxymethylated groups that increase its solubility. All materials are natural, biocompatible, accessible, and affordable. Rheological analysis was performed on bioinks with varying concentrations of alginate, gelatin, and CCNC. Based on the rheological analysis, a bioink was selected for printing accuracy analysis, and the bioink was subsequently enriched with normal human knee articular chondrocytes (NHAC-kn) for 3D bioprinting. The constructs were created with an extrusion-based bioprinter. The viability and gene expression of the embedded cells were assessed.

2. Materials and methods

2.1. Bioink preparation for rheological analysis
Table 1 presents the investigated bioink formulations. Firstly, weighted sodium alginate (Sigma-Aldrich), gelatin from porcine skin (Sigma-Aldrich), and CCNC (Cellulose Lab) were sterilized under ultraviolet (UV) light for 30 minutes. The components were then dissolved in

Table 1. Bioink formulations for rheological analysis

	Concentrations (w/v)		
	Gelatin	**Alginate**	**CCNC**
Bioink A	3.0%	0.5%	1.4%
Bioink B	4.0%	0.5%	1.4%
Bioink C	5.0%	0.5%	1.4%
Bioink D	4.0%	0.75%	1.4%
Bioink E	4.0%	1.0%	1.4%
Bioink F	4.0%	0.75%	1.0%
Bioink G	4.0%	0.75%	2.0%

Abbreviation: CCNC, carboxymethylated cellulose nanocrystal.

sterile 4.6% (w/v) D-mannitol (Sigma-Aldrich) solution. The components were added in the following order: alginate, gelatin, and CCNC; the mixture was shaken after each addition for at least 30 minutes at 37°C. The prepared bioinks were mixed overnight. During bioink formulation, the EFD Optimum dispensing equipment (Nordson) ensures a high repeatability of bioink composition by wiping the residues from the walls with a piston.

2.2. Rheological analysis
Rheological analysis was performed using the Anton Paar 302 rheometer, equipped with 25 mm, smooth, parallel plates (PP25). The gap between plates was set to 1 mm, and measurements were conducted at 23°C, unless stated otherwise. The performed rheological measurements included amplitude sweep test, temperature sweep test, and rotation. Temperature sweep experiments were performed at a rate of 2°C·min^{-1} from 20°C to 40°C. In the rotation study, the shear rate range was set to 0.01–200.00 s^{-1}. The oscillatory measurement was divided into three intervals[36]. The first interval was a pre-shear step conducted at a constant strain amplitude (γ) of 0.01% and an angular frequency (ω) of 10 s^{-1}. The next interval was a rest time (t = 10 minutes), followed by an amplitude sweep test with varying strain amplitude (0.01%–500.00%) and a constant angular frequency (1 rad·s^{-1}). A layer of silicone oil was spread over the surface of the sample to prevent water evaporation from the bioink samples during rheological measurements[36,37]. All rheological measurements were performed in triplicate, including sample preparation, and at least three measurements were performed for further calculations.

2.3. 3D model design
Three computer-aided design (CAD) models were developed. The first model was developed for printing accuracy analysis, while the second model was developed to test the feasibility of bioprinting a meniscus-like shape model (approximately 29 mm × 39 mm × 11 mm). Both were prepared with Inventor Professional 2020. The

stereolithography (STL) models were adjusted based on the bioprinter requirements in Slic3r. The third model (10 mm × 10 mm × 1 mm cylinder) was less challenging, and it was prepared using Thinkercad for 3D bioprinting. This model was uploaded to the BIO X bioprinter (Cellink) and sliced using a bioprinting software with infill set at a 35% rectilinear pattern.

2.4. Printing accuracy analysis
The bioink selection for 3D bioprinting accuracy analysis was based on the former rheological analysis. The bioink was prepared as described above, transferred to a cartridge, and precooled in a 25°C water bath. The BIO X bioprinter (Cellink) with temperature-controlled, pressure extrusion printhead was used. Its printhead and printbed temperatures were set to 25°C and 10°C, respectively. A 22 G needle (inner diameter = 410 μm) was used. After printing, the constructs were photographed on millimeter paper, and all measurements were taken from 15 individually printed constructs. The length and width measurements for printing accuracy were performed on ImageJ software. The printing accuracy in percentage was assessed with a previously proposed equation[38] as follows:

$$Printing\ accuracy\left[\%\right]=\left[1-\frac{\left|A_i\left[mm\right]-A\left[mm\right]\right|}{A\left[mm\right]}\right]*100$$

where A_i is the measurement of a printed construct, and A is the measurement of a 3D model.

2.5. Culture of NHAC
Normal human knee articular chondrocytes (NHAC-kn, Lonza) were cultured in the recommended CGM™ Chondrocyte Growth Medium (Lonza) for expansion of chondrocytes, with supplementation at standard conditions (37°C, 5% CO_2, and 95% relative humidity). Cell passaging was performed with TrypLE™ Express Enzyme (Gibco) when the cells reached 80%–90% confluence. Chondrocytes up to the sixth passage were used for 3D bioprinting.

2.6. Bioink preparation for 3D bioprinting
The bioink prepared as described above was further mixed by using two syringes clipped with the female/female luer lock adapter. The prepared bioink was mixed with 1 × 10^7 cells·mL^{-1} of bioink in the same way. Specifically, the cells were suspended in 100 μL of chondrocyte medium and transferred to a syringe, while 1 mL of bioink was transferred to another syringe; then, the syringes were clipped with a female/female luer lock adapter prior to mixing the content. Before bioprinting, the bioink with cells was placed in a cartridge and held in a 25°C water bath to induce gelatin gelation.

2.7. 3D bioprinting

The 3D bioprinting proceeded with the same parameters as those in the printing accuracy analysis; the only difference was the printing nozzle, which was 25 G. After bioprinting, the constructs were crosslinked with sterile 200 mM calcium chloride ($CaCl_2$) (Sigma-Aldrich) dissolved in 4.6% (w/v) D-mannitol for 10 minutes at room temperature. Then, the constructs were cultured in supplemented CGM™ Chondrocyte Growth Medium with 5 mM $CaCl_2$ in standard conditions.

2.8. Live/dead assay

After 24 h, 7 days, 14 days, and 28 days, three bioprinted constructs were divided for viability and gene expression analyses. The live/dead assay was performed according to the product manual (LIVE/DEAD® Viability/Cytotoxicity Kit, Invitrogen), with the utilization of confocal microscopy (IX83, Olympus). Scans for viability assessment were taken from the approximate midpoint of three different constructs at each time point. From each of these scans, two middle slices were selected for live and dead cell counting. These images were analyzed with the ImageJ software.

2.9. Gene expression analysis

Three constructs from each time point were dissolved in 100 mM sodium citrate, containing 0.08 U·µL⁻¹ Proteinase K and 1.0 U·µL⁻¹ RNAse Inhibitor (A&A Biotechnology), while shaking for 5 minutes at 37°C, followed by ribonucleic acid (RNA) isolation with TriReagent (Sigma-Aldrich). Chloroform was then added, and the probes were centrifuged at 12,000 RCF for 15 minutes at 4°C. The supernatant was collected and mixed with a 1:1 volume of cold 99% ethanol. The solution was then transferred to the columns from RNeasy Mini Kit. The isolation steps were performed according to the RNeasy Mini Kit manual. The RNA concentration was measured using the Qubit 4 Fluorometer. For reverse transcription polymerase chain reaction (RT-PCR), TranScriba Kit (A&A Biotechnology) was used with random hexamer primers and 300 ng of total RNA. The following genes for real-time PCR were selected: *COL1A1*, *COL2A1*, *COL10A1*, *SOX9*, and *RUNX2*, with *GAPDH* as the housekeeping gene. The

Table 2. Primer sequences used for gene expression analysis

Gene name	Forward/Reverse	Sequence
COL1A1	F	5'-ACGTCCTGGTGAAGTTGGTC-3'
	R	5'-ACGTCCTGGTGAAGTTGGTC-3'
COL2A1	F	5'-CTGGAAAAGATGGTCCCAAAG-3'
	R	5'-CAGGGAATCCTCTCTCACCAC-3'
COL10A1	F	5'-TTACGCTGAACGATACCAAATG-3'
	R	5'-GACTTCCGTAGCCTGGTTTTC-3'
SOX9	F	5'-GACTCGCCACACTCCTCCT-3'
	R	5'-AGGTCTCGATGTTGGAGATGAC-3'
RUNX2	F	5'-ACCAGATGGGACTGTGGTTACT-3'
	R	5'-TGTGAAGACGGTTATGGTCAAG-3'
GAPDH	F	5'-TGACATCAAGAAGGTGGTGAAG-3'
	R	5'-TTCGTTGTCATACCAGGAAATG-3'

designed starters are shown in Table 2. The QuantStudio 6k Flex Real-Time PCR System (Applied Biosystems) with 1 µL of complementary deoxyribonucleic acid (cDNA) and Maxima SYBR Green/ROX qPCR Master Mix (Thermo Scientific) was used to evaluate the expression of these genes. Primers were used at a final concentration of 0.5 µM. The gene expression results were tested with the two-way analysis of variance (ANOVA).

2.10. Data analysis

GraphPad Prism 8.0.1 was used for statistical computing and graph preparation.

3. Results

3.1. Rheology

The temperature sweep test compared the storage modulus (G'), the loss modulus (G"), and the cross-over temperature (G' = G") between bioink A, B, and C (Figure 1). G'/G" cross-over indicates the temperature at which the bioink changes its state. If G' is above G", the elastic part dominates in the viscoelastic spectrum, and the bioink is solid. Conversely, if G" is above G', the viscous part dominates,
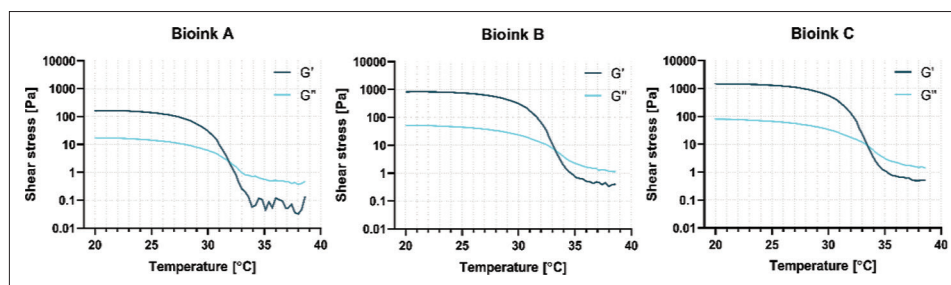

Figure 1. The temperature-dependent functions of storage modulus G' and loss modulus G" of bioinks A, B, and C.
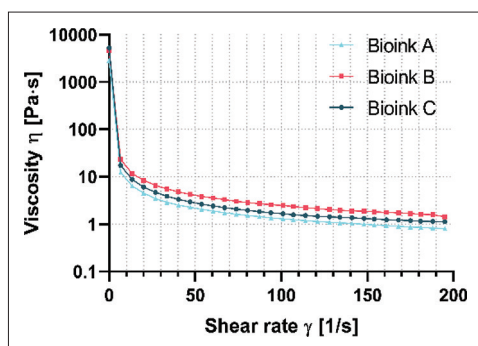
Figure 2. Flow curves of bioinks A, B, and C.

and the bioink is liquid. Bioink A reached its lowest G'/G" at 32.3°C. Bioinks B and C obtained similar G'/G" values at 33.1°C and 33.3°C, respectively. These bioinks also had higher values of both, storage and loss modulus, particularly in the temperature range of 20°C to 35°C.

Bioink flow analysis with gelatin content from 3.0% to 5.0% enables the estimation of printability (Figure 2). All bioinks exhibited a shear-thinning behavior, in which shear rate (γ) increases and shear stress (τ) decreases viscosity (η). In the conducted research, the viscosity range for all bioinks was similar. It was 2863–0.08 Pa·s for bioink A, 4630–0.02 Pa·s for bioink B, and 5210–0.05 Pa·s for bioink C at a shear rate range of 0.01–200.00 s^{-1}.

In the amplitude sweep test, bioinks with varying concentrations of each component were tested, beginning with bioinks with different gelatin content (3.0%, 4.0%, and 5.0%) (Figure 3). All bioinks displayed a solid-like

behavior (G' > G") until G'/G" cross over. Expectedly, a lower gelatin content corresponded to the cross-over at lower strain rates, while higher gelatin content resulted in higher values of G'. Hydrogels with 3.0% and 5.0% of gelatin showed a slight increase in the storage modulus followed by a steep downward slope. From the above results, the gelatin content was set at 4.0%.

Subsequently, amplitude sweep tests were performed on bioinks with varying alginate content (0.5%, 0.75%, and 1.0 %) (Figure 4). Bioink B revealed the highest constancy in G' values resulting in a broad linear viscoelastic (LVE) region. Interestingly, bioinks D and E with higher alginate content revealed a similar spike in G' as observed for bioinks A and C. Bioinks B, D, and E reached G'/G" crossover at 239%, 340%, and 396% strain, respectively. The 0.75% alginate content was selected for further analysis.

The next step involved testing bioinks with fixed gelatin (4.0%) and alginate (0.75%) contents but varying CCNC concentrations (bioink D, 1.4%; bioink F, 1.0%; and bioink G, 2.0%) using the amplitude sweep test (Figure 5). There was a significant increase in G' with increasing CCNC concentration, but the increase in G" was less noticeable. This could be explained by the hydrophilic properties of CCNC that contribute to an overall increase in the solid component of the bioinks, resulting in elevated G'. Bioinks F, D, and G reached the G'/G" crossover at 366%, 340%, and 256% strain, respectively, demonstrating the improvement of shear-thinning properties with the addition of CCNC.
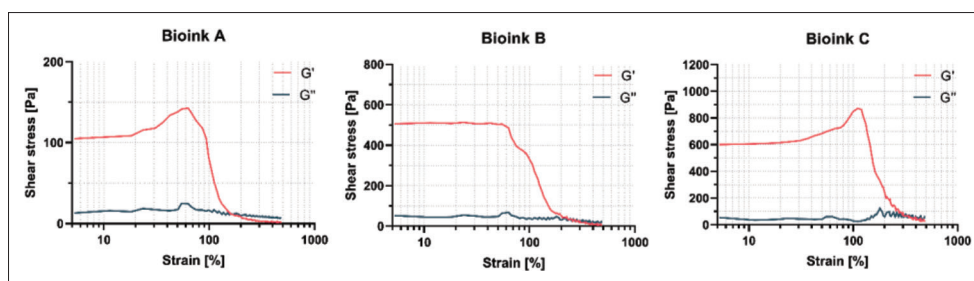

Figure 3. The results of amplitude sweeps of bioinks A, B, and C (increasing gelatin content: 1.0%, 1.4%, 2.0%).
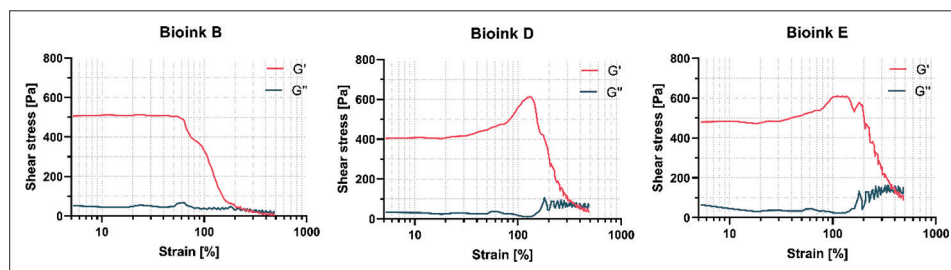
Figure 4. The results of amplitude sweeps of bioinks B, D, and E (increasing alginate content: 0.5%, 0.75%, 1.0%).
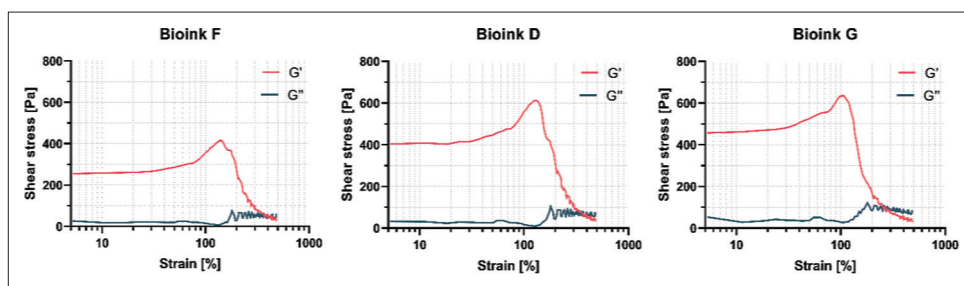
Figure 5. The results of amplitude sweeps of bioinks F, D, and G (increasing CCNC content: 1.0%, 1.4%, 2.0%).
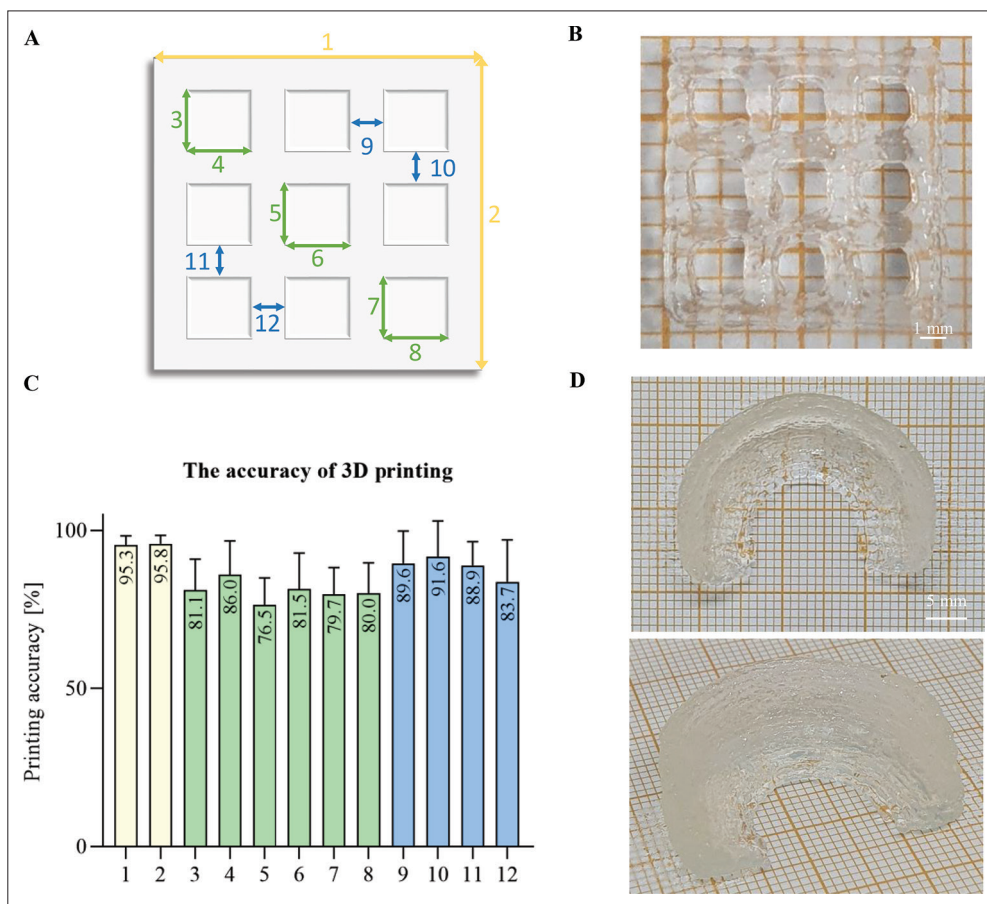
Figure 6. The accuracy of 3D printing with 0.75% alginate_4.0% gelatin_1.4% CCNC bioink without cells. (A) Measured dimensions for calculating the accuracy of 3D printing. (B) A representative image of the printed construct used for calculating the accuracy of 3D printing. (C) The accuracy of 3D printing. The colors of columns correspond to the colors in A; consequently, yellow indicates the measurements outside, green indicates the measurements inside the holes, and blue indicates the measurements within the walls. (D) A bioprinted meniscus-like shape model.

The bioink with 4.0% gelatin, 0.75% alginate, and 1.4% CCNC (Bioink D) was selected for further analysis.

3.2. Printing accuracy

The printing accuracy of constructs developed with bioink D was compared to the CAD model (Figure 6A and B). The best accuracy was obtained with a 25 G nozzle that operates at 40–55 kPa with a speed of 22–30 mm·s⁻¹. We observed a steady flow of bioink through the 25 G nozzle, contrary to the clogged 27 G nozzle. The measurements outside (dimensions 1 and 2, Figure 6A) were approximately 96.0% accurate (Figure 6C). Inside the walls, a similarly high level of accuracy (between 92.5% and 97.1%) was obtained (dimensions from 9 to 12, Figure 6A and C). The lowest accuracy with the highest deviations was observed for measurements inside the holes (dimensions from 3 to 8,
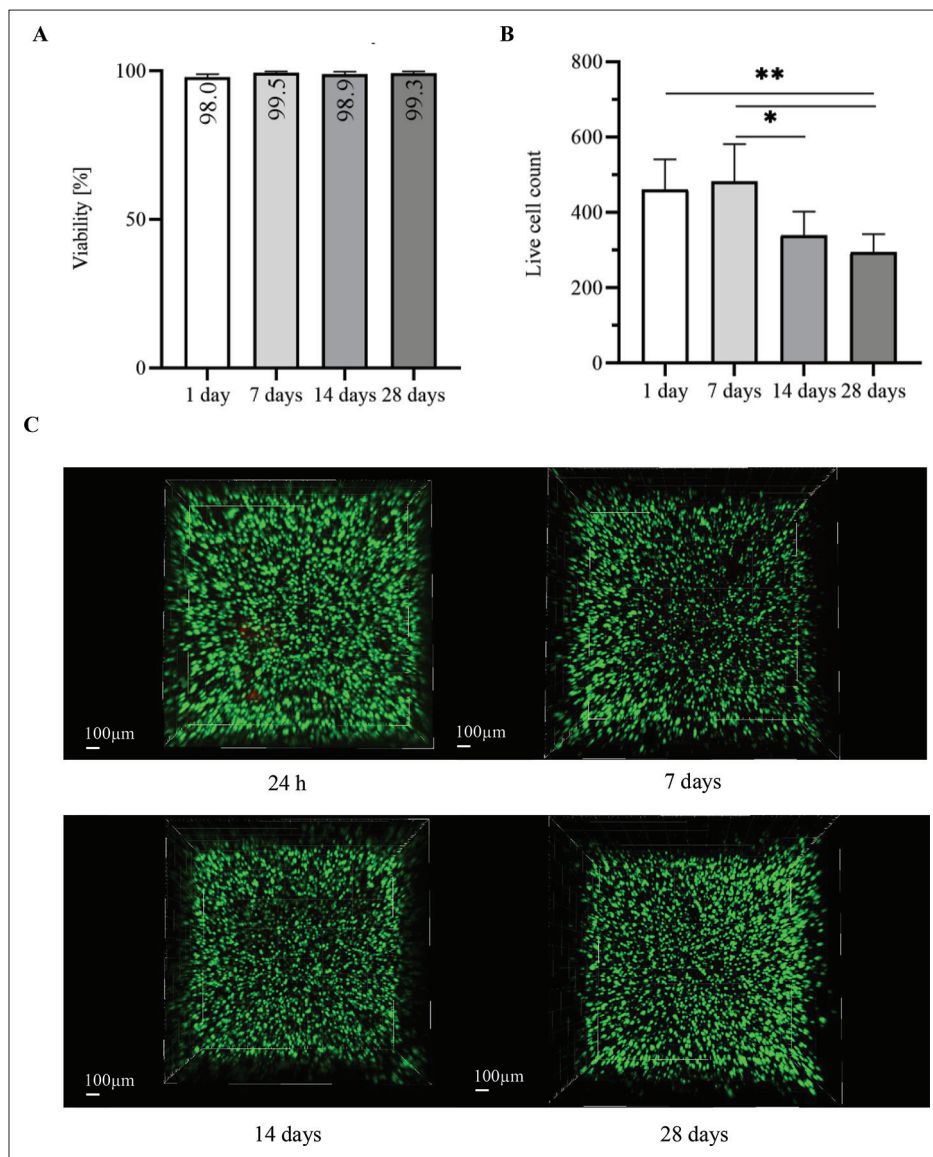
Figure 7. Viability of normal human knee articular chondrocytes (1×10^7 cells·mL^{-1}) bioprinted with 0.75% alginate_4.0% gelatin_1.4% CCNC bioink assessed by LIVE/DEAD assay (Invitrogen). (A) Viability at different time points. (B) Changes in cell count during culture. Note: *P value ≤ 0.05; **P value ≤ 0.02. (C) Representative 3D confocal scans from the constructs.

Figure 6A and C). The meniscus-like shape model was also bioprinted (Figure 6D).

3.3. Cell viability

The cell viabilities at all time points were above 98% (Figure 7A); however, there was a significant drop in cell count after one week (Figure 7B). Figure 7C represents the 3D confocal scans from the constructs. Since each scan has a different layer number, it could be mistakenly deduced that the cell quantity is the same. We also noticed cell release from the construct under optical microscopy. The homogenous cell distribution inside the construct indicates a successful mixing process.

3.4. Gene expression

The RNA isolation resulted in a low nucleic acid yield; therefore, only five chondrogenesis marker genes were selected from previous research[5]. Figure 8 shows the changes in gene expressions. There were no significant alterations to the expressions of *COL1A1* and *COL10A1* during the investigated time. On the other hand, the expression of *COL2A1* increased during culture in the bioprinted construct, with a significant change after four weeks. It resulted in a high *COL2A1/COL1A1* ratio. In terms of transcription factor genes, *SOX9* and *RUNX2* expressions were higher after bioprinting but decreased

Figure 8. Gene expression analysis. There are only two biological replicates in 28-day group, while the number of replicates of other groups is indicated in Materials and methods. Note: ****$P < 0.0001$.

during culture in the construct; nonetheless, the change was statistically insignificant.

4. Discussion

This work focused on the formulation of a bioink composed of alginate, gelatin, and CCNC for meniscal 3D bioprinting. Rheological analysis enabled us to determine the optimal concentration of components.

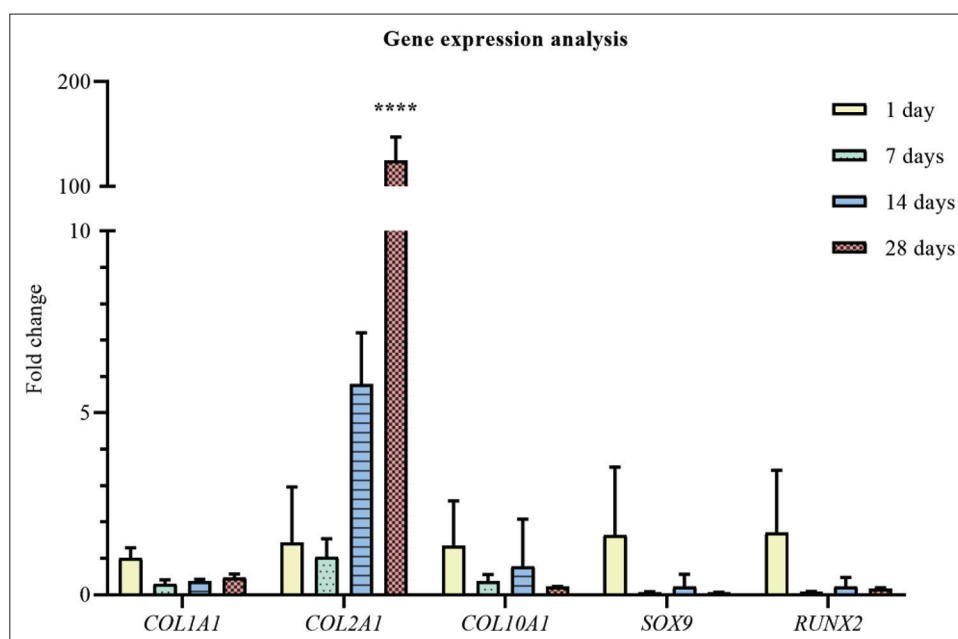Firstly, the temperature sweep test was performed to establish an optimal gelatin content, since gelatin contributes the most to the temperature-dependent rheological properties of bioinks[37,39]. The onset of a significant decrease in G' was observed for all bioinks at 28°C, which is closely related to the sol-gel transition temperature of gelatin[40,41]. Overall, gelatin is suitable for bioprinting at temperatures below 28°C[41,42]. These results imply that the bioink should be cooled to at least 25°C before bioprinting.

The shear-thinning behavior is another essential property of bioinks, which allows for precise and stable prints[43,44]. Bioink viscosities in the range of 30 mPa·s^{-1} to over $6 \cdot 10^7$ mPa·s^{-1} are considered compatible for 3D extrusion bioprinting, and the viscosities of bioinks A, B, and C were within this range[45,46]. An increased concentration of gelatin stiffens the bioinks within the tested temperature range and ensures better printability and stability of bioprinted constructs. However, an excessive gelatin content may negatively affect the printing process due to nozzle clogging or non-uniform bioink flow. Higher viscosity also causes cellular damage; hence, bioinks with

low viscosity provide a cell-friendly environment for longer culturing periods although their printability is usually poor[47,48]. The amplitude sweep test proved that a lower gelatin content corresponded with the occurrence of cross-over at lower strain rates. Concomitantly, higher G' values were observed for bioinks with a higher gelatin content, which improves material strength but may result in poor printability[49]. Taking into account the entire viscosity range and the temperature sweep test, the composition of bioink B with a gelatin content of 4.0% has the most suitable rheological properties for 3D bioprinting and was chosen for further analysis. More precisely, the pivotal impact on this selection includes the broad LVE region, the reasonably high G' values, and the cross-over occurrence after a non-rapid decrease of the storage modulus of bioink B.

The amplitude sweep tests of bioinks with different alginate concentrations (bioinks B, D, and E) revealed the complexity of their viscoelastic properties and the inability to predict their properties solely from the concentrations of their constituents. The optimization of the alginate concentration is not only crucial for the printability and mechanical properties of the construct, but also for cell viability and proliferation[41,50]. Based on the rheological tests and the biological properties of alginate, the 0.75% alginate concentration was selected for further studies.

Lastly, the rheological dissimilarities between bioinks with different CCNC concentrations (bioinks D, F, and G) were assessed. This component has a significant impact on bioink reinforcement and the improvement of shear-

thinning behavior[51,52]. The CCNC concentration of 1.4% is optimal for preventing tears and clogs with higher values of the storage modulus and maintaining print integrity. From the rheological analysis, the selected bioink formulation is 4.0% gelatin, 0.75% alginate, and 1.4% CCNC.

We have formulated a printable bioink with the lowest shear stress and the highest printing accuracy by selecting the lowest possible concentration of components. The best printing accuracy was obtained with a 25 G nozzle for pressure below 55 kPa. This pressure is applicable for 3D bioprinting since higher pressures might increase shear stress in the nozzle and damage the cell membrane[53]. The shear forces exerted on cells may elicit alterations in the gene expression profile. Excess mechanical stress downregulates collagen type I and II expressions and upregulates matrix metallopeptidase (MMP) 1 and 13[24,54]. The MMPs encode collagenases that are involved in endochondral ossification or osteoarthritis through the degradation of ECM proteins, such as collagen type II and aggrecan. This situation is highly undesirable for cartilage tissue engineering. An attempt was made to perform a dynamic mechanical analysis (DMA 242 D, Netzsch) to compare the mechanical strength of the constructs; however, the scaffolds were too soft for the analyzer's detector (results not shown). We intended to repeat a dynamic mechanical analysis following the production of ECM proteins by cells. It is a feasible step since our bioprinted constructs were stable in culture medium for more than six months (results not shown). Another possibility is to enhance mechanical properties by introducing other materials, like PCL, as mentioned in the introduction[10,11,14].

Various crosslinking strategies may also be used to control the mechanical stress and bioprinting parameters. Gelatin with chemical modification can be subjected to enzymatic crosslinking to enable 3D bioprinting[55]. Besides, gelatin can be crosslinked with a chemical crosslinker, such as glutaraldehyde, which was used with a hydrogel composed of alginate, gelatin, and nanocellulose and compared with the Ca^{2+} alginate crosslinking[56]. Based on mechanical and structural differences, the divalent cation crosslinking of alginate was considered most suitable for 3D bioprinting. The selection of divalent ions and their concentration also influences the mechanical properties of alginate hydrogel; for example, strontium ions create more durable constructs than calcium ions[57]. Moreover, the proper use of cations can direct cell differentiation. Cobalt ions (Co^{2+}) mimic hypoxic conditions by inhibiting hypoxia-inducible factors[58]. Research performed on human mesenchymal stem cells encapsulated in alginate beads crosslinked with Co^{2+} revealed significant changes in cartilage-specific gene expression[59]. Live/dead assay and real-time PCR were performed to assess the biocompatibility of bioink. The high

cell viability within the bioprinted construct was observed at all time points. However, the decrease in cell count indicates that chondrocytes do not proliferate inside the construct, which is contrary to other research conducted on bioink composed of alginate and nanofibrillated cellulose[60]. In the future, the identification of proliferation markers, like Ki-67, should be carried out to prove the presence of proliferating cells[61]. The transcriptional control of the avascular meniscus phenotype is regulated by transcription factors SOX-9 and SOX-8 that upregulate $COL2\alpha1$, $COL11\alpha2$, and $ACAN$ expressions[62]. Products of these genes, namely collagen type II, type XI, and aggrecan, are the main structural proteins of the cartilaginous ECM. Endochondral ossification is a process in which bones replace the hyaline cartilage; hence, it is important to observe the expression of osteogenesis marker genes[63]. RUNX family transcription factor 2 (RUNX2) is the main transcription factor associated with osteogenesis. The change in $SOX9$ and $RUNX2$ expressions reduces $COL2\alpha1$ expression and initiates collagen type X synthesis, followed by increased collagen type I synthesis. Due to low yields of RNA extractions, only five genes' expressions were measured (Table 2). A significant change was observed only in the expression of $COL2A1$, which increased during the culture. The high accumulation of type II collagen is characteristic of the inner (white-white) and middle (white-red) zones of the meniscus[64]. However, collagen type I is still the most prevalent in the native meniscus. There were no observable significant changes in the rest of the analyzed genes. Perhaps, longer culture periods may allow for the observation of more significant changes.

The present study has several limitations. A good practice in bioink research is to conduct disintegration studies and pore size evaluation with the diffusion of nutrients[23]. The absence of these tests is due to the limited number of constructs, ensuing from the cells' low proliferative capacity and the high cell count required for 3D bioprinting, which is a challenge often underscored in the tissue engineering community[5,65,66]. Our team is also working on this issue (including 3D scaffold-free cultures and mesenchymal stem cell application).

Bioink with higher component concentrations (1.25% alginate, 20% gelatin, and 0.25% of cellulose nanofiber) was also proven succesful for meniscal bioprinting[7]. The viability of fibrochondorocytes was equally high (> 95 %). The most relevant differences were bioprinting with a wider nozzle (22 G) in comparison to the results presented in this study (25 G). The other bioink composed of 4% alginate, 35% gelatine, and 2% carboxymethyl cellulose was also succesfully used for extrusion into the negative mould[67]. Encapsulated MG-63 osteosarcoma cells proliferated and produced collagen inside the construct.

Finally, bioinks based on alginate, gelatine, and nanocellulose have also been extensively investigated for bone tissue engineering. Besides enhancing printability, cellulose also increases the expression of the osteogenic marker gene[22,68]. Dutta et al. observed notable gene expression changes; however, the mesenchymal stem cells were seeded on the construct composed of 3% alginate, 4% gelatin, and 1% cellulose nanocrystals rather than being encapsulated inside the bioink[68]. Nevertheless, only osteogenic-specific genes were studied. Finally, a comparable bioink formulation of 2.0% alginate, 3.3% gelatin, and 0.93% diethylaminoethyl cellulose was used for skin bioprinting, yielding promising results[69,70]. These studies suggest that the proposed bioink could be used for other 3D bioprinting applications.

5. Conclusion

This study presents the formulation and evaluation of a bioink dedicated to extrusion-based 3D bioprinting of meniscal tissue. The rheological analysis included the amplitude sweep test, temperature sweep test, and rotation. The selected bioink was used for bioprinting with normal human knee articular chondrocytes. Subsequently, the encapsulated cell viability and the gene expression of chondrogenic markers were investigated. In the course of rheological and biological analyses, we established an optimal bioink composition and proved that the bioink is printable, stable in cell culture, biocompatible, and able to maintain the native phenotype of chondrocytes. We intend to investigate the chondrogenic potential of bioink with human adipose-derived mesenchymal stem cells. In our ongoing research, the formulated bioink is used as a basis to promote the chondrogenesis of encapsulated cells through supplementation with hyaluronic acid, carbon nanotubes, or collagen and alterations in alginate crosslinking.

Conflict of interest

The authors declare no conflicts of interest.

Author contributions

Conceptualization: Julia Anna Semba, Adam Aron Mieloch, Jakub Dalibor Rybka
Investigation: Julia Anna Semba, Ewa Tomaszewska, Piotr Cywoniuk
Methodology: Julia Anna Semba, Adam Aron Mieloch
Supervision: Adam Aron Mieloch, Jakub Dalibor Rybka
Writing – original draft: Julia Anna Semba
Writing – review & editing: Adam Aron Mieloch, Jakub Dalibor Rybka

References

1. Pereira H, Varatojo R, Sevivas N, *et al.,* 2016, Physiopathology of the meniscal lesions, in: *Surgery of the Meniscus*, Springer Berlin Heidelberg, 47–61.

   https://doi:10.1007/978-3-662-49188-1_5

2. Doral MN, Bilge O, Huri G, *et al.*, 2018, Modern treatment of meniscal tears. *EFORT Open Rev*, 3:260–268.

   https://doi.org/10.1302/2058-5241.3.170067

3. Beaufils P, Becker R, Kopf S, *et al.*, 2017, The knee meniscus: Management of traumatic tears and degenerative lesions. *EFORT Open Rev*, 2:195–203.

   https://doi.org/10.1302/2058-5241.2.160056

4. Vaishya R, Patralekh MK, Vaish A, *et al.*, 2018, Publication trends and knowledge mapping in 3D printing in orthopaedics. *J Clin Orthop Trauma*, 9:194–201.

   https://doi.org/10.1016/j.jcot.2018.07.006

5. Semba JA, Mieloch AA, Rybka JD, 2020, Introduction to the state-of-the-art 3D bioprinting methods, design, and applications in orthopedics. *Bioprinting*, 18:e00070.

   https://doi.org/10.1016/j.bprint.2019.e00070

6. Agarwal S, Saha S, Balla VK, *et al.,* 2020, Current developments in 3D bioprinting for tissue and organ regeneration–A review. *Front Mech Eng*, 6:589171.

   https://doi.org/10.3389/fmech.2020.589171

7. Luo W, Song Z, Wang Z, *et al.*, 2020, Printability optimization of gelatin-alginate bioinks by cellulose nanofiber modification for potential meniscus bioprinting. *J Nanomater*.

   https://doi.org/10.1155/2020/3863428

8. Stanco D, Urbán P, Tirendi S, *et al.*, 2020, 3D bioprinting for orthopaedic applications: Current advances, challenges and regulatory considerations. *Bioprinting*, 20:e00103.

   https://doi.org/10.1016/j.bprint.2020.e00103

9. Ma X, Liu J, Zhu W, *et al.*, 2018, 3D bioprinting of functional tissue models for personalized drug screening and in vitro disease modeling. *Adv Drug Deliv Rev*, 132:235–251.

   https://doi.org/10.1016/j.addr.2018.06.011

10. Chae S, Lee SS, Choi YJ, *et al.*, 2021, 3D cell-printing of biocompatible and functional meniscus constructs using meniscus-derived bioink. *Biomaterials*, 267:120466.

https://doi.org/10.1016/j.biomaterials.2020.120466

11. Jian Z, Zhuang T, Qinyu T, *et al.*, 2021, 3D bioprinting of a biomimetic meniscal scaffold for application in tissue engineering. *Bioact Mater*, 6:1711–1726.

https://doi.org/10.1016/j.bioactmat.2020.11.027

12. Mieloch AA, Semba JA, Rybka JD, 2022, CNT-type dependent cellular adhesion on 3D-printed nanocomposite for tissue engineering. *Int J Bioprint*, 8(2):548.

https://doi.org/10.18063/ijb.v8i2.548

13. Vahedi P, Jarolmasjed S, Shafaei H, *et al.*, 2019, In vivo articular cartilage regeneration through infrapatellar adipose tissue derived stem cell in nanofiber polycaprolactone scaffold. Tissue and Cell 57:49–56.

https://doi.org/10.1016/j.tice.2019.02.002

14. Romanazzo S, Vedicherla S, Moran C, *et al.*, 2018, Meniscus ECM-functionalised hydrogels containing infrapatellar fat pad-derived stem cells for bioprinting of regionally defined meniscal tissue. J *Tissue Eng Regen Med*, 12:e1826–e1835.

https://doi.org/10.1002/term.2602

15. Saldin LT, Cramer MC, Velankar SS, *et al.*, 2017, Extracellular matrix hydrogels from decellularized tissues: Structure and function. *Acta Biomaterialia* 49:1–15

16. Ng WL, Chua CK, Shen YF, 2019, Print me an organ! Why we are not there yet. *Prog Polym Sci*, 97:101145.

https://doi.org/10.1016/j.progpolymsci.2019.101145

17. Liu D, Nikoo M, Boran G, *et al.*, 2015, Collagen and gelatin. Annu Rev Food Sci Technol, 6:527–557.

https://doi.org/10.1146/annurev-food-031414-111800

18. Ojansivu M, Rashad A, Ahlinder A, *et al.*, 2019, Wood-based nanocellulose and bioactive glass modified gelatin-alginate bioinks for 3D bioprinting of bone cells. *Biofabrication*, 11:35010.

https://doi.org/10.1088/1758-5090/ab0692

19. Leite ÁJ, Sarker B, Zehnder T, *et al.*, 2016, Bioplotting of a bioactive alginate dialdehyde-gelatin composite hydrogel containing bioactive glass nanoparticles. *Biofabrication*, 8:035005.

https://doi.org/10.1088/1758-5090/8/3/035005

20. Costantini M, Idaszek J, Szöke K, *et al.*, 2016, 3D bioprinting of BM-MSCs-loaded ECM biomimetic hydrogels for in vitro neocartilage formation. *Biofabrication*, 8:035002.

https://doi.org/10.1088/1758-5090/8/3/035002

21. Markstedt K, Mantas A, Tournier I, *et al.*, 2015, 3D bioprinting human chondrocytes with nanocellulose-alginate bioink for cartilage tissue engineering applications. *Biomacromolecules*, 16:1489–1496.

https://doi.org/10.1021/acs.biomac.5b00188

22. Ojansivu M, Rashad A, Ahlinder A, *et al.*, 2019, Wood-based nanocellulose and bioactive glass modified gelatin-alginate bioinks for 3D bioprinting of bone cells. *Biofabrication*, 11:035010.

https://doi.org/10.1088/1758-5090/ab0692

23. Zaeri A, Cao K, Zhang F, *et al.*, 2022, A review of the structural and physical properties that govern cell interactions with structured biomaterials enabled by additive manufacturing. *Bioprinting*, 26:e00201.

https://doi.org/10.1016/j.bprint.2022.e00201

24. Zhao Z, Li Y, Wang M, *et al.*, 2020, Mechanotransduction pathways in the regulation of cartilage chondrocyte homoeostasis. *Journal of Cellular and Molecular Medicine*, 24:5408–5419.

https://doi.org/10.1111/jcmm.15204

25. Möller T, Amoroso M, Hägg D, *et al.*, 2017, In vivo chondrogenesis in 3D bioprinted human cell-laden hydrogel constructs. *Plast Reconstr Surg—Glob Open*, 5:e1227.

https://doi.org/10.1097/GOX.0000000000001227

26. Jiang T, Munguia-Lopez JG, Flores-Torres S, *et al.*, 2019, Extrusion bioprinting of soft materials: An emerging technique for biological model fabrication. *Appl Phys Rev*, 6:011310.

https://doi.org/10.1063/1.5059393

27. Dravid A, McCaughey-Chapman A, Raos B, *et al.*, 2022, Development of agarose-gelatin bioinks for extrusion-based bioprinting and cell encapsulation. *Biomed Mater* (Bristol), 17:055001.

https://doi.org/10.1088/1748-605X/ac759f

28. Li Z, Huang S, Liu Y, *et al.*, 2018, Tuning alginate-gelatin bioink properties by varying solvent and their impact on stem cell behavior. *Sci Rep*, 8:8020.

https://doi.org/10.1038/s41598-018-26407-3

29. Zhuang P, Ng WL, An J, *et al.*, 2019, Layer-by-layer ultraviolet assisted extrusion-based (UAE) bioprinting of hydrogel constructs with high aspect ratio for soft tissue engineering applications. *PLoS ONE*, 14:1–21.

https://doi.org/10.1371/journal.pone.0216776

30. Zaeri A, Zgeib R, Cao K, *et al.*, 2022, Numerical analysis on the effects of microfluidic-based bioprinting parameters on the microfiber geometrical outcomes. *Sci Rep*, 12:1–16.

https://doi.org/10.1038/s41598-022-07392-0

31. Li X, Liu B, Pei B, *et al.*, 2020, Inkjet bioprinting of biomaterials. *Chem Rev*, 120:10793–10833.

https://doi.org/10.1021/acs.chemrev.0c00008

32. Ng WL, Huang X, Shkolnikov V, *et al.*, 2022, Controlling droplet impact velocity and droplet volume: key factors to achieving high cell viability in sub-nanoliter droplet-based bioprinting. *Int J Bioprint*, 8:424.

https://doi.org/10.18063/ijb.v8i1.424

33. Xiong R, Zhang Z, Chai W, *et al.*, 2017, Study of gelatin as an effective energy absorbing layer for laser bioprinting. *Biofabrication*, 9:024103.

https://doi.org/10.1088/1758-5090/aa74f2

34. Ng WL, Lee JM, Zhou M, *et al.*, 2020, Vat polymerization-based bioprinting—process, materials, applications and regulatory challenges. *Biofabrication*, 12:022001.

https://doi.org/10.1088/1758-5090/ab6034

35. Li W, Mille LS, Robledo JA, *et al.*, 2020, Recent advances in formulating and processing biomaterial inks for vat polymerization-based 3D printing. *Adv Healthc Mater*, 9:1–18.

https://doi.org/10.1002/adhm.202000156

36. Pääkkönen T, Dimic-Misic K, Orelma H, *et al.*, 2016, Effect of xylan in hardwood pulp on the reaction rate of TEMPO-mediated oxidation and the rheology of the final nanofibrillated cellulose gel. *Cellulose*, 23:277–293.

https://doi.org/https://doi.org/10.1007/s10570-015-0824-7

37. Jessop ZM, Al-Sabah A, Gardiner MD, *et al.,* 2017, 3D bioprinting for reconstructive surgery: Principles, applications and challenges. *J Plast Reconstr Aesthetic Surg*, 70(9):1155–1170.

https://doi.org/10.1016/j.bjps.2017.06.001

38. Giuseppe M di, Law N, Webb B, *et al.*, 2018, Mechanical behaviour of alginate-gelatin hydrogels for 3D bioprinting. *J Mech Behav Biomed Mater*, 79:150–157.

https://doi.org/10.1016/j.jmbbm.2017.12.018

39. Ning L, Gil CJ, Hwang B, *et al.*, 2020, Biomechanical factors in three-dimensional tissue bioprinting. *Appl Phys Rev*, 7:041319.

https://doi.org/10.1063/5.0023206

40. Kawabe S, Seki M, Tabata H, 2014, Investigation of the sol-gel transition of gelatin using terahertz time-domain spectroscopy. *J Appl Phys*, 115:143103.

https://doi.org/10.1063/1.4870954

41. Liu F, Chen Q, Liu C, *et al.*, 2018, Natural polymers for organ 3D bioprinting. *Polymers (Basel)*, 10:1278.

https://doi.org/10.3390/polym10111278

42. Kačarević ŽP, Rider PM, Alkildani S, *et al.*, 2018, An introduction to 3D bioprinting: Possibilities, challenges and future aspects. *Materials*, 11:2199.

https://doi.org/10.3390/ma11112199

43. Dimitreli G, Thomareis AS, 2004, Effect of temperature and chemical composition on processed cheese apparent viscosity. *J Food Eng*, 64:265–271.

https://doi.org/10.1016/j.jfoodeng.2003.10.008

44. Li MG, Tian XY, Chen XB, 2009, A brief review of dispensing-based rapid prototyping techniques in tissue scaffold fabrication: Role of modeling on scaffold properties prediction. *Biofabrication*, 1:032001.

https://doi.org/10.1088/1758-5082/1/3/032001

45. Murphy S V., Atala A, 2014, 3D bioprinting of tissues and organs. *Nat Biotechnol*, 32:773–785.

https://doi.org/10.1038/nbt.2958

46. Jones N, 2012, Science in three dimensions: The print revolution. *Nature*, 487:22–23.

https://doi.org/10.1038/487022a

47. Rutz AL, Hyland KE, Jakus AE, *et al.*, 2015, A multimaterial bioink method for 3D printing tunable, cell-compatible hydrogels. *Adv Mater*, 27:1607–1614.

https://doi.org/10.1002/adma.201405076

48. Blaeser A, Duarte Campos DF, Puster U, *et al.*, 2016, Controlling shear stress in 3D bioprinting is a key factor to balance printing resolution and stem cell integrity. *Adv Healthc Mater*, 5:326–333.

https://doi.org/10.1002/adhm.201500677

49. Jin Y, Zhao D, Huang Y, 2018, Study of extrudability and standoff distance effect during nanoclay-enabled direct printing. *Bio-Des Manuf*, 1:123–134.

https://doi.org/10.1007/s42242-018-0009-y

50. Markstedt K, Mantas A, Tournier I, *et al.*, 2015, 3D bioprinting human chondrocytes with nanocellulose-alginate bioink for cartilage tissue engineering applications. *Biomacromolecules*, 16:1489–1496.

https://doi.org/10.1021/acs.biomac.5b00188

51. Athukoralalage SS, Balu R, Dutta NK, *et al.,* 2019, 3D bioprinted nanocellulose-based hydrogels for tissue engineering applications: A brief review. *Polymers*, 11(5):898.

https://doi.org/10.3390/polym11050898

52. Han C, Wang X, Ni Z, *et al.*, 2020, Effects of nanocellulose on alginate/gelatin bio-inks for extrusion-based 3D printing. *BioResources*, 15:7357–7373.

https://doi.org/10.15376/biores.15.4.7357-7373

53. Fakhruddin K, Hamzah MSA, Razak SIA, 2018, Effects of extrusion pressure and printing speed of 3D bioprinted construct on the fibroblast cells viability. *IOP Conf Ser: Mater Sci Eng*, 440:012042.

https://doi.org/10.1088/1757-899X/440/1/012042

54. Liu Q, Hu X, Zhang X, *et al.*, 2016, Effects of mechanical stress on chondrocyte phenotype and chondrocyte extracellular matrix expression. *Sci Rep*, 6:1–8.

https://doi.org/10.1038/srep37268

55. He H, Li D, Lin Z, *et al.*, 2020, Temperature-programmable and enzymatically solidifiable gelatin-based bioinks enable facile extrusion bioprinting. *Biofabrication*, 12.

https://doi.org/10.1088/1758-5090/ab9906

56. Erkoc P, Uvak I, Nazeer MA, *et al.*, 2020, 3D printing of cytocompatible gelatin-cellulose-alginate blend hydrogels. *Macromol Biosci*, 20:1–15.

https://doi.org/10.1002/mabi.202000106

57. Place ES, Rojo L, Gentleman E, *et al.*, 2011, Strontium-and zinc-alginate hydrogels for bone tissue engineering. *Tissue Eng Part A*, 17:2713–2722.

https://doi.org/10.1089/ten.tea.2011.0059

58. Teti G, Focaroli S, Salvatore V, *et al.*, 2018, The hypoxia-mimetic agent cobalt chloride differently affects human mesenchymal stem cells in their chondrogenic potential. *Stem Cells Int*, 2018: 3237253.

https://doi.org/10.1155/2018/3237253

59. Focaroli S, Teti G, Salvatore V, *et al.*, 2016, Calcium/cobalt alginate beads as functional scaffolds for cartilage tissue engineering. *Stem Cells Int*, 2016:20–22.

https://doi.org/10.1155/2016/2030478

60. Nguyen D, Hgg DA, Forsman A, *et al.*, 2017, Cartilage tissue engineering by the 3D bioprinting of iPS cells in a nanocellulose/alginate bioink. *Sci Rep*, 7:658.

https://doi.org/10.1038/s41598-017-00690-y

61. Apelgren P, Amoroso M, Lindahl A, *et al.*, (2017) Chondrocytes and stem cells in 3D-bioprinted structures create human cartilage in vivo. *PLoS ONE*, 12:e0189428.

https://doi.org/10.1371/journal.pone.0189428

62. Grogan SP, Duffy SF, Pauli C, *et al.*, 2018, Gene expression profiles of the meniscus avascular phenotype: A guide for meniscus tissue engineering. *J Orthop Res*, 36:1947–1958.

https://doi.org/10.1002/jor.23864

63. Mackie EJ, Ahmed YA, Tatarczuch L, *et al.*, 2008, Endochondral ossification: how cartilage is converted into bone in the developing skeleton. *Int J Biochem Cell Biol*, 40:46–62.

https://doi.org/10.1016/j.biocel.2007.06.009

64. Folkesson E, Turkiewicz A, Rydén M, *et al.*, 2020, Proteomic characterization of the normal human medial meniscus body using data-independent acquisition mass spectrometry. *J Orthop Res*, 38:1735–1745.

https://doi.org/10.1002/jor.24602

65. Francis SL, di Bella C, Wallace GG, *et al.*, 2018, Cartilage tissue engineering using stem cells and bioprinting technology—barriers to clinical translation. *Front Surg*, 5:1–12.

https://doi.org/10.3389/fsurg.2018.00070

66. Sharma P, Kumar P, Sharma R, *et al.*, 2019, Tissue engineering; current status & futuristic scope. *J Med Life*, 12:225–229.

https://doi.org/10.25122/jml-2019-0032

67. Sathish PB, Gayathri S, Priyanka J, *et al.*, 2022, Tricomposite gelatin-carboxymethylcellulose-alginate bioink for direct and indirect 3D printing of human knee meniscal scaffold. *Int J Biol Macromol*, 195:179–189.

https://doi.org/10.1016/j.ijbiomac.2021.11.184

68. Dutta SD, Hexiu J, Patel DK, *et al.*, 2021, 3D-printed bioactive and biodegradable hydrogel scaffolds of alginate/gelatin/cellulose nanocrystals for tissue engineering. *Int J Biol* Macromol, 167:644–658.

https://doi.org/10.1016/j.ijbiomac.2020.12.011

69. Ramakrishnan R, Kasoju N, Raju R, *et al.*, 2022, Exploring the potential of alginate-gelatin-diethylaminoethyl cellulose-fibrinogen based bioink for 3d bioprinting of skin tissue constructs. *Carbohydr Polym Technol Appl*, 3:100184.

https://doi.org/10.1016/j.carpta.2022.100184

70. Somasekharan LT, Raju R, Kumar S, *et al.*, 2021, Biofabrication of skin tissue constructs using alginate, gelatin and diethylaminoethyl cellulose bioink. *Int J Biol* Macromol, 189:398–409.

https://doi.org/10.1016/j.ijbiomac.2021.08.114

Julia Semba

Laboratory of Applied Biotechnology
Center for Advanced Technology
Adam Mickiewicz University in Poznan
e-mail: jsemba@amu.edu.pl

Author contribution statement

I declare that I am the first author of the article "Formulation and evaluation of a bioink composed of alginate, gelatin, and nanocellulose for meniscal tissue engineering" by Julia Anna Semba, Adam Aron Mieloch, Ewa Tomaszewska, Piotr Cywoniuk, and Jakub Dalibor Rybka, published in *International Journal of Bioprinting* in 2023. The author's contribution is as follows:

Julia Semba designed the study, prepared bioinks formula, and 3D bioprinted constructs. The rheological analysis and 3D model design were made and analyzed by Julia Semba (with Ewa Tomaszewska help). Julia Semba designed, made, and analyzed printing accuracy and cell viability after 3D bioprinting. Julia Semba designed (with P. Cywoniuk assistance), made, and analyzed gene expression. Julia Semba wrote the original draft with all Figures.

Adam Mieloch designed the study, supervised the experiments, and revised the draft.

Ewa Tomaszewska made the rheological analysis and 3D model design with Julia Semba. Wrote draft of section 3.1. "Rheology".

Piotr Cywoniuk helps with primer designed and qPCR data analysis.

Jakub Rybka designed the study, supervised the experiments and the technical part of the research, and revised the draft. Jakub Rybka acquired funding and corresponded with the journal and reviewers.

Date: 18.08. 2023

Signature: *Julia Semba*

prof. UAM dr hab. Inż. Jakub D. Rybka

Dr Adam Mieloch

Laboratory of Applied Biotechnology
Center for Advanced Technology
Adam Mickiewicz University in Poznan
e-mail: amieloch@amu.edu.pl

Author contribution statement

I declare that I am the co-author of the article "Formulation and evaluation of a bioink composed of alginate, gelatin, and nanocellulose for meniscal tissue engineering" by Julia Anna Semba, Adam Aron Mieloch, Ewa Tomaszewska, Piotr Cywoniuk, and Jakub Dalibor Rybka, published in *International Journal of Bioprinting* in 2023 and I am aware that this publication is a part of Julia Semba PhD dissertation. The author's contribution is as follows:

Julia Semba designed the study, prepared bioinks formula, and 3D bioprinted constructs. The rheological analysis and 3D model design were made and analyzed by Julia Semba (with Ewa Tomaszewska help). Julia Semba designed, made, and analyzed printing accuracy and cell viability after 3D bioprinting. Julia Semba designed (with P. Cywoniuk assistance), made, and analyzed gene expression. Julia Semba wrote the original draft with all Figures.
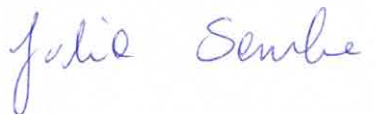
Adam Mieloch designed the study, supervised the experiments, and revised the draft.

Ewa Tomaszewska made the rheological analysis and 3D model design with Julia Semba. Wrote draft of section 3.1. "Rheology".

Piotr Cywoniuk helps with primer designed and qPCR data analysis.

Jakub Rybka designed the study, supervised the experiments and the technical part of the research, and revised the draft. Jakub Rybka acquired funding and corresponded with the journal and reviewers.

Date: 21.08.2023

Signature:

Ewa Tomaszewska

e-mail: ewa.t.tomaszewska@outlook.com

Author contribution statement

I declare that I am the co-author of the article "Formulation and evaluation of a bioink composed of alginate, gelatin, and nanocellulose for meniscal tissue engineering" by Julia Anna Semba, Adam Aron Mieloch, Ewa Tomaszewska, Piotr Cywoniuk, and Jakub Dalibor Rybka, published in *International Journal of Bioprinting* in 2023 and I am aware that this publication is a part of Julia Semba PhD dissertation. The author's contribution is as follows:

Julia Semba designed the study, prepared bioinks formula, and 3D bioprinted constructs. The rheological analysis and 3D model design were made and analyzed by Julia Semba (with Ewa Tomaszewska help). Julia Semba designed, made, and analyzed printing accuracy and cell viability after 3D bioprinting. Julia Semba designed (with P. Cywoniuk assistance), made, and analyzed gene expression. Julia Semba wrote the original draft with all Figures.

Adam Mieloch designed the study, supervised the experiments, and revised the draft.

Ewa Tomaszewska made the rheological analysis and 3D model design with Julia Semba. Wrote draft of section 3.1. "Rheology".

Piotr Cywoniuk helps with primer designed and qPCR data analysis.

Jakub Rybka designed the study, supervised the experiments and the technical part of the research, and revised the draft. Jakub Rybka acquired funding and corresponded with the journal and reviewers.

Date: 20.08.2023

Signature: *Ewa Tomaszewska*

Dr Piotr Cywoniuk

Laboratory of Applied Biotechnology
Center for Advanced Technology
Adam Mickiewicz University in Poznan
e-mail: pcywoniuk@amu.edu.pl

Author contribution statement

I declare that I am the co-author of the article "Formulation and evaluation of a bioink composed of alginate, gelatin, and nanocellulose for meniscal tissue engineering" by Julia Anna Semba, Adam Aron Mieloch, Ewa Tomaszewska, Piotr Cywoniuk, and Jakub Dalibor Rybka, published in *International Journal of Bioprinting* in 2023 and I am aware that this publication is a part of Julia Semba PhD dissertation. The author's contribution is as follows:

Julia Semba designed the study, prepared bioinks formula, and 3D bioprinted constructs. The rheological analysis and 3D model design were made and analyzed by Julia Semba (with Ewa Tomaszewska help). Julia Semba designed, made, and analyzed printing accuracy and cell viability after 3D bioprinting. Julia Semba designed (with P. Cywoniuk assistance), made, and analyzed gene expression. Julia Semba wrote the original draft with all Figures.

Adam Mieloch designed the study, supervised the experiments, and revised the draft.

Ewa Tomaszewska made the rheological analysis and 3D model design with Julia Semba. Wrote draft of section 3.1. "Rheology".

Piotr Cywoniuk helps with primer designed and qPCR data analysis.

Jakub Rybka designed the study, supervised the experiments and the technical part of the research, and revised the draft. Jakub Rybka acquired funding and corresponded with the journal and reviewers.

Date: 22.08.2023

Signature:

Dr hab. inż. Jakub Rybka, prof. UAM

Laboratory of Applied Biotechnology
Center for Advanced Technology
Adam Mickiewicz University in Poznan
e-mail: jrybka@amu.edu.pl

Author contribution statement

I declare that I am the corresponding author of the article "Formulation and evaluation of a bioink composed of alginate, gelatin, and nanocellulose for meniscal tissue engineering" by Julia Anna Semba, Adam Aron Mieloch, Ewa Tomaszewska, Piotr Cywoniuk, and Jakub Dalibor Rybka, published in *International Journal of Bioprinting* in 2023 and I am aware that this publication is a part of Julia Semba PhD dissertation. The author's contribution is as follows:

Julia Semba designed the study, prepared bioinks formula, and 3D bioprinted constructs. The rheological analysis and 3D model design were made and analyzed by Julia Semba (with Ewa Tomaszewska help). Julia Semba designed, made, and analyzed printing accuracy and cell viability after 3D bioprinting. Julia Semba designed (with P. Cywoniuk assistance), made, and analyzed gene expression. Julia Semba papered the original draft with Figures 6, 7, and 8. Figures 1 to 5 were made by Julia Semba and Ewa Tomaszewska.

Adam Mieloch designed the study, supervised the experiments, and revised the draft.

Ewa Tomaszewska made the rheological analysis and 3D model design with Julia Semba. Figures 1 to 5 were made by Julia Semba and Ewa Tomaszewska.

Piotr Cywoniuk helps with primer designed and qPCR data analysis.

Jakub Rybka designed the study, supervised the experiments and the technical part of the research, and revised the draft. Jakub Rybka acquired funding and corresponded with the journal and reviewers.

Date: 1 8. 08. 2023

Signature: prof. UAM dr hab. Inż. Jakub D. Rybka

scientific reports

OPEN

Hyaluronic acid and multiwalled carbon nanotubes as bioink additives for cartilage tissue engineering

Tomasz Szymański[1,2], Julia Anna Semba[1,3], Adam Aron Mieloch[1], Piotr Cywoniuk[1], Marcelina Kempa[1,3] & Jakub Dalibor Rybka[1]✉

Articular cartilage and meniscus injuries are prevalent disorders with insufficient regeneration responses offered by available treatment methods. In this regard, 3D bioprinting has emerged as one of the most promising new technologies, offering novel treatment options. Additionally, the latest achievements from the fields of biomaterials and tissue engineering research identified constituents facilitating the creation of biocompatible scaffolds. In this study, we looked closer at hyaluronic acid and multi-walled carbon nanotubes as bioink additives. Firstly, we assessed the minimal concentrations that stimulate cell viability, and decrease reactive oxygen species and apoptosis levels in 2D cell cultures of normal human knee articular chondrocytes (NHAC) and human adipose-derived mesenchymal stem cells (hMSC-AT). In this regard, 0.25 mg/ml of hyaluronic acid and 0.0625 mg/ml of carbon nanotubes were selected as the most optimal concentrations. In addition, we investigated the protective influence of 2-phospho-L-ascorbic acid in samples with carbon nanotubes. Tests conducted on 3D bioprinted constructs revealed that only a combination of components positively impacted cell viability throughout the whole experiment. Gene expression analysis of *COL1A1*, *COL6A1*, *HIF1A*, *COMP*, *RUNX2*, and *POU5F1* showed significant changes in the expression of all analyzed genes with a progressive overall loss of transcriptional activity in most of them.

Joint degeneration resulting from articular cartilage and meniscus defects is one of the most prevalent disorders of the musculoskeletal system. Cartilage's low healing capacity and poor regeneration effects with available treatments motivate further research into new solutions[1]. A part of the effort is directed at new surgical techniques and more advanced biomaterials, facilitating the creation of biocompatible cartilage scaffolds[2]. Raising interest is observed in the field of biologically active materials, focused on the maintenance of cell viability and proper phenotype. Collagens in cartilage tissue form complex extracellular scaffolds to bear mechanical forces, maintain homeostasis and provide anchoring sites for chondrocytes, extracellular matrix (ECM) molecules, and growth factors[3]. For many years collagen was considered to be only a structural component of the cartilage matrix, but recently, its role in extracellular signaling, mainly via integrin receptors, was discovered[4]. Collagens regulate chondrocyte proliferation, metabolism, and differentiation; similarly to soluble signaling molecules. Additionally, they significantly suppress chondrocyte hypertrophy, which is the pathological process in osteoarthritic cartilage, leading to cell senescence and death. Interestingly, carbon nanotubes (CNTs) share similar dimensions to collagen fibrils, rendering them a potential collagen biomimetic[5,6]. Hyaluronic acid (HA) is another major ECM component, performing a dual role as a structural and signaling molecule. It has exceptional water retention properties, forming a gel-like environment within the tissue, and providing elasticity for the whole structure[7].

In this study, we investigated multi-walled carbon nanotubes (MWCNTs) and hyaluronic acid (HA) as bioink additives for the 3D bioprinting of cartilage constructs. 3D bioprinting is a tissue engineering technology, which allows for precise spatial deposition of cell-enriched biomaterials, and recreation of tissue-specific structures capable to restore, maintain or improve damaged tissue through 3D scaffolds[2].

Due to their unique biological and mechanical properties, carbon nanotubes are the subject of research in cartilage regenerative medicine. The MWCNTs are concentrically rolled graphene layers forming a cylindrical structure. Surfaces of synthetic materials functionalized with CNTs stimulate chondrocyte growth and facilitate

[1]Center for Advanced Technology, Adam Mickiewicz University, Poznan, Poland. [2]Faculty of Chemistry, Adam Mickiewicz University, Poznan, Poland. [3]Faculty of Biology, Adam Mickiewicz University, Poznan, Poland. ✉email: jrybka@amu.edu.pl

1

the maintenance of their native phenotype[8,9]. The incorporation of CNTs also improves the mechanical properties of constructs, rendering them useful in scaffold reinforcement[10]. Most studies emphasize concentration-dependent effects. The cytotoxicity of carbon nanotubes is frequently emphasized and observed through an increase in reactive oxygen species (ROS) production. To mitigate cellular damage elicited by high ROS levels, antioxidant compounds such as L-ascorbic can be utilized. Due to its additional role in collagen production, a more stable analog, 2-phospho- L-ascorbic acid, was used in our study[11–13].

In the case of cartilage tissue engineering, ECM components are of special interest not only due to their mechanical properties, ensuring the physiological functioning of cartilage as a shock absorber, but also due to their biological properties. Hyaluronic acid (HA) is a glycosaminoglycan prevalent in abundance in ECM of articular cartilage[14]. It provides antioxidative, anti-inflammatory, and chondroprotective effects, which are beneficial for cartilage repair. The concentration and molecular weight of HA determines its biological activity. This component was previously utilized as an additive to bioprint the articular cartilage constructs with auspicious stimulation of cell viability and phenotype[15]. HA has also been chemically modified to improve its mechanical, and biological properties, or enable UV cross-linking[16,17].

This study assesses the chondrogenic properties of multi-walled carbon nanotubes and hyaluronic acid as bioink additives. In the first step, the minimal stimulating concentration of these components was determined with the 2D culture of normal human knee articular chondrocytes (NHAC) and human adipose-derived mesenchymal stem cells (hMSC-AT). Then, cell-containing 3D constructs were created using extrusion-based 3D bioprinting and formulated bioink. The bioink composition was based on alginate, gelatin, and carboxymethylated cellulose nanocrystals (CCNC), supplemented with MWCNTs or HA. Subsequently, the viability and gene expression of chondrogenesis markers were evaluated.

Methods

MWCNTs functionalization. MWCNTs were purchased and characterized as described in our previous work[18]. MWCNTs with diameters of 15–30 nm, lengths of 15–20 μm, and purity up to 95% produced by chemical vapor deposition (CVD) were functionalized by oxidation according to the following method. 30 mg of MWCNTs were sonicated at 70 °C in a mixture of concentrated sulfuric (H_2SO_4) and nitric (HNO_3) acids in a ratio of 3:1. Then, the mixture was neutralized with 300 ml of 3 M sodium hydroxide (NaOH). Purification of the oxidized carbon nanotubes was carried out in cycles of centrifugation and resuspension in miliQ water at 9000×g at 20 °C for: (a) 15 min, (b) 30 min, (c) 40 min, and then 12,000×g at 4 °C for 40 min. The resulting carbon nanotube solution was dried using a vacuum evaporator. The MWCNTs were suspended in a phosphate buffer (PBS). The mass of nanotubes in a given volume of the solution was determined by the thermogravimetric method to calculate the concentration of the functionalized MWCNTs (which was 2.02 mg/ml).

Cell culture. Normal Human Articular Chondrocytes (NHAC, LONZA Catalog #: CC-2550) were cultured in CGM™ Chondrocyte Growth Medium (LONZA), while human adipose tissue-derived mesenchymal stem cells (hMSC-AT, PromoCell) were cultured in supplemented Mesenchymal Stem Cells Growth Medium 2 (PromoCell); both in a humidified 5% CO_2 atmosphere, at 37 °C in tissue culture flasks (Falcon®). The culture medium was changed every three days and cells were passaged with TrypLE (Gibco) at 80–85% confluency. Additionally, hMSC-AT were cultured in Mesenchymal Stem Cell Chondrogenic Differentiation Medium (PromoCell) as a reference for gene expression analysis.

Determination of the cell viability, reactive oxygen species, and apoptosis levels in 2D cell cultures stimulated with MWCNTs and 2-phospho-L-ascorbic acid. For all tests, NHAC and hMSC-AT were seeded in a clear bottom 96-well plate (Corning) at a density of 1000 cells/well. After 24 h, medium with 0.015, 0.03, 0.0625, and 0.125 mg/ml MWCNTs was added to each well; the total volume was 100 μl medium/well. To investigate the antioxidant effect of vitamin C, the same replicates were performed with the addition of 50 μg/ml.

2-phospho-L-ascorbic acid in a cell culture medium. This salt was used instead of regular ascorbic acid, due to its increased stability in water solutions[19]. The viability was assessed with the CellTiter-Glo® Luminescent Cell Viability Assay (Promega) as described above.

The level of H_2O_2 and reactive oxygen species (ROS) were determined according to the manufacturer protocol of the ROS-Glo™ H_2O_2 Assay (Promega). Briefly, 24 h after seeding, 20 μl of H_2O_2 substrate solution was added to each well. The samples were incubated for 2 h at 37 °C with 5% CO_2. Subsequently, 100 μl of ROS-Glo™ Detection Solution was added to each well, and samples were incubated for 30 min at room temperature. The luminescent signal was read with a microplate reader (Infinite® 200 PRO, TECAN). ROS-Glo™ H_2O_2 Assay results were correlated with the CellTiter-Glo® Luminescent Cell Viability Assay. In an analogical way, Caspase-Glo® 3/7 Assay Systems (Promega) were conducted to investigate apoptosis via caspase activity. All samples were conducted in triplicate. The luminescence values were normalized to respective control samples (100%). The statistical significance was determined by a two-tailed Student's t-test (n = 3; additive vs control: *P < 0.05; **P < 0.01 and ***P < 0.001).

Determination of cell viability in 2D cultures supplemented with HA. For all experiments, NHAC, and hMSC-AT cells were seeded in a clear bottom 96-well plate (Corning) at a density of 1000 cells/well. After 24 h, medium with 0.125, 0.25, 0.5, or 1 mg/ml HA (Contipro) was added to each well; the total volume was 100 μl medium/well. Cells were cultured in the supplemented medium at 37 °C with 5% CO_2. The experiment was performed according to the producer protocol of the CellTiter-Glo® Luminescent Cell Viability Assay (Promega). CGM™ medium and Mesenchymal Stem Cells Growth Medium 2 without HA were used as a control.

After 24 h, 48 h, and 72 h, 100 µl of CellTiter-Glo® Reagent was added to each well. The samples were incubated for 30 min at room temperature. The luminescent signal was read with a microplate reader (Infinite® 200 PRO, TECAN). All samples were conducted in triplicate. The luminescence values were normalized to respective control samples (100%). The statistical significance was determined by a two-tailed Student's t-test (n = 3; additive vs control: *$P < 0.05$; **$P < 0.01$ and ***$P < 0.001$).

The preparation of bioink.   The bioink was prepared as follows. Weighted and UV-sterilized sodium alginate (Sigma-Aldrich) was dissolved in a sterile 4.6% (w/v) D-mannitol (Sigma-Aldrich) solution. Subsequently, weighted and UV-sterilized porcine skin gelatin (Sigma-Aldrich), and CCNC (Cellulose Lab) were separately added and mixed with the alginate solution with two syringes connected with the female/female Luer-lock adapter. The materials were shaken each time at 37 °C for at least 30 min with HulaMixer™ Sample Mixer, followed by overnight mixing. The final concentrations of bioink components were 4.0% gelatin, 0.75% alginate, and 1.4% CCNC. Before adding cells, HA or/and MWCNTs were added and bioink was additionally mixed with two syringes connected with the female/female Luer-lock adapter. The prepared bioink was mixed with 8×10^6 cells/ml of bioink in an analogical way. Only hMSC-AT were utilized for 3D bioprinting. Before bioprinting, the bioink with cells was placed in a cartridge and held at a 25 °C water bath to induce gelatin gelation.

The rheological tests.   The rheological evaluation was performed on Anton Paar 302 rheometer, equipped with 25 mm, smooth, parallel plates (PP25) with bioink without cells and before crosslinking. The gap between plates was set to 1 mm and—unless stated otherwise—measurements were conducted at 23 °C. Performed rheological measurements were temperature sweep test and rotation. Temperature sweep experiments were performed at a rate of 2 °C/min from 20 to 40 °C. In the rotation study, the shear rate range was set to 0.01–1000.00 s^{-1}. A layer of silicone oil was spread over the verge surface of the sample to prevent water evaporation from bioink samples during rheological measurements. All rheological tests were performed in at least two repeats.

3D bioprinting.   The BioX printer (Cellink) with temperature-control, pressure extrusion printhead was used, with printhead temperature set at 25 °C, and printbed temperature set at 10 °C.

After bioprinting, the constructs were crosslinked with sterile 200 mM $CaCl_2$ (Sigma-Aldrich) dissolved in 4.6% (w/v) D-mannitol (Sigma-Aldrich) for 10 min at room temperature.

The constructs were cultured in Mesenchymal Stem Cell Growth Medium 2 (Promocell), and the Mesenchymal Stem Cell Chondrogenic Differentiation Medium (Promocell) in the case of cells used as differentiation control. The constructs were cultured in standard conditions (37 °C, 5% CO_2) and the medium was changed every 3 days.

SEM–EDX.   The constructs bioprinted without cells were subjected to Scanning Electron Microscopy (SEM) with Energy Dispersive X-Ray Analysis (EDX). The analyzed scaffolds were with or without the addition of the MWCNTs. The morphology of samples was characterized by scanning electron microscope Quanta FEG 250 (FEI) in low vacuum conditions at the pressure of 70 Pa with an electron beam energy of 10 keV. EDS spectra were collected with an electron beam energy of 30 keV using an EDS Octane SDD detector (EDAX). Prior to analysis, the scaffolds were frozen at −80 °C for 2 h and then lyophilized (Christ, Alpha 1–2 LDplus lyophilizer) for 12 h, at the pressure of 1 mBar. Subsequently, the pressure was decreased to 0.18 mBar and the process was carried out for another 4 h.

The live/dead assay of cells encapsulated in bioprinted construct.   After 24 h, 14 days, and 21 days, bioprinted constructs were analyzed with the LIVE/DEAD assay performed according to the manufacturer`s protocol (LIVE/DEAD® Viability/Cytotoxicity Kit, Invitrogen). Stained cells were visualized on a confocal microscope (IX83, Olympus). Scans for viability counting were taken from the lateral part of three different constructs at each time point. From each of these scans, two middle slices were chosen for live and dead cell counting. Obtained images were analyzed with Fiji software using ITCN functionality. The viability was calculated as a % of live cells. The statistical significance was determined by two-tailed Student's t-test (n = 3; additive vs control: $P^a < 0.05$; $P^b < 0.01$ and $P^c < 0.001$; timepoint vs timepoint (within the particular additive group): *$P < 0.05$; **$P < 0.01$ and ***$P < 0.001$).

Analysis of gene expression of cell-laden constructs.   Three constructs from each time point were dissolved in 100 mM sodium citrate containing 0.08 U/µl of Proteinase K and 1.0 U/µl of RNAse Inhibitor (A&A Biotechnology) with shaking at 37 °C for 5 min and followed by the RNA isolation with TriReagent (Sigma-Aldrich) and chloroform/phenol extraction. Isolated total RNA concentration was measured with the Qubit 4 fluorometer (Invitrogen) and reversely transcribed with the High-Capacity cDNA Reverse Transcription Kit (Thermo Scientific). Gene expression was analyzed from 7.5 ng of cDNA per sample with real-time PCR using Maxima SYBR Green/ROX qPCR Master Mix (Thermo Scientific) on QuantStudio 7 Flex (Applied Biosystems). The qPCR data were statistically analyzed with GraphPad Prism software. Relative expression was calculated with ddCt and referred to *RPS29* gene expression. The variations in gene expression were determined by two-tailed Student's t-test (n ≥ 2); P-values were considered significant as follows: additive vs control: $P^a < 0.05$; $P^b < 0.01$ and $P^c < 0.001$; timepoint vs timepoint (within the particular additive group): *$P < 0.05$; **$P < 0.01$ and ***$P < 0.001$. Sequences of primers used are listed in Supp. Tab. 1.

Results

Analysis of viability, ROS, and caspase 3/7 generation in 2D NHAC and hMSC-AT cell cultures.

In NHAC 2D culture, 1 mg/ml of HA addition had no significant effect on cell proliferation (Fig. 1a). The culture exposed to 0.25 mg/ml of HA showed negligible changes in viability after 24 h. However, increased proliferation was observed after 72 h of culture. Similar results were obtained for hMSC-AT (Fig. 2a). The highest increase in proliferation was observed at the HA concentration of 0.25 mg/ml. A decrease in cell viability of both NHAC and hMSC-AT cultures was observed for all MWCNTs concentrations. The highest decrease of about 50% in viability was observed for 0.125 mg/ml. Interestingly, in the culture with the lower range of MWCNTs concentrations (0.015 mg/mL and 0.03 mg/ml), cell viability was diminished in comparison to a higher concentration of 0.0625 mg/ml at all time points (Figs. 1b and 2b). Observed dependency was corroborated by analyses of ROS production and active caspases 3/7 (Figs. 1 c,d and 2c,d). The stable form of vitamin C (2-phospho-l-ascorbic acid) yields protective and antioxidative effects in the NHAC and hMSC-AT cell culture with CNTs. The strongest antioxidant effect of vitamin C is seen at the highest concentration of MWCNTs (0.125 mg/ml). Its supplementation causes a significant reduction in the production of reactive oxygen species and inhibits cell death compared to the medium without 2-phospho-l-ascorbic acid supplementation (Figs. 1 c,d and 2c,d).

Analysis of bioink and 3D bioprinting.

The addition of 0.25 mg/ml HA and 0.0625 mg/ml MWCNTs yielded the most beneficial effect in 2D tests, therefore these concentrations were selected for 3D bioprinting. The aim was to assess whether selected additives influence cell viability and induce chondrogenic differentiation in 3D culture. The hMSC-AT cell line at a concentration of 8×10^6 cells/ml was used in the study due to a higher proliferation rate than NHAC.

The MWCNTs or HA addition showed negligible influence on the rheological properties of bioinks. All of them exhibit a shear-thinning behavior and have similar cross-over temperatures (G' = G"), which signifies good printability (Fig. 3). Table 1 presents parameters set for 3D bioprinting.

Figure 1. Relative cell viability, ROS levels and caspase 3/7 activity in 2D NHACs culture. (**a**) Relative viability of NHACs after exposure to different concentrations of HA. (**b**) Relative viability of NHACs after exposure to different concentrations of MWCNTs. (**c**) Relative ROS generation after 24 h exposure to MWCNTs. (**d**) Relative Caspase 3/7 activity after 24 h incubation with MWCNTs. The data are presented as the mean ± SD. The statistical significance was determined by two-tailed Student's t-test (n = 3; additive vs control: *P < 0.05; **P < 0.01 and ***P < 0.001).
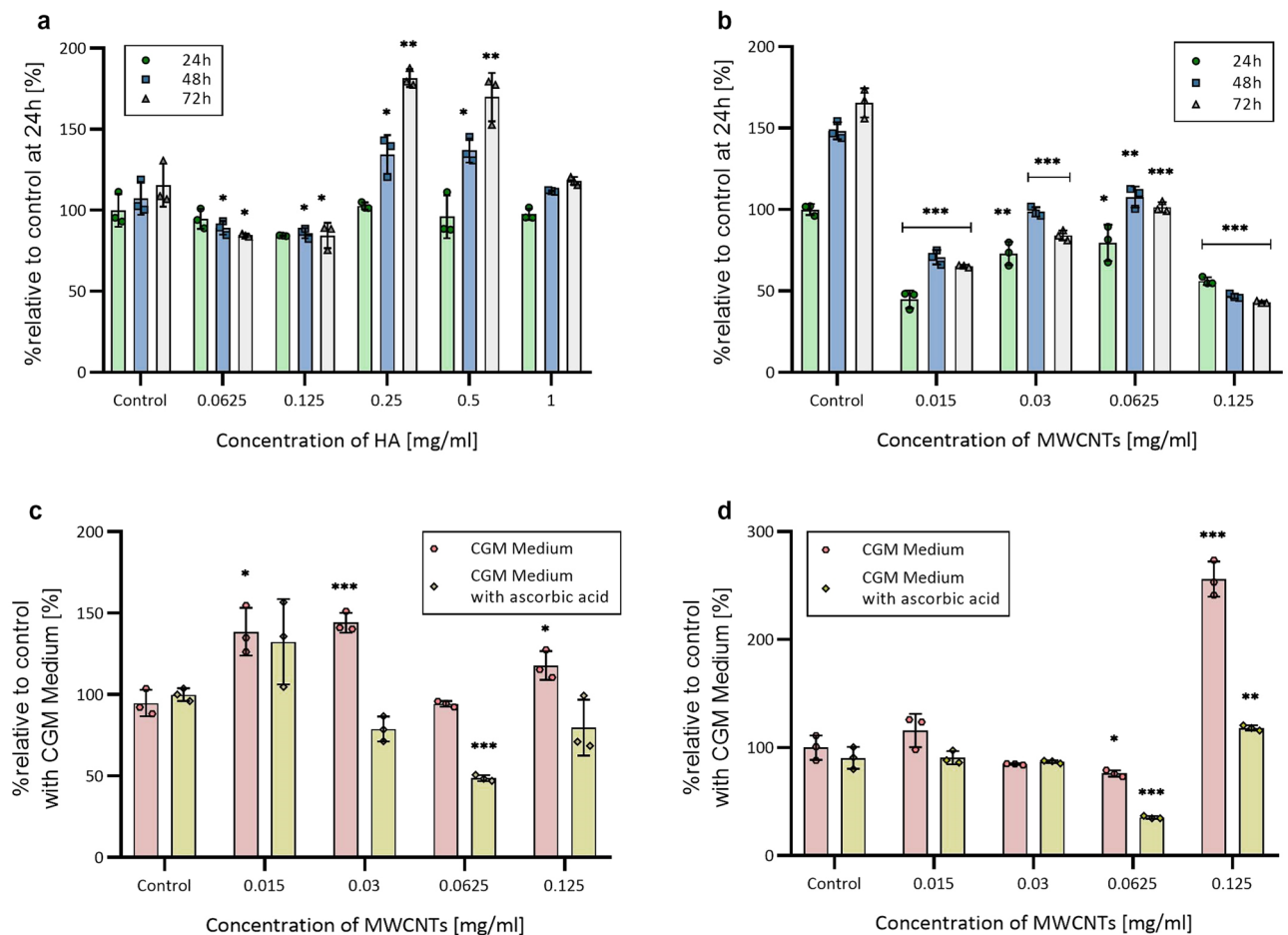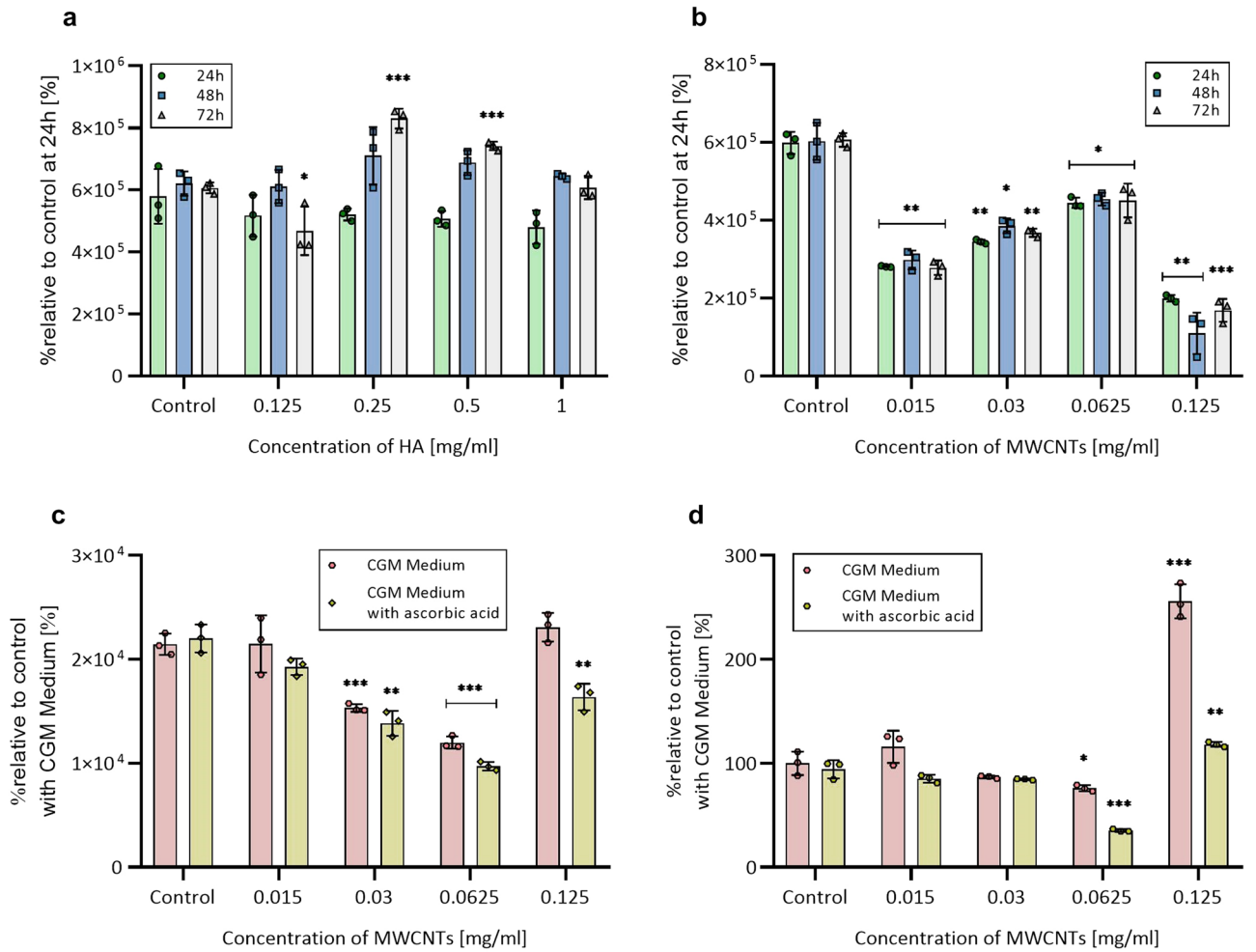
Figure 2. Relative cell viability, ROS levels, and caspase 3/7 activity in 2D hMSC-AT culture. (**a**) Relativeiability of hMSC-AT after exposure to different concentrations of HA. (**b**) Relative viability of hMSC-AT after exposure to different concentrations of MWCNTs. (**c**) Relative ROS generation after 24 h exposure to MWCNTs. (**d**) Relative caspase 3/7 activity after 24 h incubation with MWCNTs. The data are presented as the mean ± SD. The statistical significance was determined by two-tailed Student's t-test (n = 3; additive vs control: *P < 0.05; **P < 0.01 and ***P < 0.001).

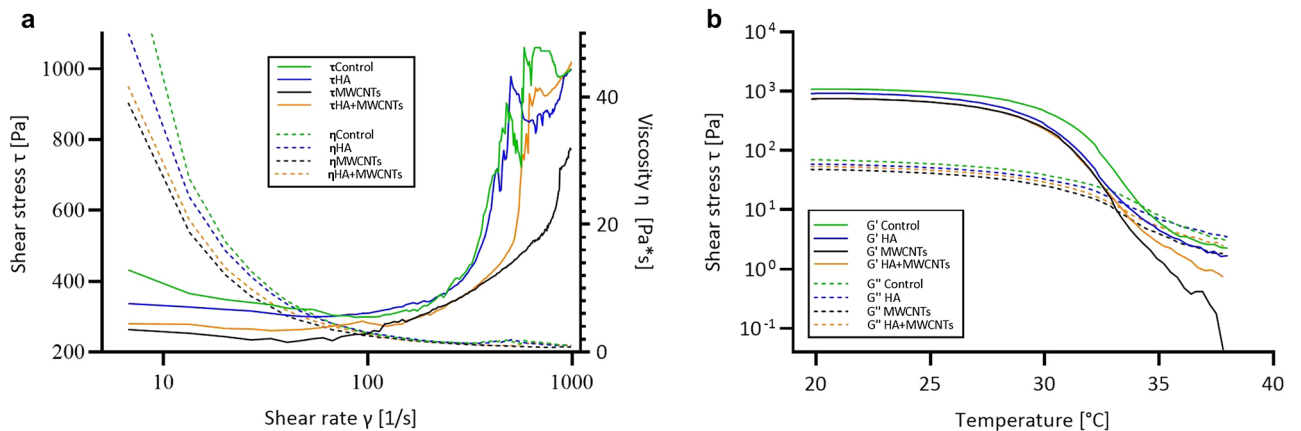**Figure 3.** Rheological analysis of bioinks with MWCNTs or HA addition. Control is bioink without MWCNTs and HA. (**a**) Shear stress and viscosity as a function of shear rate. (**b**) The temperature-dependent functions of storage modulus G' and loss modulus G".

	No additives	Bioink with 0.25 mg/ml HA	Bioink with 0.0625 mg/ml MWCNTs	Bioink with 0.25 mg/ml HA and 0.0625 mg/ml MWCNTs
Needle	22 gauge (inner diameter = 410 μm)			
Pressure	60–68 kPa	65–70 kPa	55–60 kPa	65–70 kPa
Speed	14–15 mm/s	15–18 mm/s	14–15 mm/s	16–18 mm/s
Preflow	200 ms			
Postflow	0 ms			

Table 1. 3D bioprinting parameters.

SEM–EDX analysis showed insignificant changes in structure and elemental composition (Supp. Fig. 1). In the SEM images, regular pores can be observed, which match our bioprinting model. scaffolds also present highly fibrous structures.

Cell viability in bioprinted scaffolds. Live/dead assay was performed in order to determine the hMSC-AT viability in the 3D scaffolds (Fig. 4). In the control medium, a constant decrease in total viability was observed. Interestingly, the biggest decline in viability was observed in the differentiation medium, despite the cells having the highest transcriptional activity (see paragraph 3.4.). A similar decline was observed in HA-enriched constructs. In the case of MWCNTs-containing constructs, the decline was not observed, which implies a stimulating or protective effect on the cells. HA and MWCNTs combined were the only compositions, showing a synergistic effect, which has a positive impact on cell viability throughout the whole experiment.

HA and MWCNTs supplementation affect the expression of chondrogenic markers. To evaluate the chondrogenic potential of HA and functionalized MWCNTs, the gene expression analysis of genetic markers of chondrogenesis and stemness was performed (Fig. 5). Based on available data, the following genes were selected as chondrogenic markers: *COL1A1, COL6A1, COL10A1* and *COMP* (encoding collagen type I, VI, X, and Cartilage Oligomeric Matrix Protein, respectively—ECM components), *RUNX2, HIF1A,* and *SOX9*; (transcription factors)[3,20]. Additionally, to monitor the stemness of hMSCs we analyzed the expression of transcription factor Oct-4 (*POU5F1* gene)[21]. hMSC-AT-containing scaffolds of each bioink variant were maintained in culture for 1, 14, or 21 days. At each time point, expression of the hMSC-AT in bioink variants was normalized to hMSC-AT 3D bioprinted with bioink without additives (Fig. 5, green dashed lines). An additional group of control scaffolds was maintained in the chondrogenic medium for the same time intervals to define reference expression profiles in differentiated cells (DIFF) (Supp. Fig. 2). Gene expression profiles of cells from the same bioink variant between different time points were juxtaposed. A set of analyzed genes demonstrates expression fluctuations across subsequent time points (Fig. 5a–c,e,f) when compared to the control group (Fig. 5a–c,e,f, green dashed lines). The expression of two analyzed genes, *SOX9* and *COL10A1*, dropped below detectable lev-
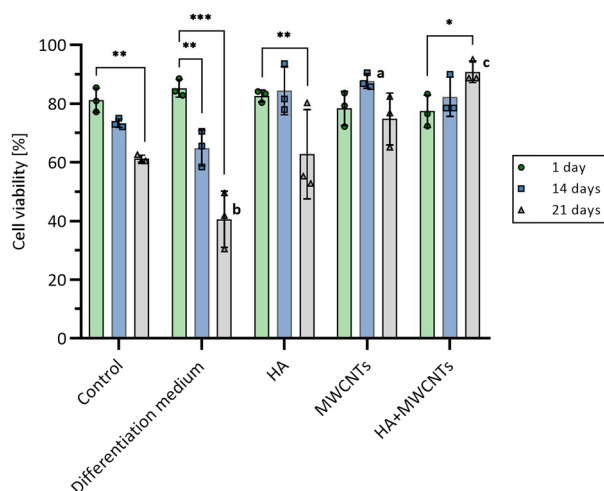
Figure 4. Viability of hMSC-AT cells in bioprinted scaffolds. Loss of viability over time can be observed in control media, supplemented with HA, and most profoundly, in commercial differentiation medium. Addition of the MWCNTs alone results in a protective or stimulating effect on cells, because the decrease in viability is not observed. Combined with HA, the viability has even increased over 21-day period. The data are presented as the mean ± SD. The statistical significance was determined by two-tailed Student's t-test (n = 3; additive vs control: [a]P < 0.05; [b]P < 0.01 and [c]P < 0.001; timepoint vs timepoint (within particular additive group): *P < 0.05; **P < 0.01 and ***P < 0.001).
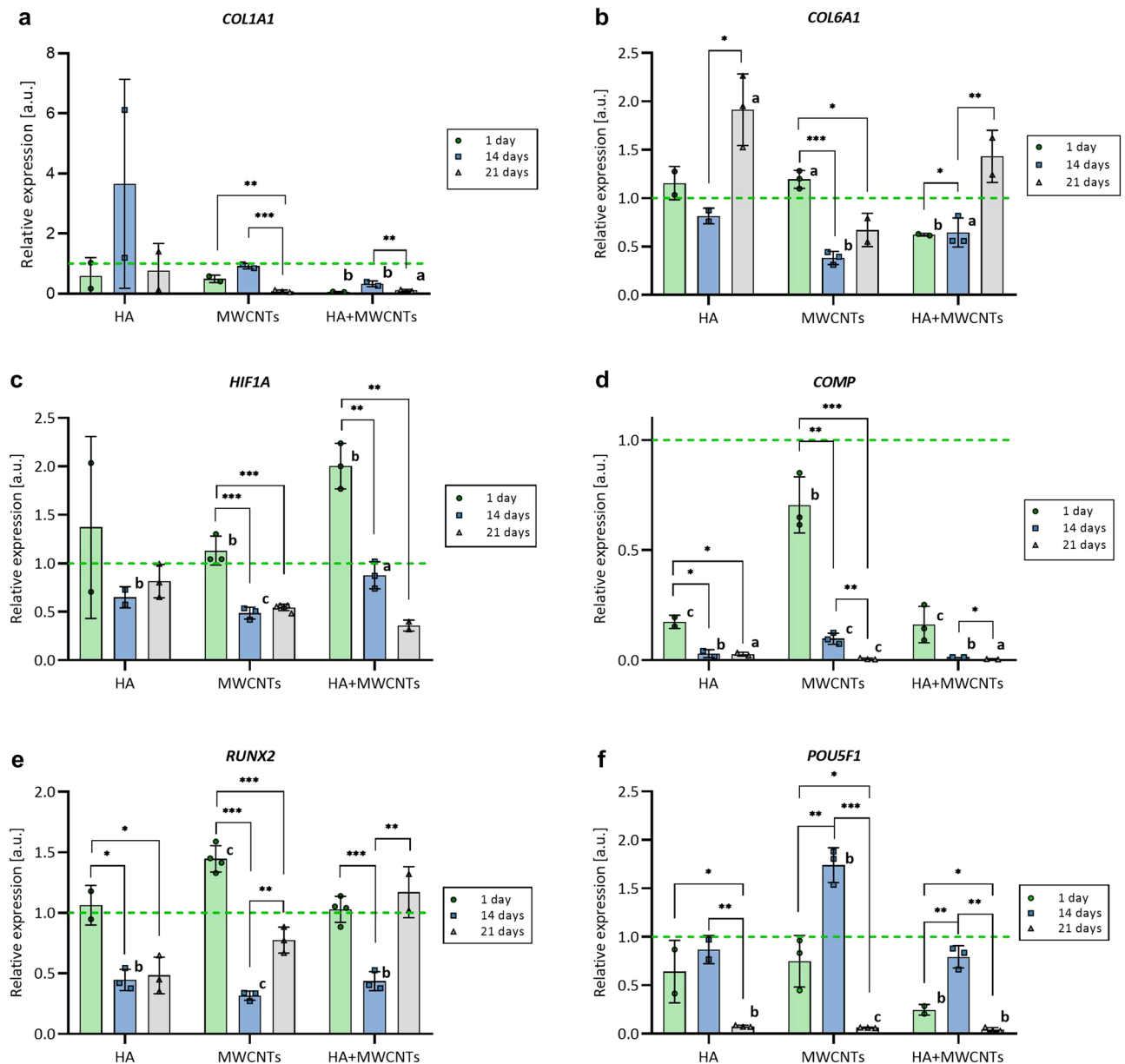
Figure 5. Bioink additives affect the expression of chondrogenic markers. Real-time analysis of COL1A1 (**a**), COL6A1 (**b**), HIF1A (**c**), COMP (**d**), RUNX2 (**e**) and POU5F1 (**f**) gene expression in hMSCs 3D-printed with bioink containing 0.25 mg/ml of hyaluronic acid (HA), 0.0625 mg/ml of multi-walled carbon nanotubes (MWCNTs) or mix of HA and MWCNTs (HA + MWCNTs) (0.25 mg/ml and 0.0625 mg/ml, respectively) 1 day (1d), 14 days (14d) and 21 days (21d) post-printing. The expression of each variant is normalized to the average expression in hMSCs 3D-printed with bioink without additives at a particular time point (green dashed line). The statistical significance was determined by two-tailed Student's t-test (n ≥ 2; additive vs control (green dashed line): [a]P < 0.05; [b]P < 0.01 and [c]P < 0.001; timepoint vs timepoint (within particular additive group): *P < 0.05; **P < 0.01 and ***P < 0.001).

els on day 14 and 21, respectively, for all analyzed bioink variants including control scaffolds (data not shown), therefore, they were excluded from further analysis. Incubation for 21 days revealed an intense decrease of *COL1A1, HIF1A, COMP*, and *POU5F1* genes expression in MWCNTs and HA + MWCNTs bioink variants and *COMP* and *POU5F1* expression in HA variant (Fig. 5a,c,d,f). In parallel, expression analysis of the same genes in DIFF medium 21 days post-printing showed a rapid increase of *COL1A1* and *COMP* activity, and a significant decrease of *POU5F1* while expression of *HIF1A* remained unchanged (Supp. Fig. 2a,c,d,f). For HA and HA + MWCNTs variants, a significant increase in *COL6A1* expression was observed on day 21 (Fig. 5b) as well as for DIFF (Supp. Fig. 2b). The initial significant increase was also detected in *HIF1A* and *RUNX2* genes for MWC-NTs and HA + MWCNTs (*HIF1A*) and MWCNTs (*RUNX2*) followed by a deep decrease on day 14 (Fig. 5c,e). For MWCNTs on day 21 expression of *RUNX2* was restored to the control level as well as for HA + MWCNTs, yet, without expression boost on day 1 (Fig. 5e). Expression of *RUNX2* in DIFF progressively elevated (Supp.

Fig. 2e). Temporal transcriptional activation has also been observed for MWCNTs and HA + MWCNthe Ts in the *POU5F1* gene, where 14 days post-printing gene expression strongly increased to drop to a barely detectable level at day 21 (Fig. 5f) which reflects the expression profile of *POU5F1* in DIFF (Supp. Fig. 2f). Noteworthy, despite the same dynamics, *POU5F1* expression for HA + MWCNTs was much lower than for MWCNTs and did not reach the expression level observed in control scaffolds (Fig. 5f, 1 day, and 14 days).

Discussion

Bioink development is an inextricable part of 3D bioprinting for tissue engineering. Structural materials, like alginate or cellulose, are responsible for construct integrity and proper mechanical features; whereas biologically active substances are added to maintain cell functionality or stimulate various biological effects. This work investigated the influence of HA and functionalized MWCNTs firstly in 2D culture and then as additives to bioink designed for cartilage regeneration.

The toxicity of carbon nanotubes is a frequently raised concern regarding its utilization in tissue engineering[22]. The addition of the MWCNTs in all tested concentrations decreased cell viability and resulted in an increased ROS production in 2D cultures (Figs. 1b and 2b). These results confirm our previous reports[18]. Interestingly, R OS production diminished with increasing concentrations of MWCNTs, but when the concentration exceeded 0.0625 mg/ml, a robust generation of ROS occurred. This phenomenon could be elucidated by ROS scavenging facilitated by the CNTs, as described earlier. Our previous research reveals the interference of CNTs with luminescence-based assays, yielding nonrepresentative results, falsely indicating the high toxicity of this nanomaterial. However, at low concentrations used in this study, this interference may be omitted. Additionally, combining the assay with the measurement of caspase activity provides a double check on the reliability of the assay.

Additionally, to mitigate oxidative stress elicited by the MWCNTs, a more stable analog of vitamin C was tested. It has been demonstrated that ascorbic acid promotes chondrogenic cell differentiation, and helps to maintain a chondrogenic phenotype, especially in pathological conditions[23]. Our study corroborates the beneficial effects of ascorbic acid on oxidative stress and the viability of cells.

Alginate-HA bioink has been previously utilized to bioprint articular cartilage constructs[15]. In the study, the authors demonstrated that HA addition increased chondrogenic gene expression; however, in a contrast to our experimental design, a thermoplastic polymer was used as a structural material. The addition of HA was shown to affect the viscosity of bioink and, consequently, printability[24]. The rheological analysis of our bioinks showed inconsiderable variation. This discrepancy could be explained by the relatively low concentration of HA in the bioink (0.25 mg/ml).

The lowest level of the MWCNTs cytotoxicity in 2D culture was observed at a concentration of 0.0625 mg/ml which was subsequently used for bioink formulation. Cells cultured in 3D bioprinted constructs showed higher tolerance to increasing concentrations of carbon nanotubes, compared to 2D culture[25]. In 3D culture, carbon nanotubes are embedded in a hydrogel matrix, which limits their ability to be absorbed by the cells, while in 2D cultures carbon nanotubes diffuse into the medium facilitating cellular uptake by endocytosis[26]. In our previous study, 0.01% of CNTs embedded in polycaprolactone scaffold increased chondrocyte adhesion and proliferation[8].

Live/dead analysis showed that in the scaffold without additives (control and differentiation medium), as well as with HA, the viability of cells decreased over time. This is not the case in the scaffolds supplemented with MWCNTs. It may be attributed to the CNTs' resemblance to collagen fibrils, forming a 3D intricate mesh-like structure (Supp. Fig. 1), which may have a stimulating effect on the cells. Partial degradation of the HA-supplemented scaffolds could be caused by an increase in water content due to the strong hydrophilicity of HA, leading to the loss of integrity and subsequent degradation. Scaffolds with both MWCNTs and HA showed the highest viability of cells. They were also more stable than HA-supplemented scaffolds. This observation can further corroborate the CNTs' resemblance to collagens since collagen's main structural function is to provide tensile strength to the whole tissue.

In general, significant changes in expression of all analyzed genes with a progressive overall loss of transcriptional activity were observed (*COL1A1, HIF1A, COMP, POU5F1*—Fig. 5a,c,d,f, *COL10A1, SOX9*—data not shown). However, in DIFF samples the expression of *COL1A1* and *COMP* increased intensively while the *HIF1A* level remained stable (Supp. Fig. 2a,c,d). HIF1A protein is prone to oxygenation as a target of HIF hydroxylases and its level is elevated during hypoxia[27]. The initial increase of *HIF1A* expression observed on day 1 for all bioink variants may be due to culture format conversion from 2 to 3D which resulted in temporal hypoxia or hypoxia-like conditions, however, a stable level of *HIF1A* in DIFF does not support such hypothesis. On the other hand, the chondrogenic medium contains a variety of components that intensively stimulate the differentiation process (a detailed formulation of the medium was unavailable) some of which may exhibit antagonistic properties regarding *HIF1A* activation.

Since *HIF1A* positively regulates the expression of *SOX9*, it may explain the dramatic loss of its expression observed on days 14 and 21[28]. Collagen type I, VI, X, and COMP protein are constituents of cartilage ECM and their increased expression is observed at different stages of chondrogenic differentiation[3]. Although all bioink variants revealed an intense decrease in expression of *COL1A1* (except for HA, however, insignificant), *COL10A1,* and *COMP*, expression of *COL6A1* increased in HA and HA + MWCNTs. It also reflects a similar expression pattern in MWCNTs samples, yet, insignificant. It has been shown that the expression of *COL1A1* is prone to the presence of collagen type I-derived fragments[29,30]. As gelatin is one of the main components of the bioink formulation, it is plausible that short collagen fragments inhibit *COL1A1* transcription. A significant increase of *COL1A1* expression in DIFF might be, contrastingly, a result of the dominant stimulatory effect of the chondrogenic medium which ameliorates collagen fragment inhibitory properties. Little is known about the regulation of *COMP* expression. However, previous studies show that COMP binds to collagen type I which might point to mutual or synergistic regulation and explain the simultaneous decrease of *COMP* gene expression

in all bioink variants, in contrast to DIFF where expression of both genes is dramatically increased[31]. Collagen type X is abundant in hypertrophic chondrocytes, therefore, intense loss of its expression in bioprinted hMSCs might be a hallmark of early-stage chondrogenic differentiation[32]. Although collagen type VI comprises up to 1% of total collagen in articular cartilage it plays important role in ECM organization and governing chondrocyte fate and, therefore, serves as an indicator of chondrogenesis[33–35]. The moderate increase observed in HA and HA + MWCNTs corresponds to changes in *COL6A1* observed in DIFF. Although the magnitude of change in *POU5F1* expression in MWCNTs and HA + MWCNTs is notably lower, its profile is similar to this observed in DIFF. Interestingly, while the *POU5F1* gene tends to deactivate in differentiating cells, its expression at day 14 in DIFF (as well as in CNTs and HA + MWCNTs) strongly elevates to almost complete deactivation on day 21. That might point to significant transcriptional rearrangement in hMSCs during incubation in a chondrogenic medium but in the presence of MWCNTs or a mix of HA and MWCNTs as well. Taken together, the addition of HA or MWCNTs, alone or in tandem, to the bioink provokes alterations in the expression of genes related to chondrogenic differentiation. Although the expression patterns are not identical for all selected genes and the magnitude of observed changes is considerably lower when compared to the expression induced by the chondrogenic medium, effects elicited by additives, MWCNTs, and HA + MWCNTs, in the expression of *COL6A1*, *RUNX2,* and *POU5F1* might point to low-efficient or time-shifted differentiation.

Summary

The effects of hyaluronic acid and carbon nanotubes were investigated in 2D and 3D in vitro cell cultures. Results were concentration-dependent and differ in models (2D or 3D). HA stimulates cell viability in monolayer culture. In bioprinted constructs, MWCNTs have a beneficial influence on cell viability while HA inclusion in examined concentration has a negative impact on constructs integrity. The profile of the analyzed gene changed significantly and we observed the overall loss of transcriptional activity in most of them. These results suggest the need for more complex gene expression analysis combined with protein accumulation studies, also in extended time points. In general, promising results from 3D bioprinted scaffolds encourage undertaking in vivo tests to investigate the precise mechanism of CNTs' interaction with cells. This may elucidate further whether they act as collagen mimetics.

Data availability

All data generated or analyzed during this study are included in this published article [and its supplementary information files].

References

1. Kwon, H. *et al.* Surgical and tissue engineering strategies for articular cartilage and meniscus repair. *Nat. Rev. Rheumatol.* **15**, 550–570 (2019).
2. Semba, J. A., Mieloch, A. A. & Rybka, J. D. Introduction to the state-of-the-art 3D bioprinting methods, design, and applications in orthopedics. *Bioprinting* **18**, e00070 (2020).
3. Gelse, K., Pöschl, E. & Aigner, T. Collagens—Structure, function, and biosynthesis. *Adv. Drug Deliv. Rev.* **55**, 1531–1546 (2003).
4. Xin, W., Heilig, J., Paulsson, M. & Zaucke, F. Collagen II regulates chondrocyte integrin expression profile and differentiation. *Connect. Tissue Res.* **56**, 307–314 (2015).
5. Holmes, D. F., Lu, Y., Starborg, T. & Kadler, K. E. Collagen fibril assembly and function. *Curr. Top. Dev. Biol.* **130**, 107–142 (2018).
6. Koláčná, L. *et al.* Biochemical and biophysical aspects of collagen nanostructure in the extracellular matrix. *Physiol. Res.* **56**, 51–60 (2007).
7. Garantziotis, S. & Savani, R. C. Hyaluronan biology: A complex balancing act of structure, function, location and context. *Matrix Biol.* **78–79**, 1–10 (2019).
8. Mieloch, A. A., Semba, J. A. & Rybka, J. D. CNT-type dependent cellular adhesion on 3D-printed nanocomposite for tissue engineering. *Int. J. Bioprint.* **8**, 70–79 (2022).
9. Chahine, N. O., Collette, N. M., Thomas, C. B., Genetos, D. C. & Loots, G. G. Nanocomposite scaffold for chondrocyte growth and cartilage tissue engineering: Effects of carbon nanotube surface functionalization. *Tissue Eng. Part A* **20**, 2305–2315 (2014).
10. Mirmusavi, M. H., Ahmadian, M. & Karbasi, S. Polycaprolactone-chitosan/multi-walled carbon nanotube: A highly strengthened electrospun nanocomposite Scaffold for cartilage tissue engineering. *Int. J. Biol. Macromol.* **209**, 1801–1814 (2022).
11. Pinnell, S. R. Regulation of collagen biosynthesis by ascorbic acid: A review. *Yale J. Biol. Med.* **58**, 553–559 (1985).
12. Murad, S. *et al.* Regulation of collagen synthesis by ascorbic acid. *Proc. Natl. Acad. Sci. USA* **78**, 2879–2882 (1981).
13. Ibold, Y. *et al.* Effect of different ascorbate supplementations on in vitro cartilage formation in porcine high-density pellet cultures. *Tissue Cell* **41**, 249–256 (2009).
14. Charan, T. R. *et al.* "Nanomaterials of curcumin-hyaluronic acid": Their various methods of formulations, clinical and therapeutic applications, present gap, and future directions. *Futur. J. Pharm. Sci.* **7**, 1–17 (2021).
15. Antich, C. *et al.* Bio-inspired hydrogel composed of hyaluronic acid and alginate as a potential bioink for 3D bioprinting of articular cartilage engineering constructs. *Acta Biomater.* **106**, 114–123 (2020).
16. Poldervaart, M. T. *et al.* 3D bioprinting of methacrylated hyaluronic acid (MeHA) hydrogel with intrinsic osteogenicity. *PLoS ONE* **12**, e0177628 (2017).
17. Hauptstein, J. *et al.* Hyaluronic acid-based bioink composition enabling 3D bioprinting and improving quality of deposited cartilaginous extracellular matrix. *Adv. Healthc. Mater.* **9**, 2000737 (2020).
18. Szymański, T., Kempa, M., Giersig, M. & Rybka, J. D. Carbon nanotubes interference with luminescence-based assays. *Materials (Basel)* **13**, 4270 (2020).
19. Hata, R.-I. & Senoo, H. L-Ascorbic acid 2-phosphate stimulates collagen accumulation, cell proliferation, and formation of a three-dimensional tissuelike substance by skin fibroblasts. *J. Cell. Physiol.* **138**, 8–16 (1989).
20. Di Cesare, P. E. *et al.* Expression of cartilage oligomeric matrix protein (COMP) by embryonic and adult osteoblasts. *J. Orthop. Res.* **18**, 713–720 (2000).
21. Niwa, H., Miyazaki, J. I. & Smith, A. G. Quantitative expression of Oct-3/4 defines differentiation, dedifferentiation or self-renewal of ES cells. *Nat. Genet.* **24**, 372–376 (2000).

22. Szymański, T. *et al.* Utilization of carbon nanotubes in manufacturing of 3D cartilage and bone scaffolds. *Materials* **13**, 4039 (2020).
23. Chang, Z., Huo, L., Li, P., Wu, Y. & Zhang, P. Ascorbic acid provides protection for human chondrocytes against oxidative stress. *Mol. Med. Rep.* **12**, 7086–7092 (2015).
24. Lee, S. J. *et al.* Three-dimensional printable hydrogel using a hyaluronic acid/sodium alginate bio-ink. *Polymers (Basel)* **13**, 1–8 (2021).
25. Chahine, N. O., Collette, N. M., Thomas, C. B., Genetos, D. C. & Loots, G. G. Nanocomposite scaffold for chondrocyte growth and cartilage tissue engineering: Effects of carbon nanotube surface functionalization. *Tissue Eng.-Part A* **20**, 2305–2315 (2014).
26. Maruyama, K. *et al.* Endocytosis of multiwalled carbon nanotubes in bronchial epithelial and mesothelial cells. *Biomed. Res. Int.* **2015** (2015).
27. Schofield, C. J. & Ratcliffe, P. J. Oxygen sensing by HIF hydroxylases. *Nat. Rev. Mol. Cell Biol.* **5**, 343–354 (2004).
28. Zhang, C. *et al.* Hypoxia-inducible factor-1 is a positive regulator of Sox9 activity in femoral head osteonecrosis. *Bone* **48**, 507–513 (2011).
29. Horlein, D., McPherson, J., Goh, S. H. & Bornstein, P. Regulation of protein synthesis: Translational controls by procollagen-derived fragments. *Proc. Natl. Acad. Sci. USA* **78**, 6163–6167 (1981).
30. Wiestner, M. *et al.* Inhibiting effect of procollagen peptides on collagen biosynthesis in fibroblast cultures. *J. Biol. Chem.* **254**, 7016–7023 (1979).
31. Rosenberg, K., Olsson, H., Mörgelin, M. & Heinegård, D. Cartilage oligomeric matrix protein shows high affinity zinc-dependent interaction with triple helical collagen. *J. Biol. Chem.* **273**, 20397–20403 (1998).
32. Smith, D. E. & Fisher, P. A. Identification, developmental regulation, and response to heat shock of two antigenically related forms of a major nuclear envelope protein in Drosophila embryos: Application of an improved method for affinity purification of antibodies using polypeptides. *J. Cell Biol.* **99**, 20–28 (1984).
33. Hou, W. *et al.* Cross-tissue characterization of heterogeneities of mesenchymal stem cells and their differentiation potentials. *Front. Cell Dev. Biol.* **9**, 3493 (2021).
34. Zelenski, N. A. *et al.* Type VI collagen regulates pericellular matrix properties, chondrocyte swelling, and mechanotransduction in mouse articular cartilage. *Arthritis Rheumatol.* **67**, 1286–1294 (2015).
35. Eyre, D. R., Weis, M. A. & Wu, J. J. Articular cartilage collagen: An irreplaceable framework?. *Eur. Cell. Mater.* **12**, 57–63 (2006).

Acknowledgements

Author contributions

J.D.R. guided and supervised the project. T.S. and A. A. M. designed and supervised the experiments. T.S., J.A.S., M.K. and P.C., conducted experiments, T.S. and J.D.R. contributed intellectually to the scientific design of the project. A.A.M. and J.D.R. mentored the technical part of the project; manuscript preparation T.S., J.A.S.; manuscript edition A.A.M, J.D.R.

Funding

Competing interests

The authors declare no competing interests.

Additional information

Supplementary Information The online version contains supplementary material available at https://doi.org/10.1038/s41598-023-27901-z.

Correspondence and requests for materials should be addressed to J.D.R.

Reprints and permissions information is available at www.nature.com/reprints.

Publisher's note Springer Nature remains neutral with regard to jurisdictional claims in published maps and institutional affiliations.

Supplementary data

Supplementary Figure 1. SEM and EDX analysis. SEM images of scaffolds without addition of the MWCNTs (A, B, C) and scaffolds supplemented with CNTs (D, E, F). EDX spectra of CNT supplemented (G) and non-supplmented scaffolds (H). There is no significant difference in atomic composition.
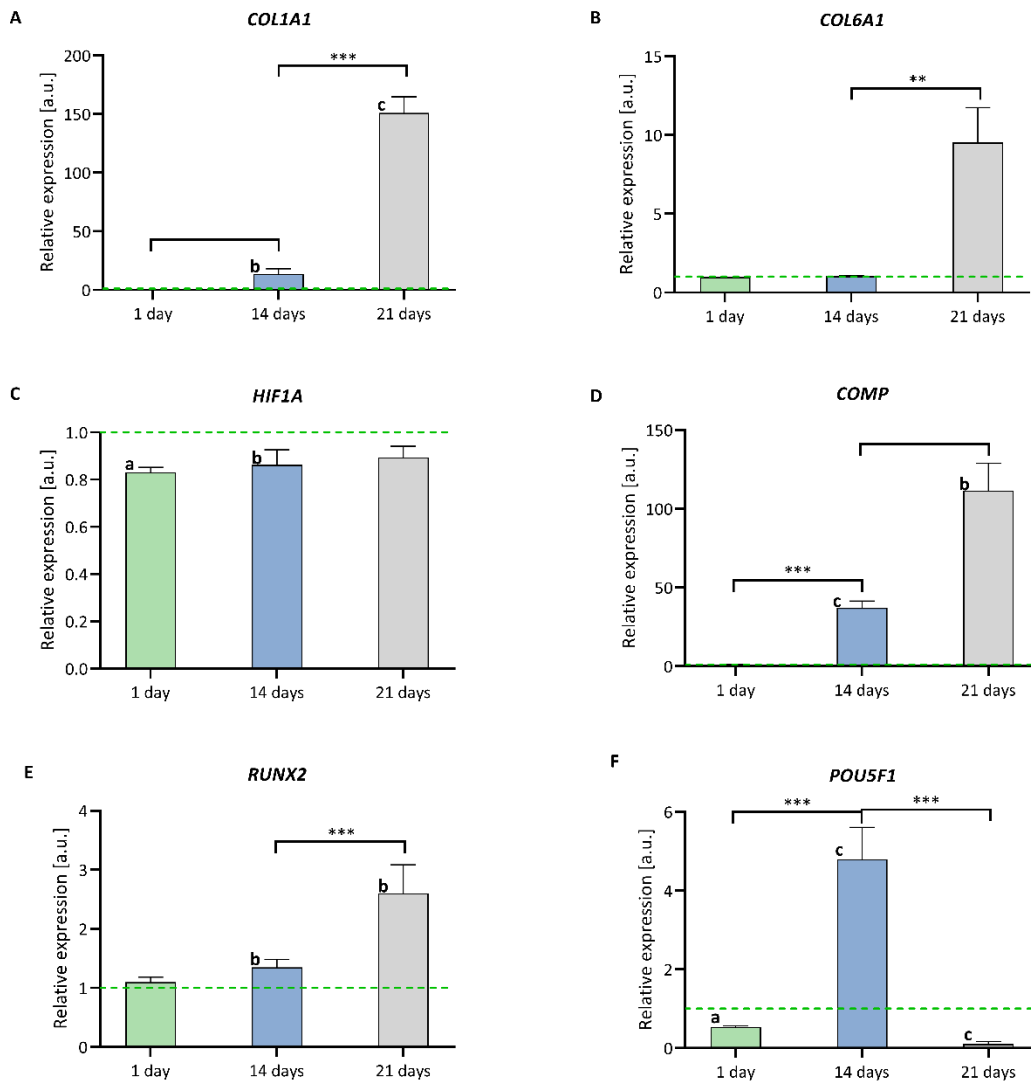
Supplementary Figure 2. **Differentiation medium affects expression of chondrogenic markers.** Real-time analysis of COL1A1 (A), COL6A1 (B), HIF1A (C), COMP (D), RUNX2 (E) and POU5F1 (F) gene expression in hMSCs 3D-printed with bioink without HA or MWCNTs supplementation 1 day (1d), 14 days (14d) and 21 days (21d) post-printing. Expression is normalized to average expression in hMSCs 3D-printed with bioink without additives and cultured in regular medium at particular time point (green dashed line). The statistical significance was determined by two-tailed Student's t-test (n≥2; chondrogenic vs control: $P^a < 0.05$; $P^b < 0.01$ and $P^c < 0.001$; timepoint vs time point $P^* < 0.05$; $P^{**} < 0.01$ and $P^{***} < 0.001$).

Supplementary Tabel 1. Primer sequences used in real-time analysis.

RPS29	forward 5'-AGATGGGTCACCAGCAGCTGTACTG-3'
	reverse 5'-AGACACGACAAGAGCGAGAA-3'
COL1A1	forward 5'-ACGTCCTGGTGAAGTTGGTC-3'
	reverse 5'-AGCCTCTCTCTCCTCTCTGACC-3'
COL6A1	forward 5'-CTCGTGGACAAAGTCAAGTCCT-3'
	reverse 5'-GTAGGTGCCCTTCCCAAAGTA-3'
COL10A1	forward 5'-TTACGCTGAACGATACCAAATG-3'
	reverse 5'-GACTTCCGTAGCCTGGTTTTC-3'
RUNX2	forward 5'-ACCAGATGGGACTGTGGTTACT-3'
	reverse 5'-TGTGAAGACGGTTATGGTCAAG-3'
HIF1A	forward 5'-CCAACAGTAACCAACCTCAGTG-3'
	reverse 5'-GCCTAAAAGTTCTTCTGGCTCA-3'
COMP	forward 5'-ACAATGACGGAGTCCCTGAC-3'
	reverse 5'-TCTGCATCAAAGTCGTCCTG-3'
SOX9	forward 5'-GACTCGCCACACTCCTCCT-3'
	reverse 5'-AGGTCTCGATGTTGGAGATGAC-3'
POU5F1	forward 5'-GGAGATATGCAAAGCAGAAACC-3'
	reverse 5'-CTCAAAATCCTCTCGTTGTGC-3'

Julia Semba

Laboratory of Applied Biotechnology
Center for Advanced Technology
Adam Mickiewicz University in Poznan
e-mail: jsemba@amu.edu.pl

Author contribution statement

I declare that I am the co-author of the article "Hyaluronic acid and multiwalled carbon nanotubes as bioink additives for cartilage tissue engineering" by Tomasz Szymański, Julia Anna Semba, Adam Aron Mieloch, Piotr Cywoniuk, Marcelina Kempa and Jakub Dalibor Rybka, published in *Scientific reports* in 2023. The author's contribution is as follows:

Tomasz Szymański designed the study and supervised the experiments. Tomasz Szymański made MWCNTs functionalization and determined the cell viability, reactive oxygen species, and apoptosis levels in 2D cell cultures stimulated with MWCNTs, 2-phospho-l-ascorbic acid, and hyaluronic acid. Tomasz Szymański with Julia Semba prepared the original draft and Supp. Figure 1.

Julia Semba co-designed the study. She was responsible for cell culture. Julia Semba prepared bioinks, made rheological analysis, and 3D bioprinted. Julia Semba prepared and analyzed SEM. Julia Semba with Piotr Cywoniuk prepared, made, and analyzed gene expression. Julia Semba with Tomasz Szymański prepared the original draft. She prepared Figures 1 to 3, as well as Figure 4 and Supp. Figure 1 with Tomasz Szymański and Figure 5 and Supp. Figure 2 with Piotr Cywoniuk.

Adam Mieloch designed the study, supervised the experiments, and revised the draft.

Piotr Cywoniuk helps with primer design and qPCR data analysis. Made Figure 5 and Supp. Figure 2 with Julia Semba.

Marcelina Kempa helped to determine the cell viability, reactive oxygen species, and apoptosis levels in 2D cell cultures stimulated with MWCNTs, 2-phospho-l-ascorbic acid, and hyaluronic acid.

Jakub Rybka guided and supervised the research and revised the draft. Jakub Rybka also acquired funding and corresponded with the journal and reviewers.

Date: 18.08. 2023

Signature: *Julia Semba*

prof. UAM dr hab. inż. Jakub D. Rybka

Tomasz Szymański

Laboratory of Applied Biotechnology
Center for Advanced Technology
Adam Mickiewicz University in Poznan
e-mail: tomszy1@amu.edu.pl

Author contribution statement

I declare that I am the first author of the article "Hyaluronic acid and multiwalled carbon nanotubes as bioink additives for cartilage tissue engineering" by Tomasz Szymański, Julia Anna Semba, Adam Aron Mieloch, Piotr Cywoniuk, Marcelina Kempa and Jakub Dalibor Rybka, published in *Scientific reports* in 2023 and I am aware that this publication is a part of Julia Semba PhD dissertation. The author's contribution is as follows:

Tomasz Szymański designed the study and supervised the experiments. Tomasz Szymański made MWCNTs functionalization and determined the cell viability, reactive oxygen species, and apoptosis levels in 2D cell cultures stimulated with MWCNTs, 2-phospho-l-ascorbic acid, and hyaluronic acid. Tomasz Szymański with Julia Semba prepared the original draft and Supp. Figure 1.

Julia Semba co-designed the study. She was responsible for cell culture. Julia Semba prepared bioinks, made rheological analysis, and 3D bioprinted. Julia Semba prepared and analyzed SEM. Julia Semba with Piotr Cywoniuk prepared, made, and analyzed gene expression. Julia Semba with Tomasz Szymański prepared the original draft. She prepared Figures 1 to 3, as well as Figure 4 and Supp. Figure 1 with Tomasz Szymański and Figure 5 and Supp. Figure 2 with Piotr Cywoniuk.

Adam Mieloch designed the study, supervised the experiments, and revised the draft.

Piotr Cywoniuk helps with primer design and qPCR data analysis. Made Figure 5 and Supp. Figure 2 with Julia Semba.

Marcelina Kempa helped to determine the cell viability, reactive oxygen species, and apoptosis levels in 2D cell cultures stimulated with MWCNTs, 2-phospho-l-ascorbic acid, and hyaluronic acid.

Jakub Rybka guided and supervised the research and revised the draft. Jakub Rybka also acquired funding and corresponded with the journal and reviewers.

Date: 22.08.2023

Signature:

Dr Adam Mieloch

Laboratory of Applied Biotechnology
Center for Advanced Technology
Adam Mickiewicz University in Poznan
e-mail: amieloch@amu.edu.pl

Author contribution statement

I declare that I am the co-author of the article "Hyaluronic acid and multiwalled carbon nanotubes as bioink additives for cartilage tissue engineering" by Tomasz Szymański, Julia Anna Semba, Adam Aron Mieloch, Piotr Cywoniuk, Marcelina Kempa and Jakub Dalibor Rybka, published in *Scientific reports* in 2023 and I am aware that this publication is a part of Julia Semba PhD dissertation. The author's contribution is as follows:

Tomasz Szymański designed the study and supervised the experiments. Tomasz Szymański made MWCNTs functionalization and determined the cell viability, reactive oxygen species, and apoptosis levels in 2D cell cultures stimulated with MWCNTs, 2-phospho-l-ascorbic acid, and hyaluronic acid. Tomasz Szymański with Julia Semba prepared the original draft and Supp. Figure 1.

Julia Semba co-designed the study. She was responsible for cell culture. Julia Semba prepared bioinks, made rheological analysis, and 3D bioprinted. Julia Semba prepared and analyzed SEM. Julia Semba with Piotr Cywoniuk prepared, made, and analyzed gene expression. Julia Semba with Tomasz Szymański prepared the original draft. She prepared Figures 1 to 3, as well as Figure 4 and Supp. Figure 1 with Tomasz Szymański and Figure 5 and Supp. Figure 2 with Piotr Cywoniuk.
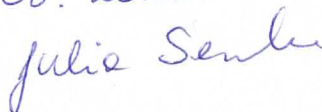
Adam Mieloch designed the study, supervised the experiments, and revised the draft.

Piotr Cywoniuk helps with primer design and qPCR data analysis. Made Figure 5 and Supp. Figure 2 with Julia Semba.

Marcelina Kempa helped to determine the cell viability, reactive oxygen species, and apoptosis levels in 2D cell cultures stimulated with MWCNTs, 2-phospho-l-ascorbic acid, and hyaluronic acid.

Jakub Rybka guided and supervised the research and revised the draft. Jakub Rybka also acquired funding and corresponded with the journal and reviewers.

Date: 21.08.2023

Signature:

Dr Piotr Cywoniuk

Laboratory of Applied Biotechnology
Center for Advanced Technology
Adam Mickiewicz University in Poznan
e-mail: pcywoniuk@amu.edu.pl

Author contribution statement

I declare that I am the co-author of the article "Hyaluronic acid and multiwalled carbon nanotubes as bioink additives for cartilage tissue engineering" by Tomasz Szymański, Julia Anna Semba, Adam Aron Mieloch, Piotr Cywoniuk, Marcelina Kempa and Jakub Dalibor Rybka, published in *Scientific reports* in 2023 and I am aware that this publication is a part of Julia Semba PhD dissertation. The author's contribution is as follows:

Tomasz Szymański designed the study and supervised the experiments. Tomasz Szymański made MWCNTs functionalization and determined the cell viability, reactive oxygen species, and apoptosis levels in 2D cell cultures stimulated with MWCNTs, 2-phospho-l-ascorbic acid, and hyaluronic acid. Tomasz Szymański with Julia Semba prepared the original draft and Supp. Figure 1.

Julia Semba co-designed the study. She was responsible for cell culture. Julia Semba prepared bioinks, made rheological analysis, and 3D bioprinted. Julia Semba prepared and analyzed SEM. Julia Semba with Piotr Cywoniuk prepared, made, and analyzed gene expression. Julia Semba with Tomasz Szymański prepared the original draft. She prepared Figures 1 to 3, as well as Figure 4 and Supp. Figure 1 with Tomasz Szymański and Figure 5 and Supp. Figure 2 with Piotr Cywoniuk.

Adam Mieloch designed the study, supervised the experiments, and revised the draft.

Piotr Cywoniuk helps with primer design and qPCR data analysis. Made Figure 5 and Supp. Figure 2 with Julia Semba.

Marcelina Kempa helped to determine the cell viability, reactive oxygen species, and apoptosis levels in 2D cell cultures stimulated with MWCNTs, 2-phospho-l-ascorbic acid, and hyaluronic acid.

Jakub Rybka guided and supervised the research and revised the draft. Jakub Rybka also acquired funding and corresponded with the journal and reviewers.

Date: 22.08.2023

Signature:

Dr hab. inż. Jakub Rybka, prof. UAM

Laboratory of Applied Biotechnology
Center for Advanced Technology
Adam Mickiewicz University in Poznan
e-mail: jrybka@amu.edu.pl

Author contribution statement

I declare that I am the corresponding author of the article "Hyaluronic acid and multiwalled carbon nanotubes as bioink additives for cartilage tissue engineering" by Tomasz Szymański, Julia Anna Semba, Adam Aron Mieloch, Piotr Cywoniuk, Marcelina Kempa and Jakub Dalibor Rybka, published in *Scientific reports* in 2023 and I am aware that this publication is a part of Julia Semba PhD dissertation. The author's contribution is as follows:

Tomasz Szymański designed the study and supervised the experiments. Tomasz Szymański made MWCNTs functionalization and determined the cell viability, reactive oxygen species, and apoptosis levels in 2D cell cultures stimulated with MWCNTs, 2-phospho-l-ascorbic acid, and hyaluronic acid. Tomasz Szymański with Julia Semba prepared the original draft and Supp. Figure 1.

Julia Semba co-designed the study. She was responsible for cell culture. Julia Semba prepared bioinks, made rheological analysis, and 3D bioprinted. Julia Semba prepared and analyzed SEM. Julia Semba with Piotr Cywoniuk prepared, made, and analyzed gene expression. Julia Semba with Tomasz Szymański prepared the original draft. She prepared Figures 1 to 3, as well as Figure 4 and Supp. Figure 1 with Tomasz Szymański and Figure 5 and Supp. Figure 2 with Piotr Cywoniuk.

Adam Mieloch designed the study, supervised the experiments, and revised the draft.

Piotr Cywoniuk helps with primer design and qPCR data analysis. Made Figure 5 and Supp. Figure 2 with Julia Semba.

Marcelina Kempa helped to determine the cell viability, reactive oxygen species, and apoptosis levels in 2D cell cultures stimulated with MWCNTs, 2-phospho-l-ascorbic acid, and hyaluronic acid.

Jakub Rybka guided and supervised the research and revised the draft. Jakub Rybka also acquired funding and corresponded with the journal and reviewers.

Date: 1 8. 08. 2023

Signature: prof. UAM dr hab. inż. Jakub D. Rybka

Mechanical testing of 3D printed constructs for meniscal tissue engineering.

Julia Anna Semba[1, 2], Adam Aron Mieloch[1], Ana M Teixeira[3], Pedro Martins[3,4], and Jakub Dalibor Rybka[1 *]

1 – Center for Advanced Technology, Adam Mickiewicz University, Poznan, Poland

2 – Faculty of Biology, Adam Mickiewicz University, Poznan, Poland

3 – FEUP/INEGI, Faculdade de Engenharia da Universidade do Porto, Porto, Portugal

4 – Aragón Institute of Engineering Research(i3A), University of Zaragoza, Zaragoza, Spain

* Correspondence to: Jakub Dalibor Rybka, jrybka@amu.edu.pl, +48 61829 1875

Abstract

One of the avenues for application of 3D bioprinting in orthopedics is the treatment of meniscal tears. Low viscosity biomaterials including hydrogel-based bioinks - are incompatible with most analytical devices available on the market. Hence, a custom-made equipment was applied to test the feasibility of compression analysis and stiffness estimation of freshly 3D printed constructs (composed of alginate, gelatin, and nanocellulose). In addition, the effects of time, hydrostatic pressure, and multiwalled carbon nanotubes (MWCNTs) addition on the mechanical properties were investigated. The drastic decrease in stiffness of constructs measured in PBS at 37 °C could be attributed to gelatin dissolution; while, the MWCNT addition almost doubled the stiffness of constructs, even at low concentrations - 0.125 mg MWCNTs per ml of bioink. To our knowledge, this is the first study demonstrating that MWCNTs enhance the stiffness of scaffolds created with bioink used for 3D bioprinting with cells.

Key words: hydrogels, mechanical testing, bioink, carbon nanotubes, 3D bioprinting

Graphical abstract

alginate

carboxymethylated
cellulose nanocrystal

gelatin

multiwalled carbon
nanotubes

3D printing

Compression
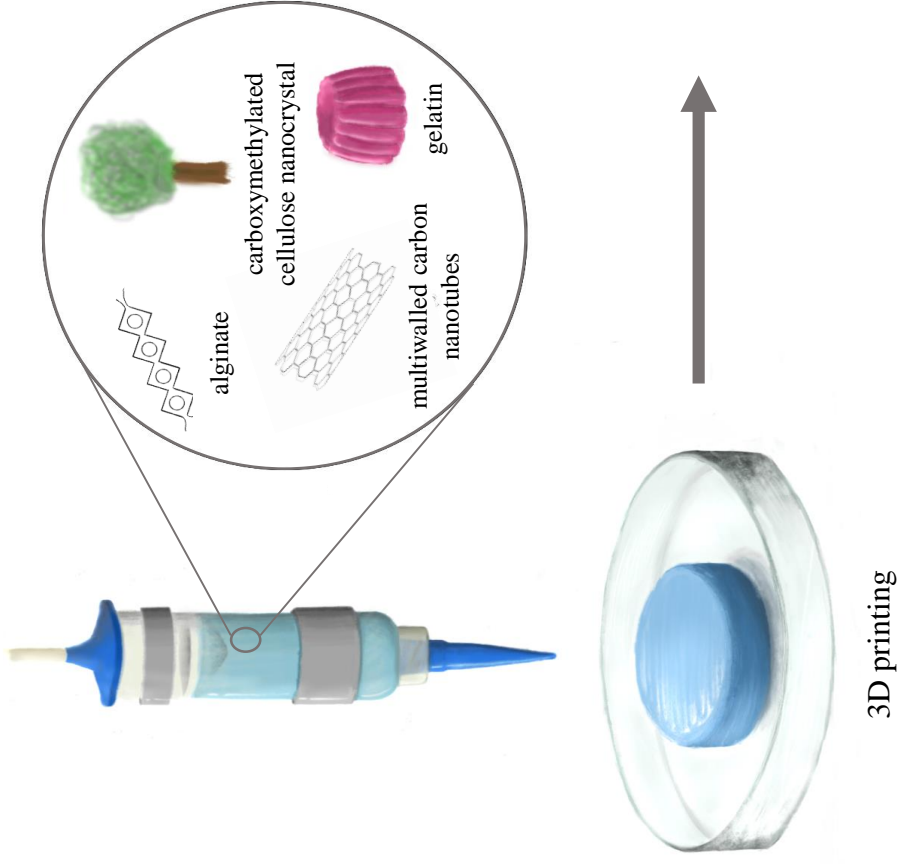
Introduction

Menisci are cartilaginous structures located in the knee between the femoral condyle and the tibial plateau (1,2). The mature meniscus is a heterogeneous tissue of zonal architecture varying in extracellular matrix (ECM), vascularity, and cellular phenotype. The red-red zone contains oval, fibroblast-like cells embedded in ECM composed predominantly of type I collagen (90 % of dry weight). In contrast, the white-white zone contains round, chondrocyte-like cells surrounded by ECM abundant in type II collagen (60 % of dry weight) with a decreased amount of type I collagen (40 %). The red-white zone shows attributes of red-red and white-white regions. The orientation of collagen fibers is circumferential within the meniscus, while random orientation is present on the surface of the meniscus. Due to these structural and physiological differences, the meniscus presents inhomogeneous mechanical properties, contributing to the proper functioning of the meniscus and the knee joint (2).

Menisci stabilize and transfer load in the knee joints. These functions entail prevalent meniscal injuries, associated with pain and joint dysfunction leading to articular cartilage degeneration (3). The treatment of meniscal tears is therefore crucial for long-term health and proper functioning of the knee joint. The most popular methods of treatment are meniscectomy and suturing, the results of which depend on patient physical condition (age, weight, and physical activity) and type of injury (size and location) (4). These methods usually yield insubstantial and unsatisfactory long-term outcomes, especially in the case of complex or extensive injuries. Therefore, alternative therapeutic methods are needed.

Tissue engineering offers tools to manufacture personalized constructs which provide a suitable mechanical and chemical environment to regenerate or replace damaged tissue (5). 3D bioprinting is currently a frontier technology in tissue engineering used for scaffold production through "layer-by-layer" assembly. This technology enables the creation of patient-specific constructs mimicking the native tissue in geometry and function more accurately than ever before (6). Among various 3D bioprinting techniques, extrusion-based bioprinting is the most popular. It utilizes pneumatic pressure or mechanical pistons for the continuous deposition of bioink (5). It is a relatively cheap technology applicable to bioinks with a wide range of viscosities.

Usually, bioinks are based on hydrogels or crosslinked polymers, the flow of which can be controlled (by adjusting printing parameters to the physicochemical properties of the bioink). The liquid-solid transition is an essential parameter to adjust the viscosity of bioinks and subsequently the stiffness of constructs to the desired application. In general, mechanical conformity between an implant and native tissue is one of the main factors affecting biocompatibility. Therefore, mechanical characterization is an important aspect of 3D bioprinted scaffold design.

While rheological measurement protocols have been established for bioinks, mechanical analysis of bioprinted scaffolds is challenging. Materials are tested with different setups and loading conditions, such as tension, compression, indentations, or dynamic mechanical analysis (DMA) (7). The goal is to obtain load-displacement data, which are typically converted to stress-strain or force-displacement curves. With this information,

various mechanical properties can be calculated e.g. stiffness, Young modulus, or yield strength. However, most devices available on the market are inadequate for displacement measurements at the low end of the viscoelastic spectrum, to which hydrogels pertain.

The aim of this work was to perform the mechanical characterization of freshly bioprinted scaffolds with custom-built prototype equipment. The bioink selected was developed for 3D bioprinting of meniscus-like constructs (8), as the main objective of meniscus tissue engineering is to recreate the mechanical characteristics of the native tissue (8). Physiologically, menisci are under constant hydrostatic pressure with direct compression and tension (9). These mechanical stimulations are essential for the development and maintenance of healthy cartilage. As demonstrated, insufficient or excessive mechanical loads may negatively alter gene expression profiles, e.g. the excessive mechanical stress upregulates the matrix metallopeptidase 13 (MMP13) expression (10). *MMP13* encodes collagenase 3, which degrades collagen type II and aggrecan. This variation is involved in endochondral ossification or osteoarthritis. Therefore, the successful application of 3D bioprinted constructs for meniscus tissue engineering relies heavily on its mechanical properties, affecting durability, biocompatibility, and overall performance (11).

Compression tests were performed on bioprinted constructs with bioink composed of alginate, gelatin, and carboxymethylated cellulose nanocrystals (CCNC) (8). The experiments were conducted with custom-made equipment built at INEGI (Institute of Science and Innovation in Mechanical and Industrial Engineering, Faculty of Engineering, University of Porto). At first, the protocol for compression testing of 3D bioprinted constructs was established. Then, the protocol was applied to investigate the influence of time, hydrostatic pressure, and multiwalled carbon nanotubes (MWCNTs) addition on the mechanical properties of the 3D constructs. Carbon nanotubes are concentrically rolled layers of graphene that form a cylindrical structure (12,13). The similarity of carbon nanotubes to collagen fibrils and their superior strength renders them a promising material for meniscus tissue engineering (14,15).

Methods

Bioink Preparation

Sodium alginate (Sigma-Aldrich), gelatin from porcine skin (Sigma-Aldrich), and CCNC (Cellulose Lab) were dissolved in a 4.6 % (w/V) D-mannitol (Sigma-Aldrich) solution. The components were added in the following order: alginate, gelatin, and CCNC; mixed each time with two syringes clipped with the female/female Luer lock adapter and left for 30 minutes at 37 °C. The final concentration was 0.75 % alginate, 4 % gelatin, and 1.4 % CCNC, as established previously (8).

MWCNTs were added at a concentration of 0.125 mg/ml; this concentration displayed the most beneficial biological effect in our prior research (16). MWCNTs were purchased (Nanolab Inc.) and functionalized as described earlier (12). Briefly, the MWCNTs (diameter: 15 nm – 30 nm; length: 15 µm – 20 µm: purity: ~95 %) were sonicated at 70 °C in a mix of

concentrated H_2SO_4 and HNO_3. This mixture was then neutralized with NaOH. The purification of the oxidized carbon nanotubes was carried out in cycles of centrifugation and resuspension in miliQ water. The resulting solution of carbon nanotubes was dried and suspended in phosphate buffer (PBS). The thermogravimetric method was applied to calculate the concentration of the functionalized MWCNTs.

3D Bioprinting

Prior to bioprinting, the bioink was placed in a cartridge and kept in a 25 °C water bath to induce gelatin gelation. The bioprinter (BioX or Inkredible, Cellink) with pressure extrusion printhead was used for printing of the cylindrical model (diameter = 8 mm; high = 6 mm) with an infill set at 35 % rectilinear pattern. A 22gauge needle (inner diameter = 410 µm) was utilized as the printing tip.

After bioprinting, the constructs were crosslinked with 200 mM $CaCl_2$ (Sigma-Aldrich) dissolved in 4.6 % (w/V) D-mannitol for 10 minutes at RT. The constructs were then immersed in Dulbecco's Modified Eagle Medium (DMEM, Corning) for 10 min to wash out the excess of $CaCl_2$. The samples measured after seven days were kept at DMEM supplemented with penicillin (100 U/ml) and streptomycin (100 µg/ml) at 4 °C.

Compression test

Each sample was measured before testing (diameter and height). The compression tests were performed with a flat-ended circular indenter (15 mm) (**Fig. 1**). The experimental apparatus was a custom-built prototype, which consist of an actuator (with a load capacity of 12 kg and a resolution of 3.05×10^{-4} mm), a load cell of 10 N (DBBSMM-1 kg), and a computer (17). The custom-made software was used for test definition, actuator control, and force-displacement data acquisition. Before each compression test, a preload of 0.02 N was applied to contact the indenter with the sample surface.
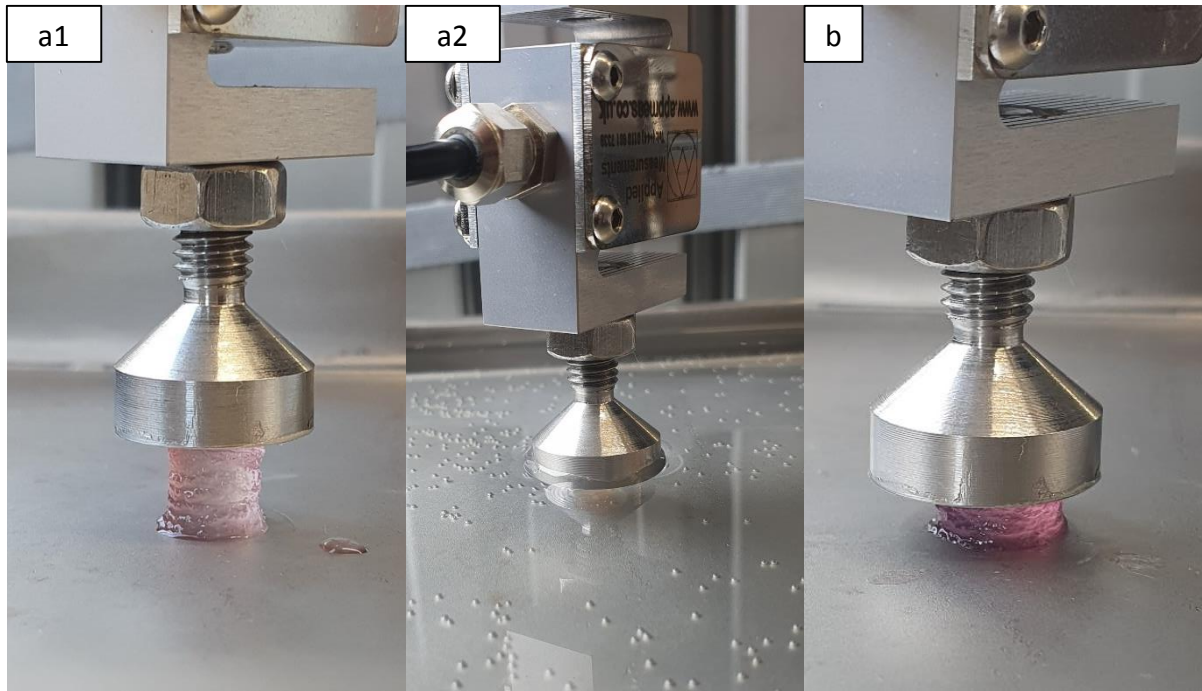
Figure 1. *Compression tests. Sample before (**a1**) and after (**b**) measurement and immersed in PBS (**a2**) before measurement.*

The first measurements were set at 80 % of a construct height to set up the appropriate strain range to consider during the experimental program. In practice the strain limits varied and were constrained to values below 80% (total sample destruction), to explore the optimal strain range per sample type. Then, to evaluate the effect of preconditioning, a preconditioning stage was applied with ten cycles of compression at 10 % of the height of the constructs at 1 mm/min.

The influence of hydrostatic pressure and temperature on the force-displacement curve was investigated using the apparatus` container filled with PBS (**Fig. 1 a2**). The temperature control module was set at 37 °C.

Data analysis

The force-displacement experimental data was acquired at a maximum sampling of 100 Hz. Due to fluctuations in the sampling, data from individual samples add to be regularized by interpolation procedure, to enable proper statistical treatment. The statistics carried out over each experimental batch consider the following:

1. it considers each experimental curve

$$i \in \{1, \dots, n\}: i, n \ \in N$$

   of the form

$$c_j^{(i)} = (f_j, d_j)$$

   with a total of j

$$j \in \{1, \dots, m\}: j, m \ \in N$$

experimental data points, as an individual experiment

2. it considers that all the curves $c^{(i)}$ describe the same phenomenon, i.e., the same testing protocol is applied to (n) identical samples corresponding to the experimental batch

3. After the data regularization (via interpolation), it is possible to apply a point-wise statistical treatment to the curves of a given batch, allowing us to calculate:
   a. a mean curve $c^{(mean)}$ representative of the whole batch, made of the point wise means, carried over the n curves for each point j
   b. statistical quantities such as the standard deviation (SD) and the standard error of the mean (SEM)

Stiffness estimation was carried out considering the slope of the second linear region of the loading curve (between the toe region and the yield point).

Results

Table 1 presents the established protocol for unconfined compression testing of cylindrical constructs (8 mm x 6 mm). The ultimate load to displacements ranging from 2.5 mm to 3.5 mm (**Fig. 2 a**). We added the preconditioning step since the meniscus is mechanosensitive tissue under constant cyclic loads (9). The stiffness of constructs measured with precondition was insignificantly higher (p-value = 0.0975) than the constructs measured without preconditioning (**Fig. 2 b**, **Tab. 2**). A preconditioning of ten cycles at 10 % strain reduced the experimental variability.

*Table 1. Parameters for compression testing of cylindrical constructs
(diameter = 8 mm; high = 6 mm).*

Parameter	Value
Speed	1 mm/min
Preconditioning	10 cycles; 10 % strain
Ramp	3.5 mm (approximately 60 % strain)
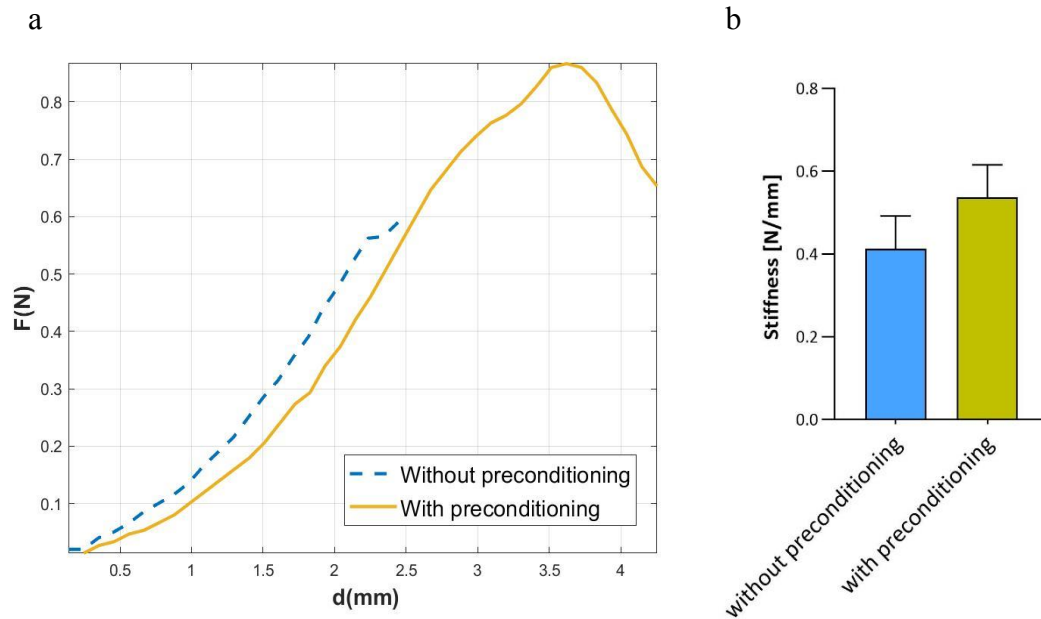
Figure 2. *Influence of preconditioning on force-displacement curves (**a**) and stiffness (**b**) of printed constructs. The data shown are mean (SD). The statistical significance was determined by unpaired Student's t-test (n ≥ 3; P* < .05; P** < .01 and P*** < .001).*

Fresh and 7-day-old constructs were evaluated to investigate the influence of time on mechanical properties (**Fig. 3 a** and **3 d**, **Tab. 2**). The difference in stiffness was statistically insignificant (p-value = 0.4376).

Table 2*. Values of stiffness of printed constructs with different variables.*

	Stiffness [N/mm]	
	n	Mean ± SD
Without preconditioning	4	0.4127 ± 0.07952
With preconditioning	3	0.5362 ± 0.07934
Control	7	0.3374 ± 0.09422
7-day old constructs	4	0.4127 ± 0.07952
In PBS at 37 °C	4	0.08916 ± 0.01721
With MWCNTs	3	0.6542 ± 0.1336
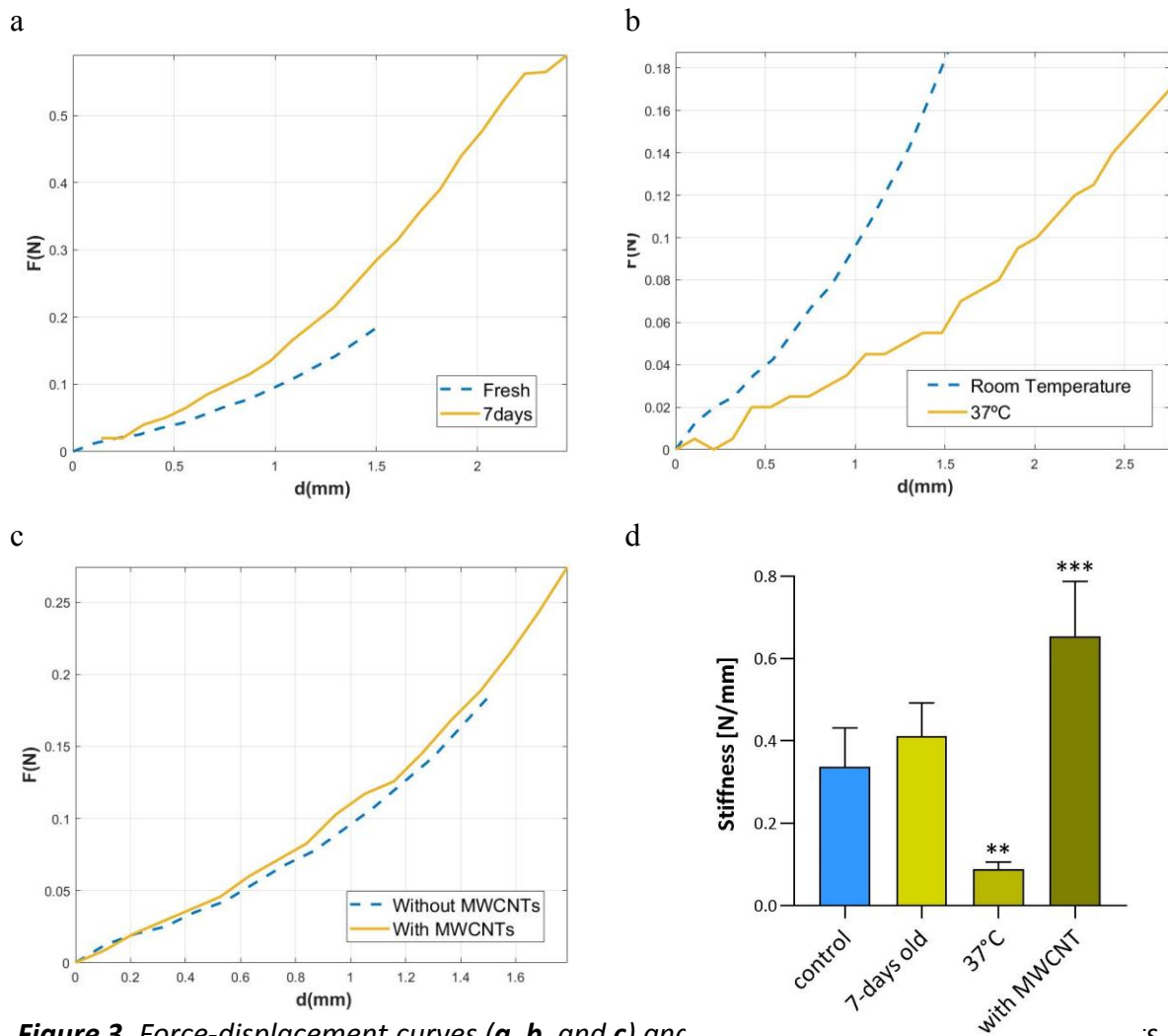
Figure 3. *Force-displacement curves (**a**, **b**, and **c**) and stiffness (**d**) of bioprinted constructs with different variables. Force-displacement curves of freshly bioprinted and 7-day-old constructs (**a**), constructs measured in and out of water bath (**b**), and constructs with and without MWCNTs addition (**c**). The data shown are mean (SD). The statistical significance was determined by one-way ANOVA (n ≥ 3; P* < 0.05; P** < 0.01 and P*** < 0.001).*

The tests were also performed on samples immersed in PBS at 37 °C (**Fig. 1 a2**). The results showed different mechanical behavior of constructs (**Fig. 3 b** and **3 d**, **Tab. 2**). The stiffness of constructs immersed in PBS decreases significantly (p-value = 0.0015). Finally, the mechanical properties of constructs enriched with MWCNTs were tested (**Fig. 3 c** and **3 d**, **Tab. 2**). The stiffness was significantly higher (p-value = 0.0004) for constructs with incorporated MWCNTs.

Discussion

The meniscus is a heterogeneous and mechanically sensitive tissue with complex biomechanics. Mechanical stimuli are essential for its proper development and functioning (18). Therefore, implant candidates must reproduce qualities of native tissue to fulfill their function. Investigating the mechanical attributes of bioprinted constructs is of fundamental

importance for the implementation of meniscal tissue engineering in medicine. The freshly bioprinted constructs are too soft for mechanical analysis with most commercially available devices, such as nanoindentation or DMA instruments. The present study faced this challenge and delivered a protocol for measuring the mechanical properties of bioprinted constructs. The methodology was then applied to investigate the effects of time, hydrostatic pressure, and MWCNTs supplement on mechanical behavior. Mechanical tests were performed with the custom-made machine at INEGI. Similar compression tests were performed by Giuseppe et al. with gelatin-alginate constructs and a custom-made machine (19).

The measurements were relatively simple and repeatable. The preconditioning strain was added to obtain consistent and repeatable responses (20). This strategy lowered variation, which was also observed in other studies (19,21). The parameters (ten cycles with 10 % of strain) were based on available literature (17,19). The strain value and number of cycles were demonstrated to affect the viscoelastic behavior of soft tissues, including the meniscus (21,22). Increased frequency resulted in an increase in meniscus stiffness, providing a starting point for further investigations (18).

The biomechanics of the knee joint subject menisci to constant cyclic loads, which affects their physiology. Dynamic compression studies have revealed the influence of cyclic loading, on the expression of cartilage-specific genes in mesenchymal stem cells encapsulated in agarose (23,24). Cells sense mechanical stress through mechanoreceptors, such as integrins, Ca^{2+} channels, and cytoskeleton (25). Mechanical signals are translated into various biomolecular pathways, stimulating chondrogenesis and maintenance of chondrogenic phenotype. However, the compression start time strongly affects the expression shifts (23,24). Therefore, submitting bioprinted implants to cyclic loads may provide a stimulus facilitating differentiation and/or maintenance of a proper cell phenotype (9).

Variations in mechanical strength over time were expected; since hydrogels display time-dependent mechanical behavior due to the intrinsic viscoelasticity of the polymer network (7). The analysis revealed insignificant differences between fresh and 7-day-old constructs. However, the 7-day-old constructs were kept at 4 °C, which does not correspond to the human physiological temperature or environment of the cell culture. Presumably, different storage conditions (e.g. at 37 °C with a humidified atmosphere) with extended time points would yield more significant changes (19). Hence, compression tests performed in PBS at 37 °C were designed to imitate the cell culture environment. A drastic decrease in stiffness was observed, which may be attributed to gelatin dissolution. The cross-over temperature of the bioink is 33.1 °C (8). Nevertheless, it is desired to measure the influence of cell activity on construct stiffness in solution at 37 °C for extended time points.

In this study, we observed that the MWCNTs addition narrowed the variability and almost doubled the stiffness of constructs even at concentrations as low as 0.125 mg/ml (**Fig. 3 c and 3 d**). These results confirm the viability for using carbon nanotubes in the regeneration of meniscal tissue. A higher concentration of MWCNTs is expected to further increase the stiffness of scaffolds, but our previous study has shown that higher concentrations are toxic to mesenchymal stem cells in 2D cultures (14,16). The MWCNTs

addition had a negligible influence on the viscoelasticity of the bioink (16). Moreover, the MWCNTs were shown to enhance the viability of mesenchymal stem cells and the expression of chondrogenic ECM genes (16,26). Interestingly, surfaces of synthetic materials functionalized with carbon nanotubes stimulate the growth of chondrocytes and help maintain their native phenotype (15,26–28). The toxicity of carbon nanotubes is a frequently raised issue. However, this effect could be partially mitigated by encapsulating cells in hydrogel with a low concentration of MWCNTs (16).

Ideally, the mechanics of meniscus scaffolds should correlate with the features of patients' native tissue or at least with established standard parameters. Individual lifestyle and age strongly affect the composition of ECM and the forces (compression and tension) acting on the menisci (29). The presented protocol enables to control the stiffness at an initial stage of constructs' production. This approach, combined with the reconstruction of the tissue geometry via computer-aided design and 3D printing technology, ensures better functionality of constructs adapted to lifestyles and physical conditions of patients.

We have presented the idea to measure stiffness of future implants created with 3D bioprinting. However, the mechanical analysis of freshly harvested, healthy human menisci remain an issue, due to limited availability. The meniscectomy is performed only in case of complex injuries, with advanced arthritis and inflammation. Therefore, most measurements are made on damaged or frozen tissues. These conditions affect the structure of meniscal ECM and, consequently, the mechanical properties (29,30). Alternatively, animal menisci can be used; however, differences in mechanical properties were observed (30). In addition, the lack of a standardized methods for estimation of meniscal features leads to notable variability in the values of stiffness and tensile modulus (2). Heterogeneity and complexity of the meniscal structure impose further difficulties regarding a reliable mechanical analysis. A unified approach to the characterization of human menisci is a matter that needs to be addressed.

The tested constructs were printed without cellular material which is a limitation of this study. Nonetheless, the aim of this study was to showcase the measurement approach of constructs created with the proposed bioink. Subsequent studies will assess the mechanical behavior of constructs seeded with mesenchymal stem cells guided toward chondrogenesis. The encapsulated cells remodel their environment through the activity of proteinases and the synthesis of ECM proteins; especially when natural hydrogels are used as bioink components (31–33). Additionally, the 3D bioprinting technique with compression apparatus enables the application of additional stimulators to intensive chondrogenesis process. Cell differentiation could be prompted not only by bioink supplementation with growth factors, ECM extracts, or MWCNTs, but also by dynamic compression (23,24,34,35).

The mechanical tests should be considered a standard practice in meniscal tissue engineering, allowing mechanical personalization of an implant. This research presented an approach to investigate the mechanical behavior of freshly bioprinted constructs with low stiffness. It is a simple and quick method, which allows for high-throughput mechanical testing of bioprinted constructs. It is desirable to test longer culture scaffolds with encapsulated cells, like mesenchymal stem cells. Such research would allow to assess the effect of structural

materials (like MWCNTs) on the mechanical properties of constructs and the mechanical stimulation on chondrogenesis over time. Moreover, the change of mechanical properties could also enable to track progression of chondrogenesis.

Funding

References

1.	Fox AJS, Bedi A, Rodeo SA. The Basic Science of Human Knee Menisci: Structure, Composition, and Function. Sports Health. 2012;4:340–351. doi: 10.1177/1941738111429419. Cited: in: : PMID: 23016106.

2.	Murphy CA, Garg AK, Silva-Correia J, Reis RL, Oliveira JM, Collins MN. The Meniscus in Normal and Osteoarthritic Tissues: Facing the Structure Property Challenges and Current Treatment Trends. Annu Rev Biomed Eng. 2019;21:495–521. doi: 10.1146/annurev-bioeng-060418-052547.

3.	Logerstedt DS, Ebert JR, MacLeod TD, Heiderscheit BC, Gabbett TJ, Eckenrode BJ. Effects of and Response to Mechanical Loading on the Knee [Internet]. Sports Medicine. Springer International Publishing; 2022. Available from: https://doi.org/10.1007/s40279-021-01579-7.

4.	Doral MN, Bilge O, Huri G, Turhan E, Verdonk R. Modern treatment of meniscal tears. EFORT Open Rev. 2018;3:260–268. doi: 10.1302/2058-5241.3.170067.

5.	Semba JA, Mieloch AA, Rybka JD. Introduction to the state-of-the-art 3D bioprinting methods, design, and applications in orthopedics. Bioprinting [Internet]. 2020;18:e00070. doi: 10.1016/j.bprint.2019.e00070.

6.	Filardo G, Petretta M, Cavallo C, Roseti L, Durante S, Albisinni U, Grigolo B. Patient-specific meniscus prototype based on 3D bioprinting of human cell-laden scaffold. Bone Joint Res [Internet]. 2019;8:101–106. doi: 10.1302/2046-3758.82.BJR-2018-0134.R1.

7.	Oyen ML. Mechanical characterisation of hydrogel materials. International Materials Reviews. 2014;59:44–59. doi: 10.1179/1743280413Y.0000000022.

8.	Semba JA, Mieloch AA, Tomaszewska E, Cywoniuk P, Rybka JD. Formulation and evaluation of a bioink composed of alginate, gelatin, and nanocellulose for meniscal tissue engineering. Int J Bioprint. 2023;9.

9.	Dai W, Wu T, Leng X, Yan W, Hu X, Ao Y. Advances in biomechanical and biochemical engineering methods to stimulate meniscus tissue. Am J Transl Res. 2021;13:8540–8560. Cited: in: : PMID: 34539978.

10.   Hall BK. Chondrocyte Diversity. Bones and Cartilage. 2007;301–315. doi: 10.1016/b978-012319060-4/50024-5.

11.   Quiroga JMP, Ito K, van Donkelaar CC. Meniscus replacement: Influence of geometrical mismatches on chondroprotective capabilities. J Biomech. 2015;48:1371–1376. doi: 10.1016/j.jbiomech.2015.02.063. Cited: in: : PMID: 25835788.

12.   Szymanski T, Kempa M, Giersig M, Rybka JD. Carbon Nanotubes Interference with Luminescence-Based Assays. Materials. 2020;13 (19):1–14. doi: doi:10.3390/ma13194270.

13.   Szymański, T.; Mieloch, A.A.; Richter, M.; Trzeciak, T.; Florek, E.; Rybka, J.D.; Giersig M, Szymański T, Mieloch AA, Richter M, Trzeciak T, Florek E, Dalibor Rybka J, Giersig M. Utilization of Carbon Nanotubes in Manufacturing of. Materials. 2020. p. 1–25.

14.   Mirmusavi MH, Ahmadian M, Karbasi S. Polycaprolactone-chitosan/multi-walled carbon nanotube: A highly strengthened electrospun nanocomposite scaffold for cartilage tissue engineering. Int J Biol Macromol [Internet]. 2022;209:1801–1814. doi: 10.1016/j.ijbiomac.2022.04.152. Cited: in: : PMID: 35487378.

15.   Zadehnajar P, Akbari B, Karbasi S, Mirmusavi MH. Preparation and characterization of poly ε-caprolactone-gelatin/multi-walled carbon nanotubes electrospun scaffolds for cartilage tissue engineering applications. International Journal of Polymeric Materials and Polymeric Biomaterials [Internet]. 2020;69:326–337. doi: 10.1080/00914037.2018.1563088.

16.   Szymański T, Semba JA, Mieloch AA, Cywoniuk P, Kempa M, Rybka JD. Hyaluronic acid and multiwalled carbon nanotubes as bioink additives for cartilage tissue engineering. Sci Rep [Internet]. 2023;1–10. doi: 10.1038/s41598-023-27901-z.

17.   Teixeira AM, Martins P. Mechanical characterisation of an organic phantom candidate for breast tissue. J Biomater Appl [Internet]. 2020;34:1163–1170. doi: 10.1177/0885328219895738. Cited: in: : PMID: 31876237.

18.   Pereira H, Caridade SG, Frias AM, Silva-correia J, Pereira DR, Cengiz IF, Mano JF, Oliveira JM, Espregueira-mendes J, Reis RL. Biomechanical and cellular segmental characterization of human meniscus : building the basis for Tissue Engineering therapies. Osteoarthritis Cartilage [Internet]. 2014;22:1271–1281. doi: 10.1016/j.joca.2014.07.001.

19.   Giuseppe M di, Law N, Webb B, A. Macrae R, Liew LJ, Sercombe TB, Dilley RJ, Doyle BJ. Mechanical behaviour of alginate-gelatin hydrogels for 3D bioprinting. J Mech Behav Biomed Mater. 2018;79:150–157. doi: 10.1016/j.jmbbm.2017.12.018.

20.   Cheng S, Clarke EC, Bilston LE. The effects of preconditioning strain on measured tissue properties. J Biomech. 2009;42:1360–1362. doi: 10.1016/j.jbiomech.2009.03.023. Cited: in: : PMID: 19394022.

21.   Ebrahimi M, Mohammadi A, Ristaniemi A, Stenroth L, Korhonen RK. The effect of different preconditioning protocols on repeatability of bovine ACL stress-relaxation response in tension. J Mech Behav Biomed Mater [Internet]. 2019;90:493–501. doi: 10.1016/j.jmbbm.2018.10.041. Cited: in: : PMID: 30448563.

22. Hosseini SM, Wilson W, Ito K, van Donkelaar CC. How preconditioning affects the measurement of poro-viscoelastic mechanical properties in biological tissues. Biomech Model Mechanobiol. 2014;13:503–513. doi: 10.1007/s10237-013-0511-2. Cited: in: : PMID: 23864393.

23. Haugh MG, Meyer EG, Thorpe SD, Vinardell T, Duffy GP, Kelly DJ. Temporal and spatial changes in cartilage-matrix-specific gene expression in mesenchymal stem cells in response to dynamic compression. Tissue Eng Part A. 2011;17:3085–3093. doi: 10.1089/ten.tea.2011.0198. Cited: in: : PMID: 21870950.

24. Ge Y, Li Y, Wang Z, Li L, Teng H, Jiang Q. Effects of Mechanical Compression on Chondrogenesis of Human Synovium-Derived Mesenchymal Stem Cells in Agarose Hydrogel. Front Bioeng Biotechnol. 2021;9:1–12. doi: 10.3389/fbioe.2021.697281.

25. Zhao Z, Li Y, Wang M, Zhao S, Zhao Z, Fang J. Mechanotransduction pathways in the regulation of cartilage chondrocyte homoeostasis. J Cell Mol Med. 2020;24:5408–5419. doi: 10.1111/jcmm.15204. Cited: in: : PMID: 32237113.

26. Chahine NO, Collette NM, Thomas CB, Genetos DC, Loots GG. Nanocomposite scaffold for chondrocyte growth and cartilage tissue engineering: Effects of carbon nanotube surface functionalization. Tissue Eng Part A. 2014;20:2305–2315. doi: 10.1089/ten.tea.2013.0328.

27. Mieloch AA, Semba JA, Rybka JD. CNT-Type Dependent Cellular Adhesion on 3D-Printed Nanocomposite for Tissue Engineering. Int J Bioprint. 2022; doi: http://doi.org/10.18063/ijb.v8i2.0018.

28. Mirmusavi MH, Ahmadian M, Karbasi S. Polycaprolactone-chitosan/multi-walled carbon nanotube: A highly strengthened electrospun nanocomposite scaffold for cartilage tissue engineering. Int J Biol Macromol. 2022;209:1801–1814. doi: 10.1016/j.ijbiomac.2022.04.152. Cited: in: : PMID: 35487378.

29. Mohamadi A, Momenzadeh K, Masoudi A, Walley KC, Ierardi K, Ramappa A, DeAngelis JP, Nazarian A. Evolution of knowledge on meniscal biomechanics: a 40 year perspective. BMC Musculoskelet Disord [Internet]. 2021;22:1–13. doi: 10.1186/s12891-021-04492-2. Cited: in: : PMID: 34266442.

30. Sandmann GH, Adamczyk C, Garcia EG, Doebele S, Buettner A, Milz S, Imhoff AB, Vogt S, Burgkart R, Tischer T. Biomechanical comparison of menisci from different species and artificial constructs. BMC Musculoskelet Disord. 2013;14. doi: 10.1186/1471-2474-14-324. Cited: in: : PMID: 24237933.

31. Martínez Ávila H, Schwarz S, Rotter N, Gatenholm P. 3D bioprinting of human chondrocyte-laden nanocellulose hydrogels for patient-specific auricular cartilage regeneration. Bioprinting [Internet]. 2016;1–2:22–35. doi: 10.1016/j.bprint.2016.08.003.

32. Daly AC, Critchley SE, Rencsok EM, Kelly DJ. A comparison of different bioinks for 3D bioprinting of fibrocartilage and hyaline cartilage. Biofabrication. 2016;8:045002. doi: 10.1088/1758-5090/8/4/045002.

33. Apelgren P, Amoroso M, Lindahl A, Brantsing C, Rotter N, Gatenholm P, Kölby L. Chondrocytes and stem cells in 3D-bioprinted structures create human cartilage in vivo. PLoS One. 2017;12:e0189428. doi: 10.1371/journal.pone.0189428.

34. Romanazzo S, Vedicherla S, Moran C, Kelly DJ. Meniscus ECM-functionalised hydrogels containing infrapatellar fat pad-derived stem cells for bioprinting of regionally defined meniscal tissue. J Tissue Eng Regen Med. 2018;12:e1826–e1835. doi: 10.1002/term.2602.

35. Jian Z, Zhuang T, Qinyu T, Liqing P, Kun L, Xujiang L, Diaodiao W, Zhen Y, Shuangpeng J, Xiang S, et al. 3D bioprinting of a biomimetic meniscal scaffold for application in tissue engineering. Bioact Mater [Internet]. 2021;6:1711–1726. doi: 10.1016/j.bioactmat.2020.11.027. Cited: in: : PMID: 33313450.

Julia Semba

Laboratory of Applied Biotechnology
Center for Advanced Technology
Adam Mickiewicz University in Poznan
e-mail: jsemba@amu.edu.pl

Author contribution statement

I declare that I am the first author of the unpublished article "Mechanical testing of 3D printed constructs for meniscal tissue engineering" by Julia Anna Semba, Adam Aron Mieloch, Ana M Teixeira, Pedro Martins, and Jakub Dalibor Rybka. The author's contribution is as follows:

Julia Semba designed the study. Julia Semba prepared the bioinks, 3D bioprinted constructs and done compression tests. Julia Semba wrote the original manuscript.

Adam Mieloch designed the study and mentor the technical part of the project. Adam Mieloch functionalized MWCNTs. Adam Mieloch revised the manuscript.

Ana M Teixeira assisted with compression testing and done data analysis with Pedro Matins.

Pedro Matins designed the study and supervised the experiments. Pedro Martins done data analysis with Ana M Teixeira and revised the manuscript.

Jakub Rybka supervised the technical part of the project, and revised the manuscript. Jakub Rybka acquired funding and has been corresponding with the journal.

Date: 18.08.2023

Signature: *Julia Semba*

prof. UAM dr hab. Inż. Jakub D. Rybka

Dr Adam Mieloch

Laboratory of Applied Biotechnology
Center for Advanced Technology
Adam Mickiewicz University in Poznan
e-mail: amieloch@amu.edu.pl

Author contribution statement

I declare that I am the co-author of the unpublished article "Mechanical testing of 3D printed constructs for meniscal tissue engineering" by Julia Anna Semba, Adam Aron Mieloch, Ana M Teixeira, Pedro Martins, and Jakub Dalibor Rybka and I am aware that this publication is a part of Julia Semba PhD dissertation. The author's contribution is as follows:

Julia Semba designed the study. Julia Semba prepared the bioinks, 3D bioprinted constructs and done compression tests. Julia Semba wrote the original manuscript.

Adam Mieloch designed the study and mentor the technical part of the project. Adam Mieloch functionalized MWCNTs and revised the manuscript.

Ana M Teixeira assisted with compression testing and done data analysis with Pedro Matins.

Pedro Matins designed the study and supervised the experiments. Pedro Martins done data analysis with Ana M Teixeira and revised the manuscript.

Jakub Rybka supervised the technical part of the project, and revised the manuscript. Jakub Rybka acquired funding and has been corresponding with the journal.

Date: 21.08.2023

Signature:

Ana M Teixeira

INEGI, Faculdade de Engenharia da Universidade do Porto
Campus da FEUP, Porto
e-mail: margarida.t28@gmail.com

Author contribution statement

I declare that I am the co-author of the unpublished article "Mechanical testing of 3D printed constructs for meniscal tissue engineering" by Julia Anna Semba, Adam Aron Mieloch, Ana M Teixeira, Pedro Martins, and Jakub Dalibor Rybka and I am aware that this publication is a part of Julia Semba PhD dissertation. The author's contribution is as follows:

Julia Semba designed the study. Julia Semba prepared the bioinks, 3D bioprinted constructs and done compression tests. Julia Semba wrote the original manuscript.

Adam Mieloch designed the study and mentor the technical part of the project. Adam Mieloch functionalized MWCNTs. Adam Mieloch revised the manuscript.

Ana M Teixeira assisted with compression testing and done data analysis with Pedro Matins.

Pedro Matins designed the study and supervised the experiments. Pedro Martins done data analysis with Ana M Teixeira and revised the manuscript.

Jakub Rybka supervised the technical part of the project, and revised the manuscript. Jakub Rybka acquired funding and has been corresponding with the journal.

Date: 28.8.2023

Signature: *Ana Margarida Teixeira*

Dr Pedro Martins

INEGI, Faculdade de Engenharia da Universidade do Porto
Campus da FEUP, Porto
e-mail: palsm@fe.up.pt

Author contribution statement

I declare that I am the co-author of the unpublished article "Mechanical testing of 3D printed constructs for meniscal tissue engineering" by Julia Anna Semba, Adam Aron Mieloch, Ana M Teixeira, Pedro Martins, and Jakub Dalibor Rybka and I am aware that this publication is a part of Julia Semba PhD dissertation. The author's contribution is as follows:

Julia Semba designed the study. Julia Semba prepared the bioinks, 3D bioprinted constructs and done compression tests. Julia Semba wrote the original manuscript.

Adam Mieloch designed the study and mentor the technical part of the project. Adam Mieloch functionalized MWCNTs. Adam Mieloch revised the manuscript.

Ana M Teixeira assisted with compression testing and done data analysis with Pedro Matins.

Pedro Matins designed the study and supervised the experiments. Pedro Martins done data analysis with Ana M Teixeira and revised the manuscript.

Jakub Rybka supervised the technical part of the project, and revised the manuscript. Jakub Rybka acquired funding and has been corresponding with the journal.

Date: 2023/08/23

Signature:

Dr hab. inż. Jakub Rybka, prof. UAM

Laboratory of Applied Biotechnology
Center for Advanced Technology
Adam Mickiewicz University in Poznan
e-mail: jrybka@amu.edu.pl

Author contribution statement

I declare that I am the corresponding author of the unpublished article "Mechanical testing of 3D printed constructs for meniscal tissue engineering" by Julia Anna Semba, Adam Aron Mieloch, Ana M Teixeira, Pedro Martins, and Jakub Dalibor Rybka, and I am aware that this publication is a part of Julia Semba PhD dissertation. The author's contribution is as follows:

Julia Semba designed the study. Julia Semba prepared the bioinks, 3D bioprinted constructs and done compression tests. Julia Semba wrote the original manuscript.

Adam Mieloch designed the study and mentor the technical part of the project. Adam Mieloch functionalized MWCNTs. Adam Mieloch revised the manuscript.

Ana M Teixeira assisted with compression testing and done data analysis with Pedro Matins.

Pedro Matins designed the study and supervised the experiments. Pedro Martins done data analysis with Ana M Teixeira and revised the manuscript.

Jakub Rybka supervised the technical part of the project, and revised the manuscript. Jakub Rybka acquired funding and has been corresponding with the journal.

Date: 1 8. 08. 2023

Signature:

prof. UAM dr hab. inż. Jakub D. ...

1 **Single-Cell Transcriptomic Atlas of Porcine Meniscus: Paving the Way for Advanced Therapies**

2

3 Monika Mankowska[1], Monika Stefanska[2], Anna Maria Mleczko[1], Witold Kot[3], Lukasz Krych[4], Julia Anna
4 Semba[1,5], Jakub Dalibor Rybka[1]

5 1 Center for Advanced Technology, Adam Mickiewicz University, Uniwersytetu Poznańskiego 10, 61-614 Poznań, Poland.
6 2 Department of Clinical Immunology, Jagiellonian University Medical College, Wielicka 265, 30-663 Kraków, Poland
7 3 Department of Plant and Environmental Sciences, University of Copenhagen, 1871 Frederiksberg C, Denmark.
8 4 Department of Food Science, Faculty of Science, University of Copenhagen, Rolighedsvej 26, 1958 Frederiksberg C,
9 Denmark.
10 5 Faculty of Biology, Adam Mickiewicz University in Poznań, Uniwersytetu Poznańskiego 6, 61-614 Poznań, Poland.

11

12

13 **Abstract**

14   Meniscus injuries are widespread among people, and the treatments that are now available
15 do not offer enough healing potential. In this study, we present a single-cell transcriptome atlas of the
16 meniscus, consisting of several cell clusters corresponding to four major cell types: chondrocytes,
17 endothelial cells, smooth muscle cells and immune cells. Furthermore, we conducted a thorough
18 investigation of chondrocyte clusters and discovered considerably different cellular compositions of
19 red and white zones, which elucidate their healing potential. We have also proven that the medial and
20 lateral menisci of pigs have comparable molecular landscapes. Finally, we have shown that the
21 transcriptome of pig tissue is comparable to that of human tissue. Our data provides critical support
22 for the use of pigs as a biological model for meniscal degeneration and the development of cutting-
23 edge therapies such as tissue engineering and xenotransplantation.

24
25
26 **Keywords**
27 single-cell sequencing, transcriptome atlas, meniscus, chondrocyte, pig model, orthopaedics

Introduction

The meniscus is a fibrocartilaginous tissue essential for stress distribution and knee joint stability. The structure of the meniscus is divided into three zones based on its extracellular matrix composition and degree of microvascularization: the outermost red zone, which is rich in blood vessels; the innermost white zone with a low blood supply; and the intermediate red-white zone. The meniscus has a minimal ability to repair and is prone to damage due to the transfer of heavy loads and shear forces in the knee [1]. Meniscus injuries in the outer zone are more likely to heal, but those in the internal zone often result in irreversible damage [2]. Although suturing and partial or complete meniscectomy are still the most prevalent methods of treating meniscus tears, the majority of patients develop osteoarthritis between ten and twenty years after an injury. The long-term success rate of meniscal repair is only 23,1% as shown by a meta-analysis published in 2012 [3–6]. This data suggests that novel therapies should focus on avoiding surgery while maintaining the mechanical characteristics of the meniscus. Therefore, it is hoped that developing treatment strategies like tissue engineering (TE) and xenotransplantation will considerably benefit meniscus repair.

Domestic pigs (*Sus scrofa domesticus*), being physiologically and anatomically similar to humans, has already proven to be a valuable model in studying human diseases, testing new treatments and medical devices [7]. The field of orthopaedic research is no exception, as pig models have been widely used for health conditions such as juvenile osteochondritis dissecans, meniscal degeneration, or post-traumatic osteoarthritis [8–10]. Xenotransplantation between pigs and humans, particularly for the transplantation of bones and cartilage-like structures, has already emerged as a promising area of research [11,12]. Also TE uses a range of cell types and organic scaffolds originating from pigs for facilitating tissue repair, regeneration in 3D and recapitulation of meniscus functions after severe trauma [13, 14]. This means that pigs could become a solution for the constant shortage of organ donors and lack of an efficient treatment methods, by offering high tissue availability and genetic engineering capabilities. Although both pig-based TE and xenotransplantation offer the chance to restore an organ's physiological function, an in-depth understanding of its genetics is necessary for the highest level of performance. While there are challenges that must be addressed, ongoing research on the exploration of pig's omics data aims to improve our understanding of the profound degree of biological similarities and differences between humans and pigs. With the use of single-cell sequencing of porcine menisci, we attempted to fill in a knowledge gap that will open new possibilities for advanced orthopaedic treatments.

For this purpose we have chosen single-cell RNA sequencing (scRNAseq) technology, which has emerged as the most cutting-edge method for exposing the diversity and complexity of individual cells transcriptomes. Moreover, it reveals the hierarchical architecture of many cell types and their roles within highly organized tissues and organs [15]. The 10x Genomics Gene Expression microfluidic approach, which involves the production of millions of microdroplets, each comprising a single cell, reverse transcription mixture, and a gel bead coupled with oligo sequences, enables deep investigation of single cells transcriptomes. The oligos are designed to catch poliA transcripts, tag them with a cell-identifying barcode and a unique mRNA ID (for further quantitative investigation), and ultimately allow the production of libraries compatible with long and short-read sequencing platforms. In contrast to bulk NGS approaches, this cutting-edge technology allows not only cell type identification but also enables uncovering the regulatory connections between genes and monitoring of developmental trajectories of various cellular lineages.

72   To date, only one publication using a single-cell transcriptome sequencing approach focused
73 on zonal characterization has presented the entire spectrum of cell populations that constitute the
74 human meniscus [16]. To the best of our knowledge, no data on pig meniscus cell composition are
75 currently available. In this study, single-cell transcriptome sequencing (scRNA-seq) was performed to
76 define and juxtapose cell populations that occur in specific zones of the pig meniscus. Results were
77 compared with the data from human studies.
78
79 **Results**
80
81   1. **scRNA-seq of pig menisci reveals the presence of 12 cell clusters and high similarity between**
82   **medial and lateral meniscus**
83
84 Two porcine menisci - one lateral and one medial, each divided into red and white zones, were
85 retrieved from a single pig for single-cell sequencing, resulting in the construction of the very first cell
86 transcriptome atlas for this tissue in pigs (Fig 1A). The cell type composition was compared across
87 these two anatomically divergent menisci and between zones with varying degrees of vascularity. All
88 samples achieved a satisfying percentage of living cells (ranging from 85 to 100%) enabling the capture
89 the majority of transcripts from cells and the generation of a reliable dataset. The sequencing data
90 underwent a quality control procedure, excluding cells with more than 8% of mitochondrial transcripts
91 and less than 200 genes detected in each cell (nFeatures_RNA), as they indicated apoptosis, cell lysis,
92 or empty droplets. Eventually, a dataset of 26928 high-quality cells was used for cluster identification
93 and cell type annotation (Supplementary 1). Of these cells, 14,233 originated from the medial
94 meniscus, and 12,695 from the lateral meniscus. When divided based on zonal distribution, 12,168
95 cells came from the red regions and 14,760 from the white regions.
96   Seven cell clusters corresponding to four major cell types were identified and visualized on a
97 UMAP plot (Fig 1B). Cell clusters were annotated based on the highly expressed marker genes [17]
98 (Supplementary 2). We distinguished a cluster of chondrocyte cells (Ch) expressing collagens (*COL1A1*,
99 *COL2A1, COL11A1*), aggrecan (*ACAN*), decorin (*DCN*) and *SOX9*, a transcription factor involved in
100 chondrocyte differentiation and maintenance of the chondrocytic phenotype [18–21] (Fig 1C).
101 Chondrocyte clusters constituted almost 75% of the meniscus's cells making them the majority in each
102 analysed sample (Fig 1D). The characteristics of specific chondrocytic subclusters are presented in the
103 following part of this paper. The next most abundant cell type (9.3%) comprised two clusters of
104 endothelial cells (EC), identified based on the expression of canonical markers *PECAM1* and *PLVAP*
105 [22,23](Fig 1C). Within this group, a small subpopulation of proliferating EC (PEC) was identified. Besides
106 markers typical for EC, this cluster expressed genes involved in cell proliferation (*TOP2A*) and mitosis
107 such as *SMC4* and KIF11 responsible for chromatin condensation and spindle formation during mitosis
108 [24–26] (Supplementary 2). EC populations, along with another identified cell type, smooth muscle cells
109 (SM accounting for 8.3%) expressing *ACTA2* and *MYL9*, were derived from blood vessels [27,28]. The last
110 identified group of three clusters belonged to immune cells, representing approximately 7.5% of the
111 meniscus population, and most likely comprised macrophages (MC, *CD68+*), T-cells (Tc, *CCL5+*) and
112 monocytes (mono, *HLA-DRA+*) [29–31](Supplementary 2).
113   We then compared the distribution of cell clusters in the medial and the lateral menisci. This
114 comparison was conducted due to previously documented variability between these two menisci in
115 terms of susceptibility and prevalence of injuries, as well as clinical outcomes after treatment. It was
116 revealed that all the identified clusters were observed in both menisci (Fig 1E), and the cells within

117 them exhibited similar expression profiles and cell-type specific markers [32]. The high similarity of the
118 two studied types of menisci was confirmed through analysis of variance, which showed no statistically
119 significant difference in cluster frequencies at p=0.05. The analysis showed no significant divergences
120 in either cell type composition or in frequencies between the medial and lateral menisci. Therefore
121 we chose to combine data from the scRNA-seq of the same zones originating from the medial and
122 lateral menisci in the following integrative analysis of cells within zones.
123
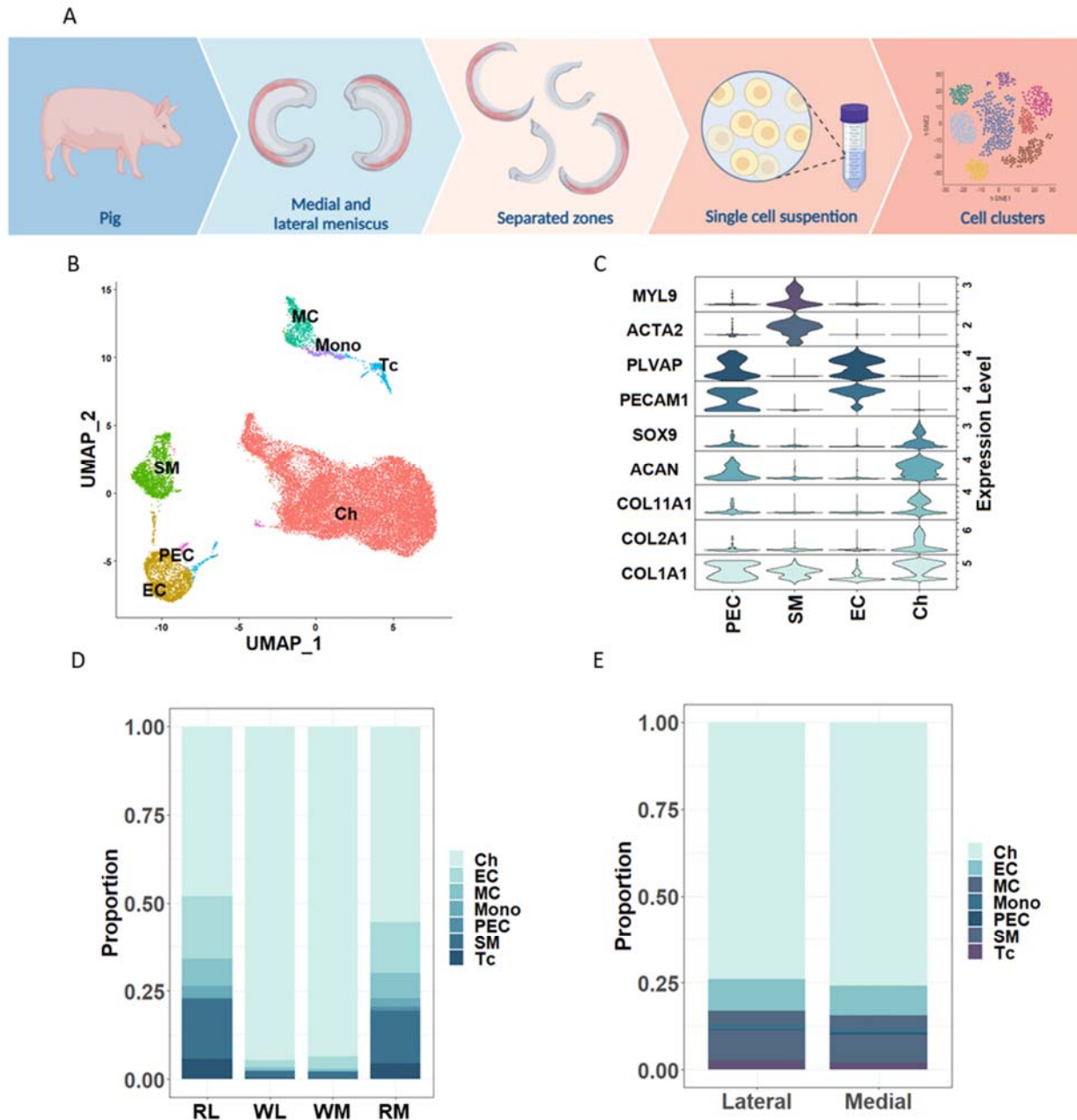
Figure 1. scRNA-seq analysis of pig menisci.
A. Sample preparation scheme. B. UMAP plot of identified clusters corresponding to cell types: Ch – chondrocytes, EC – endothelial cells, PEC – proliferating endothelial cells, SM – smooth muscle cells, Mono – monocytes, Tc- T-cells, MC - macrophages C. Marker genes expression levels. D. Cluster proportion in each analysed sample. RL – red zone, lateral meniscus, WL – white zone, lateral meniscus, WM – white zone, medial meniscus, RM – red zone, medial meniscus E. Clusters proportion in the medial and lateral meniscus.

124
125   **2. Zonal comparison of cell type composition**
126

127 To further explore the intricate nature of porcine meniscus, we compared two distinct zones that are
128 known to be anatomically different. This difference is largely due to the level of vascularization and
129 divergent extracellular matrix (ECM) composition resulting in different healing capacities [2,33]. Firstly,
130 we visualized the distribution of cells using UMAP plots (Fig 2A) and examined the percentage of
131 clusters in each zone (Fig 1D), followed by statistical analysis. All the annotated clusters were present
132 in both zones, yet their distribution differed significantly. The main factor contributing to this
133 significant discrepancy is the degree of vascularization. In the red zone, approximately 33% of cells
134 were annotated to clusters forming blood vessels, with 17% being endothelial cells (EC+PEC) and
135 another 16% marked as smooth muscle cells. On the contrary, only 2.8% and 1.9% of cells originating
136 from the white zone were identified as endothelial and smooth muscle cells, respectively. This
137 indicates the presence of only trace vascularity in the white zone, but not its complete absence.
138 Consequently, the distribution of immune cells also varies greatly, ranging from 15.4% in the red zone
139 to 1.06% in the white zone.
140   The remaining cell types predominately consist of chondrocyte clusters, which make up 51.5%
141 in the red zone and over 94% in the white zone. Furthermore, the expression patterns of certain genes
142 encoding extracellular matrix components showed distinct differences. Of particular relevance to the
143 functional biology of cartilage-like tissue is the production of collagens. As anticipated, chondrocytes
144 in the white zone exhibited elevated levels of *COL2A1*, while *COL1A1* was more abundant in
145 chondrocytes from the red zone. Additionally, genes encoding proteoglycans characteristic of
146 meniscus tissue displayed zone-specific expression patterns. Among them, *COMP* and *VCAN* were
147 strongly expressed in the red zone, while *ACAN* appeared to be more characteristic in the white zone
148 (Fig 2B). Furthermore, a differential analysis of cells forming this chondrocyte cluster (Ch) revealed
149 striking variation in gene expression patterns, indicating their involvement in distinct metabolic
150 pathways (Fig 2C, Supplementary 3 and 4).
151   Significant gene enrichment was observed in the red zone of chondrocytes, particularly in
152 metabolic pathways associated with cell-cell signalling, migration, adhesion, and communication.
153 Proliferation, immune system control, and the formation of blood vessels also appeared to be critical
154 aspects of red chondrocyte biology. Hence, it is considered that these cells exhibit a high rate of
155 metabolism, significant proliferative capacity, and tissue healing ability. In contrast, chondrocytes
156 specific to the white zone showed gene enrichment related to chondrocyte and mesenchymal stem
157 cells differentiation. Of particular importance are *SOX5* and *SOX6, which,* unlike *SOX9* activated in the
158 early stages of pre-chondrocyte formation, control the late stages of chondrocyte differentiation and
159 have a positive effect on their proliferation and cartilage matrix formation [34]. The abundance of
160 Collagen IX transcripts, which play a crucial role in connecting collagen fibres and proteoglycans to
161 provide mechanical strength, further indicates the structural role of white chondrocytes and their
162 propensity to develop cartilage tissue [35]. Additionally, these cells are closer to their final
163 developmental stage and show signs of declining metabolic activity, as expected in meniscus tissue.
164
165

Figure 2. Zonal comparison of cell type composition
A. UMAP plot comparing clusters in menisci zones – red and white. **Ch** – chondrocytes, **EC** – endothelial cells, **PEC** – proliferating endothelial cells, **SM** – smooth muscle cells, **Mono** – monocytes, **Tc**- T-cells, **MC** - macrophages **B.** Chondrocyte subclusters marker genes expression in the white and red zones. **C.** Enreached GO pathways in red (left) and white (right) zones.

3. Chondrocyte cells heterogeneity

167

168

169   Due to the above-mentioned discrepancies, additional investigation of the large cell cluster
170   expressing chondrocyte-specific molecular markers was conducted to better discriminate between
171   different cell populations. As a result, five subclusters were identified (Ch0-Ch4, Fig 3A) with distinct
172   frequencies in the white and red zone samples (Fig 3B). The subclusters were analysed based on the
173   identification of highly expressed genes (Supplementary 5).

174   Subcluster Ch0 exhibited differential expression of genes involved in osteogenesis and chondrocyte
175   ossification. Among them, *OMD* positively regulates osteogenesis, *OGN* enhances bone formation,
176   and *ASP* is a negative regulator of chondrogenesis involved in collagen biomineralization [36–41].
177   Additionally, genes involved in the negative regulation of vasculature development pathways were
178   enriched, including *SERPINF1*, *SPARC*, and *THBS4*. This expression profile suggests that the detected
179   subcluster has an osteophytic phenotype. However, osteophytes are not only osteo-cartilaginous
180   outgrowths in osteoarthritic joints; they are also considered transient repair tissue derived from
181   precursor cells [42]. The top differentiating gene for this subcluster, *ANGPTL7*, has been linked to
182   chondrocyte differentiation, endochondral ossification, and tissue remodelling [43,44]. Therefore, we
183   anticipate that this subcluster plays an important role in the meniscus remodelling process, which
184   likely results from mechanical stimuli [45]. Consequently, we believe that referring to the subcluster "0"
185   as osteophytic is inadequate since it implies that the cells are a step toward bone formation. Instead,
186   we believe that this subcluster reflects the cells' ability to respond to increasing mechanical pressure.
187   Another distinctive gene expressed in this cell group is the proapoptotic gene PEDF, suggesting a
188   transient phenotype of chondrocyte-like cells vulnerable to terminal differentiation and cell death.
189   The presence of these cells in both the red and white zones indicates that this may represent the last
190   stage of chondrocyte differentiation in the meniscus tissue. Therefore, we classified them as "end-
191   stage chondrocytes" for that reason.

192   In the white zone, subcluster Ch1, the second most frequent subcluster, predominantly expressed
193   genes encoding ECM proteins. Among them, collagens such as *COL2A1*, *COL9A1*, and *COL11A1*,
194   proteoglycans such as *ACAN* and *SNORC*, and the ECM stabilizing protein *HAPLN1* were highly
195   expressed. Due to the elevated expression of genes associated with maintaining stemness (*SCRG1*)
196   and differentiation status (*S100A1*), this population appears to have recently undergone
197   differentiation. The elevated expression of *EFEMP1*, a gene responsible for ECM integrity maintenance
198   and trafficking, and VIT, involved in matrix assembly and cell proliferation, indicates that this
199   subcluster is undergoing constant remodelling [46–48]. Pathway analysis also showed clear enrichment
200   in genes responsible for collagen synthesis, modification and degradation, as well as the assembly of
201   collagen fibrils and other multimeric structures. Since this profile closely resembles what is believed
202   to be the canonical cartilage chondrocyte transcriptome, we have named subcluster 1 "matrix-
203   depositing chondrocytes."

204   The third most common subcluster of cells, Ch2, is rich in gene transcripts connected to stress
205   response, inflammation, and tissue remodelling. Overexpression of the *GADD45* gene family,
206   implicated in response to cell injury, suggests stressful environmental growth conditions and the
207   presence of DNA-damaging agents [49]. The presence of several cytoprotective gene transcripts such as
208   *CLU* (anti-apoptotic, anti-inflammatory, and antioxidant properties), *SOD2* (coding for superoxide
209   dismutase), *CP* (a metalloprotein involved in the peroxidation of transferrin), and *MT1A* (an oxidative
210   stress-response gene protecting against hydroxyl free radicals), as well as the abundance of gene
211   transcripts connected to inflammatory response (*NFKBIA*), post-traumatic cartilage destruction (*LBP*),

212 or inflammation processes and tissue remodelling (*CHI3L1*), suggests a suboptimal meniscal
213 microenvironment for cells [50–57]. However, the overexpression of *SPP1* (a matrix remodelling marker)
214 noted in the meniscus model of post-traumatic osteoarthritis, *HPS5* (a regulator of lysosome synthesis
215 and vesicular trafficking), *CCDC80* (a promoter of cell adhesion and matrix assembly), *THBS* (an
216 adhesive glycoprotein induced in sites of tissue damage or active remodelling that mediates cell-to-
217 cell and cell-to-matrix interactions as an adaptive stress response), and *MGP* (a powerful inhibitor of
218 cartilage mineralization) indicates that the cells are remodelling in response to these stressful
219 conditions [58–62]. Additionally, the abundance of *FOS* and *CCN2* gene transcripts, both involved in cell
220 proliferation and differentiation, suggests that these cells can handle stressful growth conditions quite
221 well and are unlikely to undergo apoptotic pathways [63,64]. In summary, these cells exhibit anti-
222 oxidative and anti-inflammatory properties against the stressful growth conditions within the
223 meniscus, and in response, they remodel the ECM and clear the microenvironment to ensure the
224 survival of neighbouring cells. Therefore, we refer to them as "protective chondrocytes."
225   Cells forming subcluster Ch3, which constitute most of the red zone, express genes with divergent
226 functions. They appear to play a role in stem cell modulation, matrix remodelling, and inflammatory
227 responses simultaneously. Several gene transcripts connected to stem cell regulation, including
228 *CRABP1* and *IGFBP2*, known to modulate stem cell behaviour by suppressing cell proliferation and
229 sensitizing them to growth factors, were highly expressed [65,66]. Similarly, *SFRP2* and *TNC*, proteins
230 characteristic of mesenchymal stem cells, exhibited elevated expression levels in this subcluster. Both
231 proteins enhance mesenchymal stem cell survival rates, regulate differentiation, and enhance
232 therapeutic efficacy when exposed to unfavourable factors [67,68]. Other intensively transcribed genes
233 identified in this subcluster are important for matrix organization. For example, *MMP2*, typical for the
234 red zone, is involved in vascular remodelling and angiogenesis within the meniscus due to its degrading
235 potential toward aggrecan and collagens [69]. *ADAMTS1*, a hypoxia-induced disintegrin and
236 metalloproteinase, promotes cell proliferation and migration. Lumican is a collagen-binding
237 proteoglycan responsible for biomechanical strength in connective tissues [70]. Taken together, the
238 genes suggest a predicted pattern characteristic of vascularized, mechanically durable tissue with the
239 ability to differentiate. Overexpression of anti-inflammatory genes is a well-known phenomenon
240 specific to MSCs. On one hand, the remodelling and healing process is facilitated by the production of
241 anti-inflammatory agents that enable the recruitment of other MSCs to the site of injury. On the other
242 hand, MSCs, by modifying immune cells, foster a microenvironment favourable to the healing process
243 [71]. In a highly expressed gene set specific to cluster Ch3, antiviral *ISG12* and *IGS15*, antimicrobial
244 chemokines *CXCL2* and *CXCL14*, involved in allergic inflammation POSTN, and genes responsible for
245 immune cell infiltration *ABL2* were identified [72–75]. Considering the aforementioned, we predict that
246 the Ch3 population would closely resemble the phenotype of mesenchymal stem cells while also
247 displaying certain chondrocytic characteristics, allowing us to refer to them as "chondrocyte
248 progenitor cells." Due to their immunomodulatory and matrix remodelling properties, these cells are
249 of great interest in tissue engineering and the management of meniscus injuries.
250   The smallest subcluster, Ch4, expresses many genes involved in the breakdown of the extracellular
251 matrix, as well as those implicated in cell migration and proliferation. Genes such as apolipoprotein E
252 (*APOE*), responsible for clearing lipoproteins, lumican (*LUM*), which induces matrix degradation, and
253 serpin family E member 2 (*SERPINE2*), which regulates metalloproteinases, are implicated in catabolic
254 pathways [76–78]. Versican, a key ECM component involved in cell migration and proliferation due to its
255 matrix-loosening and hydrating capabilities, is encoded by the highly expressed *VCAN* gene. Versican
256 is a hygroscopic proteoglycan that interacts with other ECM components, affecting their assembly and

257 remodelling. In the meniscus, it has an exceptional ability to resist compressive and tensile stresses
258 caused by loading, thanks to its binding with hyaluronan [79]. *SDC2* and *GSN*, two additional abundant
259 gene transcripts in this subcluster, are linked to cell migration and proliferation. Additionally, this
260 subcluster has high quantities of various collagen transcripts that code for collagen IV, which forms a
261 basement membrane, collagen V, which plays a key role in the healing process, and collagen VI, an
262 ECM organizer [80]. Based on this transcriptional profile, the cells forming this subcluster could be
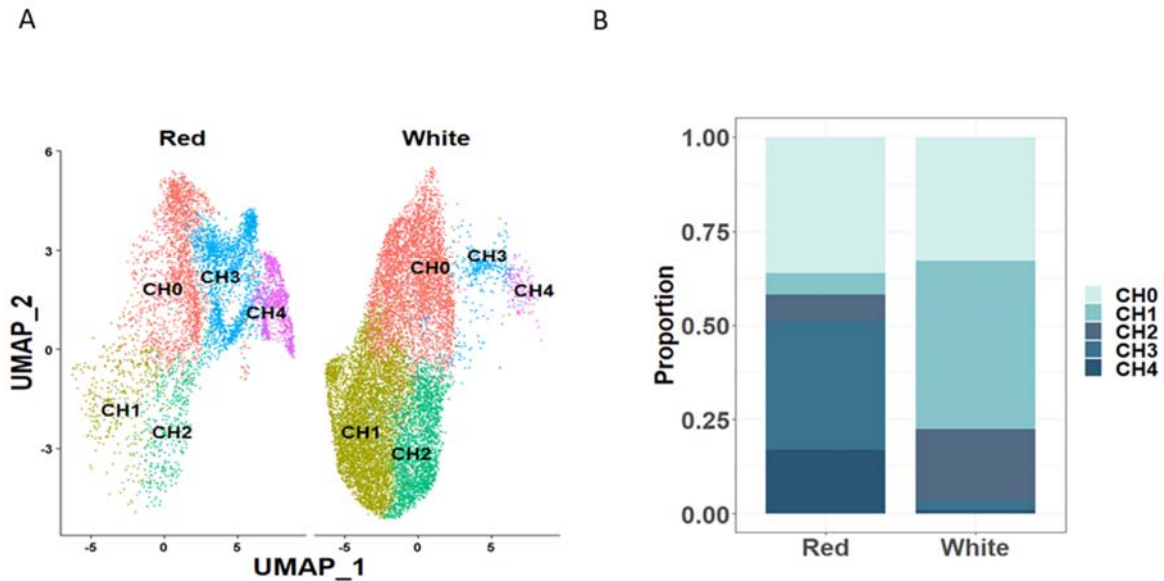263 referred to as "remodelling chondrocytes".
264
265

Figure 3. Chondrocyte cluster heterogeneity.
A. UMAP plot of chondrocyte cell subpopulations in red and white zones. **B.** Chondrocyte subclusters proportion in each zone.

Discussion

Seven cell clusters corresponding to four major cell types were identified based on the expression of marker genes: chondrocyte-like cells (Ch) expressing collagens, aggrecan, and positive for SOX9; endothelial cells (EC) expressing *PECAM+* and *PLVAP+*; proliferating endothelial cells (PEC) expressing *TOP2A+, SMC4+,* and *KIF11+*; smooth muscle cells (SM) expressing *ACTA2+* and *MYL9+*; and immune cells, most likely macrophages (MC) expressing *CD68+*, T-cells (Tc) expressing *CCL5+*, and monocytes (mono) expressing *HLA-DRA+*.

While the frequencies of these clusters differed significantly when comparing zones, the comparison analysis of medial and lateral menisci revealed no qualitative or quantitative differences in cell type distribution and cell transcriptional profiles. This leads to the conclusion that the variable prevalence and treatment outcomes observed between medial and lateral meniscus injuries are most likely due to the higher forces acting on the medial side of the knee [81]. Epidemiological studies support this hypothesis, indicating that medial meniscus tears are more common in older patients with elevated BMI and suffering from a range of degenerative knee conditions, whereas lateral meniscus injuries more frequently concern young, male patients with no history of osteoarthritis or similar conditions and are often connected to ligament injury, suggesting that those tears are sport-related [82,83]. It is not surprising, therefore, that lateral meniscus tears heal more efficiently and require fewer total or partial meniscectomy surgeries, even though there is no specific genetic component that can be added [32].

After thoroughly investigating the chondrocyte-like cluster, five subclusters (Ch0-Ch4) were discovered. Only Ch0, which we referred to as "end-stage chondrocytes," was abundant in both of the regions under study. Subclusters Ch1 and Ch2, which are most likely responsible for cartilage-specific matrix deposition and protection against adverse microenvironment factors, respectively, were distinctive to the white zone. In addition to being metabolically active and expressing chondrocyte-specific genes encoding collagens and proteoglycans, Ch3 (chondrocyte progenitor) and Ch4 (remodelling chondrocytes), which make up the majority of the red zone, also exhibit characteristics of mesenchymal stem cells and are prone to proliferation and migration. Therefore, they possess greater healing capacity and remodelling properties.

These findings are consistent with the work by Fu et al., who performed single-cell sequencing on healthy human menisci and detected chondrocytes, endothelial cells, and immune cells [16]. In contrast to their research, they additionally annotated a group of cells known as "pericytes." However, this cell population expresses significant quantities of *ACTA2*, *MYL9*, and other muscle contractile genes and is primarily found in the red zone of the meniscus, resembling the "smooth muscle cells" discovered in our investigations. Furthermore, Fu et al. noted that using only genetic markers makes it extremely difficult to differentiate between pericytes and smooth muscle cells. It is assumed that the functional characteristics of these two populations are identical, and any differences exist only in terms of nomenclature.

Regarding chondrocyte populations, the majority of our results agree with Fu et al. However, comparing cell subtypes is challenging due to the abundance of data and the subtle variations between distinct cell clusters. Except for the fact that we identified three clusters for white zone chondrocytes instead of two, the gene markers reported by Fu et al. as specific for the white zone are present in our data labelled as white zone chondrocytes. Our "end-stage chondrocytes" share *APOD*, *FN1*, and *ECRG* markers with Fu's chondrocyte-1 population and exhibit anti-angiogenic characteristics and remodelling actions. The subcluster named "matrix-depositing chondrocytes" in our study displays

311   similar genetic markers and ECM remodelling capabilities as Fu's chondrocyte-1 population (both
312   clusters are positive for *CHI3L1*, *HTRA1*, *FN1*, and *TIMP* superfamily). The "protective chondrocytes"
313   in our study, which correspond to the white zone, express markers common to Fu's chondrocyte-3 cell
314   type (*CHI3L1, CDON*). Similar to this work, Fu et al. found two red zone clusters expressing genes such
315   as *POSTN, MMP2, ADAMTS2, CFD, FNDC, VCAN*, and genes from the *CXCL* superfamily, which suggest
316   remodelling and immunomodulatory effects. The main discrepancy concerns the last chondrocyte
317   cluster identified by Fu et al. as expressing genes linked to proliferation; these markers were not found
318   in any of our chondrocyte clusters but were prevalent in the *PECAM/PLVAP+* proliferating endothelial
319   cells (PEC). Interestingly, in our dataset, the cells referred to as "chondrocyte progenitors" associated
320   with the chondrocyte-2 and chondrocyte-4 clusters were found to express MSC markers and display
321   early signals of differentiation, which were not reported by Fu et al. Although more thorough research
322   on the integration of data from different species is needed for a detailed examination of cell type
323   similarities, it is clear that the cell types found in porcine-origin menisci are consistent with data from
324   humans. Due to the lack of automated software for functional annotation of detected clusters, single-
325   cell data analysis studies are currently focused on subjective approaches and addressing specific
326   hypotheses.
327   Single-cell sequencing of the human meniscus has been covered in another study by Sun et al.
328   [84]. However, we have chosen not to compare our data with those results due to several concerns, the
329   primary one being sample treatment prior to sequencing. Our and Fu's experiment settings used
330   freshly extracted meniscus tissue cells that had been subjected to single-cell library preparation,
331   whereas the study of the Sun et al. analysed in vitro cultured cells. Sun's study focused solely on
332   adherent cell populations, and it is highly possible that the cells' expression patterns were dramatically
333   changed during the culture process. Additionally, the single cell suspension and partitioning methods
334   were different (cell sorting as opposed to droplets generation). Fu discussed this in significant detail
335   and claimed that these differences led to discrepancies in the generated data, resulting in significantly
336   distinct cell clustering. The mismatch in results highlights the necessity of thoroughly reviewing the
337   methodology before attempting to compare the data.
338   Our study was conducted solely on one individual. However, analysing 26,928 cells seems
339   adequate for creating a cell atlas for a single, specific tissue, especially since Wang et al.'s pig cell atlas
340   included a comparable number of analysed cells for only two tissue types (liver and lung), while some
341   tissues were described based on a few thousand cells (with a minimal number of 1,527 for subfornical
342   organ) [85].
343   In this paper, we present a single-cell transcriptome atlas of the medial and lateral menisci of
344   pig, demonstrating that their molecular landscapes are identical. By dividing the meniscus into red
345   and white zones prior to sequencing, we identified significantly diverse cellular component that
346   support the zones' capacity for healing. Additionally, we have shown that the cellular makeup of pig
347   tissue is similar to that of human tissue, providing crucial support for the use of pigs as a biological
348   model for meniscal degeneration and the development of cutting-edge therapies like tissue
349   engineering and xenotransplantation.
350
351

Methods

Material

Medial and lateral menisci originating from one pig donor were collected from a local slaughterhouse. Tissues were rinsed in 5% Betadine (Egis) in PBS solution followed by two rinses in PBS. They were then transported in MACS® Tissue Storage Solution (Miltenyi Biotec, #130-100-008) on ice for up to 1 hour and processed immediately after arrival.

Single-cell suspension preparation

The tissue was dissected away from the synovium, segmented into white and red zones, and then cut into small pieces. This was followed by enzymatic digestion and disaggregation steps. First, incubation was carried out with 4mg/mL Pronase enzyme blend (Sigma-Aldrich, #10165921001) at 37°C for one hour, followed by a second incubation in 3 mg/mL Collagenase P (Sigma-Aldrich, #11213873001) at 37°C for another two hours. The mixture was then filtered through a 70 μm pluriStrainer® (pluriSelect, #43-57070-51) and centrifuged. The cell pellet was resuspended in 0.1% BSA (Sigma-Aldrich, #A9418-50G) in PBS and centrifuged to remove dead cells. Finally, the cells were filtered through a 30 μm pluriStrainer® (pluriSelect, #43-50030-03) and resuspended in 1% BSA in PBS to prevent cell re-aggregation.

Library generation

Subsequently, the cells isolated from meniscal zones were subjected to library construction using the Chromium Next GEM Single Cell 3' Reagent Kit v3.1 (10x Genomics, #PN-1000269). Samples were processed according to the manufacturer's protocol. Cell suspensions were first divided into the single-cell format with a Chromium X Series controller (10x Genomics), which encapsulates single cells within nanoliter-scale Gel Beads-in-emulsion (GEMs), where all generated cDNA shares a common barcode. The GEMs produced barcoded full-length cDNA from polyadenylated mRNA during incubation. After incubation, the GEMs were ruptured, and the pooled fractions were recovered. Silane magnetic beads were used to purify the first-strand cDNA from the reaction mixture. Barcoded, full-length cDNA was then amplified via PCR to generate sufficient mass for library construction. Enzymatic fragmentation and size selection were employed to optimize the size of the cDNA amplicons. Indexes and TruSeq Read 2 were added to the samples via End Repair, A-tailing, Adaptor Ligation, and PCR. The final libraries contained the P5 and P7 primers used in Illumina bridge amplification. The prepared libraries were sequenced on the NextSeq500 (Illumina) device with the Mid Output Kit v2.5 (300 cycles).

scRNA-seq data pre-processing and quality control

Following sequencing, the output fastq files were uploaded to the 10x Genomics Cell Ranger Software (cellranger-6.1.2). The cells were pre-analysed and mapped to the custom-built pig reference genome (Sscrofa11.1) using the cellranger mkref pipeline provided by 10x Genomics. Downstream analysis was performed using R and RStudio software. Cell doublets, cells expressing more than 8% of mitochondria-related genes ("ATP6", "ATP8", "COX1", "COX2", "CYTB", "ND2", "ND3", "ND4", "ND4L",

397 "ND5", "ND6"), and cells with fewer than 200 genes (nFeature_RNA) per cell were excluded from
398 downstream analysis.
399
400 **Identification and analysis of cell clusters**
401
402 Clustering of cells was performed using the Seurat package (v4.3.0). The data were first
403 normalized, and then integration was performed using the IntegrateData function. The results were
404 displayed as UMAP plots. The identification of main cell populations, such as chondrocytes,
405 endothelial cells, proliferating endothelial cells, smooth muscle cells, monocytes, T-cells, and
406 macrophages, was based on the expression of 30 marker genes with the highest expression within
407 each cluster (FindAllMarkers). Genes with differential expression between the groups were identified
408 using the FindMarkers function, which is based on the non-parametric Wilcoxon rank sum test.
409 Adjusted p-values were calculated based on Bonferroni correction using all features in the dataset.
410
411 **Pathway analysis**
412
413 Pathway analysis was carried out with GO term enrichment using the GOnet software and the
414 dataset of differentially expressed genes (adjusted p-value < 0.05).
415
416 **Statistical analysis**
417
418 For all statistical analyses, GraphPad Prism 8.0.1 was used. The statistical significance of cell
419 cluster distribution within menisci and zones was calculated using a two-way ANOVA test.
420
421 **Data availability**
422
423 Data are available in a public, open access repository Gene Expression Omnibus
424 (https://www.ncbi.nlm.nih.gov/geo/) with the accession number GSE241228.
425

426 **References**
427 1. Rai, M. F. & McNulty, A. L. Meniscus beyond mechanics: Using biology to advance
428   our understanding of meniscus injury and treatment. *Connect Tissue Res* **58**, 221–
429   224 (2017).
430 2. Makris, E. A., Hadidi, P. & Athanasiou, K. A. The knee meniscus: Structure–function,
431   pathophysiology, current repair techniques, and prospects for regeneration.
432   *Biomaterials* **32**, 7411–7431 (2011).
433 3. Doral, M. N., Bilge, O., Huri, G., Turhan, E. & Verdonk, R. Modern treatment of
434   meniscal tears. *EFORT Open Rev* **3**, 260–268 (2018).
435 4. Andersson-Molina, H., Karlsson, H. & Rockborn, P. Arthroscopic partial and total
436   meniscectomy. *Arthroscopy: The Journal of Arthroscopic & Related Surgery* **18**, 183–
437   189 (2002).
438 5. Beaufils, P., Becker, R., Kopf, S., Matthieu, O. & Pujol, N. The knee meniscus:
439   management of traumatic tears and degenerative lesions. *EFORT Open Rev* **2**, 195–
440   203 (2017).

441   6.   Nepple, J. J., Dunn, W. R. & Wright, R. W. Meniscal Repair Outcomes at Greater
442   Than Five Years. *The Journal of Bone and Joint Surgery-American Volume* **94**, 2222–
443   2227 (2012).

444   7.   Lunney, J. K. *et al.* Importance of the pig as a human biomedical model. *Sci Transl*
445   *Med* **13**, (2021).

446   8.   Tóth, F. *et al.* Evaluation of the Suitability of Miniature Pigs as an Animal Model of
447   Juvenile Osteochondritis Dissecans. *Journal of Orthopaedic Research* **37**, 2130–2137
448   (2019).

449   9.   Fang, Y. *et al.* An animal model study on the gene expression profile of meniscal
450   degeneration. *Sci Rep* **10**, 21469 (2020).

451   10.   Goetz, J. E. *et al.* A clinically realistic large animal model of intra-articular fracture
452   that progresses to post-traumatic osteoarthritis. *Osteoarthritis Cartilage* **23**, 1797–
453   1805 (2015).

454   11.   Bracey, D. N. *et al.* A porcine xenograft-derived bone scaffold is a biocompatible bone
455   graft substitute: An assessment of cytocompatibility and the alpha-Gal epitope.
456   *Xenotransplantation* **26**, (2019).

457   12.   Sommaggio, R., Uribe-Herranz, M., Marquina, M. & Costa, C. Xenotransplantation of
458   pig chondrocytes: therapeutic potential and barriers for cartilage repair. *Eur Cell Mater*
459   **32**, 24–39 (2016).

460   13.   Kwon, H. *et al.* Surgical and tissue engineering strategies for articular cartilage and
461   meniscus repair. *Nat Rev Rheumatol* **15**, 550–570 (2019).

462   14.   Semba, J. A., Mieloch, A. A. & Rybka, J. D. Introduction to the state-of-the-art 3D
463   bioprinting methods, design, and applications in orthopedics. *Bioprinting* **18**, e00070
464   (2020).

465   15.   Jovic, D. *et al.* Single-cell RNA sequencing technologies and applications: A brief
466   overview. *Clin Transl Med* **12**, (2022).

467   16.   Fu, W. *et al.* Cellular features of localized microenvironments in human meniscal
468   degeneration: a single-cell transcriptomic study. *Elife* **11**, (2022).

469   17.   Kozhemyakina, E., Lassar, A. B. & Zelzer, E. A pathway to bone: signaling molecules
470   and transcription factors involved in chondrocyte development and maturation.
471   *Development* **142**, 817–831 (2015).

472   18.   Gelse, K. Collagens—structure, function, and biosynthesis. *Adv Drug Deliv Rev* **55**,
473   1531–1546 (2003).

474   19.   Li, I. M. H. *et al.* Differential tissue specific, temporal and spatial expression patterns
475   of the Aggrecan gene is modulated by independent enhancer elements. *Sci Rep* **8**,
476   950 (2018).

477   20.   Akiyama, H., Chaboissier, M.-C., Martin, J. F., Schedl, A. & de Crombrugghe, B. The
478   transcription factor Sox9 has essential roles in successive steps of the chondrocyte
479   differentiation pathway and is required for expression of *Sox5* and *Sox6. Genes Dev*
480   **16**, 2813–2828 (2002).

481   21.   Lefebvre, V. & Dvir-Ginzberg, M. SOX9 and the many facets of its regulation in the
482   chondrocyte lineage. *Connect Tissue Res* **58**, 2–14 (2017).

483   22.   Privratsky, J. R. & Newman, P. J. PECAM-1: regulator of endothelial junctional
484   integrity. *Cell Tissue Res* **355**, 607–619 (2014).

485   23.   Guo, L., Zhang, H., Hou, Y., Wei, T. & Liu, J. Plasmalemma vesicle-associated
486   protein: A crucial component of vascular homeostasis. *Exp Ther Med* **12**, 1639–1644
487   (2016).

488 24. Ali, Y. & Abd Hamid, S. Human topoisomerase II alpha as a prognostic biomarker in
489   cancer chemotherapy. *Tumor Biology* **37**, 47–55 (2016).
490 25. Thadani, R., Kamenz, J., Heeger, S., Muñoz, S. & Uhlmann, F. Cell-Cycle Regulation
491   of Dynamic Chromosome Association of the Condensin Complex. *Cell Rep* **23**, 2308–
492   2317 (2018).
493 26. Rapley, J. *et al.* The NIMA-family kinase Nek6 phosphorylates the kinesin Eg5 at a
494   novel site necessary for mitotic spindle formation. *J Cell Sci* **121**, 3912–3921 (2008).
495 27. Xu, C. *et al.* Single-Cell RNA Sequencing Reveals Smooth Muscle Cells
496   Heterogeneity in Experimental Aortic Dissection. *Front Genet* **13**, (2022).
497 28. Sun, J. *et al.* Distinct Roles of Smooth Muscle and Non-muscle Myosin Light Chain-
498   Mediated Smooth Muscle Contraction. *Front Physiol* **11**, (2020).
499 29. Chistiakov, D. A., Killingsworth, M. C., Myasoedova, V. A., Orekhov, A. N. &
500   Bobryshev, Y. V. CD68/macrosialin: not just a histochemical marker. *Laboratory
501   Investigation* **97**, 4–13 (2017).
502 30. Korbecki, J., Grochans, S., Gutowska, I., Barczak, K. & Baranowska-Bosiacka, I. CC
503   Chemokines in a Tumor: A Review of Pro-Cancer and Anti-Cancer Properties of
504   Receptors CCR5, CCR6, CCR7, CCR8, CCR9, and CCR10 Ligands. *Int J Mol Sci* **21**,
505   7619 (2020).
506 31. Cajander, S. *et al.* Quantitative Real-Time Polymerase Chain Reaction Measurement
507   of HLA-DRA Gene Expression in Whole Blood Is Highly Reproducible and Shows
508   Changes That Reflect Dynamic Shifts in Monocyte Surface HLA-DR Expression
509   during the Course of Sepsis. *PLoS One* **11**, e0154690 (2016).
510 32. Krych, A. J. *et al.* Medial Versus Lateral Meniscus Root Tears: Is There a Difference
511   in Injury Presentation, Treatment Decisions, and Surgical Repair Outcomes?
512   *Arthroscopy: The Journal of Arthroscopic & Related Surgery* **36**, 1135–1141 (2020).
513 33. Heckmann, T. P., Barber-Westin, S. D. & Noyes, F. R. Meniscal Repair and
514   Transplantation: Indications, Techniques, Rehabilitation, and Clinical Outcome.
515   *Journal of Orthopaedic & Sports Physical Therapy* **36**, 795–814 (2006).
516 34. Smits, P. *et al.* The Transcription Factors L-Sox5 and Sox6 Are Essential for Cartilage
517   Formation. *Dev Cell* **1**, 277–290 (2001).
518 35. Yan, D. *et al.* The impact of low levels of collagen IX and pyridinoline on the
519   mechanical properties of in vitro engineered cartilage. *Biomaterials* **30**, 814–821
520   (2009).
521 36. Lin, W. *et al.* Osteomodulin positively regulates osteogenesis through interaction with
522   BMP2. *Cell Death Dis* **12**, 147 (2021).
523 37. Eyre, D. R. & Weis, M. A. Bone Collagen: New Clues to Its Mineralization Mechanism
524   from Recessive Osteogenesis Imperfecta. *Calcif Tissue Int* **93**, 338–347 (2013).
525 38. Rajagopal, A. *et al.* Restoration of the serum level of SERPINF1 does not correct the
526   bone phenotype in Serpinf1 null mice. *Mol Genet Metab* **117**, 378–382 (2016).
527 39. Nakamura, D. S., Hollander, J. M., Uchimura, T., Nielsen, H. C. & Zeng, L. Pigment
528   Epithelium-Derived Factor (PEDF) mediates cartilage matrix loss in an age-dependent
529   manner under inflammatory conditions. *BMC Musculoskelet Disord* **18**, 39 (2017).
530 40. Tagliaferri, C., Wittrant, Y., Davicco, M.-J., Walrand, S. & Coxam, V. Muscle and
531   bone, two interconnected tissues. *Ageing Res Rev* **21**, 55–70 (2015).
532 41. Xu, L., Li, Z., Liu, S.-Y., Xu, S.-Y. & Ni, G.-X. Asporin and osteoarthritis. *Osteoarthritis
533   Cartilage* **23**, 933–939 (2015).

534 42. Gelse, K., Söder, S., Eger, W., Diemtar, T. & Aigner, T. Osteophyte development—
535 molecular characterization of differentiation stages. *Osteoarthritis Cartilage* **11**, 141–
536 148 (2003).
537 43. Takano, M. *et al.* ANGPTL2 Promotes Inflammation via Integrin α5β1 in
538 Chondrocytes. *Cartilage* **13**, 885S-897S (2021).
539 44. Nishiyama, S. *et al.* ANGPTL2 Induces Synovial Inflammation via LILRB2.
540 *Inflammation* **44**, 1108–1118 (2021).
541 45. Hashimoto, S. *et al.* Development and regulation of osteophyte formation during
542 experimental osteoarthritis. *Osteoarthritis Cartilage* **10**, 180–187 (2002).
543 46. de Vega, S., Iwamoto, T. & Yamada, Y. Fibulins: Multiple roles in matrix structures
544 and tissue functions. *Cellular and Molecular Life Sciences* **66**, 1890–1902 (2009).
545 47. Wilson, R. *et al.* Changes in the Chondrocyte and Extracellular Matrix Proteome
546 during Post-natal Mouse Cartilage Development. *Molecular & Cellular Proteomics* **11**,
547 M111.014159 (2012).
548 48. Zhang, Y. & Marmorstein, L. Y. Focus on molecules: Fibulin-3 (EFEMP1). *Exp Eye*
549 *Res* **90**, 374–375 (2010).
550 49. Salvador, J. M., Brown-Clay, J. D. & Fornace, A. J. Gadd45 in Stress Signaling, Cell
551 Cycle Control, and Apoptosis. in 1–19 (2013). doi:10.1007/978-1-4614-8289-5_1.
552 50. Zhang, T., Ma, C., Zhang, Z., Zhang, H. & Hu, H. NF-κB signaling in inflammation and
553 cancer. *MedComm (Beijing)* **2**, 618–653 (2021).
554 51. Won, Y., Yang, J., Park, S. & Chun, J. Lipopolysaccharide Binding Protein and CD14,
555 Cofactors of Toll-like Receptors, Are Essential for Low-Grade Inflammation–Induced
556 Exacerbation of Cartilage Damage in Mouse Models of Posttraumatic Osteoarthritis.
557 *Arthritis & Rheumatology* **73**, 1451–1460 (2021).
558 52. Zhao, T., Su, Z., Li, Y., Zhang, X. & You, Q. Chitinase-3 like-protein-1 function and its
559 role in diseases. *Signal Transduct Target Ther* **5**, 201 (2020).
560 53. Tarquini, C. *et al.* Clusterin exerts a cytoprotective and antioxidant effect in human
561 osteoarthritic cartilage. *Aging* **12**, 10129–10146 (2020).
562 54. Ungsudechachai, T., Honsawek, S., Jittikoon, J. & Udomsinprasert, W. Clusterin Is
563 Associated with Systemic and Synovial Inflammation in Knee Osteoarthritis. *Cartilage*
564 **13**, 1557S-1565S (2021).
565 55. Koike, M. *et al.* Mechanical overloading causes mitochondrial superoxide and SOD2
566 imbalance in chondrocytes resulting in cartilage degeneration. *Sci Rep* **5**, 11722
567 (2015).
568 56. Duprez, J., Roma, L. P., Close, A.-F. & Jonas, J.-C. Protective Antioxidant and
569 Antiapoptotic Effects of ZnCl2 in Rat Pancreatic Islets Cultured in Low and High
570 Glucose Concentrations. *PLoS One* **7**, e46831 (2012).
571 57. Drecourt, A. *et al.* Impaired Transferrin Receptor Palmitoylation and Recycling in
572 Neurodegeneration with Brain Iron Accumulation. *The American Journal of Human*
573 *Genetics* **102**, 266–277 (2018).
574 58. Salazar-Noratto, G. E., De Nijs, N., Stevens, H. Y., Gibson, G. & Guldberg, R. E.
575 Regional gene expression analysis of multiple tissues in an experimental animal
576 model of post-traumatic osteoarthritis. *Osteoarthritis Cartilage* **27**, 294–303 (2019).
577 59. Gautam, R. *et al.* The Hermansky-Pudlak Syndrome 3 (Cocoa) Protein Is a
578 Component of the Biogenesis of Lysosome-related Organelles Complex-2 (BLOC-2).
579 *Journal of Biological Chemistry* **279**, 12935–12942 (2004).

580 60. Manabe, R. *et al.* Transcriptome-based systematic identification of extracellular matrix
581   proteins. *Proceedings of the National Academy of Sciences* **105**, 12849–12854
582   (2008).
583 61. Lynch, J. M. *et al.* A Thrombospondin-Dependent Pathway for a Protective ER Stress
584   Response. *Cell* **149**, 1257–1268 (2012).
585 62. Yagami, K. *et al.* Matrix Gla Protein Is a Developmental Regulator of Chondrocyte
586   Mineralization And, When Constitutively Expressed, Blocks Endochondral and
587   Intramembranous Ossification in the Limb. *Journal of Cell Biology* **147**, 1097–1108
588   (1999).
589 63. Takigawa, M. CCN2: a master regulator of the genesis of bone and cartilage. *J Cell*
590   *Commun Signal* **7**, 191–201 (2013).
591 64. Güller, M. *et al.* c-Fos overexpression increases the proliferation of human
592   hepatocytes by stabilizing nuclear Cyclin D1. *World J Gastroenterol* **14**, 6339 (2008).
593 65. Lin, Y.-L., Persaud, S. D., Nhieu, J. & Wei, L.-N. Cellular Retinoic Acid–Binding
594   Protein 1 Modulates Stem Cell Proliferation to Affect Learning and Memory in Male
595   Mice. *Endocrinology* **158**, 3004–3014 (2017).
596 66. Fisher, M. C., Meyer, C., Garber, G. & Dealy, C. N. Role of IGFBP2, IGF-I and IGF-II
597   in regulating long bone growth. *Bone* **37**, 741–750 (2005).
598 67. Alfaro, M. P. *et al.* The Wnt modulator sFRP2 enhances mesenchymal stem cell
599   engraftment, granulation tissue formation and myocardial repair. *Proceedings of the*
600   *National Academy of Sciences* **105**, 18366–18371 (2008).
601 68. Rodrigues, M., Yates, C. C., Nuschke, A., Griffith, L. & Wells, A. The Matrikine
602   Tenascin-C Protects Multipotential Stromal Cells/Mesenchymal Stem Cells from
603   Death Cytokines Such as FasL. *Tissue Eng Part A* **19**, 1972–1983 (2013).
604 69. Fuller, E. S., Smith, M. M., Little, C. B. & Melrose, J. Zonal differences in meniscus
605   matrix turnover and cytokine response. *Osteoarthritis Cartilage* **20**, 49–59 (2012).
606 70. Chakravarti, S. Functions of lumican and fibromodulin: Lessons from knockout mice.
607   *Glycoconj J* **19**, 287–293 (2002).
608 71. Liu, H., Li, D., Zhang, Y. & Li, M. Inflammation, mesenchymal stem cells and bone
609   regeneration. *Histochem Cell Biol* **149**, 393–404 (2018).
610 72. Wang, S. *et al.* Dynamic Changes in the Expression of Interferon-Stimulated Genes in
611   Joints of SPF Chickens Infected With Avian Reovirus. *Front Vet Sci* **8**, (2021).
612 73. Hara, T. & Tanegashima, K. Pleiotropic functions of the CXC-type chemokine
613   CXCL14 in mammals. *J Biochem* **151**, 469–476 (2012).
614 74. Li, Z. *et al.* Integrated Analysis of miRNAs and Gene Expression Profiles Reveals
615   Potential Biomarkers for Osteoarthritis. *Front Genet* **13**, (2022).
616 75. Izuhara, K. *et al.* Periostin in Allergic Inflammation. *Allergology International* **63**, 143–
617   151 (2014).
618 76. Barreto, G. *et al.* Lumican is upregulated in osteoarthritis and contributes to TLR4-
619   induced pro-inflammatory activation of cartilage degradation and macrophage
620   polarization. *Osteoarthritis Cartilage* **28**, 92–101 (2020).
621 77. Zhou, Y. *et al.* Deletion of ApoE Leads to Intervertebral Disc Degeneration via
622   Aberrant Activation of Adipokines. *Spine (Phila Pa 1976)* **47**, 899–907 (2022).
623 78. Santoro, A. *et al.* SERPINE2 Inhibits IL-1α-Induced MMP-13 Expression in Human
624   Chondrocytes: Involvement of ERK/NF-κB/AP-1 Pathways. *PLoS One* **10**, e0135979
625   (2015).

626   79.   Rahmani, M. *et al.* Versican: signaling to transcriptional control pathwaysThis paper is
627   one of a selection of papers published in this Special Issue, entitled Young
628   Investigator's Forum. *Can J Physiol Pharmacol* **84**, 77–92 (2006).

629   80.   Theocharidis, G. & Connelly, J. T. Minor collagens of the skin with not so minor
630   functions. *J Anat* **235**, 418–429 (2019).

631   81.   Halder, A. *et al.* Influence of Limb Alignment on Mediolateral Loading in Total Knee
632   Replacement. *Journal of Bone and Joint Surgery* **94**, 1023–1029 (2012).

633   82.   Thein, R. *et al.* The Prevalence of Cruciate Ligament and Meniscus Knee Injury in
634   Young Adults and Associations with Gender, Body Mass Index, and Height a Large
635   Cross-Sectional Study. *J Knee Surg* **30**, 565–570 (2017).

636   83.   Mitchell, J. *et al.* Epidemiology of meniscal injuries in US high school athletes between
637   2007 and 2013. *Knee Surgery, Sports Traumatology, Arthroscopy* **24**, 715–722
638   (2016).

639   84.   Sun, H. *et al.* Single-cell RNA-seq analysis identifies meniscus progenitors and
640   reveals the progression of meniscus degeneration. *Ann Rheum Dis* **79**, 408–417
641   (2020).

642   85.   Wang, F. *et al.* Endothelial cell heterogeneity and microglia regulons revealed by a pig
643   cell landscape at single-cell level. *Nat Commun* **13**, 3620 (2022).

644

Supplementary materials are available on the attached CD.

Julia Semba

Laboratory of Applied Biotechnology
Center for Advanced Technology
Adam Mickiewicz University in Poznan
e-mail: jsemba@amu.edu.pl

Author contribution statement

I declare that I am the co-author of the unpublished article "Single-Cell Transcriptomic Atlas of Porcine Meniscus: Paving the Way for Advanced Therapies" by Monika Mankowska, Monika Stefanska, Anna Maria Mleczko, Witold Kot, Lukasz Krych, Julia Anna Semba, Jakub Dalibor Rybka. The author's contribution is as follows:

Julia Semba prepared the single cell suspension preparation and helped with library generation and preliminary data analysis.

Monika Mańkowska designed the study and mentor the technical part of the project. She processed the scRNA-seq data and made data interpretations. Monika Mańkowska-Woźniak wrote the original manuscript.

Monika Stefanska made a bioinformatic analysis.

Anna Maria Mleczko prepared the single cell suspension preparation and helped with library generation. Anna Mleczko precipitated in data interpretation.

Witold Kot made library sequencing.

Łukasz Krych made a bioinformatic analysis.

Jakub Rybka supervised the technical part of the project and revised the manuscript. Jakub Rybka acquired funding and has been corresponding with the journal.

Date: 18.08.2023

Signature: *Julia Semba*

prof. UAM dr hab. inż. Jakub D. Rybka

Dr Monika Mańkowska-Woźniak

Laboratory of Applied Biotechnology
Center for Advanced Technology
Adam Mickiewicz University in Poznan
e-mail: mmankowska@amu.edu.pl

Author contribution statement

I declare that I am the first author of the unpublished article "Single-Cell Transcriptomic Atlas of Porcine Meniscus: Paving the Way for Advanced Therapies" by Monika Mankowska, Monika Stefanska, Anna Maria Mleczko, Witold Kot, Lukasz Krych, Julia Anna Semba, Jakub Dalibor Rybka, and I am aware that this publication is a part of Julia Semba PhD dissertation. The author's contribution is as follows:

Julia Semba prepared the single cell suspension preparation and helped with library generation and preliminary data analysis.

Monika Mańkowska designed the study and mentor the technical part of the project. She processed the scRNA-seq data and made data interpretations. Monika Mańkowska-Woźniak wrote the original manuscript.

Monika Stefanska made a bioinformatic analysis.

Anna Maria Mleczko prepared the single cell suspension preparation and helped with library generation. Anna Mleczko precipitated in data interpretation.

Witold Kot made library sequencing.

Łukasz Krych made a bioinformatic analysis.

Jakub Rybka supervised the technical part of the project and revised the manuscript. Jakub Rybka acquired funding and has been corresponding with the journal.

Date: 18.08.2023

Signature:

Dr Anna Mleczko

Laboratory of Applied Biotechnology
Center for Advanced Technology
Adam Mickiewicz University in Poznan
e-mail: amleczko@amu.edu.pl

Author contribution statement

I declare that I am the co-author of the unpublished article "Single-Cell Transcriptomic Atlas of Porcine Meniscus: Paving the Way for Advanced Therapies" by Monika Mankowska, Monika Stefanska, Anna Maria Mleczko, Witold Kot, Lukasz Krych, Julia Anna Semba, Jakub Dalibor Rybka, and I am aware that this publication is a part of Julia Semba PhD dissertation. The author's contribution is as follows:

Julia Semba prepared the single cell suspension preparation and helped with library generation and preliminary data analysis.

Monika Mańkowska designed the study and mentor the technical part of the project. She processed the scRNA-seq data and made data interpretations. Monika Mańkowska-Woźniak wrote the original manuscript.

Monika Stefanska made a bioinformatic analysis.

Anna Maria Mleczko prepared the single cell suspension preparation and helped with library generation. Anna Mleczko precipitated in data interpretation.

Witold Kot made library sequencing.

Łukasz Krych made a bioinformatic analysis.

Jakub Rybka supervised the technical part of the project and revised the manuscript. Jakub Rybka acquired funding and has been corresponding with the journal.

Date: 21.08.2023 r.

Signature: *Anna Mleczko*

Dr Łukasz Krych

Department of Food Science,
Faculty of Science,
University of Copenhagen
e-mail: krych@food.ku.dk

Author contribution statement

I declare that I am the co-author of the unpublished article "Single-Cell Transcriptomic Atlas of Porcine Meniscus: Paving the Way for Advanced Therapies" by Monika Mankowska, Monika Stefanska, Anna Maria Mleczko, Witold Kot, Lukasz Krych, Julia Anna Semba, Jakub Dalibor Rybka, and I am aware that this publication is a part of Julia Semba PhD dissertation. The author's contribution is as follows:

Julia Semba prepared the single cell suspension preparation and helped with library generation and preliminary data analysis.

Monika Mańkowska designed the study and mentor the technical part of the project. She processed the scRNA-seq data and made data interpretations. Monika Mańkowska-Woźniak wrote the original manuscript.

Monika Stefanska made a bioinformatic analysis.

Anna Maria Mleczko prepared the single cell suspension preparation and helped with library generation. Anna Mleczko precipitated in data interpretation.

Witold Kot made library sequencing.

Łukasz Krych made a bioinformatic analysis.

Jakub Rybka supervised the technical part of the project and revised the manuscript. Jakub Rybka acquired funding and has been corresponding with the journal.

Date: 2 7 - 08 - 202 3

Signature:

Dr hab. inż. Jakub Rybka, prof. UAM

Laboratory of Applied Biotechnology
Center for Advanced Technology
Adam Mickiewicz University in Poznan
e-mail: jrybka@amu.edu.pl

Author contribution statement

I declare that I am the corresponding author of the unpublished article "Single-Cell Transcriptomic Atlas of Porcine Meniscus: Paving the Way for Advanced Therapies" by Monika Mankowska, Monika Stefanska, Anna Maria Mleczko, Witold Kot, Lukasz Krych, Julia Anna Semba, Jakub Dalibor Rybka, and I am aware that this publication is a part of Julia Semba PhD dissertation. The author's contribution is as follows:

Julia Semba prepared the single cell suspension preparation and helped with library generation and preliminary data analysis.

Monika Mańkowska designed the study and mentor the technical part of the project. She processed the scRNA-seq data and made data interpretations. Monika Mańkowska-Woźniak wrote the original manuscript.

Monika Stefanska made a bioinformatic analysis.

Anna Maria Mleczko prepared the single cell suspension preparation and helped with library generation. Anna Mleczko precipitated in data interpretation.

Witold Kot made library sequencing.

Łukasz Krych made a bioinformatic analysis.

Jakub Rybka supervised the technical part of the project and revised the manuscript. Jakub Rybka acquired funding and has been corresponding with the journal.

Date: 1 8. 08. 2023

Signature:

prof. UAM dr hab. inż. Jakub D. Rybka